UNIVERSITY OF LEEDS

Long-term Performance of Portland cement-Slag-Limestone [CEM VI(S-LL)] Mortars and Concretes Exposed to Extreme Environments

Moro Sabtiwu

Submitted in accordance with the requirements for the degree of

Doctor of Philosophy

The University of Leeds
Faculty of Engineering and Physical Sciences
School of Civil Engineering

July 2024

UNIVERSITY OF LEEDS

Long-term Performance of Portland Slag Limestone [CEM VI(S-LL)] Mortars and Concretes Exposed to Extreme Environments

Moro Sabtiwu

Supervisors

Prof. Susan Bernal Lopez

Dr Yuvaraj Dhandapani

Dr Michal Drewniok

Submitted in accordance with the requirements for the degree of

Doctor of Philosophy

The University of Leeds

Faculty of Engineering and Physical Sciences

School of Civil Engineering

July 2024

Intellectual Property and Publication Statement

The candidate confirms that the work submitted is his own, except where work is part of jointly-authored publications. The contribution of the candidate and the other authors of such publications is explicitly indicated below. The candidate confirms that appropriate credit has been given within the thesis where reference has been made to the work of others. The author, Moro Sabtiwu, was responsible for the experimental works, including data curation, formal analysis, investigation and writing the original drafts and the interpretation of the data.

Parts of the research reported in Chapters 3, 4, 5, 6 and 7 have been featured in part or fully in the following conference publications:

1. **Sabtiwu M.**, Dhandapani Y., Adu-Amankwah and S., Bernal S.A. Carbonation performance of Portland-slag-limestone mortars. Proceeding of *the 41st Cement and Concrete Science Conference, 12 -13th September 2022,* Leeds, UK
2. **Sabtiwu, M.**, Dhandapani, Y., Drewniok, M., Adu-Amankwah, S., Bernal, S.A. Engineering and durability performance of composite Portland cement- blast furnace slag-limestone concretes. Proceedings *the 77th RILEM Annual Week & the 1st Interdisciplinary Symposium on Smart & Sustainable Infrastructures*, *4 - 8th September 2023* Vancouver, BC, Canada.
3. **Sabtiwu, M.**, Dhandapani, Y., Drewniok, M., Adu-Amankwah, S., Bernal, S.A. Impact of carbonation on chloride permeability of composite Portland cement-slag-limestone concretes. Proceedings of the *42nd Annual Cement & Concrete Science Conference*, *11 - 12th September 2023,* London, UK
4. **Sabtiwu, M.**, Dhandapani, Y., Drewniok, M., Adu-Amankwah, S., Bernal, S.A. Uniaxial compressive creep performance of concrete based on composite Portland -blast furnace slag-limestone cements. Proceedings of the *fib ICCS2024 – International Conference on Concrete Sustainability, 11 - 13th September 2024*, Guimaraes, Portugal
5. **Sabtiwu, M**., Dhandapani, Y., Drewniok, M., Adu-Amankwah, S., Bernal, S.A. Coupled action of load and carbonation on transport properties of Portland cement-slag-limestone concretes. Proceedings of the *10th International Conference on Concrete under Severe Conditions – Environment and loading, 25 - 27th September 2024*, Chennai, India

Dr Samuel Adu-Amankwah was a PhD project advisor, the other co-authors were PhD thesis supervisors who contributed to the conceptualisation of the research, methodology, supervision, resources, project administration, funding acquisition and writing – review and editing.

Awards and Media Appearances

12th April 2024: Featured in National Highways World Engineering Day for Sustainable Development Press release - https://nationalhighways.co.uk/our-work/innovation-and-research/research/our-research-fellows-and-doctoral-students/

31st January 2024: Finalist of the Surendra P. Shah Award on Technologies for Low-Carbon and Lean Construction 2024 global competition; organised by The Indian Institute of Technology Madras, Chennai, India

12th September 2023: Best Poster Award winner at the IOM^3 42nd Cement and Concrete Science Conference, London, UK

02nd March 2023: Featured in National Highways Press release: Doctoral students helping National Highways innovate for the future – https://nationalhighways.co.uk/article/doctoral-students-helping-national-highways-innovate-for-the-future/

13th September 2022: Best Poster Award winner at the IOM^3 41st Cement and Concrete Science Conference, Leeds, UK

Acknowledgement

This study was co-funded by the UK Engineering and Physical Sciences Research Council (EPSRC) and National Highways via a CASE award.

I appreciate the unflinching ‘motherly’, yet critical research support of my supervisor Prof. Susan Bernal Lopez, and the constructive inputs from co-supervisors Dr. Yuvaraj Dhandapani, Dr. Michal Drewniok and Dr. Samuel Adu-Amankwah, for making the work a reality. Their invaluable guidance and knowledge immensely contributed to shaping the trajectory of this project.

I am extremely appreciative and thankful to my wife, Taliawat and, daughters Nuha and Rahma for riding along with me in the high and low tides of the PhD journey.

My gratitude is extended to my parents, and non-exhaustive well-wishing family members who supported this journey. Special appreciation to my Dad, Wuro Alhaji Sabtiwu Gouni, the Ghana Central region Kotokoli Chief who set the pace for my education. Thanks to my mum, Rebecca Lariba, for travelling to UK to support with childcare, while I focused on research.

I also acknowledge the support of past and present technicians, here at the University of Leeds, School of Civil Engineering, Ian, Steve, Rob, Marvin, Patrick and Stuart. The readiness and approachable posture of Ian to assist is particularly recognised.

Thanks to all the non-exhaustive list of friends made during my time at University of Leeds. You all formed part of a great company to work with.

Abstract

Ternary cement (CEM VI(S-LL)) made of conventional supplementary cementitious materials (e.g. blast furnace slag) with addition of limestone powder, as Portland cement replacements, are attracting research and commercial interest for their sustainability and durability potential as viable options for concrete production.

The widespread deployment of CEM VI(S-LL) for the production of structural concrete is arguably limited despite its inclusion in standards such as the BS 8500-2:2023 and the BS EN 197-5:2021. This is a consequence of the limited track record regarding the long-term performance of concretes made from these cements, under near realistic in-service conditions. Multiscale and multi-technique approaches highlighting the synergy between microscale properties and macroscale performance are key to understanding the potential deterioration mechanisms of these materials. This research thesis centres on elucidating the implications of multiple exposure classes on the long-term performance of mortars and concrete, with or without loading, made of CEM I, binary CEM I-blast furnace slag, and ternary blast furnace slag-limestone blended cement.

The durability performance of mortars and concrete, specifically chlorides permeability and carbonation resistance, in addition to mechanical properties were determined as a function of different binder formulations and curing durations. For the concrete made of ternary cement blends, it was identified that a reduction in the blast furnace slag content, due to addition of ~10-20 wt.% limestone powder, leads to satisfactory mechanical and durability properties relative to binary blast furnace slag-blended concrete and CEM I concrete. It was established that concrete made from ternary blast furnace slag-limestone-CEM I exhibited progressive increases in compressive strength, reaching values comparable to those of the reference CEM I specimens by 365 days of curing. The flexural strength, static and dynamic elastic moduli of blast furnace slag-containing concretes, with or without limestone, is comparable to CEM I mixes at early and prolonged curing ages. An evaluation of the performance based on existing models such as the ACI, *fib* and BS EN 1992-1-1:2023 (Eurocode 2) demonstrated satisfactory conformance, suggesting concretes made from CEM VI(S-LL) can safely be adopted in structural applications. The chloride permeability and sorptivity studies demonstrated that, using composite cements containing up to ~20 wt.% limestone has no detrimental implications on the resistance to chlorides and water ingress of concrete produced with them. This is attributed to beneficial effect of pore refinement evidenced by bulk conductivity evolution.

Carbonation and chloride induced deterioration of reinforced concretes are leading causes of infrastructure damage and potential collapse. Carbonation induces pore structural changes (porosity and pore connectivity) which can exacerbate chloride and/or water ingress in structural concrete. A study on the impact of unidirectional carbonation exposure on moisture and chloride transport was conducted as part of this thesis research. The carbonation rates of binary and ternary cements based mortar and concrete mixes were higher than those of CEM I. However, the addition of limestone showed no significant impact on blast furnace slag-blended systems. Calculations of service life considering the carbonation rates determined for the assessed concretes, showed that the carbonation depths are within limits of the cover depths recommended by the BS 8500-1:2023 for concretes made from multicomponent cements designed for 50 years carbonation exposure classes XC3/XC4. Also, rather than relying solely on the design strength of concrete as the criterion for suitability in carbonation exposure classes XC3/XC4, the predicted carbonation depths for 50-100 years, and post-accelerated carbonation strength (well above design strength) achieved by CEM VI(S-LL), suggest that these materials can be suitable for use in exposure classes XC3/XC4. The increased rate of carbonation observed in binary and ternary cement based concretes did not result in detrimental shrinkage-induced dimensional instabilities and post-carbonation residual strength. Meanwhile, it is also established that despite the increased carbonation rates in blast furnace slag-containing mortars and concretes, with or without limestone, their chloride resistance was nearly two-fold better than that of CEM I.

The combined action of compressive load (~30%) and natural or accelerated carbonation was interrogated relative to non-loaded concretes, followed by studies of these combined actions on moisture transport properties. Loading under natural and accelerated carbonation exposure was sustained for 200 and 28 days respectively. It was identified that the progression of the carbonation front was limited in the stressed state relative to non-loaded concretes and independent of mix design or exposure type. The total deformation of binary and ternary mixes was lower relative to CEM I in both exposure conditions evaluated. However, the magnitude of strain was identified to be greater under accelerated carbonation (~2.5-times in CEM I and ~5-times in composite cements) relative to ambient exposure conditions. Studies of water admissibility of stressed and unstressed concretes after carbonation indicated that both materials (CEM I and blended cements) exhibited comparable rates of water ingress.

This PhD thesis research demonstrates that CEM VI(S-LL) based concrete have excellent mechanical performance, compliant with existing design codes for structural concrete. These are suitable materials for applications where high chloride and moderate carbonation resistances are required, and loading conditions will not have a negative impact on their durability performance.

Contents

List of Tables

List of Figures

List of abbreviations

Cement related nomenclature

CEM I/OPC/PC: Portland cement

GGBS/GBFS/BFS: Ground Granulated Blast Furnace Slag

CEM VI(S-LL): Composite cement made from Portland cement-slag + ~20% limestone

N: CEM I/Portland cement

NS: Portland cement + ~ 50% slag

NSL: Portland cement + ~ 40% slag + ~10% limestone

NS2L: Portland cement + ~ 30% slag + ~20% limestone

SCM: Supplementary cementitious materials

ITZ: Interfacial Transition Zone

w/b: Water-to-binder ratio

w/c: Water to cement ratio

Clinker and hydrated phases related nomenclature

C_3S: Tri calcium silicate

C_2S: Di calcium silicate

CH: Portlandite

C-S-H: Calcium Silicate Hydrate

C-A-S-H: Aluminium-substituted Calcium Silicate Hydrate

AFm: Alumina-ferric oxide-mono

AFt / Ettringite: Alumina-ferric tri-sulphate

Materials and Testing related nomenclature

RH: Relative humidity

T: Temperature

GEMS: Gibbs Energy Minimization Software for Geochemical Modelling

XRD: X-ray Diffractometry

TOC: Total Organic Carbon

RCPT: Rapid Chloride Permeability Test

UPV: Ultrasonic Pulse velocity

USB: Universal Serial Bus

QXRD: Quantitative X-Ray diffraction analysis

PONKCS: Partial or No Known Crystal Structures

PDF 4+: Powder Diffraction File

ICDD: International Centre for Diffraction Data

BPO Paste: Dibenzoyl peroxide, paste

BET: Brunauer-Emmett-Teller

SSA: Specific Surface Area

IPA: Isopropanol

BS: British Standard

EN: European Norm

ACI: American Concrete Institute

FIB: International Federation for Structural Concrete

Symbol/Units related nomenclature

g/cm^3: Grammes per cubic centimetre

m^3/s: Cubic-metre per second

Pa: Pascal

m^2/s: Metre-Squared per second

µm: Micro metre

MS/m: MilliSiemens per metre

σ_b: Bulk conductivity

D_{nnsm}: Non-steady state migration coefficient

Eq.: Equation

wt. %: Percentage by weight

Chapter 1.

1. INTRODUCTION

1.1. Background and thesis structure

The long-term performance of concrete structures, apart from their initial construction design considerations, is strongly dependent on the intrinsic properties of the material and exposure conditions during its service life. When atmospheric CO_2 diffuses into the concrete cover, it induces a degradation process referred to as carbonation. It is well known that carbonation in cement and concretes with high volumes of cement replacements, such as in binary and ternary cementitious systems, is much higher than identified in plain Portland cement materials.

The carbonation-related changes on pore structure could serve as conduits for accelerated ingress of external deleterious species in moisture and ionic forms, which can exacerbate the deterioration of concrete structures, that are typically load bearing. This has significant economic, health, safety and environmental implications (1, 2). It is thus critical to develop an understanding of the long-term performance of novel cement systems with high volume supplementary cementitious materials (SCM) replacement levels, including composite ternary cements specified in the BS EN 197-5: 2021 (3) and recently ratified in the BS 8500 - 2:2023 (4) standard.

This thesis research centres on mortars and concretes made with Portland cement (CEM I), binary blends of Portland cement with ground granulated blast furnace slag (GGBS), and blends of Portland cement GGBS-limestone (ternary). The characterisation of mortars and concretes produced with the ternary cements was conducted to assess how their engineering and durability properties compare with mortars and concretes produced with binary cements and those of CEM I at different curing times. An evaluation of the impact of carbonation on transport properties including water and chloride permeability, as well as the influence of the combined action of carbonation and compressive load on other durability performance of these materials was conducted. Studies combining different durability stresses (carbonation-chlorides) and loading (loading-carbonation) are rare, due to the complexity of the

experimental set up and lack of standardised protocols for conducting such tests; however, this approach will enable the elucidation of the material's durability under closer-to-reality in-service conditions.

A review of literature is presented in Chapter 2 where the changes in chemistry and consequently on microstructure due to inclusion of SCMs (focus on slags with/without limestone) relative to CEM I are highlighted. The gaps in the literature on the influencing parameters on carbonation-induced microstructure variations (mainly porosity and pore connectivity) and the interlink with transport properties are reviewed. Moreover, the relevance of accounting for the effect of loading on durability towards realistic performance assessment of concretes in the context of existing literature are discussed.

Chapter 3 highlights the analytical techniques employed in the PhD project for the characterisation of raw materials used for producing the different cementitious systems. The associated mode of operation of equipment for characterising fresh and, hardened mortars and concrete are expounded in this section, including methods adopted for casting, curing and sample preconditioning until testing. These methods mainly include X-ray diffractometry, laser granulometry, Helium gas pycnometry, BET surface area for raw materials, Nordtest NTBUILD 492 and ultrasonic pulse velocity (UPV) for mortars or concrete characterisation. The techniques adopted for setting up coupled action of mechanical load and carbonation are also described.

Furthermore, experimental results are shown in the subsequent three chapters, with each chapter aligning with the PhD project objectives, and each presenting a self-contained section of results and discussion. Chapter 4 reports the results and discussion on the carbonation performance of mortar mixes exposed to natural or ambient (up to 2 years) and accelerated CO_2 (up to 100 days) carbonation exposure. The compressive strength, water absorption properties, bulk conductivity and permeability to chlorides of the carbonated mortars are discussed.

Chapter 5 provides a detailed analysis of the engineering and durability performance of concrete specimens, moist cured for up to 365 days. The evolution of compressive strength, flexural strength, static and UPV dynamic elastic moduli are presented. In addition, the variations in transport properties including water absorption, chloride permeability, bulk and surface resistivity of the concretes with curing age are also discussed.

In Chapter 6, findings on determining the impact of carbonation on transport properties at the concrete scale are showcased. Specifically, the carbonation performance, water absorption properties and chloride permeability on the carbonated concretes are discussed. An additional comparative analysis of the studies on the shrinkage evolution of concretes under ambient

and accelerated carbonation is also reported. Chapter 6 is further expanded to contain an additional study (Section 6.5) focusing on the effect of the combined action of loading and carbonation on transport properties. A comparative analysis of accelerated carbonation (up to 28 days) performance under sustained uniaxial compressive load, with corresponding loaded specimens under ambient conditions (up to 28 days), and non-loaded concretes under similar conditions is reported. The impact of load on the concrete mixes under both conditions is also discussed. Additionally, the load-induced strain evolution (up to 150 days) of concretes under ambient conditions is highlighted. The residual strength, water absorption properties and open porosity changes of the concretes assessed after the loading cycle are reported and discussed in this section.

1.2. Overview of the literature

The guaranteeing of long-term performance of concrete infrastructure is one of the major engineering challenges of our time. While durability performance of concrete under a single deteriorative environment, with or without loads, has been fairly considered for Portland cement (CEM I), and for conventional SCMs (such as fly ash and GGBS), only a few studies on durability of ternary concrete systems have been reported in the literature (5).

Studies reflecting realistic field conditions of coupled action of loading and multiple exposure conditions to the most common durability problems, such as carbonation and/or chloride exposure are sparse. Some studies have employed indirect testing methodologies for durability assessment using only steel reinforcement under stress in simulated concrete pore solution, with or without chlorides (6, 7). However, such studies are unlikely to simulate in-service conditions, and will only provide a simplified picture of the tested concrete performance, as the influence of durability stresses on the concrete cover stability are not always considered. Factors such as the impact of pore refinement on diffusivity and chemical binding due to binding phases are unaccounted for.

The effect of mechanical loading on transport properties of concrete has been studied in the past. Although, it is believed that there is a good understanding about the alteration induced by loading on properties such as permeability and water absorption, contradictions exist regarding results obtained when testing concrete with or without loading (8-11). It is identified that these studies have been developed in the context of fracture mechanics (e.g., the use of fictitiously cracked specimens), use of short-term loading cycles, and test conducted on concretes stressed to near failure loads. There exist a limited consideration when concrete is subjected to sustained load and carbonation for long duration, and the combined impact on

other durability mechanism. A multiscale understanding in the context of the impact of SCMs on intrinsic microstructure-related properties (such as porosity and pore connectivity) development of modern concrete when subjected to loading and multiple durability exposure conditions is currently lacking. This gap exists despite its relevance for optimising concrete mixes designed for longevity, and the urgent need for identifying the best strategies for extending infrastructure service life and prediction of how different exposure conditions might influence the long-term performance of concretes. However, research efforts towards standardised experimental methodologies for such studies are gaining interest.

In response to this knowledge gap, this PhD research investigates the role of chemical and physical stresses on the performance of conventional and blended Portland cement concrete. Specifically, this project evaluates the effect of CO_2 and/or chloride/moisture ingress on the durability of these materials; given that carbonation and chloride-induced corrosion are some of the most common degradation mechanisms compromising the service life of structures globally. The coupled effect of loading is also investigated, to identify how loading a concrete system influences the progress of carbonation in these materials, and the combined impact on transport mechanisms, as this is largely unknown, particularly for composite cement concrete.

Concrete subjected to loading (under field conditions) can experience load-induced deformation and drying shrinkage, which can be associated with (micro) cracking or its propagation. These can serve as conduits (depending on the size and location of microcracks) for the ingress of deteriorative agents, which can further trigger other durability problems in structural concrete. The performance of CEM I concrete systems under the combined action of load with individual exposure conditions (here, drying environment is considered as ambient carbonation) has been addressed in the literature (12, 13). Similarly, the coupled action of load and single environmental exposure on blast furnace slags has been reported, but with conflicting results, mostly based on compressive loading. (14-16). Meanwhile, the assessment of the performance of concretes made from multicomponent cementitious systems with a high volume of SCMs and limestone addition (as specified in BS EN 197-5) under loading conditions is sparse (17). There is also a lack of studies examining the long-term performance of materials when exposed to accelerated degradation (e.g., carbonation) under mechanical loading. It is thus critical to consider the performance of modern concretes under mechanical loading when subjected to other durability actions. Additionally, it is important to elucidate the potential dependencies between loading and durability performance based on multiple exposure combinations to adequately understand the long-term behaviour of concrete under near realistic conditions. Such long-term performances under load can be achieved by

inducing accelerated degradation of the material via modification of standardised testing methodologies.

The synergistic effect of using different SCMs in improving durability performance of concrete has been gaining global attention. Generally, blast furnace slag-containing concrete systems exhibit reduced carbonation resistance relative to CEM I concrete systems, but with contradictory limiting factors (18-20). The reduction in the amount of portlandite (CH) reserves would typically lead to reduced carbonation resistance of SCM-concretes. There is a general understanding of the accelerated progression of carbonation of the main binding phases - an aluminium-substituted calcium silicate hydrate (C-A-S-H). This results in decalcification and potentially leads to pore coarsening in SCM concrete systems. For CEM I systems, the carbonation of portlandite densifies pore structure with an additional impact of pH loss in both cases. However, studies linking decalcification-induced changes in capillary porosity (closely linked to transport properties) on refined SCM porosity and impact on chloride mobility/water ingress with or without load are very limited.

It is evident that there is a lack of understanding of the existing relationships among the pore structural-related response, transport properties, and load-induced deterioration of concrete made with high volume of SCMs. Studies on the influence of the coupled effect of aggressive exposure environment (such as carbonation) on the performance of concretes under stress, and the combined impact on transport properties are urgently needed. This is critical to identify the realistic serviceability of different concrete mix designs subjected to mechanical and environmental loads. Thus, the following outstanding questions are addressed in this PhD research:

i. How does high SCM (with/without limestone addition) replacement influence the engineering and durability properties of concretes?

ii. How does carbonation influence the durability performance of concrete under compressive stress states at expected service load levels?

iii. What is the role of stress on ingress of deleterious species, such as moisture/chlorides on carbonated concretes?

iv. How does the coupled exposure to loading and aggressive species alter engineering properties of concrete?

The aims and objectives in this study are presented to answer the aforementioned research questions and are highlighted in the subsequent section, followed by a more detailed literature review.

1.3. Aims

The overall aim of this study is to elucidate the effect of the combined exposure to loading and durability stresses in the performance of low carbon mortars and concretes produced with composite cements. A concrete technology approach is adopted to simulate the deterioration mechanisms of concrete near realistic service conditions with concrete in stressed or unstressed state, and detailed characterisation of the concrete mixes is conducted to determine the mechanism leading to changes in performance. Thus, this study also contributes to the development of testing protocols for evaluating the effect of loading in durability performance of concretes, as standards for coupled durability exposure and stress testing are non-existent.

1.4. Objectives

The following specific objectives are pursued to achieve the aims of this study.

i. Determine the evolution of engineering (e.g. mechanical strengths) and transport (e.g. chloride and water ingress) properties of mortars and concretes made from Portland cement (CEM I), blends of Portland cement with slag (binary), and blends of Portland cement slag-limestone (ternary).

ii. Conduct a systematic evaluation of the impact of carbonation on chloride ingress of composite mortars and concretes.

iii. Evaluate the effect of sustained compressive loading on the progress of natural and accelerated carbonation of binary slags and ternary limestone-slag concretes at predefined compressive stress/strength ratios, while evaluating, total strain evolution and implications on the pore structure related properties (e.g. open porosity).

iv. Identify the coupled effect of compressive loading and carbonation on transport properties of concretes made from composite cements.

Chapter 2.

2. LITERATURE REVIEW

2.1. Sustainability of cements and concretes

Portland cement manufacturing contributes a remarkable amount of CO_2 emissions, which is a major contributor to climate change (21, 22). The contribution arises from high temperature limestone decomposition (with associated fuel use), producing approximately 0.53 kg CO_2 per kg of clinker (23). Research progress and global decarbonisation efforts have posited several measures to increase the sustainability of this material. This includes a balance between efficient resource utilisation, CO_2 reduction targets and enhancing concrete performance. While alternative clinkers show promise to producing low carbon concrete, with reduced CO_2 emission potential (24), compositional improvements such as high volume replacement of widely used Portland clinker offers the more immediate and practical solution to improve concrete sustainability (25-27). For achieving net zero targets, the mean global clinker factor by 2050 needs to be reduced to about 0.60 from 0.78 (26, 27). Portland clinker replacement materials, referred to as supplementary cementitious materials (SCMs) arise from natural sources (e.g. clays) or as industrial by-product e.g. ground granulated blast furnace slag (GGBS) and fly ashes. Recent developments in increasing limestone contents in concrete in addition to the use of conventional SCMs to produce ternary blends has gained research interest, not only to enhance durability potential of modern concrete, but also motivated by the great potential of CO_2 emissions reduction when using cements with a reduced clinker factor. For example, multicomponent concretes made from blast furnace slags with limestone addition up to ~20% have demonstrated through life cycle analysis to reduce the global warming potential by 35% (17). Similarly, various studies using calcined clay limestone cements have shown significant reduction in global warming potential of up to about 30% (28).

In addition to establishing the sustainability benefits of SCMs, their physical and chemical contribution to CEM I hydration is well understood in binary and ternary blended cements. However, for composite cements with high volume SCMs + high limestone content recently

added to the European BS EN 197-5: 2021 (3) and UK standards BS 8500-2:2023 (4), there is an urgent need to expand the body of knowledge on the long-term performances of concretes made from them, due to limited in-service track record. Some key aspects of the chemistry of binary and ternary cements with focus on blast furnace slag, and with limestone addition to slags are discussed in the next section. The influence on fresh and hardened properties is also discussed. It is worth noting that blast furnace slag is also referred to as GGBS/slags in the entire thesis; Portland cement is interchangeably herein referred to as CEM I or OPC or PC.

2.2. Supplementary cementitious materials (SCMs)

Supplementary cementitious (SCMs) are soluble silicates, aluminosilicates or calcium aluminosilicates in the form of fine powders, and used as replacement materials for Portland cement clinker or addition to Portland cement in concrete mixtures. They include sources from industrial waste (by-products) such, fly ashes from coal power plants and GGBS from pig iron manufacturing. Natural sources include clays, volcanic ashes and limestone fillers. Typical physical and chemical characteristics of SCMs employed in binary and ternary blends are summarised in Table 2.1. SCMs influence the hydration kinetics of Portland cement, phase assemblage evolution and pore solution chemistry. Pozzolanic SCMs such as fly ashes react by consumption of portlandite (CH) from Portland cement hydration. Slags however exhibit some latent hydraulicity and can be activated by alkalis (including hydration products from Portland cement) and sulphates (29).

Table 2.1: Physical and chemical characteristics of some SCMs (30, 31)

Material & Chemistry (%by mass)	Fineness	Remarks when blended with OPC
Fly ash – Class C [Based on ASTM C618 - 23E1 (32)] CaO = 11.6–29.0; SiO_2 = 23.1–50.5; Al_2O_3 = 13.3–21.3; Fe_2O_3 = 3.7–22.5	Particle size: <1µm to 150µm Blaine fineness 200–300 m^2/kg	• Latent hydraulicity to pozzolanic • reduces the bleeding and segregation
Fly ash – Class F [Based on ASTM C618 – 23E1 (32)] CaO = 0.7–7.5; SiO_2 = 45–64.4; Al_2O_3 = 19.6–30.1; Fe_2O_3 = 3.8–23.9		• Low reactivity, pozzolanic • slow early age strength development
Grounded Blast Furnace Slag CaO = 35–48 ; SiO_2 = 32–42 ; Al_2O_3 = 6–19 ;Fe_2O_3 = 3; MgO = 7–15	Particle size: < 45 µm; Blaine fineness on average 500 m^2/kg	• Latent hydraulic reactivity • High Al_2O_3 promotes early age strength in the presence of sulphates
Calcined clays (metakoalin) SiO_2 = ~51.5 ; Al_2O_3 = ~40.2	Particle size: ~1–2 µm; Blaine fineness 12–15 m^2/kg	• High reactivity and increases the concrete's early age strength
Limestone Mainly Calcite, dolomitic types contain magnesium	Blaine fineness 800 – 1,100 m^2/kg	• Forms carbonate-AFm phases with reactive alumina; Increasing the packing density

When Portland cement is mixed with water, it reacts. The hydration products of such reactions are mainly dominated by calcium silicate hydrates (C-S-H) formation in accordance with Equations 2.1 and 2.2. Blast furnace slag is also hydraulic but less reactive than Portland cement. Their reaction typically produces an aluminium-substituted calcium silicate hydrate (C-(A)-S-H) but with variable stoichiometry, as shown in Equation 2.4. In the case of limestone, reactions between aluminates and calcite can proceed according to Equation 2.5 yielding the formation of carboaluminates. Generally, Portland cement present higher reactivity relative to SCMs as illustrated in Figure 2.1, where a comparatively lowered degree of reaction of common SCMs to alite (dominant reactive phase in Portland cement clinker) can be seen. The reactivity of SCMs and their replacement levels strongly influence the phase assemblage (type and amount of reaction products forming) and the C-(A)-S-H phase composition. Figure 2.2(b) shows that, as SCM dissolution increases, a resultant C-(A)-S-H phase develops, characterised by a decreasing Ca/Si ratio and an increasing Al/Si ratio, depending on the SCM type. Compared to Portland cement, hydration of slags produces C-(A)-S-H with reduced Ca/Si and higher Al/Si, relatively lower AFm (monosulfate and monocarbonate) and AFt.

Reaction of clinker phases:

$2C_3S + 11H \rightarrow C_3S_2H_8 + 3CH$ **……..** Tricalcium silicate hydration to form C-S-H
Eq. 2.1

$2C_2S + 9H \rightarrow C_3S_2H_8 + CH$ **……** Hydration of dicalcium silicates to form C-S-H
Eq. 2.2

$C_3A + 3C\bar{S}H_2 + 26H \rightarrow C_6A\bar{S}_3H_{32}$ **…..** Hydration of tricalcium aluminate to form ettringite
Eq. 2.3

Reaction of SCMs:

SCM (Al) + SCM (Si) + CH → C-A-*S*-H **……** Pozzolanic reaction
Eq. 2.4

SCM (Al) + $xCaCO_3$ + 3CH → $C_3A.\ xCaCO_3.\ H_{11\text{-}12}$ **….** Carboluminate formation in limestone binder systems **Eq. 2.5**

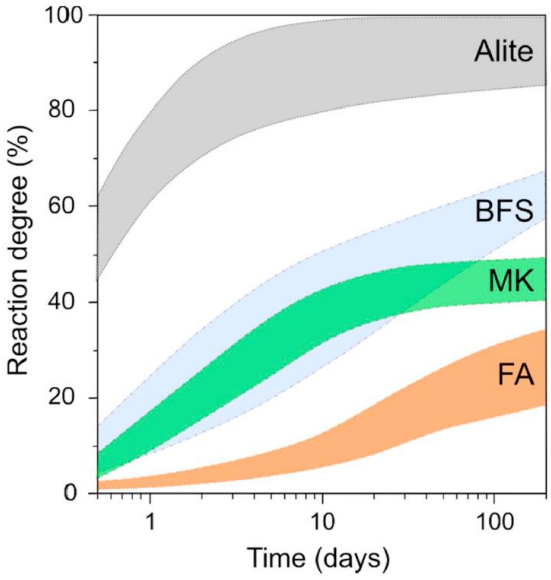

Figure 2.1 : Comparison of degree of reaction envelopes of alites and SCMs such as Fly ashes (siliceous): FA, blast furnace slag (BFS) and metakoalin (MK). Reproduced from (33)

The partial replacement of Portland cement with SCMs influences its hydration process, by acceleration of hydration of Portland cement via a ‘filler effect’ serving as additional nucleation sites due to typically high surface area, and availability of space favourable for C-S-H growth via dilution effect (34). Other studies, however, attribute the 'filler effect' to the shearing action of filler materials (35).

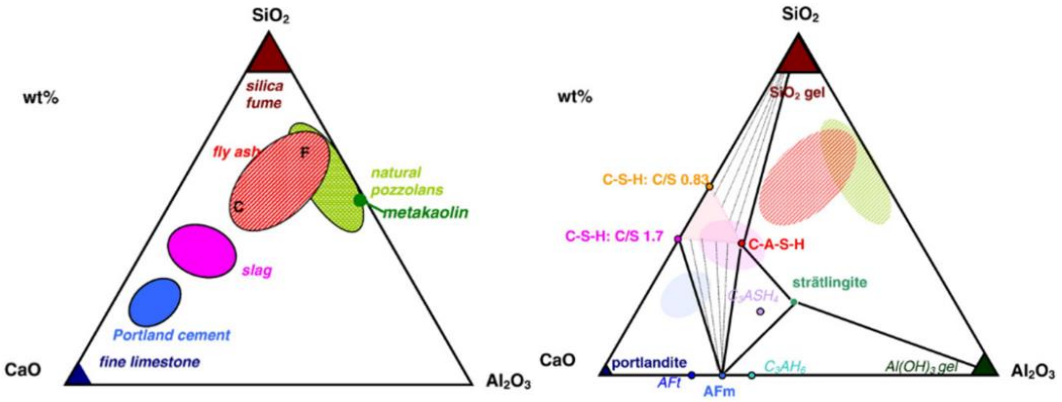

(a) (b)

Figure 2.2: (a) Ternary diagram of cementitious materials (b) Phase assemblages in CaO–Al_2O_3–SiO_2 ternary system. Reproduced from (31)

The additional hydrates forming due to SCMs reaction contribute to the space-filling, strength development and may influence durability of concrete, which is apparent at later curing ages. Generally, SCMs, such as slags refine concrete microstructure due to their reduced particle size and ongoing pozzolanic reaction. The use of GGBS also leads to reductions in porosity of the matrix and interfacial transition zone (ITZ) compared to CEM I concretes (36-38). This can be seen in Figure 2.3 where a decrease in critical pore entry radius and wider pore size distributions of slag-containing pastes in comparison to CEM I between 28 - 60 days of hydration (39). These changes in capillary porosity are closely linked to the transport properties of concrete and ultimately influence the durability performance of concrete for a given environmental exposure condition.

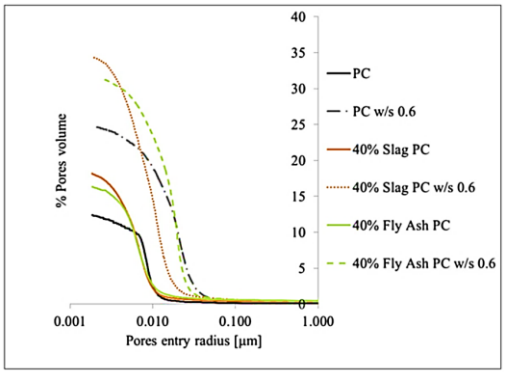

Figure 2.3: Critical pore entry curves (MIP) at different w/b for paste samples made from PC, PC-slag (40%) at 28days, and PC-fly ash (40%) at 60 days. Reproduced from (39)

Furthermore, SCMs alter the pore solution chemistry of the binder in concrete, including the alkali composition (which contributes to charge neutrality), ionic strength and pH. Anderson et al. (42) reported that Na^+ and K^+ ions dominated OPC and slags pore solution. Figure 2.4 shows the time-dependent changes in the concentration of pore solution ions in slag-containing composite cements. It can be seen in Portland cement-slag-limestone systems that, concentrations of Ca^{2+} and SO_4^{2-} dominated pore solution at early ages with decreased Al in the presence of ettringite and gypsum (40). However, the concentrations of Al in pore solution however is dependent on pH (41).

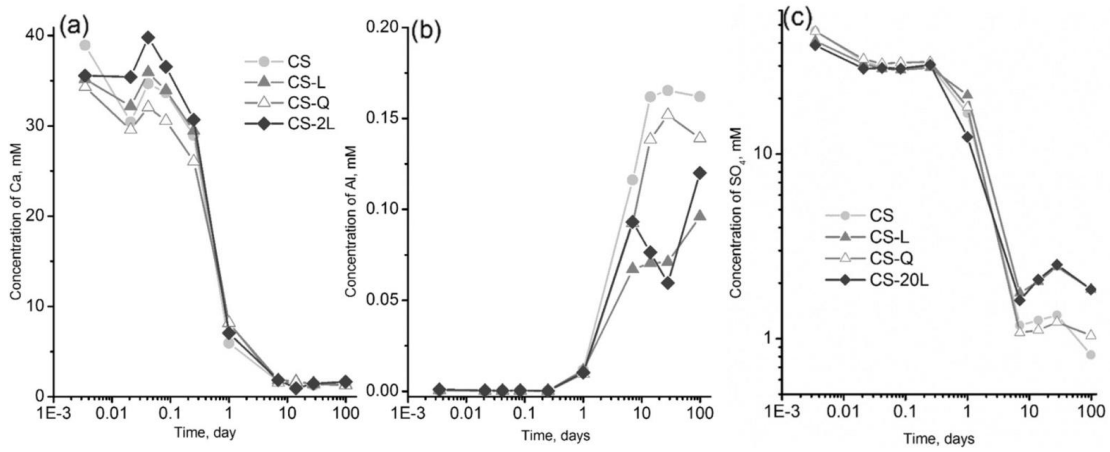

Figure 2.4: Evolution of total ion concentrations in the pore solution of composite slag cements (a) calcium and (b) aluminium (c) sulphate. [C = CEM 52.5R, S = slag, Q = Quartz, L = limestone (~10%), 2L/20L = limestone (~20%)] Adapted from (40)

These changes would largely influence the interactions of concrete with external ions as demonstrated in studies where carbonation exposure induced a further drop in alkalis (Na^+ and K^+) ion concentrations, in SCM-blended cements relative to CEM I (42, 43). The hydration of SCMs with focus on slags with or without limestone and their impact on hydration and microstructure is discussed in the next section.

2.3. Hydration of blended cement with blast furnace slags – impact on clinker hydration and microstructure-related properties

Slags latent hydraulicity or reactivity arise from nearly 2/3 of amorphous phase in quenched and granulated molten slag. The glassy phases are typically compounds of $CaO\text{-}SiO_2\text{-}Al_2O_3$ and MgO, with trace crystal compositions of mellilite (3). They possess relatively lower specific

gravity compared to Portland cement (44). As SCMs, they are substituted from a minimum of 10% - 95% levels by intergrinding with Portland clinker or direct application in concrete production. A detailed understanding of the reactivity of slags exists in the literature, and it is well known that increased slag loadings have a diminishing impact on not only reactivity but also strength properties, as reported for slag loadings exceeding 80% (45-48).

The hydration of clinker and slags proceeds almost simultaneously. Thus, their reactivities influence each other, and experimental methods (49) and thermodynamic models (31) have been used to explore the phase assemblage evolution of binary slags with some agreement in their findings. Figure 2.5 shows phase assemblages formed when about 75% slag has reacted in blended binary slag cements as determined by thermodynamic modelling.

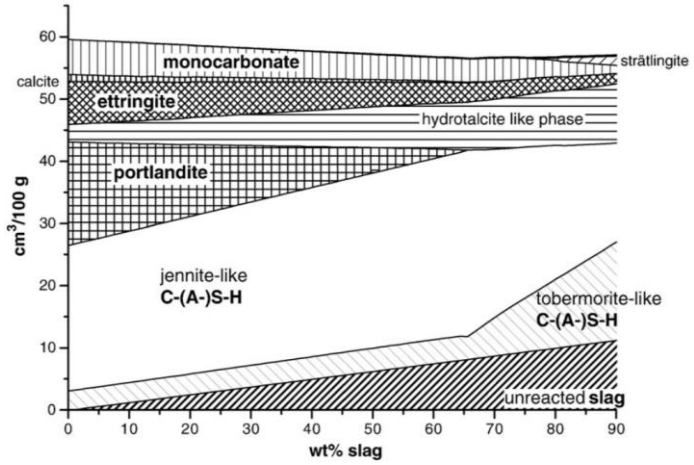

Figure 2.5: Thermodynamic modelling of phase assemblage evolution of blended hydrated Portland-slag cement. A Complete Portland cement reaction and 75% slag reaction was assumed. Adapted from (31)

In addition to main C-(A)-S-H phases, hydrotalcite-like phases can also form, in high MgO content of slags. Stratlingite may be formed depending on the slags alumina content/or the C-S-H uptake of Al. Portlandite reduces progressively with hydration time as reported for blended slag paste studied after 20 years, as well as Mg/Al ratio in hydrotalcite-like phases (49). The reactivity of slag influences the fresh properties and the strength development of mortars and concretes made from them. This is further discussed below.

2.4. Characteristics of fresh and hardened state of blended blast furnace slag concretes

The workability of concrete refers to the compactability, mobility and stability of fresh concrete. It can be assessed by flow characteristics such as slump and spread of fresh concretes, which influence the setting times. The workability of slag-blended cements is notably greater in relation to CEM I systems for similar water-to-binder ratios. Slags have been shown to exhibit prolonged setting times in relation to Portland cement for the same water-to-cement ratio, which increases at higher slag replacement levels (50, 51) as shown in Table 2.2. However, it is worth noting that the specific surface area (SSA) would largely influence these characteristics so that Portland cement with lower SSA/high fineness could exhibit extended setting times than slag-containing mixes (even at lower substitution levels) (52). The improved workability is attributable to smooth slip planes provided by surface characteristics of slags. While this presents benefits for placements and transportation of ready mixed concrete, extended final set times can influence the finishing operations of as-cast structural concrete.

Table 2.2: Comparison of setting times of concretes made from neat cements and slags (at different replacement levels). Adapted from (51)

Cement type	Slag loading (mass %)	Setting time* (final set – initial set) (h:min)
CEM I 32.5	0	20 minutes
CEM III/A 42.5	45	35 minutes
CEM III/A 32.5	62	45 minutes
CEM III/B 32.5	73	50 minutes

* Reported setting time is difference between final set and initial set time

Hardened concrete made from blended slag cements exhibits reduced early age strength in comparison to Portland cement, at a similar water-to-binder ratio and curing conditions, which is attributable to their slower rate of hydration. This is influenced by the slag characteristics and level of substitution. Generally, slag contents of < 60% have resulted in improved strength development for a comparable strength to OPC (50, 53). For structural concrete, considering slags react slowly in relation to Portland cement, the associated reduced heat of hydration of slag cements presents a technical advantage when used for massive concrete operations. This can help mitigate early-age thermal cracking, depending on the pouring height, when

used in mass concrete pouring operations (54, 55). The slow early age strength development can nonetheless be accelerated by thermal curing, but this has implications for long-term strength and the tendency for delayed ettringite formation or coarse porosity (51). However, with prolonged water curing, the strength evolution approaches or equals that of OPC at advanced ages depending on the concrete mix design (56).

In addition to improving compressive strength, hardened slag-blended concrete have shown satisfactory flexural strength (53, 57) and elastic modulus (53) compared to Portland cement concretes after 28 days curing. Considering the great interest in adopting ternary slags cements with limestone addition, it has become necessary to understand the synergistic impact of limestone addition on clinker and slag hydration, and how the microstructure of such ternary blends evolve. This is discussed in the next section.

2.5. Influence of limestone on fresh properties of composite clinker – slag cements

Limestone addition has been reported to influence the fresh properties of concretes in both binary and ternary mixtures, although there are limited reports on ternary slag multicomponent systems. As shown in Table 2.3, limestone addition to Portland clinker can be used to produce workable fresh concrete; however, increasing the limestone content above 20% necessitated the addition of a superplasticizer (58). While some studies reported a decreasing impact of limestone on flow properties, others observed an increasing trend (59).

Table 2.3: Impact of powdered limestone addition to clinker on fresh properties of concrete

Mix ID	Limestone loading (mass %)	Slump (mm)	Flow (mm)
LC1	0	130	460
LC2	10	120	440
LC3	15	120	420
LC4	20	110	420
LC5*	35	110	400

* Plasticizer (Pozzolith 390 N) added

Similarly, in multicomponent slag systems with limestone addition, while some studies demonstrated satisfactory flow properties without superplasticizer addition at 20% limestone loading (60), other studies with comparable formulations reported the need for superplasticizer dosing to achieve workable concrete compared to CEM I (61). Several factors account for the discrepancies in the impact of limestone on fresh properties when it directly replaces clinker or is used in multicomponent systems. The morphology of limestone, which relates to its specific surface area, is expected to influence the extent of filler effects on hydration kinetics. Meanwhile, the purity of the limestone used can also affect the fresh properties of concrete mixes.

2.6. Influence of limestone on composite clinker – impact on blended blast furnace slag hydration and microstructure

The contribution of limestone to hydration has received considerable attention in the literature (40, 62, 63). It acts as a filler and provides nucleation sites, which improve hydration. By acting as a filler, it has the so called ‘dilution effect’ which refers to an increase in water and space available for hydrates from reactive component of the binder to grow (34, 64). The reaction with tricalcium aluminate yields mono-carboaluminates formation, which stabilises ettringite (41) and further contributes to increasing the solid volume due to the low density of ettringite. In ternary slag systems, in addition to enhancing clinker hydration (63), limestone addition has been demonstrated to favour slag dissolution, thus facilitating accelerated hydration, limiting retarding effect of slag hydration by high alumina concentrations (40). Figure 2.6 shows the interaction between slag and 10-20% limestone addition on slag hydration evaluated via isothermal calorimetry. It can be seen that slag hydration increased at higher limestone content. The hydration products in ternary slag-limestone systems as predicted by GEMS thermodynamic modelling are C-(A)-S-H (reported as C-S(A)-H; C-S-H phase with alumina incorporation in the GEMS model), CH, carboaluminates and hydrogarnets, as shown in Figure 2.7. The combined effect of limestone interaction in composite cements pore filling and additional hydrates formation is consequential to refined pore structure, which has a bearing on strength development and durability properties.

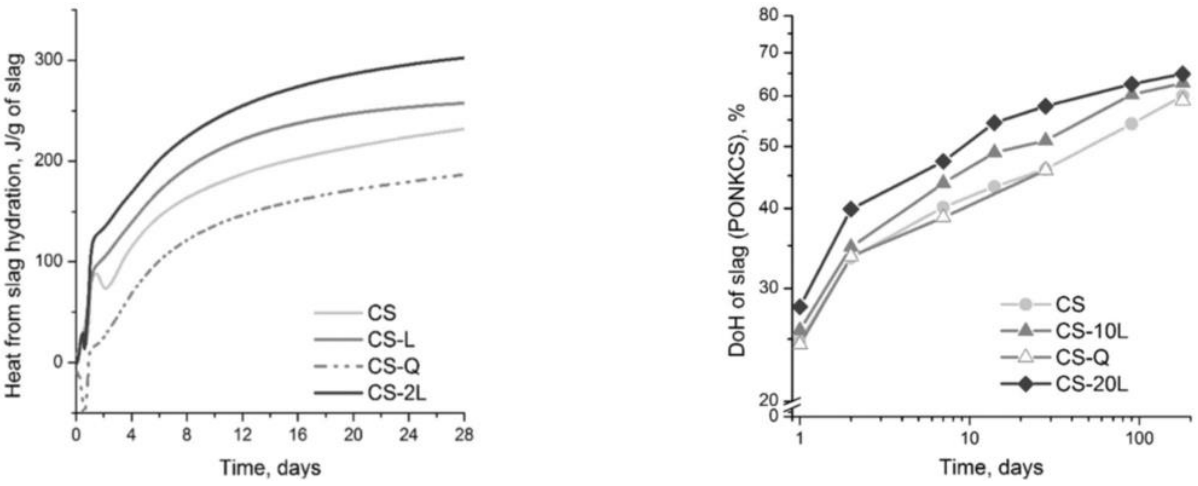

(a) (b)

Figure 2.6: Effect of limestone on slag hydration as determined by (a) isothermal calorimetry and (b) QXRD/PONKCS. [C = CEM 52.5R, S = slag, Q = Quartz, L = limestone (~10%), 2L or 20L = limestone (~20%)] Adapted from (40)

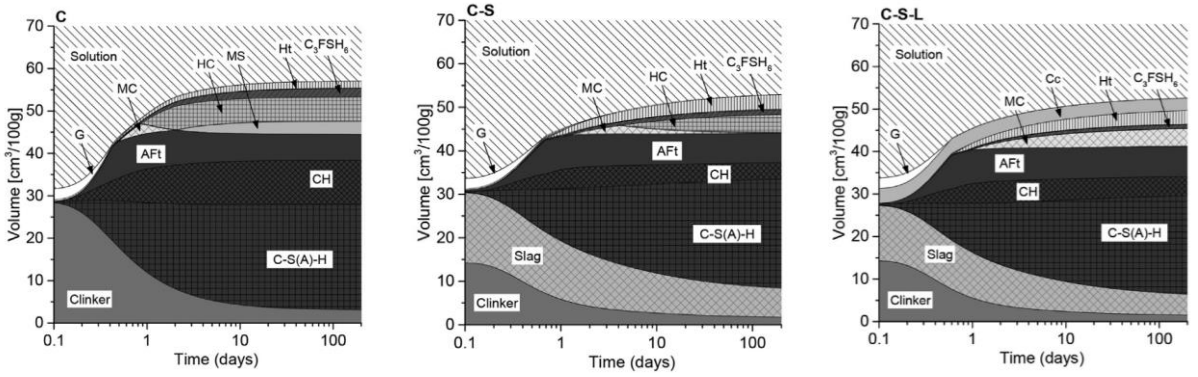

(a) (b) (c)

Figure 2.7: Predicted time-dependent phase assemblage volume fractions of hydrating binders modelled by GEMS (a) 100 wt.% CEM I(52.5R) (b) CEM I(52.5R) + 47.08 wt. % Slag (c) CEM I(52.5R) + wt. % 38.03 Slag + 8.55 wt.%. [C-S(A)-H: C-S-H phase with alumina incorporation, C_3FSH_6: iron containing hydrogarnets, CH: portlandite, AFt: ettringite, Ht: hydrotalcite, G: gypsum, Cc: calcite, MC: Monocarbonate, HC: hemicarbonate]. Model assumptions: congruent dissolution of all anhydrous phases, free dissolution of calcite and gypsum, C-SH corrected for Al uptake, gel porosity unaccounted for in C-S-H volume. Adapted from (65)

The synergistic benefits identified between slag and limestone in ternary blended Portland-slag-limestone systems have recently attracted research attention (17, 40, 66). However, there is great uncertainty about the longer-term performance of concretes produced with such composite cements. This limits their widespread use as structural concrete and adoption into standards, globally. The current state of knowledge on durability and overall performance when considered under the combined action of mechanical load, of slag concrete systems with or without limestone, in comparison with CEM I, is reviewed in the following section.

2.7. Durability of concrete structures

The design for durability of concrete ensures its long-term performance. This approach accounts for the ability of a structural concrete element to withstand deteriorative conditions which can affect the expected performance over its intended design service life (67, 68). The deteriorative environmental factors may be chemical, physical, or a combination of different mechanisms (69). The interaction between the permeation properties of concrete cover and the prevailing exposure environment of the concrete structure primarily governs the durability performance of concrete.

Over the past three decades, performance based durability frameworks have been considered and implemented to shift from prescriptive design approaches towards considerations of long-term performance of concrete, independently of the type of binder the concrete is made of (70-72). Such performance-based specifications provide conformity criteria of verifying factors that influence durability, conversely to prescriptive/deemed to satisfy specifications. Prescriptive specifications have been based on satisfying mix design limit values such as binder content, water/binder ratios, while acceptance criteria has been largely based on compressive strength (73).

However, using compressive strength as the sole parameter for indirectly estimating the durability potential of binary or ternary blended cements containing slags is not adequate. For example, Nganga et al (74) showed no correlation between compressive strength and oxygen permeability index for various binary mixes containing slags, even though they were designed to achieve high compressive strengths, and would be expected to exhibit satisfactory durability performance as per prescriptive standards. Similarly, varied conclusions exist on the relationship between compressive strength and carbonation performance (18, 19). Also, studies have reported poor correlation between the compressive strength evolution and chloride permeability test in concretes made from slags (75). The relative differences in strength evolution of SCMs with Portland cement makes the sole use of compressive strength

an unsuitable parameter for durability performance prediction. A rationale or pragmatic approach thus can be developed by understanding key influencing parameters on hardened concrete under field conditions, and then experimentally implementing at the laboratory scale using reproducible test methods.

In hardened concrete, the impairment of transport properties and subsequent acceleration of fluid ingress would not only promote deterioration mechanisms within the hydrated matrix, but could also lead to deformation issues (expansion and/or shrinkage) arising from the rehydration of previously anhydrous binders. This becomes a complex phenomenon in SCM concrete systems where long-term natural carbonation of phase assemblages will further have implications on pH, alkalinity reserves and carbonation shrinkage. For example, in Portland-limestone multicomponent systems, carbonation-induced shrinkage could include carbonation of hemi-carboaluminates to mono-carbonates, and or portlandite to calcite ($CaCO_3$). This represents density changes from 1.99 to 2.18 g/cm^3 and 2.25 to 2.71 g/cm^3 respectively (76). Meanwhile, the release of bound water due to carbonation may also contribute to further volume changes. These complex phenomena may undermine the benefits of autogenous self-healing in minimising carbonation in cracked slag-blended concrete relative to CEM I, as recently reported (77).

Concrete under realistic in-service conditions is typically subjected to loading, and this is expected to influence the rate of deterioration of concrete. The stress type and stress states can influence the pore structure of concrete and, hence the transport properties (8, 10, 78). Load-induced pore structure response may arise from the collapse or dislocation of C-S-H due to pore humidity changes arising from consolidation and sliding effect attributable to rearrangement of water molecules which result in the generation of micro strains (79, 80). Meanwhile load-induced microcracking tendencies (81) can potentially facilitate the faster transport of aggressive species, which may be linked to microcrack induced pore connectivity. In SCM concrete systems, there is an additional propensity of carbonation-induced coarsening of pores unlike in CEM I (82). The relationship between these phenomena and the impact on durability performance of multicomponent concrete systems is critical due to the heterogeneity of phase assemblages and their potential impact on porosity and pore connectivity.

Towards addressing the research challenges of the current study, literature on chlorides and carbonation resistance are discussed, as these stresses are considered the major problems affecting long-term performance of infrastructure. The main permeation properties governing these durability mechanisms are also addressed. Furthermore, the effect of loading on the carbonation and chloride ingress are discussed while comparing CEM I, CEM I-slag and CEM

I-slag-limestone concrete systems. In addition, their deformation characteristics with or without the influence of load are discussed.

2.7.1. Open porosity and transport mechanisms in concrete

Generally, the porosity of concrete influences its transport and mechanical properties. Porosity affects the permeation of fluids into the concrete cover. Thus, it is considered one of the principal factors controlling the durability of concrete structures, and this is dependent on pore connectivity. The effect of SCMs on pore structure (porosity, pore size distribution and interconnectivity) related to other properties has been discussed in Section 2.2. In hardened concretes, volume not occupied by anhydrous cement grains or hydrated phase assemblages corresponds to porosity. The connectivity of these pores is known as tortuosity and can be influenced by factors including the water-to-binder ratio (83). For the same binder system, a high water-to-binder ratio could indicate increased porosity and less connected pores due to ill-formed microstructure. The transport of aggressive species within the matrix from the external environment occurs via capillary pores, and gel pores. Various standards provide testing methodologies and empirical equations to quantify the transport properties of concrete. Water or chloride penetrability is typically used as a measure of the transport characteristics of concrete and will be discussed in the following sections. This is followed by a review of the literature on the impact of loading on transport mechanisms in different concrete systems.

2.7.1.1. Permeability of concrete

The permeability of concrete is an important property for assessing the long-term durability in severe environments. Intrinsic properties such as degree of saturation and microstructure related properties; and external parameters such as hydraulic or pressure gradient and temperature influence concrete permeability (84). Lower water/binder ratios reduce permeability of concrete due to reduced porosity, thus improving performance related to permeability of moisture or external ions.

Permeability in porous media such as concrete generally follows Darcy's law (Equation 2.6), but its validity is limited for cases such as load-induced cracked concrete. Alternative approaches using Dupuit-Forcheimer's law have been adopted by some authors to account for alterations in the permeability of fluids due to inertia and turbulence effect in load-induced cracked concrete (85). In addition, the Klinkerberg correction has been employed to account

for gas percolation characterised by viscous flow as well as slip flows in high performance concretes and said to represent an intrinsic coefficient of permeability associated with the viscous flow. Meanwhile, idealised recommendations such the RILEM report by Reinhardt et al. (86), have suggested that, despite the heterogeneous nature of concrete microstructure, the concrete matrix, as well as a uniformly cracked matrix, may be considered as homogenous on a large scale. Considering that crack formation and propagation can be triggered by many factors other than load, such idealised assumptions may not accurately represent the overall contribution of cracks to permeability.

$$Q = \frac{kA}{\mu} * \frac{\Delta P}{L} \qquad \textbf{Eq. 2.6}$$

Where L = specimen length (m), ΔP = P1- P2 is hydrostatic pressure drop (Pa) Q = gas volumetric flow rate at pressure (m^3/s), μ = dynamic viscosity at the tested temperature (Ns/m^2), and A= cross-sectional area.

Furthermore, it must be acknowledged that, while terminology such as 'chloride permeability' is prevalent in cement and concrete literature, the mechanism should not be considered in the context of permeability as described above, but rather based on the discussions in Section 2.7.1.3.

2.7.1.2. Water absorption by capillary suction

Capillary suction or sorptivity is a measure of the admissibility and transmissibility of water through concrete via capillary forces. So that, the rate of advancement of the wetting front for a given dry or slightly saturated concrete is measured by the bulk absorption or the sorptivity. Water absorption is governed by concrete pore structural variations including open porosity and tortuosity. Thus, it serves as a relevant coefficient for durability assessment (87, 88), attributable to up to 10 μm pore size ranges of capillary pores (water accessible), unlike smaller gel pores which are in ranges of 0.5 – 4 nm (83). The sorptivity coefficient is typically used as a measure of water absorption properties, derived from the gradient of the time-dependent ratio of the mass of water absorbed per surface area to the square root of time. (89).

2.7.1.3. Diffusion and migration of external ions

Diffusion is the transport of ions due to a concentration gradient. The diffusion of external ions in concrete is governed by Fick's law for steady-state diffusion, as well as the Nernst-Planck equation (90). The coefficient of diffusion gives a measure of transport characteristics, particularly chlorides, which are used to determine the rate of penetration. This is relevant for assessing the probability of chloride-induced corrosion of steel-reinforced concrete structures based on the extent of ingress into the cover depth. Factors including pore structure (capillary porosity and pore connectivity), aggregate volume fractions, and interfacial transition zone characteristics influence the diffusion of ions in concrete. The degree of hydration, curing duration (91), and consequently, internal relative humidity also play a role. Several quantification approaches have been used for the estimation of diffusion coefficient. For example, the apparent chloride diffusivity and effective diffusivity give a measure without or with chloride binding correction respectively (92). Where the movement of ions occurs under an electric field, the mechanism is based on ion migration and has been used as a standardised method for accelerated testing of the permeability of concretes to chloride. This is reported as non-steady state migration coefficients (93). Concepts such as chloride sorption capacity have also been used to quantify variations in chloride concentrations during the ingress of ions (94). Towards addressing how loading affects these transport characteristics of concrete, the alterations of some transport properties under stress state are discussed.

2.7.2. Impact of loading on transport properties

The effect of loading on transport properties has been studied for binary and ternary concretes systems (8-11, 78), but the studies on novel ternary slag systems with limestone additions are yet to be conducted. The impact of loading on permeability and water absorption of concretes are discussed. Chloride ingress as a transport property is captured in Section 2.7.5 in conjunction with impact of load on chloride resistance.

Generally, there appears to be an increase in penetrability for concretes loaded at higher stress levels, and less detrimental impacts on the transport properties at limited stress levels; however, this can be influenced by the loading history of the tested concrete. While different critical thresholds have been reported in the literature, there is agreement that beyond a critical threshold, the tendency for coalescence of load-induced cracks (micro), increases fluid transport. Sugiyama et al. (11) investigated the variations in gas permeability (tested on hollow cylinders) of CEM I and observed that below 55% stress levels, there was no noticeable impact on gas permeability and independent on concrete mix design. However, above 76 to 79%,

permeability increased for normal weight CEM I concrete at w/c = 0.4/0.6, cured for 120 days as shown in Figure 2.8. However, studies on CEM I concretes at early ages (1-3 days) have also exhibited 40% critical thresholds (95), and 30% thresholds (96) for 28 days cured concretes above which water absorption increased.

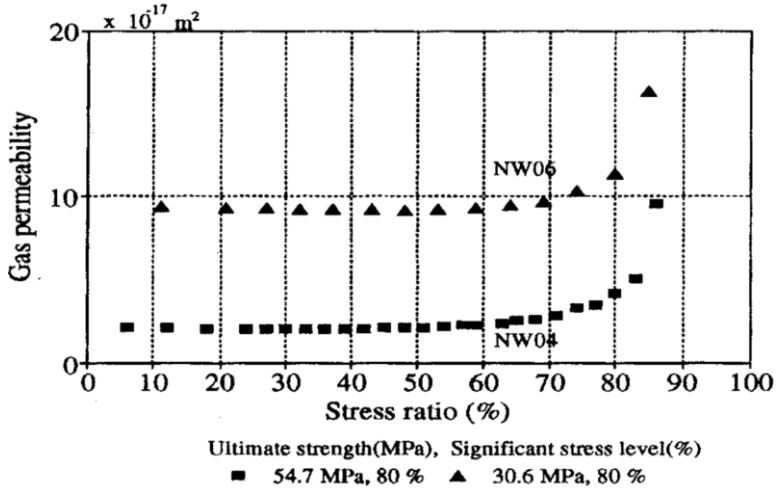

Figure 2.8: Impact of compressive stress levels on gas permeability of normal weight Portland cement (CSA A-5 Type 10) concretes at different water-to-cement ratios (NW04 = 0.4; NW06 = 0.6) moist cured for 4 months. [Preconditioning: 1 month air drying under laboratory (T= 21 ± 1 ^{o}C; %RH = 50 - 60) conditions + 7days drying at 60 ^{o}C] Reproduced from (11)

Meanwhile, slag mortars loaded to 90% of their peak load were identified to exhibit an overall increased initial sorptivity coefficient (based on the slope) relative to undamaged samples as can be seen in Figure 2.9. It is interesting to note that these materials also exhibited improved water absorption properties, attributable to self-healing, despite the samples being pre-damaged to failure. The practical relevance of such self-healing benefits can be interrogated when samples are damaged (loaded) under accelerated carbonation conditions before water transport testing.

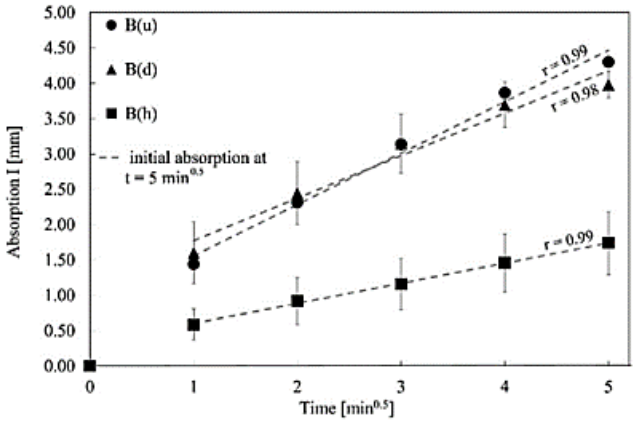

Figure 2.9 Initial water absorption of 28 days moist cured 50% slag-blended cement mortar cubes under different test conditions: (u) = undamaged(moist cured sample), (d) = damaged: mechanically damaged to 90% peak load at 0.01 mm/s load cell displacement ratio and (h)= healed (60 days immersion in deionised water). Preconditioning: 5 days oven drying at 60 ^{o}C]. Adapted from (77)

It is worth noting that, the aforementioned studies on permeability were simultaneously conducted on loaded mortars/concretes. However, some studies have used pre-loaded concrete for 'post mortem' permeability testing after unloading, but the reported findings are in disagreement among different studies. For example, Hearn et al. (9) reported that load-induced cracked or uncracked CEM I concretes (cured for at least 90 days) did not show significant increases in water permeability even for concretes prestressed at 80% load level, compared to 30% stress levels. This was attributed to partial closure of disjointed microcracks after unloading. It is interesting to note that the study reported similar observation for both cured and prolonged oven dried concretes at 105 ^{o}C, where transport characteristic would rather be expected to be largely influenced by drying shrinkage in the latter case. However, Djerbi et al. (97) identified for CEM I concretes cured for 100 days prior to loading that, permeability increased when subjected to a 60% stress level, corresponding to high residual strain. In both cases, the residual strain increased after unloading, and while Hearn (9) attributed this as sufficient to cause partial closure of microcracks, Djerbi et al (97) inferred potential increase in open porosity (not measured) and microcracking at high stress levels.

Overall, both loading approaches suffer from the rather short testing regimes in the order of few minutes to few hours. Prolonged loading duration can deepen the understanding of long-term performance. While simultaneous stress and permeability testing on the other hand provides some insights on the effect of load on permeability, they present some experimental design challenges. These tests commonly used stressed hollow cylinders, and in the case of

gas permeability testing, the gas was introduced through the hollow section and exits at the external surface (11). While this can be rationalised from a safety point of view, it is not indicative of typical fluid ingress under field conditions. When non-hollow cylinders have been used, the test methods were constrained by fluid exposure in the direction of applied load (98), which may not be representative of the typical construction practice of cored sample acquisition for further testing under laboratory conditions. In construction practice, the derivation of cored samples from structural concrete in compression is typically in the orthogonal direction to the axial loads. It does appear that the acquisition of cored samples for further testing would align more with testing conducted on pre-loaded concretes, where the load is sustained for a longer duration.

It also becomes apparent that studies based on slag cements are sparse, and none is reported for concretes made with next-generation low carbon multicomponent concretes. Meanwhile, interpretations of controlling parameters based on pore structure (related properties) evolution, which can give a deeper understanding of the impact of load on transport properties, are less emphasised, particularly at the concrete scale.

In the next section, carbonation and chloride resistance are discussed as individual durability problems, and the impact of load on concrete performance under such exposure conditions are further discussed.

2.7.3. Carbonation performance of concrete and role of SCMs

Carbonation and other potentially associated deterioration mechanism (e.g. steel reinforcement corrosion in concrete) have received considerable attention in the literature for CEM I and SCM mortar and concrete systems (82, 99, 100). It is a physico-chemical process arising from diffusion-controlled entry of atmospheric CO_2 through concrete pore system. The reaction of CO_2 dissolved in pore water forming carbonic acid leads to reduction of the pore solution pH. Its reaction with hydration products induces changes in the micro-environment at the steel-concrete-interface, and potentially make reinforcement steel bars susceptible to corrosion with gradual loss in alkalinity/pH. It must however be noted that increased susceptibility to corrosion due to reduced pH in the blended slags does not suggest initiation of steel reinforcement corrosion (99). Typical phase assemblage evolution and variations in pH for Portland cement relative to slag blends are shown in Figure 2.10. Moisture saturation (internal and external) and material (intrinsic and physical) properties impact the carbonation performance. Ambient CO_2 concentrations, temperature, relative humidity (RH) influencing the degree of concrete saturation, nature and duration of the carbonation exposure influence the

extent of CO_2 penetration (19, 101, 102). The CO_2 concentration controls the extent of carbonation and phase assemblage evolution (19, 100), and in addition to pH determines the crystal type formed. Studies have identified that, at 2-3 % CO_2 concentration, comparable calcium carbonate polymorphs (aragonite, calcite or vaterite) precipitate for both natural and accelerated carbonation, with calcite being more likely under accelerated carbonation, while metastable aragonite or vaterite are prevalent at lower CO_2 concentrations (100, 103).

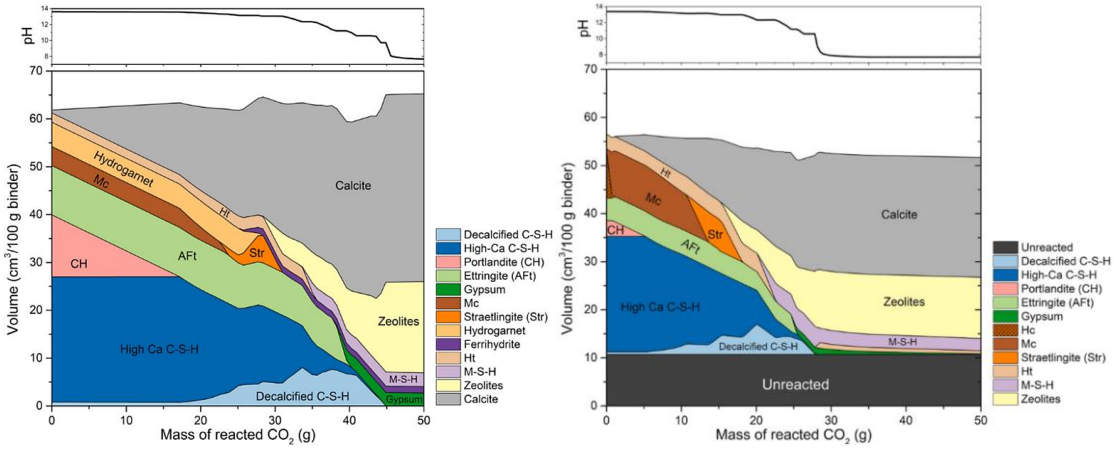

(a) (b)

Figure 2.10: Carbonation (2% accelerated) induced evolution of phase assemblages and pH profiles by thermodynamic modelling (a) Portland cement (b) 50% GGBS. Reproduced from (103)

The correlation between carbonation performance and the cementitious materials properties have been a subject of extensive discussion in the literature (19, 104, 105). These include strength properties and intrinsic matrix properties (such as buffer capacity and pore structure). While there is disagreement on the relationship between compressive strength and carbonation resistance, some studies have shown agreement on the correlation between some intrinsic properties. Leeman and Moro (19), and Sulapha et al. (20) reported a reasonable correlation between compressive strength and carbonation coefficient for binary slags concretes, however, Shah and Bishnoi (18) reported no correlation. Nonetheless, the authors confirmed the influence of the CO_2 buffer capacity (i.e., related total alkali content and reserve alkalinity) on carbonation resistance. It is evident that, estimation of carbonation performance of concrete solely considering their compressive strength is an over-simplification, particularly in systems with different cements chemistries such as those including SCMs. This calls for developing a better understanding of the fundamentals leading

to this mechanism of degradation, particularly when using SCMs, and to re-evaluate the criteria for performance prediction, including their carbonation service life.

In OPC concrete systems, the relatively higher reactive CaO improves their carbonation resistance due to greater buffer capacity (19), formation of denser carbonation products that act as ‘plugs’ and consequently inducing a pore structure refinement. On the other hand, in binary cement systems including slags, increased carbonation coefficients compared to OPC have been reported, which further decreases with increasing clinker replacement (20). This is also true for ternary Portland (PC)-slag-limestone systems (17, 60); however, a marginal rate of carbonation has also been reported for Portland cement-slag-limestone comparable to slags, as shown in Figure 2.11. In limestone ternary blends, carbonation of hemi-carbonates to more stable monocarbonates which may occur simultaneously with the carbonation of CH, has been reported and appears to bind less to alkalis than C-A-S-H phases (106, 107).

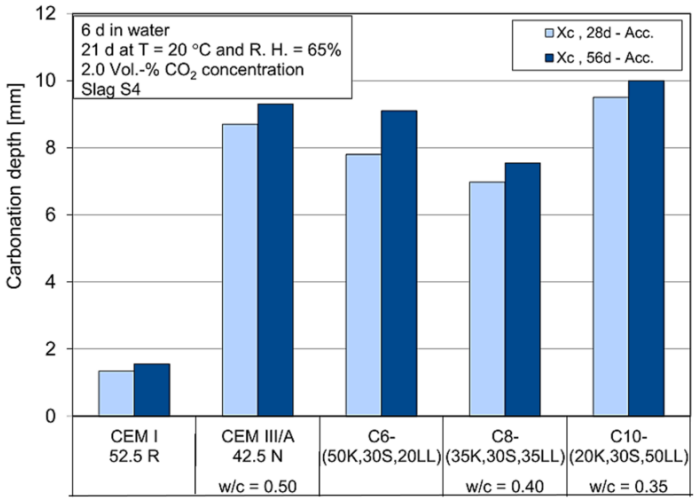

Figure 2.11: Carbonation depths of CEM I, PC-slag and PC-slag-limestone (C6, C8, C10) of concretes after 28 days and 56 days of exposure to 2 vol% CO_2 concentration. Reproduced from (17)

This is attributed to reduced availability of portlandite in systems with high volume cement replacements. However, an increase in fineness of GGBS (from 6,000 and 8,000 cm^2/g) reduces carbonation coefficients in concrete compared to OPC (20). In blended systems, limited portlandite availability due to the reduced clinker content and pozzolanic reaction, means reduced availability of carbonatable material; thus, carbonation progresses towards direct C-A-S-H decalcification with reducing Ca/Si compared to C-S-H, resulting in coarsened

pore structure, while in OPC a densified microstructure occurs via carbonation of portlandite (106, 108, 109).

On the relationship between porosity and carbonation coefficient, Shah and Bishnoi (18) and Sulapha et al. (20) reported there is no dependency on binary GGBS systems and other ternary SCM systems. A gap in such studies is the lack of clarity on the implication of pore structural changes on transport properties arising from carbonation-induced shrinkage and/or microcracking in SCM concrete systems (108). This is critical for concrete elements to assess their long-term carbonation performance with or without load, which is particularly limited for ternary concrete systems based on slag composite cements (17). Table 2.4 shows carbonation depths available in the literature for concretes made from ternary blends with high limestone addition in comparison with binary slags and CEM I. Overall, such ternary blends exhibit inferior carbonation depths relative to OPC, and the reduction of slag in lieu of limestone in the ternary blends shows comparable carbonation depths to binary slags.

Table 2.4: Summary of carbonation depths of ternary Portland-slag-limestone mortars and concretes from selected journals

Reference	Materials and method	Comments
Proske et al. (2016) (17)	- Portland cement CEM I 52.5 R (CEM I) - CEM III/A 42.5 N (with 50 wt.-% slag) - OPC + 30% Slag + (20 -50)LL - 7 d water curing; 140 days storage natural CO_2 at T=20 ± 2 C and R.H. 65 ± 3% - w/c ratios =0.35 – 0.5 - 2% CO_2 accelerated carbonation	- Ternary blends compare with binary cements and both inferior to CEM I. - carbonation depths @ 0.5 w/b ratio - 28d: CEM I = 1.7 mm, CEM III/A = 8.5, CEM I(50%) + Slag (30%) + Limestone(20%) = 7.9 mm - 56 days: CEM I = 1.8 mm, CEM III/A = 8.8, CEM I (50%) + Slag (30%) + Limestone (20%) = 8.7mm
Adu-Amankwah et al. (2017) (60)	- CEM I 42·5R - CEM I 52·5R + 47.1 Slag + 0.02 anhydrite - CEM I 52·5R + 38.02 Slag + 0.02 anhydrite + Limestone - w/c = 0.5 - Carbonation(21d natural carbonation; 20°C and 65% RH)	- Composite binders exhibit lower carbonation resistance - Depths not quantified
Lauch et al. (2016) (110)	- CEM I 52.5 R (CEM I) - CEM I(45/50) + Slag(30/20)-Limestone (25/30)) - CEM III/A 42.5 N - w/c ratios of 0.45 and 0.55 - 1% [CO_2]: T=20 ± 2^{o}C: RH= 60± 10%: 91days exposure	- Increasing limestone addition reduces carbonation resistance in slag ternary blends - CEM I(45) + Slag(30) + Limestone(25) = 12.1mm - CEM I(50) + Slag(20) + Limestone(30) = 12 mm

It must be acknowledged that, while concrete made from binary slag and ternary slag-limestone cements exhibit higher carbonation rates, the carbonation-induced pH loss only becomes a matter of relevance under multiple exposure conditions such as in the presence of chlorides. This can accelerate steel reinforcement corrosion at small concentrations as shown by Femenias *et al.*(111), where for $[Cl^-]/[OH^-] \geq 1$, corrosion is initiated due pH induced release of bound chlorides. This reinforces the urgent need to understand the underlying degradation mechanisms of SCM concrete systems under multiple environmental exposure conditions with or without loads, which reflects realistic service conditions. The impact of carbonation on transport properties, and how loading influences carbonation performance of mortars and concretes is discussed in subsequent sections.

2.7.3.1. Effect of carbonation on transport properties

Even though in slag-blended systems a refined pore structure has been identified relative to CEM I (39), the improved refinement may be compromised when subjected to carbonation. This is due to volume changes arising from phase transformation and shrinkage due to decalcification (112, 113). For the increased carbonation rates in slag systems relative to CEM I, this may be detrimental to their transport properties.

Hren et al. (114) investigated the impact of exposure to 3% CO_2 accelerated carbonation of 28 days cured mortars containing GGBS (CEM III/B (S) 32.5 N – LH/SR) relative to CEM I, on the ingress of chlorides (52 weeks; 3.5% NaCl ponding). Based on chloride profiling, it was identified that accelerated carbonation resulted in 30% increase in free chloride, but 21% reduction under natural carbonation in GGBS relative to OPC. Similarly, using experimental and analytical methods, 90 days moist cured concretes made with CEM I, and ternary slag-fly-ash concretes were subjected to 90 days natural and accelerated (20% CO_2) carbonation followed by chloride immersion (15 g/L NaCl) for 35 days (94). At the near surface carbonation front, the free chloride concentration increased under accelerated exposure relative to natural, but lower in the SCM containing concretes in all cases. Towards the boundary between carbonation front and non-carbonated area, it decreases slightly, and then progressively decreases further away from the carbonation front. It was established that the net change in apparent chloride diffusivity under accelerated and natural carbonation was lower in blended systems relative to OPC. It appears to be independent of depth increases influenced by high water binder ratios.

The impact of carbonation on transport properties has received attention in literature mostly for CEM I and binary systems or ternary systems where Portland cement is replaced with slag

in addition to other SCMs. However, such studies on CEM VI(S-LL) mortar or concrete systems are non-existent in the literature. The comparable carbonation depth reported for binary slags and Portland-slag-limestone (see Table 2.4) may indicate similar transport characteristics in both binder types, but this requires experimental validation as would be considered in this PhD.

It is further identified in the existing literature that, the evaluation of the effect of chloride exposure on carbonated materials typically follow methodologies where mortar or concrete samples are immersed in saline solutions for prolonged periods. However, for such prolonged period, there is a tendency for continued hydration of anhydrous clinker phases present in the unreacted cements which can induces pore structural changes. Thus, accelerated methods of chloride exposure can potentially mitigate such biases, as employed in this study. The impact of load on carbonation resistance are further discussed.

2.7.4. Effect of loading on carbonation resistance

Structural concrete is designed as load-bearing under field conditions. It is subjected to sustained or cyclic loading conditions (e.g. tension, compression or shear) which may be a source of deformation and cracking of carbonated concrete. As previously discussed, carbonation modifies the pore structure of concrete systems differently for SCMs systems relative to CEM I, as can be related from Auroy et al.'s. (108), where carbonation shrinkage was reported to induce microcracking in hardened PC-slag-pozzolan paste systems. Thus, the influence of loading on carbonation rate is critical.

The effect of tensile and compressive loading on carbonation performance has received attention in the literature for CEM I, blended slags, and ternary cements made from slag in addition to other SCMs (12, 115-117). The general understanding, as recently evidenced in the RILEM TC 281-CCC interlaboratory study on the impact of compressive load on carbonation rates on slags and other SCMs (117), is that, below moderate stress levels, carbonation depths are lower compared to non-loaded concretes, however carbonation depth increased at higher stress levels from 60%. This phenomenon is shown in Figure 2.12 and Figure 2.13, where it is identified that the impact of load on carbonation depth at the different stress levels are independent on the CO_2 concentration.

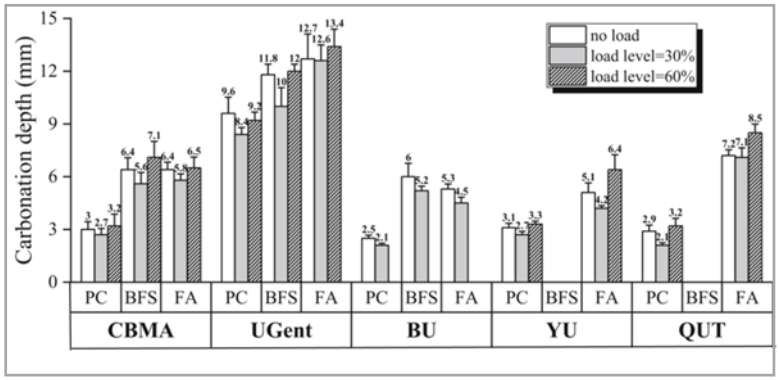

Figure 2.12: Carbonation depth under compression at 3% CO_2 exposure at different load levels. PC = Portland cement; BFS = Blast furnace slag; FA = Fly ash. Adapted from (117)

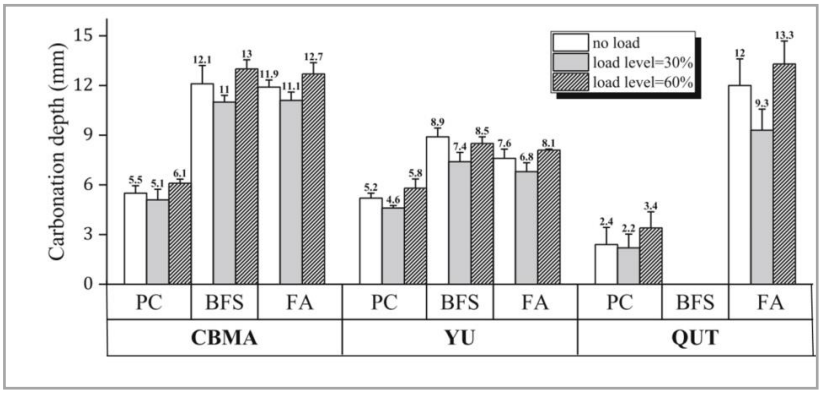

Figure 2.13: Carbonation depth under compression at 20% CO_2 exposure at different load levels. PC = Portland cement; BFS = Blast furnace slag; FA = Fly ash. Adapted from (117)

Similar observations were reported for composite fly ash-slag systems, where it was found that, a near inverse relationship exist between carbonation rate and sustained compressive loading up to about 50% stress thresholds, and evolves into a near linear relationship as stress levels increase. Conversely, a near linear relationship exist under tensile loads almost immediately below 50% stress levels. These observations have been attributed to reduced self-healing capabilities or partial closing of finer cracks for compressive stress above 50%. For tensile loadings, the rate of microcrack propagation exceeds crack closure almost immediately (115, 116).

It is evident that limited studies have focused on the direct impact of coupled action of loading and carbonation on pore structure related variations. The practical relevance of the applied stress must also be acknowledged as structural concretes are typically designed to bear load within its elastic region, other than the high stresses of most studies, even though gives insight into structures prone to persistent or transient loads (118). The load-induced variations in pore

structure is relevant in hardened concrete since it influences the ingress of other deleterious species under realistic exposure condition that is influenced under loading conditions. However, fewer attempts have been made in that regard, such as Francois and Maso (12), whose study gives insight on the influence of load-induced cracking, in the typically porous interfacial transition zone (ITZ), on carbonation rates at 50% exposure. The combined impact on transport properties are less considered (78). It thus become pertinent for studies on SCM concrete systems to understand the interplay between carbonation-induced C-A-S-H coarsening, partial crack closing and the influence on the ingress of additional aggressive species.

2.7.5. Chloride resistance of concrete and role of SCMs

Chloride ingress via microcracks or pore structure of concrete arises from mainly the exposure to seawater or de-icing salts. Other sources arise from the use of accelerators. Their main impact on durability is associated with potential depassivation of steel reinforcement when free chloride concentration in concrete exceeds critical threshold and has been widely addressed in the literature (119-121). Chlorides interact with cement paste via complex phenomena known as 'chloride binding' where chlorides attach to cement phase assemblages via chemical reactions and physical adsorption on C-S-H surface. The chemical interactions with phases such C_3A or C_4AF yield chloro-complex products such as Friedel's salt or Kuzel's salts (only forming in presence of high sulphates) (119). Meanwhile, hydrotalcite-like phases typically formed in GGBS containing paste are also reported to bound chlorides (122). The relationship between the bound chlorides and free chlorides are typically shown by chloride binding isotherms. Factors such as pH reduction (for example due to carbonation) may result in freeing or redistribution of bound chlorides, while temperature also affects chloride binding (121). Generally, binary and ternary SCM concrete systems exhibit higher resistance to chlorides than CEM I due to improved chloride binding capacity (121, 123). Portland-slags blends have shown reduced apparent diffusion coefficients relative to plain cements at different replacement as shown in Figure 2.14. For the same water-to-binder ratio, Marriaga and Claisse (123) demonstrated that up to 50% slag content replacement reduced the diffusion coefficient, however, increasing water-to-binder ratio increased the coefficient values. This is consistent with the findings of Otieno et al. (124) using slags from diverse sources and chemical compositions, where it was also identified that low Al_2O_3 in slags have a negative impact on chloride resistance of concrete.

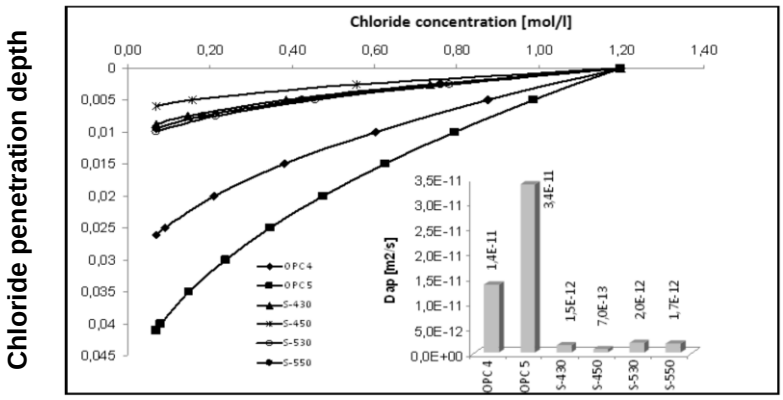

Figure 2.14: Apparent chloride diffusion coefficients [m^2/s] of CEM I and slag-blended cements. Reproduced from (123)

Proske et al. (17), evaluated Portland cement-slag-limestone materials and reported that these materials exhibited better chloride resistance related to CEM I. Nonetheless, studies on ternary Portland cement-slag-limestone systems are scanty, and further independent research is needed to compare and validate these results.

The report of higher resistivity and reduced chloride diffusivity for slag-blended cements relative to CEM I sheds light on the benefits of pore refinement on chloride resistance, however such benefits could be undermined by the progression of carbonation. This warrants further investigation under realistic conditions, where the additional contribution of carbonation to decalcification and, consequently pore coarsening can establish a strong correlation between pore structure-related variations and chloride resistance. The effect of loading on chloride resistance of different concrete systems are discussed below, with focus on variations in moisture and chloride penetration through the concrete cover.

2.7.5.1. Effect of loading on chloride resistance of concretes

Under loading conditions, stress-induced variation in the pore structure can influence the rate of chloride ingress. Experimental and simulation techniques have been employed to study the impact of load on chloride ingress in different concrete systems with some conflicting results (96, 125). Generally, chloride ingress is influenced by the load type and load level, and beyond a critical threshold, chloride penetration increases. It has been identified that the addition of SCMs such as GGBS and fly ashes, for the same water-to-binder ratio, outperformed CEM I, hence the focus of this section will be on the effect of loading on the chloride resistance of SCMs-containing concretes

Lim et al. (125), using the rapid chloride permeability test (RCPT) to determine chloride resistance, observed an increase in charge passed when CEM I specimens (water to cement (w/c) ratio 0.46) were uniaxially loaded under compression at stress levels between 0.80 and 0.95. However, Samaha and Hover (8) reported a critical stress level of 0.75 above which charged pass increases (for CEM I specimens at w/c=0.46). Meanwhile, Bao and Wan (96) identified a detrimental impact of compressive load on chloride/and or water penetration from 30% stress levels for CEM I (w/c = 0.45) systems. Also, Francois and Maso (12), used a 3-point flexure loading by coupling two beams (B on top of A), with 'A' loaded at 80% to rupture, to assess chloride diffusion in compressive and tensile zones. As can be seen from Figure 2.15, chloride penetration in tensile zones is mostly greater at tensile zones than compressive zones after prolonged exposure of CEM I concrete (w/c= 0.5) to chlorides.

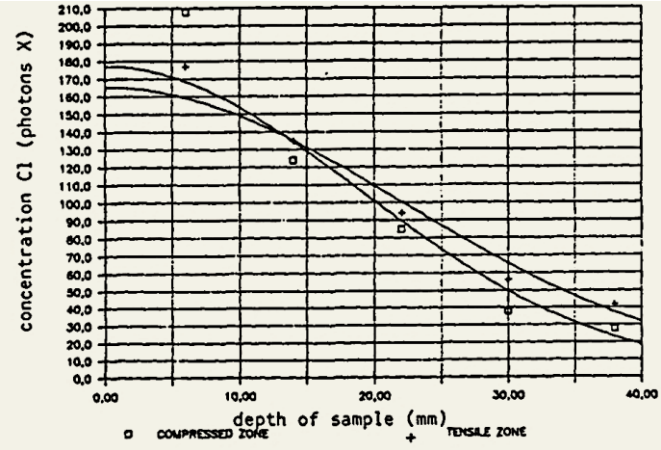

Figure 2.15: Comparison chloride diffusion in compressive and tensile zones after 43 weeks exposure of CEM I concrete (w/c= 0.5) salt fog exposure. Reproduced from (12)

Yoo and Kwon (126), reported a significant increase in diffusion coefficients at 60% compressive and tensile stress levels for both PC-slags (40%) and OPC, but higher in the case of tensile loadings. However, changes in PC-slags were marginal compared to OPC.

In summary, tensile loading affects chloride ingress more than compressive loads at the same stress levels. Meanwhile, slag concrete systems exhibit improved chloride resistance to OPC under load. However, disagreement exist on the performance for CEM I concretes. At similar w/c and adopting the RCPT test, Lim et al. (125) and Samaha and Hover (8), identified that when applying critical stress level the charged passed were not comparable.

From a practical standpoint, the studies discussed above primarily focus on load levels ranging from just above the elastic region of concrete to near failure loads, with limited consideration given to very low compressive stresses. However, considering findings that microcracking tendencies can initiate at stress levels as low as 15% (81), caution must be exercised in generalising the 30% stress level as the critical threshold above which resistance to ion and moisture ingress begins to decrease.

2.8. Time-dependent deformation

The integrity of hardened structural concrete cover can also be impaired by strain-induced damage with or without load. Strains in hardened concrete also arise from drying shrinkage, and creep when under load. Concrete as a composite material exhibit elastic behaviours as shown in Figure 2.16(a); aggregates and cement paste show near linear relationship but not in the composite form as shown in Figure 2.16(b). Aggregates, portlandite and unreacted cement have restraining effect on concrete (127). Factors, which are associated with loss of water, result in volumetric changes of concrete that leads to shrinkage. Of relevance in hardened concrete are drying shrinkage and carbonation shrinkage. Shrinkage can also arise from rehydration of anhydrous cement (autogenous or chemical shrinkage) via moisture or water ingress in compromised pore system as highlighted in Section 2.7, and may be problematic for concretes made from slow-hydrating cements. Under loading conditions, concrete creeps with time and may negatively influence durability as well as long-term serviceability. Nonetheless, creep has benefits such as retarding expansion related cracking (91). The mechanism of shrinkage and creep and impact on concrete are discussed.

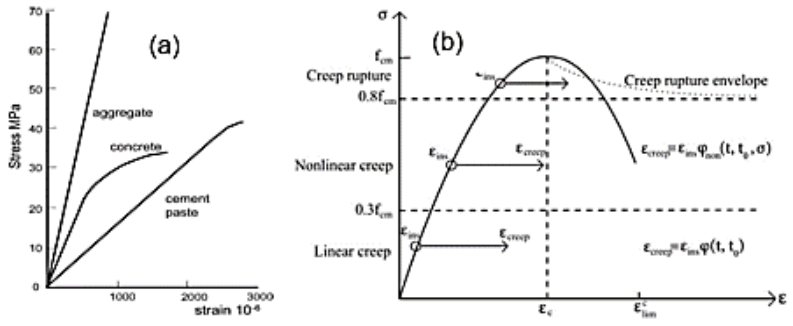

Figure 2.16: (a) Stress-strain relationship for paste, aggregate and concrete (b) Creep behaviour of concrete. Reproduced from (38, 128)

2.8.1. Shrinkage and creep – mechanism

When concrete is exposed to a dry atmosphere, it gradually shrinks due to water loss with associated rise in capillary tension of pore water and surface tension of pore walls (129). As this progress, there is a possibility of collapse of gel pores arising from loss of adsorbed water. This mechanism in normal concrete is drying shrinkage. As shown in Figure 2.17(a), this imposes a strain on concrete, which evolves over time (t_o-t). Under stress conditions, as depicted in Figure 2.17(c), an instantaneous strain (elastic strain) is imposed at time t_1 when the load is immediately applied. Sustaining the load further results in creep strain evolution, which is also time-dependent, but occurs at decreasing rate for a constant stress. The imposed microstrains within the pore structure can induce microcracking with or without load.

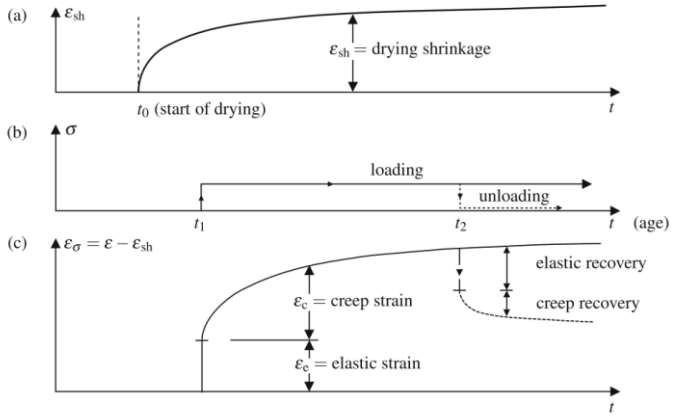

Figure 2.17: Curves for (a) shrinkage, (b) loading history (c) creep, and recovery after unloading. Reproduced from (129)

The underpinning mechanisms and limiting factors for shrinkage and creep have received considerable attention in literature via empirical and simulation approaches (130, 131). Factors such as ambient humidity, binder composition, aggregate content and type, and dimensions of concrete element influence both mechanisms. Creep is further governed by maturity of concrete upon first load application, the time and magnitude of applied load. Various integrated postulations such as consolidation, re-arrangement of hydrated assemblages, adsorbed water withdrawal (disjoining pressure), activation energy theory, solidification theory and microprestress-solidification theory, microcracking and delayed elasticity have been reported as mechanisms governing creep (80, 132-135). While opposing views exist regarding the mechanisms of induced strains in cementitious materials, there is consensus that strain can be linked to the microstructural response of C-S-H to stress.

Micromechanical techniques, such as nano-indentation, have demonstrated that C-S-H or C-(A)-S-H with high Ca/Si ratios exhibit relatively higher deformation tendencies (136, 137). This behaviour is attributed to the lower presence of defects and a greater degree of isotropy in C-S-H compared to C-(A)-S-H. The varied opinions on influencing mechanisms may for example be linked to difficulty in distinguishing intrinsic (real) and apparent shrinkage of C-S-H structure (127). The influence of moisture and humidity has also been addressed by the well-known Pickett effect discussed elsewhere (79, 138).

Meanwhile, an additional cause of shrinkage can be found in carbonation, arising from movement of bound water due to calcite precipitation with or without loading. The induced strain has been reported to be marginal in CEM I systems (102), as can be seen from Figure 2.18(a-b) where only 0.35% shrinkage is observed in carbonated concretes relative to non-carbonated, and less detrimental relative strain also recorded for axially loaded concrete carbonated at 15% CO_2, 65% relative humidity. This may be attributable to high CO_2 binding capacity and densification of microstructure, which limits CO_2 diffusion rates even for high concentrations. However, with the notable reduced carbonation resistance of SCMs, relatively higher magnitudes of strains could be induced in SCM concrete systems than OPC.

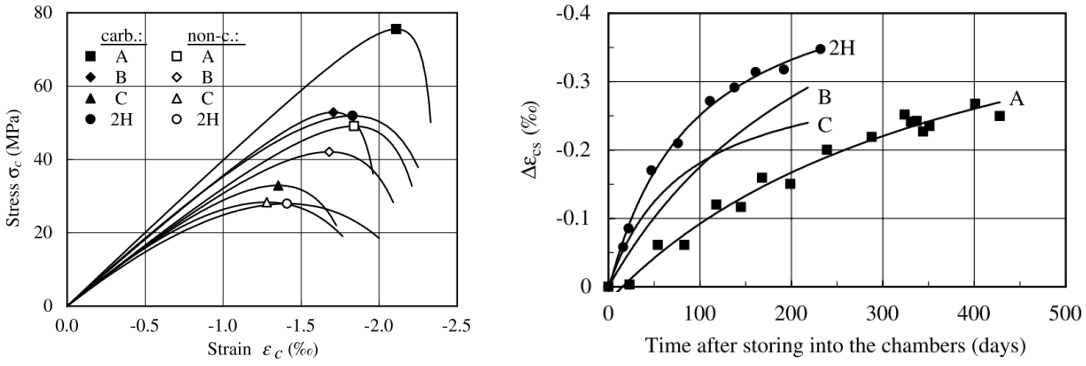

(a) (b)

Figure 2.18: (a) Stress–strain relationship of the carbonated and the non-carbonated CEM I concrete prisms (2H=improperly cured specimen) (b) carbonation-induced shrinkage evolution. Reproduced from (102)

The shrinkage or load-induced strains, which may or may not be reversible (see Figure 2.17(c)), and the associated microcracking which (81), when connected, can promote ingress of aggressive species. The load-induced dimensional stability and associated microcracking of CEM I and some SCM concrete systems are further discussed.

2.8.2. Load-induced dimensional stability of OPC and SCM concrete systems

The impact of replacing CEM I by blast furnace slag on the deformation of concrete under sustained compressive load has been reported in the literature, but with conflicting findings. Shariq et al. (16) identified an increase in the creep deformation of slag-containing concrete subjected to sustained compressive loads (~32% ultimate load) relative to CEM I-based concrete. This being more noticeable at higher slag replacement levels up to 60%. Similar findings have been reported by Chern et al (139) indicating that the creep deformation increased in slag-containing concrete when loaded at 1/4 of their compressive strength. Conversely, reduced creep deformations were reported for concretes with a higher slag content (140). However, concretes with high slag content (65%) have also exhibited comparable specific creep to CEM I based concrete, while reducing the slag content (35%) in the mix decreased the specific creep (141). Meanwhile, Proske (17) reported comparable creep performance for Portland cement-slags (50 wt. % slag) to CEM I-based concretes loaded at 1/3 of their compressive strength. As can be seen from Figure 2.19, there is a significant reduction in shrinkage of binary slags and ternary slags compared to OPC. Similarly, their creep performance was comparable to OPC systems. It can be inferred that, for an equivalent strength of binary slags and ternary PC-slag-limestone, and for w/b = 0.35 – 0.5, a reduction in shrinkage and creep performance relative to CEM I can be achieved.

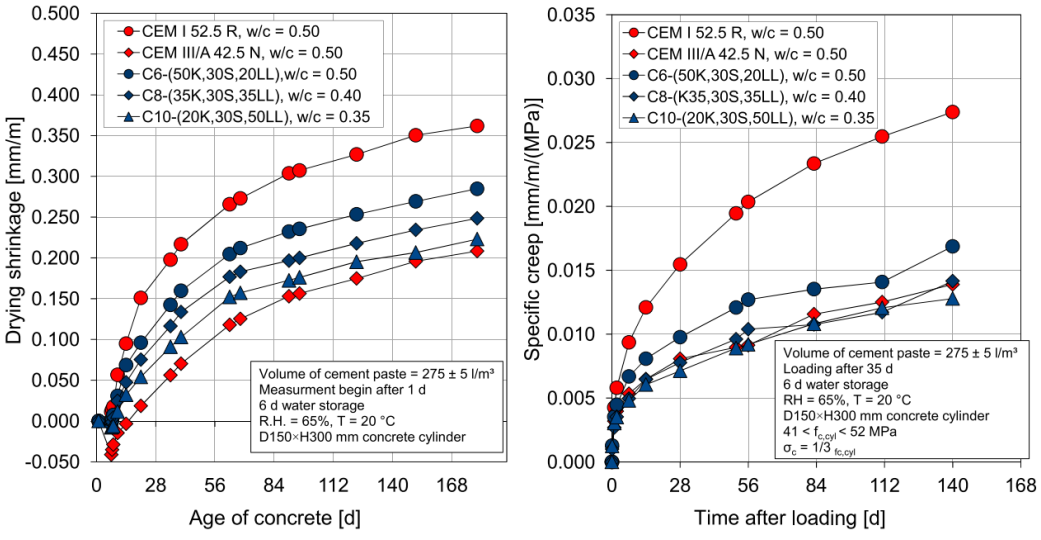

(a) (b)

Figure 2.19: Comparison of (a) shrinkage and (b) creep performance of OPC, binary slag and ternary limestone slag (C6, C8, C10). Reproduced from (17)

However, during service life, concrete will not only be subjected to loading, but it will also interact with the environment where it is being placed. Therefore, concrete is subjected to both chemical and physical stresses that will determine their long-term longevity and performance. Considering the varying deformational characteristics of blended slag cement concretes reported in the literature, it is necessary to systematically investigate how these materials will perform when subjected to close to reality exposure conditions. It is largely unknown what the effect of loading, tested under ambient conditions, might be in novel composite concrete formulations with large contents of limestone. Deformations in mechanically stressed hardened concrete made from such cements could be detrimental to deflection sensitive structures, such as long span bridges, with the passage of time. More concerning, there is very limited knowledge about the potential effect of combining loading and accelerated carbonation in the performance of such materials, which is the knowledge gap addressed in this study.

2.8.3. Shrinkage and load-induced microcracking

Figure 2.20 shows how crack development occurs when restraining tensile stresses exceed contraction. It can also be seen that the cracking of concrete can be retarded if the stress induced by free shrinkage strain, when reduced by creep, is largely lower than its tensile strength. However, once microcracks form, their evolution emanates from the conversion of conserved strain energy into surface energy for fresh crack faces (142). Microcracks affect mechanical and transport properties of concrete. The impact on transport properties can arise from modification of pore structure, due to shrinkage or creep induced damage, increasing crack sizes and/or continuity thus resulting in preferential routes for gas diffusivity or ions ingress, hence affects the overall durability of concrete. Studies of the effect of microcracks on transport properties are discussed.

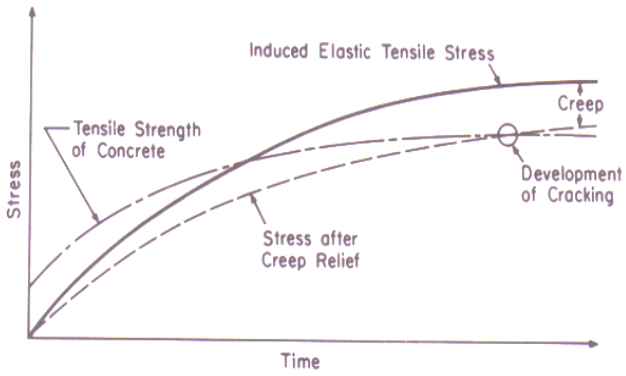

Figure 2.20: Schematic plot showing crack development when stress (tensile) due to restrained shrinkage is relieved by creep. Reproduced from (142)

Generally, the crack geometry and vicinity of the crack are controlling parameters on the ingress of ionic and gaseous species with or without load (10, 143), and are discussed. Alahmad et al. (143), investigated the CO_2 diffusivity in cracked CEM I mortar samples and observed that diffusivity is only relevant for paths perpendicular to the crack path when the crack is ≥ 60µm. However, in the vicinity of reinforcements, crack width between 12-28 µm notably influenced diffusion along the path perpendicular to the crack, and carbonation was recorded along steel embedment. Also, Picandet et al. (10) studied the impact of uniaxial compressive stress levels of 60 - 90% ultimate strength on the permeability of CEM I concrete subjected to drying. Similar to Alahmad et al. (143), diffused cracks in orders of about 3 µm width and 5 mm length were only identified in the vicinity of aggregates, reinforcing the contribution of the vicinity of cracks on transport properties. The effective permeability (difference between load-induced damage and reference) increased with drying. This is attributable to the initial emptying of capillary pores and/or large cracks while pore diameter continues to reduce so that strain induced modifications arise in the pore structure. The damage increases with increased applied-strain/yield-strain ratio. It must be highlighted that the stress levels used in the studies approached failure loads, and intended to induce microcracks, confirmed by reduction in dynamic elastic modulus of the test pieces post-loading. Inducing cracks in such a manner does not give a true representation of microcracking of typical structural concrete under sustained load for prolonged duration.

2.9. Concluding remarks

The general influence of supplementary cementitious materials (SCMs) on the chemistry, microstructure of Portland cement, and the durability performance of cement and concrete

have been reviewed, emphasising the role of slag and limestone additions, as the main materials evaluated in this study. In addition, case studies on realistic exposure of concrete to carbonation and/or chloride were reviewed, considering the testing of materials with and without load. Furthermore, deformations arising from mechanical effects were also discussed.

Overall, intrinsic properties of concretes, environmental and mechanical factors that influence durability performance under realistic conditions were analysed. This laid the basis of the current project in pursuance of 'long-term performance of concrete exposed to severe environments'. The main conclusions identified are:

- There exists a fundamental challenge of limited studies that consider realistic conditions structural concretes are exposed to, typically coupled loading and multiple durability exposure conditions. The missing link is due to the lack of standardised methods to pursue such assessment, and the complexity of the experimental setups required for producing reliable results from such tests.
- The service life prediction of concrete considering conventional durability tests (evaluating the impact of one degradation mechanism at the time without considering loading), might not be representative of what can be expected in concretes subjected to loading, considering the differences in results reported, and the limited number of studies where loading has been accounted for.
- Carbonation and chloride exposure are one of the major and costly problems affecting durability of structural concrete. The mechanisms and the influence of SCMs are fairly individually understood, but conflicting results exist in literature on the influence of stress. The focus of the conducted studies has been on identifying the interplay between stress-induced microcracking and partial crack closure as a basis for explaining the variations in transport properties. While these fracture mechanics and self-healing mechanisms are usually only implied and not always quantified, focus on pore structure related response is limited. This applies, to an extent, to studies on the coupled action of load and carbonation on transport properties.
- The synergistic benefits between GGBS and limestone in Portland-slag-limestone concrete systems are well recognised. These cements have demonstrated improved chloride resistance but with limited studies, and for an equivalent strength they can show comparable carbonation resistance to OPC. Additionally they exhibit superior creep performance relative to CEM I. Cements with slag contents between 30 – 50wt%, limestone additions between 10 - 50 wt.% and water/binder ratios of 0.35 – 0.5 have proven comparable durability to OPC (17).
- Limited long-term studies on dimensional stability related properties have been reported for Portland-slag-limestone concrete systems, while conflicting results exist

for the long-term dimensional stabilities of PC-slags concrete. It is notable that studies on load-induced dimensional stabilities discussed from the literature have focused on the creep performances with conflicting results. The load-induced deformations to be pursued in this PhD would focus on the total strain evolution from which shrinkage (of similar unloaded specimen) when subtracted could indicate creep. Thus, total strain as reported in this PhD work is solely used as basis of assessing the dimensional stabilities of materials used in this study. The study on creep performance is out of the scope of this PhD as the primary focus is how the overall load-induced total deformations influence the carbonation depths of concretes studied.

The review has highlighted that, herein lies the challenges or research gaps which need to be addressed to understand the long-term performance under coupled loading and multiple durability exposures. The conflicting results suggest that an integrated approach is required to understand the underlying degradation mechanisms to explain the performance exhibited by concrete particularly under loading testing conditions. It is suggested that a focus on pore structure (including porosity and pore connectivity) evolution which is closely related to transport properties and time-dependent deformations is necessary to adequately understand long-term performance of concrete consistent with the current project.

In response to the clear research gaps, this study focuses on evaluating the carbonation performance, and the effect of carbonation on ingress of moisture/ionic species (for example, chloride permeability and water admissibility). In this PhD research, a novel low clinker cement system containing high volume slag and limestone replacements was evaluated, mainly because these cementitious systems are gaining research interest for their durability potential, carbon reduction and resource optimisation potential, consistent with their recent addition to UK standards enabling their widespread use.

Chapter 3.

3. Methodology and analytical techniques applied for the analysis of cementitious materials

This section focuses on the materials used in this study and the techniques adopted for their characterisation in powdered, fresh or hardened states when used to produce mortars or concrete. The general working principles of equipment or devices used are also discussed. Figure 3.1 below presents the overall experimental flow chart for this study, where the main and complementary studies are illustrated. The flow chart shows multiscale studies from mortar to concrete scale, while also signifying how the multi-technique experimental methodology evolves toward near realistic field conditions where the impact of combined action of load and carbonation on transport properties is highlighted.

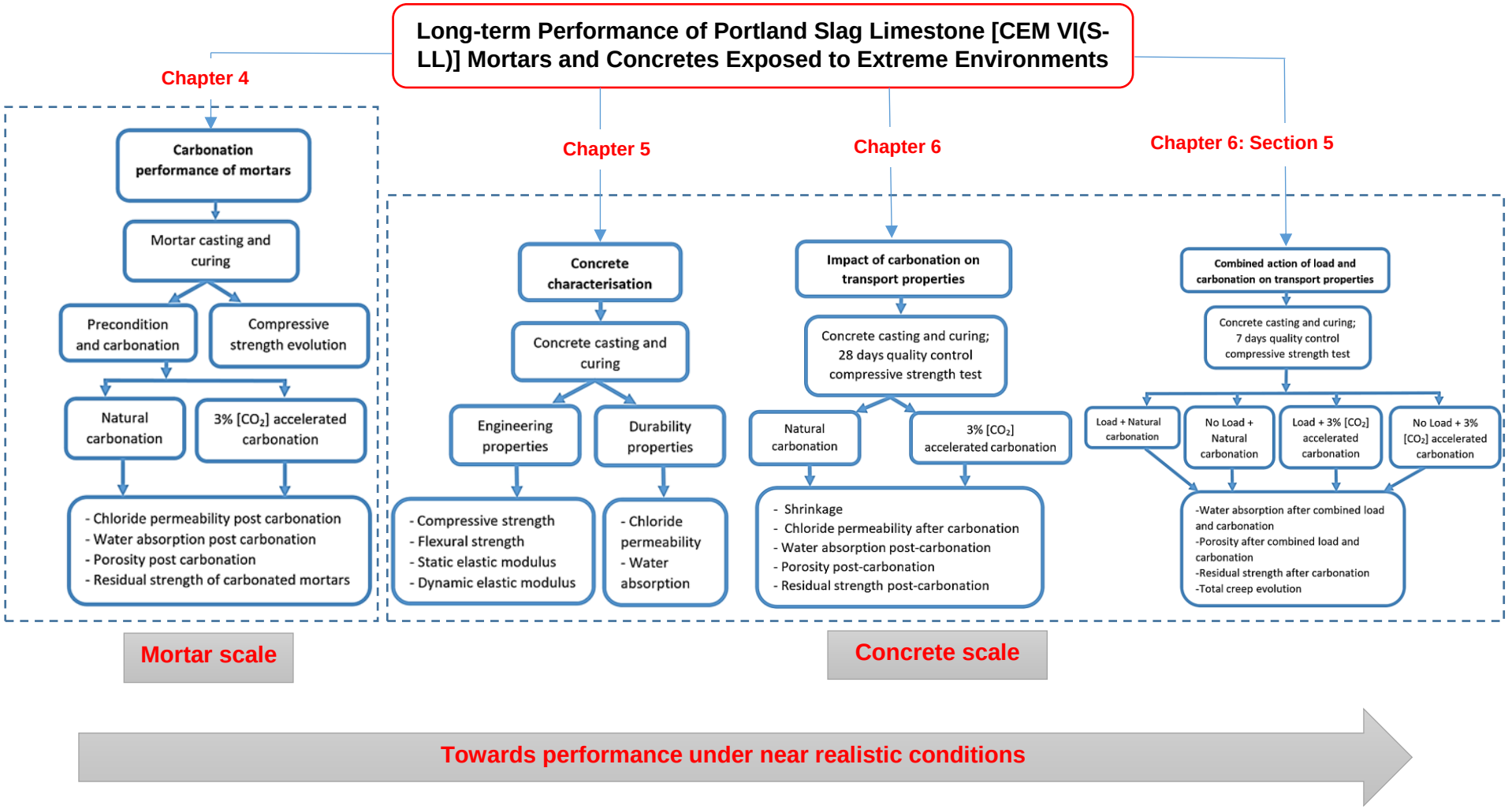

Figure 3.1: Summary flow chart for experimental programmes used in this study

3.1. Materials

In this study a CEM I 52.5N and granulated blast furnace slag (GGBS), were used as main binders. These materials were supplied by Heidelberg Materials UK, Ribblesdale and Port Talbot works, respectively. Limestone powder (conforms to BS 7979 (144)) supplied by LKAB minerals UK was used, as well as natural anhydrite (used for sulphate balancing) supplied by Heidelberg Materials, UK. The aggregates used for concrete production were uncrushed quartzite. The fine aggregate (sand) used for mortar mixing was a CEN-standard sand supplied by *Normensand Germany GMBH*, and conformed to EN 196-1 (145). Table 3.1 shows the oxide compositions of the materials used in this study, determined by X-ray fluorescence (XRF) spectroscopy using a Rigaku ZSX Primus II, with the fused bead preparation method. The quality ($CaO + Al_2O_3 + MgO / TiO_2 + SiO_2$) and basicity ($CaO + MgO /Al_2O3+ SiO_2$) coefficients of slag used are 1.65 and 1.02 respectively.

Table 3.1: Oxide compositions of CEM I, slag, limestone and anhydrite

	Al_2O_3	SiO_2	CaO	SO_3	K_2O	Na_2O	MgO	TiO_2	MnO	Fe_2O_3	Trace	LOI*
OPC	4.51	18.6	62.59	5.72	0.31	0.18	2.39	0.22	0.06	2.08	0.39	2.95
Slag	11.52	35.56	40.25	2.41	0.5	0.3	7.98	0.57	0.2	0.31	0. 41	-
Limestone	0.27	0.94	55.82	0.09	0.03	0.2	0.69	-	-	0.06	0.09	41.8
Anhydrite	0.8	2.37	38.35	52.18	0.19	0.34	1.4	-	-	0.25	0.34	3.8

*Loss on ignition (LOI) determined by wt. (%) change at room temperature and weight after 2 hours heating at 900 ^oC and ambient cooling (146)

3.2. Materials characterisation of powdered samples

3.2.1. Laser granulometry

Laser granulometry is used for measuring particle sizes, and size distribution of fine powders. It operates based on the principle of laser diffraction, following the interaction between incident laser beams and dispersed powders. Measurements from the intensity of scattered light can further be analysed for particle size calculations as a function of their scattering pattern. This method can be pursued as a dry process or wet process where liquid additives may be added in the case of wet process. In this study, the particle size distribution of the powdered cements was determined by the dry method (without liquid dispersant) using an automated Malvern Pananalytical mastersizer 3000 particle size analyser, in combination with software for setting the control parameters of the test. The size range capability of the equipment was from 0.01

µm to 3 mm. Three tests were run per sample and averaged. The particle size distribution of the cement powders is shown in Figure 3.2, the d50 of CEM I, GGBS, limestone were 17.1 µm, 14.1 µm and 11.9 µm respectively.

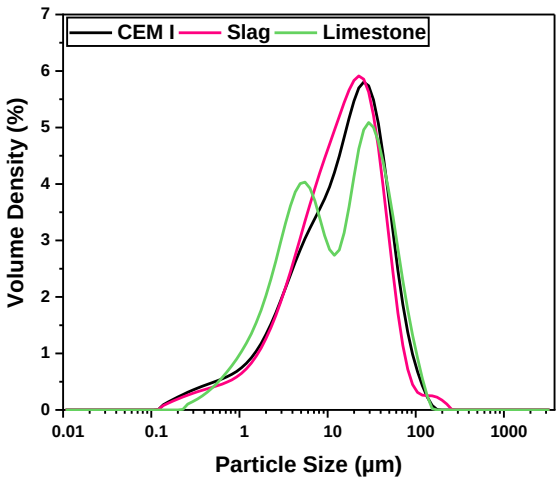

Figure 3.2: (a) Particle size distribution (dry method) of CEM I, slag and limestone

3.2.2. BET surface area analysis

BET surface area gives an indication of fineness of powdered samples. This test method follows the measurement of surface area (m^2/kg) of powdered samples via gas desorption. Samples of known mass kept in round bottom tubes were preconditioned by drying and degreasing via combined heating with nitrogen purging, using a preheated *Flowprep™ 060* sample degas system. Towards minimising any phase transformations in the cementitious powders, the heating temperature was kept at 50 ^oC for about 4 hours. Soon after, samples were cooled to room temperature and their dried mass noted.

Dried sample contained in tubes were transferred to a *micromeritics Tristar surface area and porosity analyser*, controlled by the Tristar computer software. The tubes containing samples were attached to an analysis port under vacuum condition, with about ¾ of the tube length submerged in a vessel containing the adsorptive gas, in this case liquefied nitrogen. The start of the desorption process was automated with a computer software. The setup was then run overnight with inputs, including sample mass and pre-defined degassing conditions. Following the automated sample analysis, results of desorption and pressure isotherms were generated, with associated values of BET surface areas of tested samples. The BET specific surface

(m^2/g) areas of cement materials were determined as 1.29 for CEM I, 1.38 for GGBS, and 1.04 for limestone.

3.2.3. Helium gas pycnometry - density of cements

This is a non-destructive test for ascertaining the volume and densities of dry powders, porous materials or granulates by the action of gas displacement based on pressure-volume relationships from Boyle's law. A Thermo scientific Pycnomatic equipment was used in this study. It operated using helium gas as the displacement medium. Helium gas presents a small atomic number, hence the ease of permeation of the gas in tiny pores in solids, which allows for the estimation of sample volume. Using an inbuilt programme on the equipment, input parameters such as dried mass (in grams) was used to automatically return the density/specific gravity (in grams per cubic centimetres) of tested samples.

The density (g/cm^3) of cement powders were determined for the development of concrete mix design, and the specific gravities obtained from helium pycnometer were 3.13, 2.92 and 2.72 for CEM I, GGBS, and limestone respectively.

3.2.4. X-ray diffractometry

X-ray diffraction, also known as XRD is a well-known non-destructive method for determination of crystalline phases in materials. It is extensively used for qualitative and quantitative phase identification in anhydrous and hydrated cementitious materials. Its application is based on the diffraction of X-ray photons by atoms in a periodic lattice, so that the diffracted monochromatic X-rays, which happen to be in phase, produce constructive interference. Based on Bragg's law Equation 3.1, it is possible to derive lattice spacing arising from scattering of X-rays by crystal planes (147).

$$n\lambda = 2d(\text{Sin}\ \theta) \qquad \textbf{Eq. 3.1}$$

Where d = spacing between the crystal planes, n = an integer corresponding to the order of the diffraction peak; λ = wavelength of X-ray type used; and θ = the angle of diffraction peak.

In this study, a Bruker D8 diffractomer with an X-ray source (Cu Kα1, 0.154 nm) operating at 40 kV, 40 mA was employed for sample assessment. The scan angle (2θ), step size and total

scan time (per sample) were 4 - 70°, 0.0131° and 2040 seconds. XRD characterisation technique was accompanied by the use of proprietary software High Score® equipped with international Centre for Diffraction Data (ICDD), PDF4+ 2022, which allows for phase identification by matching peaks based on diffraction patterns related to known structures indexed in the PDF4+ 2022. In this study, XRD was used for phase analysis of cement materials as shown in Figure 3.3. As expected the Portland cement is composed of the clinker phases C_3S, C_2S, C_4AF corresponding to PDF4+ 2022 powder diffraction files, 00-055-0740,01-083-0460 and 04-014-6640 respectively, similar to what has been reported in (148). Less distinct peaks were observed for expected tricalcium aluminate (C_3A) in XRD, but its presence was confirmed as ~8.4% based on Bogue calculation ($C_3A = 2.6504Al_2O_3 – 1.6920Fe_2O_3$) (149), using XRF oxide compositional data in Table 3.1. Meanwhile, the limestone peaks in the XRD data demonstrate ~98% calcite, thus validating its conformance with BS 7979 (144) which specifies a minimum of 75% calcite content in limestone fillers. It is also worth mentioning that studies have reported high calcite content in ground limestone (~95.2%), which exhibited total organic carbon (TOC) levels of less than 0.2% (150). This informs the categorisation of blended ternary mixes used in this study as CEM VI(S-LL), based on expected minimum TOC levels.

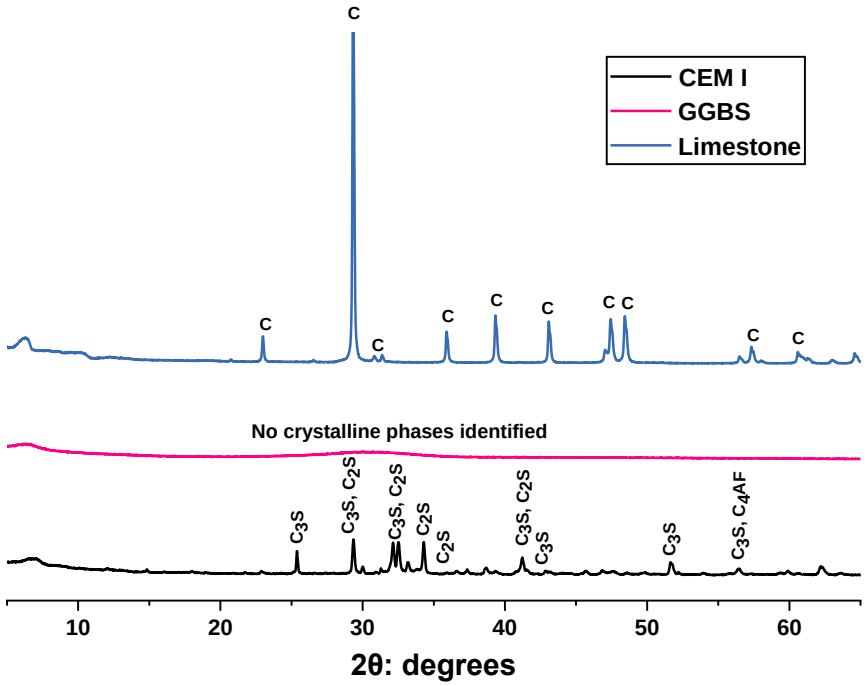

Figure 3.3: XRD patterns of CEM I 52.5N, GGBS and limestone, where C= calcite, C_3S=tricalcium silicate, C_2S= dicalcium silicate, C_4AF= tetracalcium aluminoferrite

3.3. Characterisation of Aggregates

3.3.1. Particle size distribution

The particle size distribution of aggregates was determined as prescribed by the BS 933-1: 2012 (151) standard. The dry sieving analysis method was adopted, as there was no indication of potential agglomeration of particles. Tests were conducted on fine sand, 10mm and 20mm coarse aggregates. Pre-dried aggregates stored under laboratory conditions were mechanically shaken on a vibration table, with aggregates contained in metallic sieves of different apertures stacked in descending order from top to bottom sieve. For a known mass of aggregate, the mass of aggregate retained in each sieve after vibration was recorded. The percentage of aggregates passing each sieve was calculated as the difference between the initial mass before the test and the mass retained for any given sieve, expressed as a percentage. Sieve sizes used for fines were between 75 µm to 10 mm, and for the 10 mm aggregates sieve sizes were 1.18 mm to 20 mm, while the sieve sizes for 20 mm aggregates ranged between 2.36 mm to 37.5 mm. The aggregates particle size distribution used in this study are shown in Figure 3.4 below.

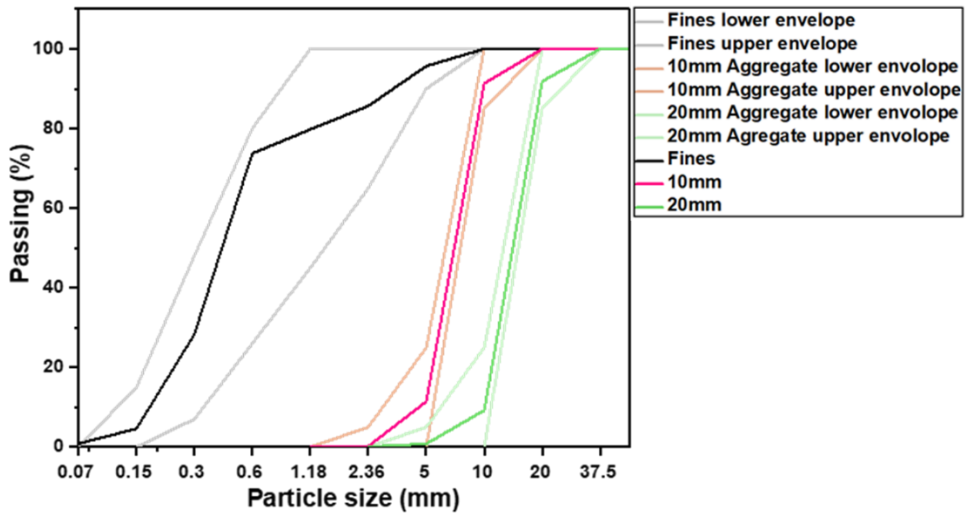

Figure 3.4: Particle size distribution of aggregates as determined by sieve analysis

3.3.2. Water absorption and density of aggregates

Density and water absorption of aggregates were determined in accordance with the BS EN 1097-6:2022 (152). The pycnometer (1 litre glass flask) method was used in these

measurements and entailed an initial placement of tested aggregates in the pycnometer, and then filled with water and saturated for 24 hours. After the 24hr saturation period, the pycnometer was overfilled with water and the mass noted, *W2*. Then the mass of surfaced dried aggregates (*W1*) removed from the pycnometer were also recorded. Meanwhile the mass of refilled pyknometer after aggregates removal was also noted (*W3*). Surface dried aggregates were then oven-dried at 105 ^{o}C for 24 hours. Air-cooled oven-dried aggregates were weighed, and the mass recorded as (*W4*). Equations 3.2 and 3.3 were used to calculate the density and water absorption of aggregates, respectively. Density of water used was 0.01 mg/m^3, and all masses recorded in grams. Three test were conducted per aggregate type and average taken.

$$Saturated\ surface\ dry\ density(g * cm^{-3}) = \rho * {}^{W1}/_{W1-(W2-W3)} \quad \textbf{Eq. 3.2}$$

$$Water\ absorption = {}^{(W1-W4)*100}/_{W4} \quad \textbf{Eq. 3.3}$$

Based on the aforementioned equations, the water absorption of sand, 10 mm and 20 mm aggregates were determined as 1.9, 1.2 and 1.1% respectively, and subsequently factored in the mix design.

3.4. Mixing, casting and fresh state testing of mortars and concretes

In this section, the methods adopted for mortar and concrete mixing are detailed. The formulation of the cement systems used in this work are also discussed. In the case of concretes, the mix design adopted for concrete mixing are described, including test methods conducted on fresh concrete mixes, casting and preconditioning.

3.4.1. Binder formulation and mortar mixing

The cements used for mortar mixing were formulated as shown in Table 3.2. The cement combinations used in this study, are herein referred to as N, NS, NSL, N2L, for plain CEM I, CEM I replaced with ~50 wt.% binary slag, ternary slag (~40 wt.%)-limestone (~10 wt.%) and ternary slag (~30 wt.%)-limestone (~20 wt.%) respectively. For the slag-containing cements, towards maintaining a maximum sulphate content at 3%, powdered natural anhydrite was added to make such adjustment, with consideration for the sulphate constituent in CEM I

slags. Similarly, for the ternary cements, the replacement levels of limestone was derived in consideration with calcite content in CEM I.

Table 3.2: Binder formulation for blended cements used in this study

ID	CEM I	Slag	Limestone	Anhydrite	Total
N	100.0				100.0
NS	51.21	48.53		0.26	100.0
NSL	51.71	39.20	8.83	0.26	100.0
NS2L	52.21	29.10	18.43	0.26	100.0

Based on the formulation above, composite binders were obtained by pre-blending the cement constituents in a roller ball mill (2.5 kg capacity) filled with plastic balls for 3 hours. The ball-milled blended cement was subsequently used for producing mortar samples. Mortar mixing was conducted with auto mixer per standard procedure specified in the EN 196-1 (145). For every standard mix, 450 g of cement, 1350 g of CEN sand and 225 g of deionised water were used. The mixing was automated at slow and fast speed with total run time of 5 minutes, with constituents added in turns. Fresh mortars were cast in moulds and compacted on vibration table for 30 seconds. It is worth noting that, the automixer per standard mix could only produce three to four 40 x 40 x 160 mm prisms, meanwhile two of such mixes were required to fill bigger moulds intended for specimens such as Ø100 x 200mm cylinders. Thus in such circumstances, a 20 kg planetary mixer was used for mortar mixes requiring higher volumes, as waiting time between successive mixing to fill larger moulds meant, the first mix typically would have started setting by the end of second mix. In all cases, cast mortars were demoulded after 24 hours and then transferred to moist room (95 %RH and 20 ± 3 ^{o}C) for curing until testing. It is acknowledged that the consistency of mortar could vary across the different mixers used. However, the aforementioned approach was adopted to minimize potential variations in fresh properties due to the setting tendencies of mortar between successive mixes. This decision was based on visual observations, as fresh properties were not measured at the mortar scale. The sample count and geometries required for hardened mortar testing are detailed in the relevant sections where the tests are discussed.

3.4.2. Concrete mix design and mixing

The mix design used for producing concrete in this study is shown in Table 3.3. It was developed on volumetric basis where the cement constituent and water/cement ratio were

kept constant at 320.3 kg/m^3 and 0.5 respectively, with additional approximate volumes apportioned to the aggregates. The density of the cement constituents, density of aggregates and water absorption of aggregates were factored in the mix design.

Table 3.3: Concrete mix design

Mix ID	CEM I 52.5N	Slag	Lime-stone	Anhy-drite	Water	Sand	10 mm Aggregates	20 mm Aggregates
N	320.3	-	-	-	160.2	651.8	237.7	950.82
NS	164.0	155.4	-	0.8	160.2	648.8	236.6	946.5
NSL	165.6	125.6	28.3	0.8	160.2	648.2	236.4	945.5
NS2L	167.2	93.2	59.0	0.8	160.2	647.5	236.1	944.5

Dry aggregates and cement constituents were transferred into a 120 L planetary mixer and homogenised for 5 minutes, then water was added, and the concrete was further mixed for another 5 minutes. The fresh properties of the concretes were immediately determined, followed by casting concrete specimens in plastic/metallic moulds as per BS EN 12390-2:2019 (153), and demoulded after 24 hours, followed by storing in a curing room (same place as mortar samples) until testing. The sample geometries and count required for hardened concrete testing are reported under relevant sections where the tests are discussed.

3.4.3. Slump and flow testing of concretes

Slump and flow testing of fresh concrete are widely used for quality control of concrete to assess the consistency (plasticity or cohesiveness) in their fresh state. Both tests give an indication of the workability of concrete. In this study, the slump test was conducted as per BS EN 12350-2:2019 (154). It entailed the filling of a standard cone (held in place on a base metal) with concrete in three layers. Each filled layer was uniformly compacted with a tamping rod up to 25 strokes. After the third layer was compacted and levelled off, the cone was steadily lifted upwards. The slump was determined by subtracting the height of the highest point of the tested (slumped) concrete from the cone height.

The flow or spread of the concretes were measured based on BS EN 12350-5:2019 (155). In this test, a standardised cone was positioned centrally on the metal plate flow table. The cone was filled in two layers with 10 strokes per layer with a tamping bar. After striking off excess concrete on top layer, the cone was lifted upwards and put away. The flow table with the concrete was lifted to prefixed levels and allowed to fall freely up to 15 cycles. The diameter

of the spread concrete was measured across two opposite directions, and the average flow diameter was determined as reported in the results section in Table 5.1.

3.4.4. Air content and density of concretes

The air content of concrete has a bearing on porosity of concrete. It can also give some insight into some durability aspects of concrete so that specifying minimum air entrainment is recommended for certain applications, for example, freeze-thaw resistance. The BS EN 12390-7:2019 (156) standard was adopted for this test. In principle, the test is based on the Boyle-Marriote's law, where an inverse relationship exists between volume of gas and pressure at constant temperatures. This test required the use of a pressure gauge meter, which is an assembly of lid/cover fitted with calibrated pressure gauges and a standard 8 litres cylindrical air test container. The mass of the empty cylinder was recorded as X1. Fresh concrete was then placed in the cylinder in three layers, with each layer compacted on a vibration table, so that the third layer completely fills the cylinder. The mass of cylinder and concrete was noted as X2. The lid of the air meter equipped with inlet, outlet valve and air pump is seal-clamped on the cylinder containing concrete. Deionised water was injected into the inlet valve until it escaped with air in the outlet valve; the setup was slightly agitated with a mallet to expel all the entrained air. Both valves were then immediately closed, followed by pumping air (with plunger connected to the air meter) into the assembly until the air meter was reset to zero. A pressure release button when pressed automatically opens the main air valve and the value of air content (%) in concrete was recorded to be as indicated on the gauge meter. The aggregate correction factor in this test was assumed zero.

The density of fresh concrete was determined in accordance with BS EN 12350-6:2019 (156). Here, the density was derived from mass of fresh concrete (X2 - X1) per unit volume of cylindrical air test container (8 litres) using masses measured in the air content measurement test.

3.5. Methods for hardened mortars and concrete testing

3.5.1. Compressive and flexural strength testing

Figure 3.5 shows photographs of the equipment used for compressive strength and flexural strength testing, which is a hydraulic operated tester, where the test type and parameters can be selected/imputed on the display unit. The compressive strength evolution of mortar or

concrete mixes were determined for moist room cured and carbonated samples. Compression test was conducted for concrete at 6 kN/s loading rate in accordance with BS EN 12390-3:2019 (157) using a 3000kN capacity MATEST crusher. Meanwhile mortar samples were tested at 2.4 kN/s as recommended in the BS 1015-11: 2019 (158). For the testing of cured mortar samples, test pieces were sawn from prisms into relevant sizes at early ages and kept under curing conditions until testing. Thus, the potential effects of sawing/cutting induced cracking was minimised prior to testing. For all the samples tested, flat steel plates corresponding to the cube length and width were placed at top and bottom of the test piece. Test on as-cast surface was avoided in all cases.

Figure 3.5: Photographs of the compressive and flexural strength testing equipment used in this study

The flexural strength of concretes was determined using the four point bending testing on duplicate 100 x 100 x 400 mm prismatic specimens, tested at 0.2 kN/s as per BS EN 12390-5:2019 (159). This was pursued by selecting the relevant program and setting the lever on the side of the equipment selector to the flexure testing rig.

3.5.2. Static elastic modulus and Poisson ratio determination

The experimental methods adopted for determining the static elastic modulus and the Poisson ratio of the concretes mixes are discussed. This was determined in accordance with the ASTM C469/C469M-22 (160) standard on two Ø100 x 200 mm cylinders per mix. Here, surface-dried concrete specimens were bonded with 60 mm, 120 Ω Tokyo measuring instrument lab-supplied strain gauges using a hardened TEROSON UP 130 (mixed with BPO paste) as substrate. The strain gauge length is dependent on largest aggregate in the concrete mixes. Before attaching strain gauges, the hardened TEROSON UP-130 was ground with successive grades of sandpaper to achieve a smooth and flattened surface, and the gauges were held in place with a Tokyo measuring instrument laboratory supplied quick-drying glue (cyanoacrylate adhesive – quick setting; operating temperature: -196 to +120 °C curing temperature & time: laboratory temperature 20 seconds to 1 minute (under 100-300 kPa thumb pressure).

Figure 3.6: Photograph showing the strain gauge attached to a cylindrical specimen for static elastic modulus determination. Method adopted based on options recommended in ASTM C469/C469M-22 (160)

Each cylinder was appended with four 120 Ω resistor strain gauges so that, two were positioned axially on the circumference at the mid-span of the cylinders in a diametrically parallel manner, and the other two strain gauges were placed laterally along the mid-height so that they are opposite to each other as shown in Figure 3.6. The strain gauges were soldered to wire leads, which were further connected to separate channels, each in a quarter-bridge circuit configuration attached to a Campbell® Scientific CR3000 micro logger. The data logger was connected to a computer program for strain data monitoring and collection, while

a USB was used to download data on applied load (kN) to failure. Figure 3.7 shows the set up for the testing procedure.

Figure 3.7: Photograph of Ø100 x 200mm cylinders subjected to incremental loads to failure

The axial and lateral strain evolution of the cylinders were recorded when subjected to compressive loads to failure using the MATEST crusher at a loading rate of 3 kN/s.

$$E_{st} = [S_2 - S_1]/(\varepsilon_2 - 0.00005) \quad \textbf{Eq. 3.4}$$

Where:

S_1 = stress corresponding to longitudinal strain, ε1, of 50 millionths, MPa; S_2 = stress corresponding to 40% ultimate load; E = chord modulus of elasticity, MPa; ε_2 = longitudinal strain produced by stress S_2.

Equation 3.4 was used to determine the static elastic modulus of the concrete mixes. The gradient of the load-displacement plot was recorded as the static elastic modulus (GPa). Meanwhile, the Poisson ratio was estimated from the axial and transverse strains corresponding to 40% of the ultimate load.

3.5.3. Ultrasonic pulse velocity (UPV) dynamic elastic modulus

For determining the evolution of dynamic properties of the concrete mixes, triplicate 100 x 100 mm cubes intended for 180 days compressive strength testing were used for measuring the

dynamic elastic modulus at curing ages of 2, 7, 28, 90 and 180 days. The non-destructive ultrasonic pulse velocity technique was implemented based on the BS EN 12504-4:2021 (161), using a Proceq Pundit PL-200PE test kit connected with 250 kHz compressional wave transducers and a receiver. Prior to every test, an OLYMPUS-supplied shear wave couplant was applied on the surfaces of the receiver to facilitate wave propagation. This was followed by a test run for transit time using a manufacturer-supplied calibration block, where a 25.4 µS value indicated very high reliability of the test. For any given sample, the transducer and receiver setup (each positioned at opposite ends of the tested cube) was used to measure the wave propagation transit time, as shown in Figure 3.8.

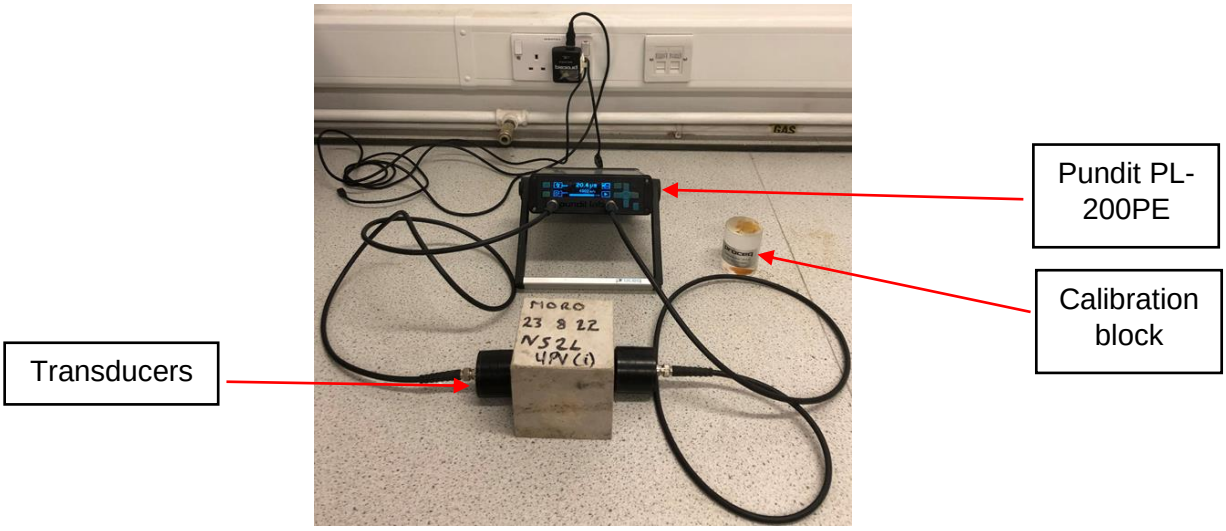

Figure 3.8: Photograph of the set up for determination of ultrasonic pulse velocity testing

Two measurements were taken per specimen on two opposite surfaces other than the as-cast surface. Prior to testing, the mass of the three concrete cubes per mix was measured in accordance with (162). Then, the density was calculated as the mass per unit volume (dimensional). Based on data collected, the UPV dynamic elastic, E_{dyn} (GPa) was calculated with Equation 3.5 as per the ASTM C 597 (163).

$$E_{dyn} = V_p{}^2 \rho(1+\nu)(1-2\nu)/(1-\nu) \qquad \textbf{Eq. 3.5}$$

Where E_{dyn} = dynamic elastic modulus ρ = density (Kg/m^3), υ= Poisson ratio, V (m/s) = velocity computed from transit time

While Equation 3.5 suggests the use of the dynamic Poisson's ratio for computing the dynamic elastic modulus, the long-term increase in the strength and maturity of concrete tends to influence both the static and dynamic Poisson's ratios in a similar manner. It has been reported that the values of static Poisson ratio and dynamic ratio appear to converge with time (164). Thus, in this study the Poisson ratio adopted in the E_{dyn} calculation is based on the poison ratio determined as described in Section 3.5.2.

3.5.4. Shrinkage and loading experiment sample preparation

Prismatic (75 x 75 x 200 mm) concrete specimens were used for shrinkage and loading experiments. These were surface prepared similar to the cylindrical specimens used for the static elastic modulus/Poisson ratio experiment as described above. The stages of sample preparation for the prisms including strain gauge and wire leads attachment are shown in Figure 3.9.

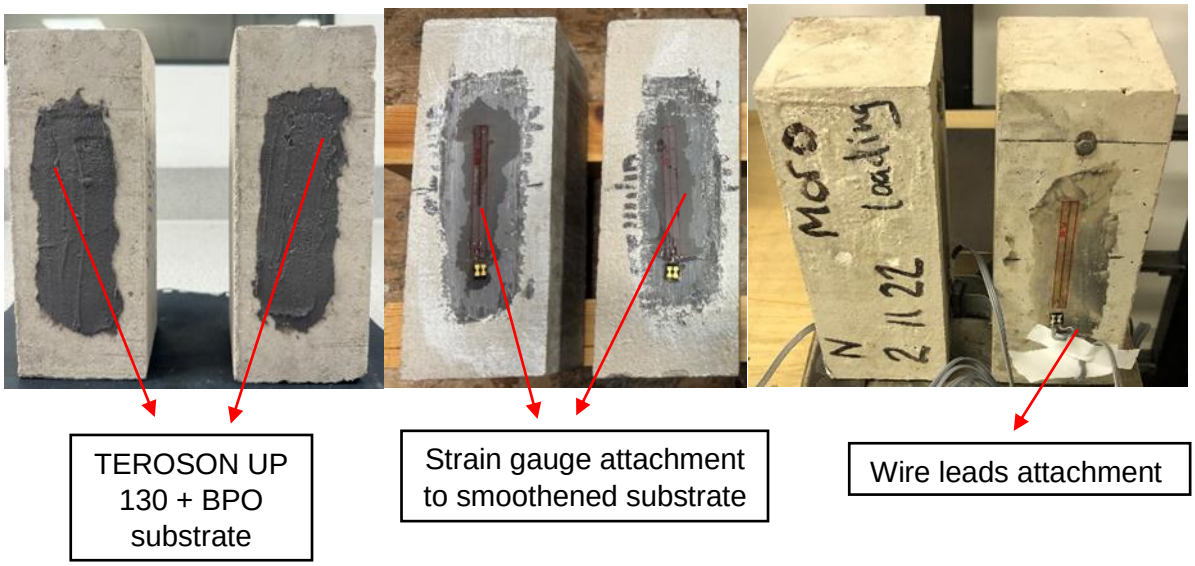

Figure 3.9: Photographs of the concretes prepared for shrinkage and loading experiments showing strain gauge locations

3.5.5. Compressive load application testing set up

The set up used in this study consisted of a base (20 x 20 x 2 cm) steel plate, and two upper (20 x 20 x 2 cm) and (20 x 20 x 1 cm) steel plates between which a 15 tonne load cell was placed. The steel plates were held in place by nutted 20 mm threaded steel rods, as seen in

Figure 3.10. Concrete specimens were centrally positioned between the base plate and top plate below the load cell. Steel spacer plates were placed between two concrete specimens. A top centrally indented spacer plate was placed on the upper concrete specimen, and it supported a Ø50 mm steel ball bearing partially machined into the 20 x 20 x 10 cm steel plate onto which the 15 tonne load cell sat. This ensured a concentric loading of concrete specimens.

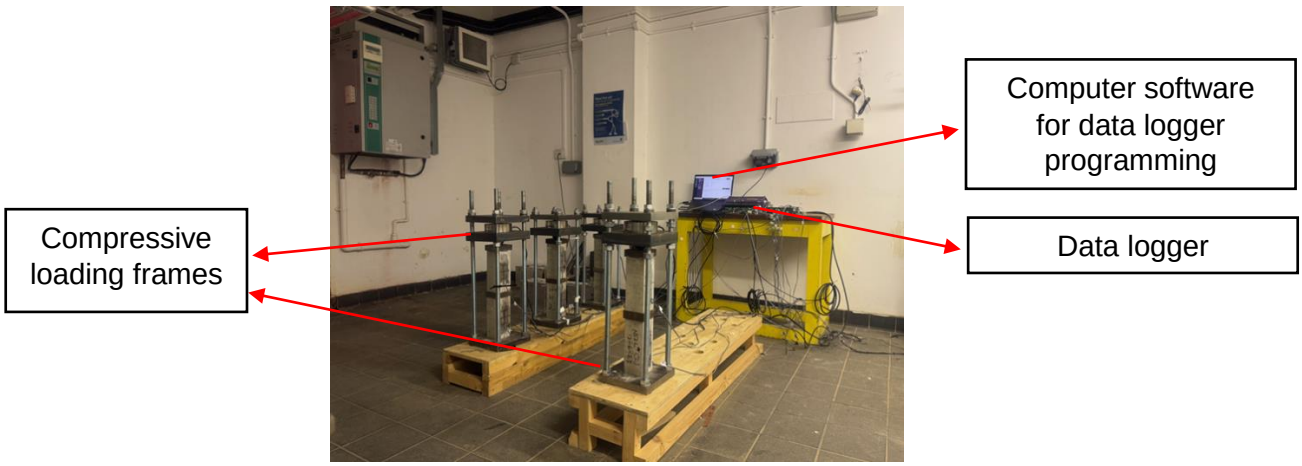

Figure 3.10: Photograph of the set up adopted for studying concretes under the combined action of compressive load and controlled ambient carbonation conditions

For every loading rig, two 75 x 75 x 200 mm prisms were simultaneously subjected to compressive load. The applied load was ~1/3 of the compressive strength at the age of loading in accordance with recommendations in (165). The predetermined stresses (kN) were applied by tensioning the set of nuts inserted on steel rods just above the 20 x 20 x 1 cm upper plate seated on the load cell. Total strain evolution was monitored over the entire period of loading using a digital strain data logger, with data stored at hourly intervals. Meanwhile the initial or elastic strain was recorded immediately at the start of loading. Due to relaxation tendencies of the setup, the applied load was closely monitored and topped up when the applied stress dropped below 0.5 - 2%. The applied load and the durations for concretes were subjected to compressive load are discussed in Section 6.5.3.2.

3.5.6. Carbonation exposure methods and performance

The carbonation performance of mortars or concrete were investigated by monitoring their carbonation depths at various times of exposure. The exposure to accelerated carbonation

was conducted according to the BS EN 12390-12:2020 (166). For specimens intended for carbonation exposure, the cast mortars or concretes were wrapped with plastic film, demoulded after 1 day and then transferred for moist room curing. After a predetermined curing period, prismatic mortars (40 x 40 x 160 mm) or concrete (75 x 75 x 200mm) samples were sealed with self-adhesive aluminium foil at the ends after surface air-drying, and then transferred for preconditioning at 20 ^{o}C, 57±3 %RH for 14 days. Preconditioning at this temperature and humidity empties curing-induced saturated pores, towards facilitating CO_2 ingress. The preconditioned samples were then transferred to a climate-controlled chamber and exposed to accelerated (3% CO_2), 57±3 %RH, and 20 ^{o}C. The evolution of carbonation depths was measured at different durations of 7, 28, 70 and 100 days. Similarly, the mortars or concretes specimens were correspondingly kept in an environmental chamber at the same RH and T without 3% CO_2; thus at environmental CO_2 conditions. Results for those samples are herein referred to as ambient or natural carbonation.

Carbonation depths were measured on freshly split surfaces at relevant testing ages and sprayed with 1% phenolphthalein solution. The regions on the sprayed split surface changing from fuscia to colourless were measured with vernier callipers. The carbonation depth corresponds to the depth measurement of the colourless region. This indicator was prepared according to the standard BS EN 12390-12:2020 (166), using IPA instead of water as dissolving media, as it provides well-delineated carbonation depths particularly in CEM I at early ages.

For all carbonated (natural and accelerated) mortars or concretes, the carbonation-induced compressive strength variations of all mixes were tested towards assessing their residual strength. Mortars were tested at 28 and 100 days post-carbonation on three dry saw-cut 40 mm cube samples. Dry saw-cutting removed the possibility of rehydration in the case of wet-saw cutting, and sawing under high vacuum extraction reduced thermal gradients, hence reducing microcracking tendencies. Post-carbonation strength test on concrete was conducted on 75 mm cubes sawn from 100 days carbonated 75 x 75 x 200 mm prisms. The strength of carbonated mortars and concretes was determined on specimens directly after the corresponding exposure without any saturation.

3.5.7. Carbonation exposure methods for transport properties studies post-carbonation

To study the impact of carbonation on transport properties of mortars and concretes, samples were systematically exposed to carbonation and then subjected to chloride or water ingress

testing. In order to replicate cored cover concrete samples derived from existing concrete infrastructure for durability testing, cylindrical specimens were exposed to unidirectional carbonation as illustrated in the schematic diagram Figure 3.11. Here, Ø100 × 200 mm mortar or concrete specimens after 28 days curing were surface dried, coated on the circumference with Sika® primer (3A:1B) and allowed to dry in a fume cupboard over 24 hours. Post drying, they were cut into Ø100 x (50±5) mm and one of the as-cut surface of the mortars or concrete were sealed with sufficient layers of self-adhesive aluminium so that only one as-cut surface was available to CO_2 ingress. These Ø100 x (50±5) mm samples were designated for studies on chloride permeability, water absorption and depth monitoring after natural and accelerated carbonation of mortars and concretes.

It was ensured that the carbonated surface was exposed to the NaCl solution in all cases. Similarly, for water ingress studies, the immersed surface was the carbonated surface. Testing of water absorption and chloride permeability of concretes was conducted after 28 and 100 days carbonation.

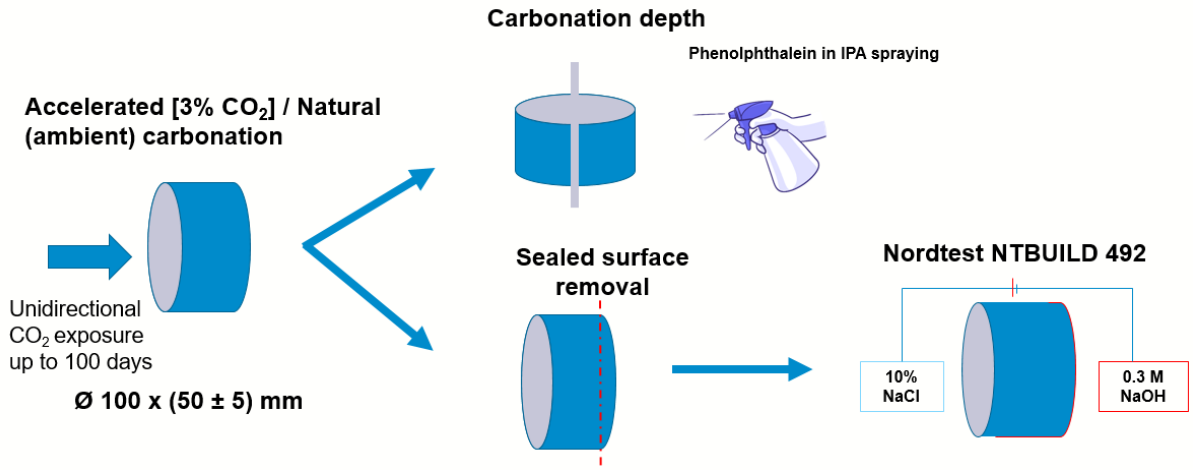

Figure 3.11: Schematic diagram of experimental methodology for investigating the effect of carbonation on transport properties of concrete

3.5.7.1. Carbonation shrinkage of concretes

To study the volumetric (bulk) shrinkage evolution of concrete mixes, 28 days moist cured 75 x 75 x 200 mm specimens were prepared as described in Section 3.5.4. The use of enclosed climatic chambers for accelerated carbonation necessitated the use of wireless/remote controlled data loggers. Thus a *lord Microstrain (WSDA-200-USB)* instrument, battery powered wireless data loggers (*V-link 200*) were used. These loggers were equipped with quarter bridge completions for connecting strain gauges to respective differential channels.

The data loggers also had the capability of logging data locally and then transmitted on demand when interfaced with the *SensorConnect* software, thus there was reduced impact on data transmission and collection, potentially from the conductive metallic chamber (behaving as a Faraday cage (167)).

Shrinkage data were collected for an initial 14 days of preconditioning and continued when transferred to the 3% [CO_2] accelerated carbonation chamber for up to 28 days. A corresponding sample was kept under ambient carbonation and shrinkage data was collected in a climatic chamber without CO_2. For carbonation shrinkage monitoring, the strain gauges were attached to sides adjacent to the as-cast surface, so that two shrinkage data were recorded per specimen. One specimen per concrete mix was used for both natural and ambient carbonation shrinkage measurements. While duplicate or triplicate specimens could offer robust experimental methodology by reducing variability in shrinkage data, restrictions such as environmental chamber capacity and voltage balancing amongst four data loggers (total of 16 channels) available for use inform the aforementioned approach.

3.5.7.2. Concrete performance under coupled load and carbonation exposure, and its impact on transport properties and residual strength

This experiment involved the exposure of 75 x 75 x 200 mm concretes to natural or accelerated carbonation while simultaneously subjecting them to compressive load. Specimens to be loaded were prepared as described in Section 3.5.4 and set up as described in Section 3.5.5. Loaded concretes were subjected to accelerated or natural carbonation for 28 days. Meanwhile, another set of concretes were subjected to long-term natural carbonation up to 200 days. Carbonation depths, strain evolution and residual strength after a loading cycle of all concrete mixes were determined.

The concretes for loading experiment were cured for 7 days prior to loading without preconditioning towards replicating typical construction practice. The testing age was adopted based on the removal of formworks during field construction for the progress of construction. This was to allow the material to gain sufficient strength in order to apply a sufficiently representative load thought out the duration of the experiment. For instance, a 2 days target strength of 10 MPa has been used as a criteria for removal of formworks (15, 168). Thus, it can also be argued that concrete structures under field conditions would start carbonating as soon as the formworks are removed. In addition, continuation of construction suggest structural members would likely be subjected to live loads from 7 days onward.

Figure 3.12 shows the loading setup adopted while inducing accelerated carbonation (3% CO_2, 57±3 %RH, and 20^{o}C). Two loading rigs, and hence two concrete mixes could be contained in the climatic chamber at a time. The load cells (1 per loading rig) were connected to two separate channels and one data logger. Then, four strain gauges (2 per either side of the upper and lower prism) per set-up were connected to dedicated channels via quarter bridge completions to one data logger. Thus, two data loggers were allocated for eight strain gauges corresponding to four strain data per rig. Here, with all connections such as load cells, and strain gauges connected to respective channels, the required stress level was applied outside the climatic chamber. The initial strain was noted, and then once the loading rig was placed in chamber, the strain gauges were immediately initialised or 'zeroed' to begin strain data acquisition.

The applied stress was ~1/3 of the 7 days compressive strength of the concrete mixes as recommended by the BS EN 12390: 17 (165).

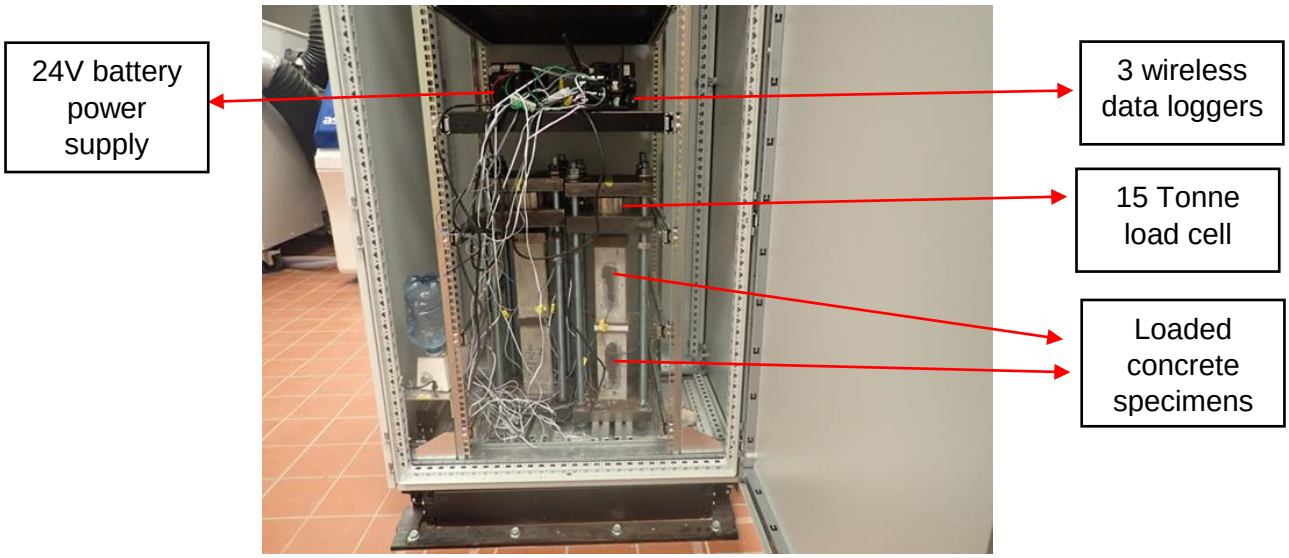

Figure 3.12: Photograph showing concrete specimens under combined action of compressive load and accelerated carbonation (3% CO_2)

In a scoping study towards establishing optimum experimental procedures, it was identified that the surface preparation for strain gauge attachment had slightly reduced carbonation ingress in that direction as per depth measurements. Thus, unlike specimens used for shrinkage measurements (not intended to be used for carbonation depth measurement), strain gauges were attached to the as-cast surface and its opposite sides so that carbonation depths were measured for sides adjacent to the as-cast surface. The availability of these surfaces

prevented the need to test residual strength on the as-cast surface, including conducting transport properties assessments such as water absorption on those surfaces.

For all loaded concretes, corresponding concretes (control specimens) cured for 7 days were kept under the same environmental conditions (T and RH) as the loaded concretes, but without load. Carbonation depth and strength after 28 days for both natural and accelerated exposure were monitored. Specimens were surface prepared similarly to loaded concretes to ensure the same surface areas for CO_2 ingress. The strain evolution was, however, not monitored for the non-loaded concretes, as the focus of the experimental programme was to obtain reference carbonation depths and strength values for comparison purposes. After completing the carbonation under loading experiments, test pieces derived from 75 × 75 × 200 prisms were obtained for the water absorption test. Specimens were dry-cut into equal parts of 50 mm thickness and the two centrally cut samples (50 mm each) were used for the water absorption test. The two central portions were chosen to give a true representation of possible variations in consolidation or settlement effects from top to bottom of loaded concrete, where consolidation or settlement effect is expected to increase towards the bottom.

3.5.8. Transport characteristics assessment of mortars and concretes

In this section the experimental methods adopted for determining permeation properties of mortars or concrete are discussed. Tests were conducted on moist room cured concretes, as well as carbonated mortars or concretes at different ages. Test on cured samples were carried out at ages 28, 90 and 180 days. Meanwhile, tests on carbonated samples were conducted post-28 and 100 days of carbonation exposure. Tests on carbonated samples subjected to load were conducted at 28 and 200 days.

3.5.8.1. Bulk conductivity

Bulk conductivity provides useful information on the pores continuity in the matrix of hardened mortars and concretes. This was performed on cylindrical samples (100Ø × 50 mm) intended for chloride permeability testing. Prior to initiating permeability test (described in Section 3.5.8.2), the bulk conductivity was recorded by subjecting the set up to 60 Volts for a duration of 60 seconds using the potentiostat operated by the Proove'it software. The software then returns the values of bulk conductivity (mS/m) after the test duration. This automated test followed the ASTM C 1760 (169). Three cylindrical samples per concrete mix were tested per

age for moist room cured concretes. Meanwhile two samples per mix were tested on carbonated mortars and concretes.

3.5.8.2. Chloride permeability/migration testing

The Nordtest NTBUILD 492 chloride migration test (93) was used for studying the resistance of mortar and concrete mixes to chloride ingress. The chloride permeability test was conducted on cured concretes after 28, 90 and 180 days, and was also applied to study mortars and concretes after 28 days and 100 days carbonation exposure (post 14 days preconditioning).

Sample preparation for chloride permeability test on carbonated mortars and concretes has been described in Section 3.5.7. Similarly, for moist room cured concretes, 100Ø × 50 mm samples were required for the test. In the case of testing on cured concretes, they were surface dried after taking from moist room, impermeabilised on the circumference with a Sika® primer (3A:1B) and allowed to dry in a fume cupboard over 24-hour period. About 15mm was cut off from the as-cast surface and the bottom, and then equal thickness of (50 ± 5) mm was then cut from remaining section.

For all mortars or concretes whose chloride permeability was investigated, the coated specimens were preconditioned before their chlorides penetrability was tested as follows. Samples were placed in an 18L preconditioning steel vessel. The vessel was covered and subjected to vacuum treatment pump for 3 hours. The vessel was then then filled with saturated lime (~3g/litre) by opening a valve connecting a hosepipe from 5L glass bottle to the vessel. Once all samples were fully immersed in lime solution, the valve was closed and set up allowed to continue running under vacuum for a further 1 hour followed by soaking the specimen fully immersed for 18 hours, and not under vacuum.

The chloride migration test is described as follows; a Germann instrument supplied, PROOVE'it equipment (with associated software) was used for the migration test by applying an electrical potential across concrete specimens with 10% (%wt.) NaCl solution and 0.3 M NaOH as catholyte and anolyte solution, respectively. Meanwhile a temperature sensor in the NaCl logged the temperature evolution during test time. Following a pre-determined test time (based on adjusted current recorded after applying 30V over 60s), the exposed surfaces were cleaned under running water. The tested cylinders were then split axially into two halves thereafter. The chloride penetration depth is measured on samples after 0.1 M $AgNO_3$

spraying of the freshly split surface. The measurement corresponds to the distance of the area showing white precipitates after $AgNO_3$ spraying as shown in Figure 3.14(b).

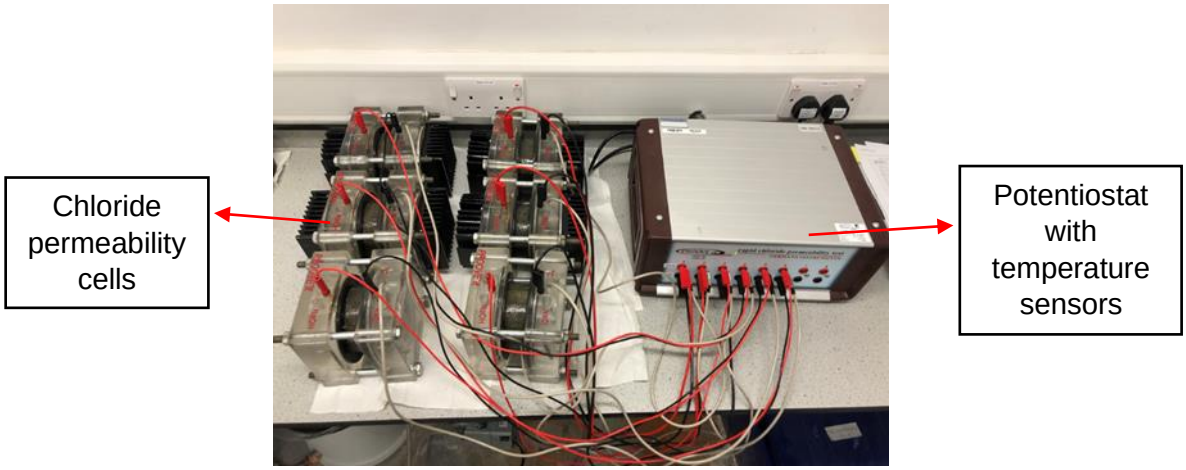

Figure 3.13: Photograph of the Setup for testing chloride permeability of mortars or concrete

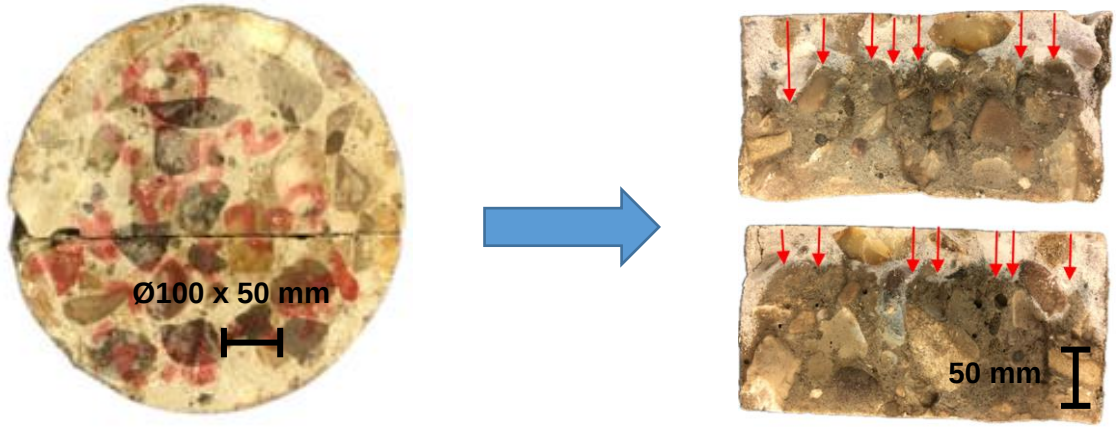

(a) (b)

Figure 3.14: Photographs showing (a) axially split (100Ø × 50 mm) concrete (using a concrete splitter) (b) white precipitate on split concrete sprayed with silver nitrate with indication of how 7 readings of chloride depths were measured. Measurement along edges (~10 mm) were avoided

Seven chloride depth data points were recorded per halved cylinder as shown in Figure 3.14(b). The average chloride depths, measured initial and final temperature, in addition to applied voltage were used as input to calculate the D_{nssm} (non-steady-state migration coefficient, $\times 10^{-12}$ m^2/s) according to Equation 3.7.

$$Dnssm = \frac{0.0239*L*(T+273)}{t*(P-2)} * \left(\bar{x} - 0.0238\sqrt{\frac{(T+273)*L*\bar{x}}{P-2}}\right) \quad \textbf{Eq. 3.7}$$

Where; P (V) = absolute value of the potential difference applied; T (°C) = mean value of initial and final temperature in the anolyte (NaCl) solution; $\bar{X}$ (mm) = mean value of measured chloride depths; t (hour) = testing time; and L (mm) = average thickness of test piece measured across four points

3.5.8.3. Surface resistivity

The surface resistivity is a non-destructive rapid electrochemical technique used for concrete structural health monitoring. It was determined using a handheld Proceq resipod device that operated based on the Wenner 4-probe resistivity measurement. The four probes of the resipod equidistant to each other were axially attached to the concrete, so that current is applied via the outer probes, and inner probes measure the voltage. The device is calibrated to return the resistivity (kOhm*cm) on its display. Test was conducted on concrete cylinders immediately they were taken out of the moist room. A total of nine readings were taken per cylinder.

3.5.8.4. Capillary suction and porosity

Sorptivity test was conducted to assess the water admissibility of mortars or concrete. Samples for sorptivity were derived from saw cutting the bulk cylindrical or prismatic specimens. Before cutting, concrete specimens were coated with epoxy on the circumference. The test was conducted following the BS EN 13057:2002 (89). Prior to the test, samples were precondtioned by drying in a ventilated oven at (105 ± 5) ^{o}C, based on (170), as initial trials demonstrated the drying process was effective at this temperature towards achieving stabilised mass changes in 7 days, relative to studies where constant mass was achieved in 2 months drying at 50 ^{o}C (97). Lower preconditioning temperatures (60, 171) have been implemented in other studies, for reasons such as thermal gradient induced cracking or phase assemblage decomposition. However, trial studies on mortars or concretes in this work showed no such indication of damage. In addition, it was decided to test the samples as per standard, so the results can be compared with those obtained in real practice, and not only used for research purposes. It must be acknowledged that, while preconditioning at 105 ^{o}C is thought to overestimate total water porosity by 15% at the paste scale, relative errors of 1% have been obtained on concrete scale (172). This suggests that the sensitivity of cement paste to preconditioning cannot necessarily be extrapolated to the mortar or concrete scale, particularly considering that low-temperature preconditioning requires an extended drying

period. After oven drying, samples were cooled to room temperature in a desiccator for 24 hours until testing.

The set up for sorptivity is shown in Figure 3.15. Here the samples were placed in a flat-bottomed container supported with an angled (L-shaped) polyvinyl chloride (PVC) pipe, so the water level traversed about 3 mm from the immersed surface of the tested sample. The mass of the cooled oven-dried samples was measured before the test. Then mass changes after immersion were further measured at predetermined durations up to 15 days. The 15-day duration was adopted to monitor whether any aberration in the sorptivity profiles exists in the concretes made from the multicomponent cement systems, as limited data exist. This also aided in establishing the saturation point. Sorptivity or sorption coefficient is determined as the slope from time t=0 to the saturation point on the sorptivity profiles. For readability, the sorptivity coefficient is used in the entire thesis.

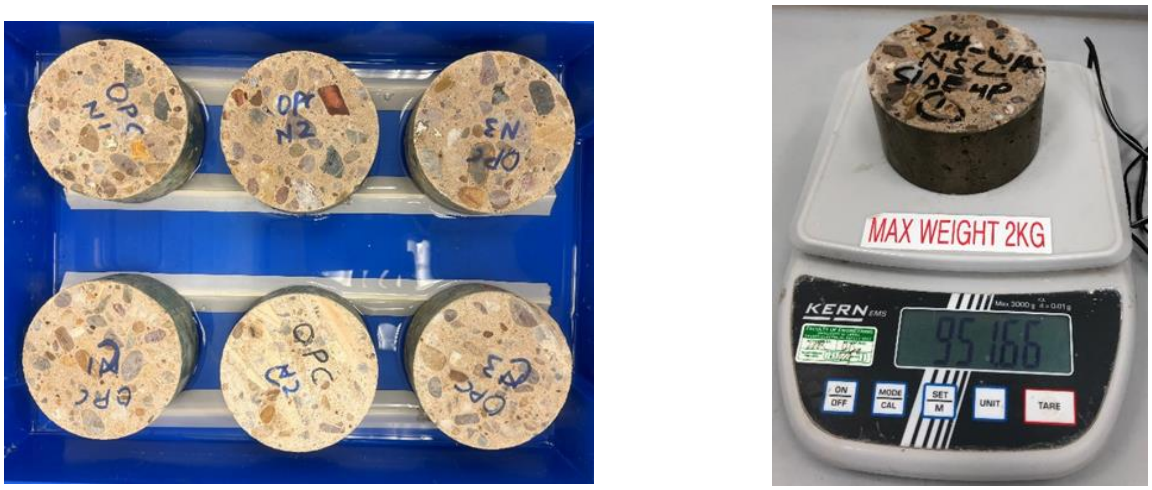

(a) (b)

Figure 3.15: Photographs of the (a) setup for conducting sorptivity test and (b) mass change measurement at predetermined time

Porosities of samples used for sorptivity test were further determined under vacuum saturation as implemented in (173). This involved placement of samples in an 18L metal vessel and under vacuum for 3 hours, followed by addition of deionised water to fill to a level just above the samples. The setup was further allowed to run under vacuum for further one hour, and then vacuum turned off thereafter. Samples were kept fully immersed in water for further 24 hours. Then after the surface dried mass post water saturation were measured. Porosity was computed as the ratio of mass differences to sample volume expressed a percentage. The

water absorption (mass %) was determined as a difference between dried and saturated mass expressed as a percentage. Sorptivity specimens of moist room cured concretes were derived similarly to cylinders used for chloride permeability testing.

3.6. Concluding remarks

Chapter 3 highlighted the key raw materials used in this study and the sample preparation methods at both mortar and concrete scales. The theoretical underpinnings for the methods adopted for characterising raw materials and techniques used to assess mechanical and durability aspects of mortars and concretes were discussed. Additionally, limitations of methods and justification for adopted approaches are provided. For example, the choice of preconditioning temperature for samples intended for water absorption and the placement of strain gauges for specimens used for combined loading and carbonation experiments. In the subsequent chapters, where results and discussion are presented, references are made to relevant sections in the experimental methodology with details of the specimen counts specific to each chapter included.

Chapter 4.

4. Carbonation Performance of blended Portland cement-slag-limestone mortars

4.1. Introduction

High-volume replacement of Portland cement is known to reduce the carbonation resistance, and can have a significant impact on the mechanical strength and transport properties of materials produced with them. A critical concern arising from higher carbonation rates in composite cement systems is how the pore structure alterations associated with carbonation can trigger other deterioration processes in the long term, for example, moisture and/or chloride ingress. The pore structure variations can increase the ions/moisture ingress in addition to carbonation-induced pH reduction, which can significantly influence susceptibility of reinforced concrete structures to corrosion-based deteriorations. The impact of carbonation on other durability mechanism is largely unknown, particularly for mortars or concrete made with next-generation multi-component composite such as the CEM VI(S-LL) or blended Portland cement-slag-limestone.

With the increased adoption of concretes with high volume of SCMs, it is crucial to evaluate and understand the factors affecting the long-term performance of the concrete structure made with such materials under realistic in-service conditions. This study addresses the implications of carbonation on the transport of aggressive species (chlorides and moisture) in partially carbonated mortar specimens, replicating the situation of a partially carbonated concrete cover in realistic concrete structures. It is acknowledged that differences in permeability and binder content between mortar and concrete will alter the quantitative results of the mechanical and transport properties evaluated. However, for the purpose of this thesis, given the complexity of some of the tests to be conducted and with no standards for multiple durability exposures, it was decided that the evaluation of mortars was required to develop an experimental protocol that can be upscaled to concretes. Studies on mortar scale was to determine optimum approach to pursue unidirectional carbonation of cylinders in a manner

that carbonation depth results can be compared to prisms as standards (BS EN 12390-12:2020 (166)) do not provide a basis for such comparison. That notwithstanding, it was also necessary to monitor the long-term carbonation progress for as long as reasonably practical within the remaining duration of the PhD, as there is no existing literature on prolonged natural carbonation exposure (for at least one year) for the ternary systems (with ~20% limestone addition) used in this study, both at the mortar and concrete scales. Conducting experiments in phases (see Figure 3.1) under COVID-19 restrictions also meant the longest carbonation ages could be achieved on mortar specimens cast during phase one. Thus, the findings in this chapter are reported as a standalone study and are not intended to explain results on a concrete scale.

Low clinker cements were produced by blending slag (~50 wt.%) with CEM I (binary cement), or blended Portland-slag composite cement with ~10 and ~20 wt.% limestone addition. The carbonation performance was monitored using the phenolphthalein indicator test, and residual compressive strength was determined after 100 days of accelerated carbonation exposure (3% CO_2 and 60% RH) for up to 100 days, and after controlled ambient exposure up to 2 years (monitored for carbonation depth as long as possible). Additionally, unidirectional carbonation was simulated using sealed cylindrical specimens.

The impact of carbonation on bulk conductivity, chloride permeability and water ingress was assessed post-carbonation exposures. While 20 wt.% limestone addition in ternary blends yielded comparable compressive strength to CEM I-based mortars at a later curing age, ternary blends exhibited a marked reduction in carbonation performance relative to CEM I. Despite higher carbonation rates, the chloride resistance and water absorption properties of composite cements are not significantly impaired by carbonation compared to CEM I.

4.2. Experimental procedures

4.2.1. Mortar mixing and sample preparation

Water, cement and a CEN-standard sand were mixed in ratios 0.5:1:3, respectively in an automated mixer. Details of the mortar mixing procedure are expounded in Section 3.4.1, using the binder formulation shown in Figure 4.1.

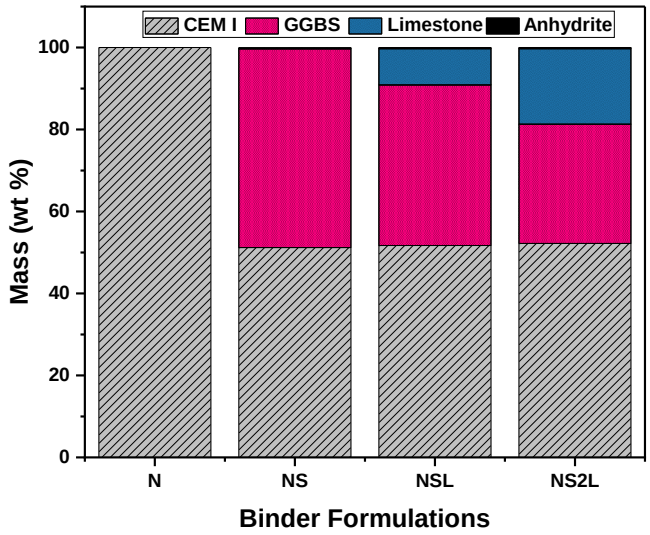

Figure 4.1: Binder formulation (wt. %) of mortar mixes evaluated

Mortar prisms (40 x 40 x 160 mm) per binder formulation were cast for compressive strength and carbonation depth evolution monitoring. Additionally, cylindrical specimens (100Ø x 200 mm) per mix were cast to interrogate the effect of carbonation on moisture and chloride ingress. All specimens were cured in a moist room (95 %RH and 20 ± 3^{o}C) for 28 days before testing.

4.2.2. Carbonation exposure of mortars

Two sets of prisms (40 x 40 x 160 mm) per exposure and mix type were used for monitoring carbonation front progression. The assessment of impact of accelerated carbonation on chloride and moisture ingress was investigated using ten (10) sets of cylindrical (100Ø × 50 mm) specimens obtained from dry-saw cutting of four cylinders (100Ø × 200 mm) per mix type. The methodology for carbonation depth monitoring, and sample preparation of samples for studying impact of unidirectional CO_2 exposure on chloride and water ingress are elaborated in experimental chapter, Section 3.5.7.

Carbonation depths at different exposure times (days) of 7, 28, 70 and 100 were measured in accelerated carbonated prisms. Similarly, the carbonation depths were measured post 28 and 100 days of exposure in cylindrical samples (100Ø x 50) mm, one per age. Correspondingly, the same set of prismatic and cylindrical mortars were simultaneously stored under sheltered conditions using similar conditions to those used in accelerated carbonation, except for

exposure to atmospheric CO_2. The carbonation depths of prismatic mortars were further measured under ambient exposure for up to 2 years using a phenolphthalein pH indicator.

Two 40 mm cubes were derived from carbonated 40 x 40 x 160 mm prisms per mix and tested for residual strength at two carbonation exposure times: 28 and 100 days. The reference compressive strength used was that of 28 days cured samples. Although it would have been ideal to test samples at comparable ages (curing + carbonation exposure) without CO_2 exposure as a reference. This study was initiated during the COVID-19 pandemic, with limited access to materials, laboratories and testing facilities, and therefore, it was prioritised to evaluate the carbonated specimens instead.

4.2.3. Studies on carbonated mortars

4.2.3.1. Sorptivity and open porosity

To investigate the moisture ingress properties after carbonation exposure, two cylindrical specimens (100Ø x 50 mm) in each mix were tested following 28 and 100 days of unidirectional natural and accelerated partial carbonation. The sorptivity profile was obtained for 15 days and the mass changes over time were analysed. The methods adopted for sample preconditioning, as well as for sorptivity testing and vacuum water saturated porosity (%), and water absorption (mass %) are described in the experimental chapter, Section 3.5.8.4.

4.2.3.2. Bulk conductivity

The bulk conductivity of carbonated cylindrical mortar samples was determined after 28 and 100 days of carbonation exposure. Two set 100Ø × 50 mm cylinders were tested per age. A Germann instrument supplied Proove'it equipment and software, which operated according to ASTM 1760 (169) was used, and the results are reported in milliSiemens/meter (mS/m) . The specimens used for testing bulk conductivity were subsequently used for chloride permeability testing as described in the next section.

4.2.3.3. Chloride Permeability

The permeability of carbonated cylindrical mortars to chloride ions were tested after 28 and 100 days of carbonation exposure as discussed in detail in Section 3.5.8.2.

4.3. Results and discussion

4.3.1. Compressive strength development

Compressive strength development of the mortars is shown in Figure 4.2. CEM I based mortars developed a higher compressive strength than composite cement based ones up to 28 days of curing. However, notable increases in compressive strength were observed when using the composite binders, NS and NSL, approaching similar strengths to CEM I by 90 days of curing. The rate of strength gain was higher for all composite binders after 7 days. Beyond 7 days, there is active contribution of slag reactivity to the formation of additional hydration products, mainly C-A-S-H and AFm phases, refining porosity and significantly improving compressive strength (31, 65). This contributes to the strength gain in the evaluated mortars. CEM I attain higher degree of reaction compared to slags during the first days of curing, consistent with what has been reported in other studies (174, 175), hence it was expected that the early age strength of NS, NSL and NS2L are relatively lower compared to CEM I. The by-product of OPC hydration including portlandite (which sustains pH levels >12) of the blended cementitious system further promotes slag dissolution as curing progresses (31, 40), thus contributing to the later age strength of composite cements due to space-filling phases. This explains the noticeable increasing rate of compressive strength of the composite binders after 7 days of curing, consistent with what has been reported in other studies (66).

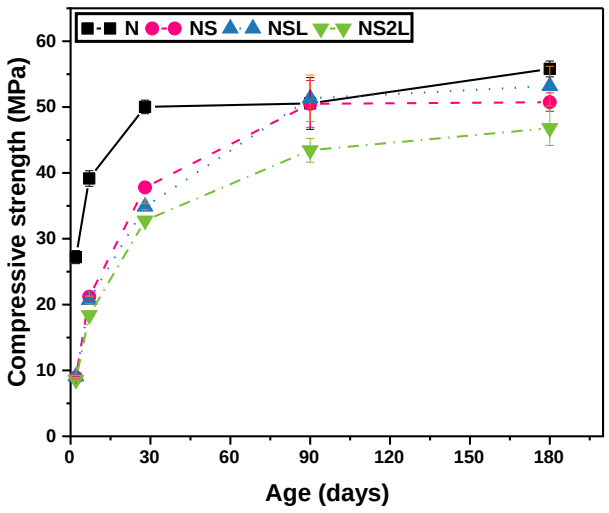

Figure 4.2: Compressive strength development of mortars as a function of curing time. Error bars correspond to one standard deviation of three measurements

The binary and ternary blends exhibited similar compressive strength evolution up to 28 days. However, at 90 days NS2L had slightly lower strength relative to NS and NSL. All composite cement (NS, NSL and NS2L) showed continuous increase in strength up to 180 days. In the ternary slag-limestone blends such as the ones evaluated in this study (NSL and NS2L), limestone plays a dual role as a reactive cement replacement and as a filler (34, 40). As a filler limestone improves the reaction of slags and CEM I by providing nucleation sites as well as increasing effective water-to-binder ratio, and space available for continuous hydration. Upon reaction, limestone participates in the CEM I hydration yielding mono- or hemi-carboaluminate reaction products by chemical reaction with alumina, and which in turn reduces aluminium concentration in the system favouring the continued slag hydration (40). Formation of carboaluminates stabilises the less dense phase ettringite, which can also contribute to the solid volume. The combined effect of limestone in Portland slag cement can lead to porosity refinement via space-filling (65), which in turn favours compressive strength gain. Such effect is noticeable in NSL mortars, whose compressive strength is comparable to those of binary slags mortars. Meanwhile, larger quantities of limestone in the binder (NS2L mortars) led to a slight reduction in the strength of NS2L, which can be attributed to dilution effects. However, by later curing ages, it is also observed that composite binders demonstrated progressive strength increases towards CEM I, with NS2L achieving ~80% of CEM I strength by 180 days. The results indicate that substituting slag with ~20 wt.% limestone is not detrimental to the compressive strength development of mortars produced with composite cements, suggesting limited dilution effects with prolonged curing age.

4.3.2. Carbonation rate at different exposure conditions

Photographs of specimens exposed to two years of natural carbonation, after being sprayed with a phenolphthalein solution, are shown Figure 4.3. The carbonation depth of CEM I at 2 years is smaller compared to that of the composite slag cements-based mortars.

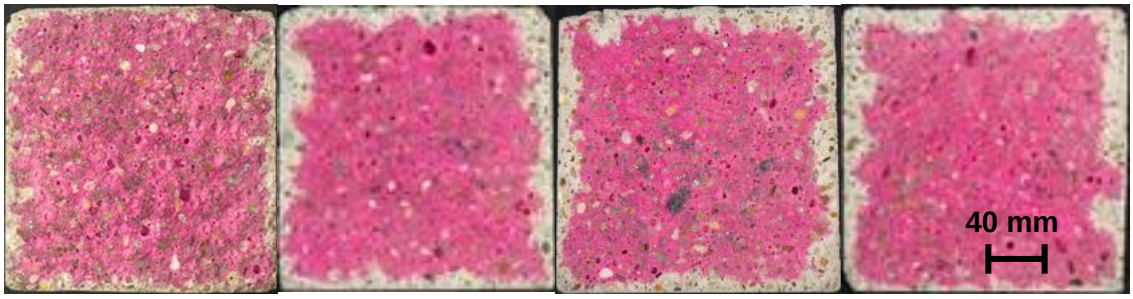

(a) (b) (c) (d)

Figure 4.3: Photographs of 40 x 40 mm mortar mixes (prisms) sprayed with a phenolphthalein solution after natural carbonation for 2 years. (a) N (b) NS (c) NSL (d) NS2L

The average carbonation depth at various exposure times is shown in Figure 4.4(a), where after 100 days ambient carbonation exposure, higher progression of carbonation front was observed for slag-containing mortars with or without limestone relative to CEM I up to 2 years. It must be highlighted that, the reported standard deviation of carbonation depth is based on 16 measurements. However, the influence of as-cast surfaces (higher measured depths) and adjacent surfaces (relatively lower measured depths) present different carbonation front progression as can be seen in Figure 4.3. This accounts for the high standard deviations. Carbonation depths was recorded in CEM I mortars after 180 days exposure and beyond. From 180 days ambient carbonation exposure, while NS2L exhibited the highest carbonation depths, it is however noticeable that, at advanced carbonation ages (2 years) the carbonation depths of all slag-containing cements with or without limestone (NS, NSL and NS2L) are comparable. In Figure 4.4(b), the plot of carbonation depths versus corresponding square root of time based on Fick's law is reported, and shows a strong correlation for all mixes, and corroborates with findings by other authors (103). Table 4.1 shows a summary of the natural carbonation rates (corresponding to the slope of linear regression for respective concrete mixes). The exposure time-specific natural carbonation coefficient ($mm/days^{0.5}$) as shown in Table 4.2 suggests a reducing trend in carbonation rates of all mortar mixes. This gives an indication that, although NS, NSL and NS2L mortars exhibited greater progression of carbonation front, the rate of progression is retarded at longer exposure durations when compared to early ages.

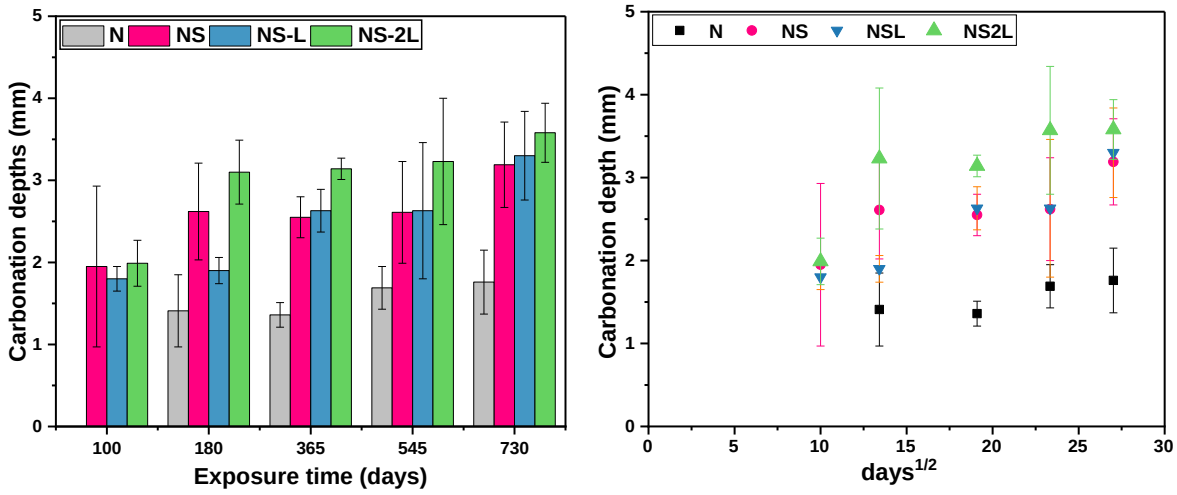

(a) (b)

Figure 4.4: Carbonation depth of mortars exposed to (a) natural carbonation up to 2 years. Figure (b) the correlation between carbonation depth and the square root of time. The values reported correspond to the average of 16 readings (four per side), and error bars correspond to one standard deviation of such measurements

Table 4.1: Natural carbonation coefficient (mm*days$^{-0.5}$) of mortar prisms based on slope of linear regression in Figure 4.4(b)

	Mix ID			
	N	**NS**	**NSL**	**NS2L**
Carbonation coefficient (mm*days$^{-0.5}$)	0.07 ± 0.004	0.13 ± 0.02	0.12 ± 0.01	0.16 ± 0.02
R^2	0.99	0.98	0.98	0.99

Table 4.2: Natural Carbonation coefficient (mm*days$^{-0.5}$) of mortar prisms as a function of the exposure time

Mix ID	**Exposure time (days)**				
	100	**180**	**365**	**545**	**730**
N	-	0.11	0.07	0.06	0.07
NS	0.20	0.2	0.13	0.1	0.12
NSL	0.18	0.14	0.14	0.1	0.12
NS2L	0.20	0.23	0.16	0.12	0.13

Carbonation progress can be further exacerbated by the induced phase changes leading to alterations in pore structure in the material. It is well known that for CEM I, the increased rate of portlandite conversion upon reaction with CO_2 to form calcium carbonate results in a

densified microstructure, where calcite precipitates act as plugs, retarding further CO_2 diffusion (100, 176), which is consistent with the reduced carbonation coefficients exhibited by CEM I-based mortars. In the case of slag-containing mortars with/without limestone, carbonation will take place in the C-(A)-S-H and/or CO_3^{2-}-AFm phases leading to its decalcification. Carbonation-related coarsening of pore structure (due to decalcification) and shrinkage related microcracking can influence transport properties (112, 113), increasing the rates of CO_2 diffusion. Therefore, there is a combined effect where a reduced portlandite content in the system, combined with an increased diffusivity of CO_2 accelerates carbonation progress. It is also noteworthy that, in the ternary limestone systems carbonation of $Ca(OH)_2$ and carbonate-AFm phases proceed almost simultaneously, resulting in synergistic benefits that can sustain their alkalinity reserves (18). This might explain the comparable carbonation rates identified in the binary and ternary mixes, at a constant clinker factor and water-to-binder ratio. This requires further investigation, as changes in porosity of the specimens, as identified in Section 4.3.4.3 may also be attributable to the differences in carbonation progress.

For mortars subjected to accelerated carbonation exposure, Figure 4.5(a) and Figure 4.5(b) show the average carbonation depths at different ages and the linear regression of carbonation depths against square root of time respectively. The carbonation depths of NS, NSL and NS2L show significant increase in carbonation depth relative CEM I at all exposure times, and the overall carbonation rates (Table 4.3) in mortars made from slag-composite cements were nearly 2 times the rates of CEM I mortars. It is worth mentioning that, even under 3% [CO_2] exposure, it appears that after prolonged exposure (100 days), the carbonation depth change is small not only in CEM I, but also for NS, NSL and NS2L consistent with the comparable carbonation coefficients identified at later exposure durations shown in Table 4.4. For example, at 100 days of exposure all mortar mixes exhibited reduced coefficients relative to the coefficients determined at day 7 of accelerated carbonation exposure. From a practical standpoint, the reliance of initial high carbonation coefficients of binary and ternary systems as a basis for increased cover depth to mitigate the progression of carbonation front towards steel reinforcement needs to be reconsidered in industrial standards.

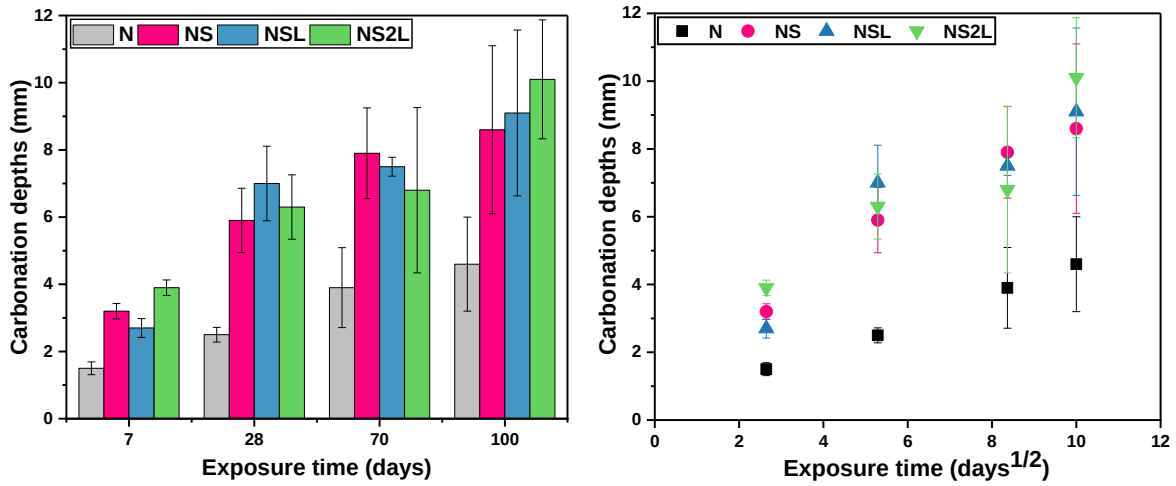

(a) (b)

Figure 4.5: Carbonation depth of mortars exposed to (a) accelerated carbonation up to 100 days. (b) Correlation between carbonation depth and the square root of time. The values reported correspond to the average of 16 readings (four per side), and error bars correspond to one standard deviation of all measurement

Table 4.3: Accelerated carbonation coefficient (mm*days$^{-0.5}$) of mortar prisms based on slope of linear regression in figure 4.5(b)

	Mix ID			
	N	**NS**	**NSL**	**NS2L**
Carbonation coefficient (mm*days$^{-0.5}$)	0.49 ± 0.02	1.12 ± 0.07	0.92 ± 0.04	0.98 ± 0.09
R^2	0.99	0.98	0.99	0.97

Table 4.4: Accelerated carbonation coefficient (mm*days$^{-0.5}$) of mortar prisms as a function of exposure time

Mix ID	**Exposure time (days)**			
	7	**28**	**70**	**100**
N	0.56	0.48	0.47	0.46
NS	1.21	1.11	0.94	0.86
NSL	1.01	1.31	0.90	0.91
NS2L	1.48	1.18	0.81	1.01

For both mortar prisms subjected to natural or accelerated carbonation exposure conditions, similar trends on the carbonation performances were identified, thus it would be expected that

some degree of dependency would exist between the two exposure methods. For estimating carbonation coefficients under natural exposure conditions considering carbonation coefficient determined in specimens exposed at higher [CO_2] concentrations, Equation 4.1 can be applied in accordance with Fick's law of diffusion (177).

$$\frac{K_{ACC}}{K_{NC}} = \frac{\sqrt{C_{Acc}}}{\sqrt{C_{NC}}} \qquad \textbf{Eq. 4.1}$$

*Where; K_{ACC} = Accelerated carbonation coefficient (mm*day$^{-0.5}$); K_{NC} = Natural carbonation coefficient (mm*day$^{-0.5}$); C_{ACC} = CO_2 concentration under natural carbonation(3%) ; and C_{NC}(mm) = CO_2 concentration under natural carbonation(0.04 % as adopted in (103))*

This was assessed by regression analysis as shown in Figure 4.6, where a good correlation (R^2 = 0.97) existed in the experimentally determined carbonation coefficients under ambient conditions versus accelerated carbonation exposure conditions.

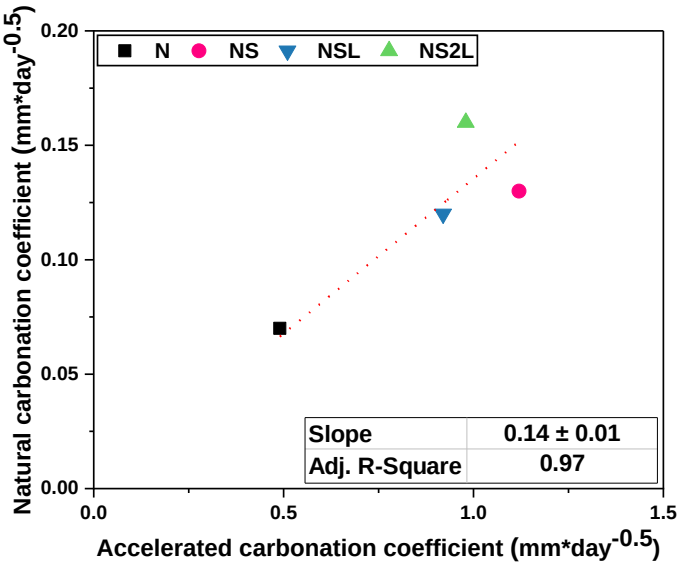

Figure 4.6: Comparison of experimentally determined natural and accelerated carbonation coefficients of mortar prisms

Table 4.5: Estimated natural carbonation coefficient from accelerated carbonation coefficient based on Equation 4.1

MIX ID	Measured (Experimental)*K_{ACC}	Measured (Experimental) *K_{NC}	Estimated K_{NC} from K_{ACC} at 3% [CO_2]
N	0.49 ± 0.21	0.07 ± 0.01	0.06 ± 0.02
NS	1.12 ± 0.07	0.13 ± 0.02	0.13 ± 0.01
NSL	0.92 ± 0.04	0.12 ± 0.01	0.11 ± 0.003
NS2L	0.98 ± 0.09	0.16 ± 0.02	0.11 ± 0.01

* K_{ACC} = Accelerated carbonation coefficient (mm*day$^{-0.5}$); K_{NC} = Natural carbonation coefficient (mm*day$^{-0.5}$)

Table 4.5 shows the estimated natural carbonation coefficients based on Equation 4.1. The estimated values are comparable to the experimental values and confirm the linear correlation between natural and accelerated carbonation coefficients for the mixes assessed, based on experimental data. The findings suggest that carbonation-induced changes (such as phase assemblage, and pore structure) of specimens exposed to accelerated carbonation are expected to be comparable to those in natural carbonation conditions. This is consistent with findings reported in other studies (100, 103), where naturally carbonated slag-blends exhibited similar phase assemblages to those identified in accelerated carbonated samples, and using comparable CO_2 concentrations of exposure to this study for each case.

4.3.3. Residual compressive strength of carbonated mortars

Figure 4.7(a-b) shows the variations in compressive strength post-natural or accelerated carbonation after 28 and 100 days of exposure. The compressive strength increased in CEM I mortar samples irrespective of the carbonation exposure conditions adopted or carbonation duration, consistent with what is known for Portland cement materials. For the composite binders, the compressive strengths were comparable at both exposure conditions, natural or accelerated carbonation at 28 days. Meanwhile, marginal increases in strength were observed for the composite binders at extended accelerated carbonation exposure times, relative to natural carbonation. When the strength evolution post-carbonation exposure are compared with the strength of the specimens cured for 28 days, all mortar mixes exhibit comparable or higher strength under both natural or accelerated carbonation. This indicates that hydration of CEM I and reaction of slag is occurring (albeit slow) in the non-carbonated regions of the specimens (49), leading to a continuous gain of strength. It was noted that the binary slags-based mortars exhibited a higher increase in the compressive strength than the ternary blended mortars after 28 days of natural or accelerated carbonation exposure, but with

prolonged carbonation, ternary blends similarly showed higher strength compared to those of 28 days cured specimens. The ternary blends also presented an increased strength close to the strength of 28 day cured reference (CEM I) mortar at 100 days of accelerated carbonation.

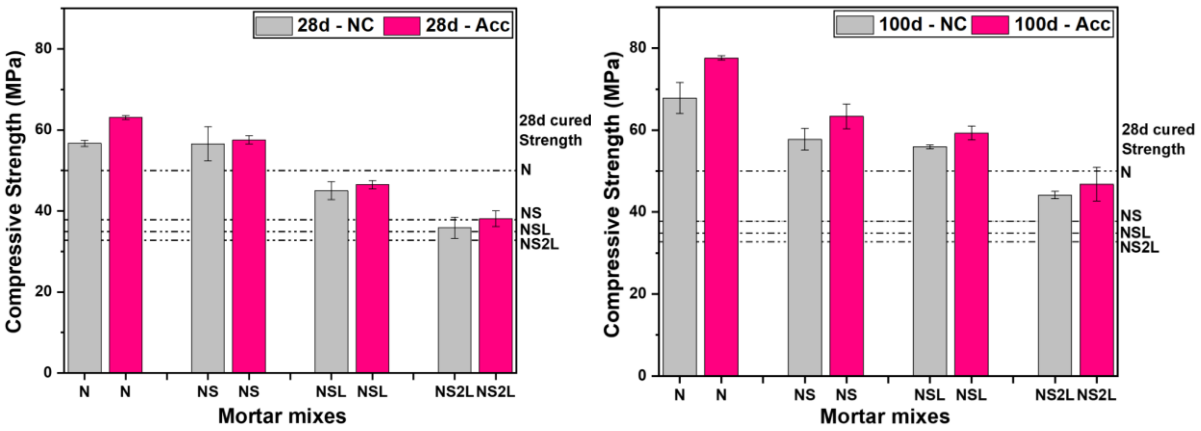

(a) (b)

Figure 4.7: Compressive strength of 28 days cured samples exposed to carbonation (a) 28 days natural or accelerated (b) 100 days natural or accelerated

The post-carbonated compressive strength will be influenced by the pore structural changes induced by carbonation and pore refinement due to ongoing hydration in the uncarbonated regions of the tested specimens. Results on the total porosity of carbonated mortars are discussed in Section 4.3.4.3 where no significant changes in the porosities were identified in accelerated carbonated mortar mixes relative to natural carbonated specimens. The correlation between the post-carbonation strength and water accessible porosity is reported in Figure 4.8, where a correlation is less apparent between the two properties considering that for similar values of porosity, significant differences in strength can be observed among the same mixes.

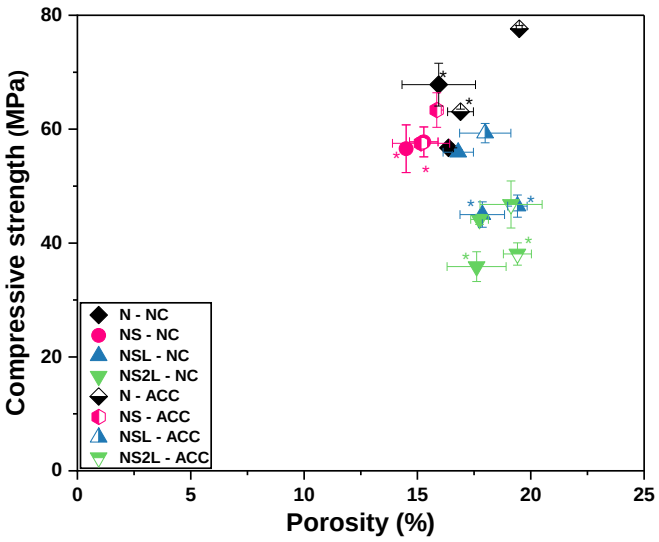

Figure 4.8: Correlation between porosity and compressive strength post 28 and 100 days natural (NC) or accelerated (ACC) carbonation exposure Note: Data points with or without asterisks (*) correspond to 28 or 100 days respectively]

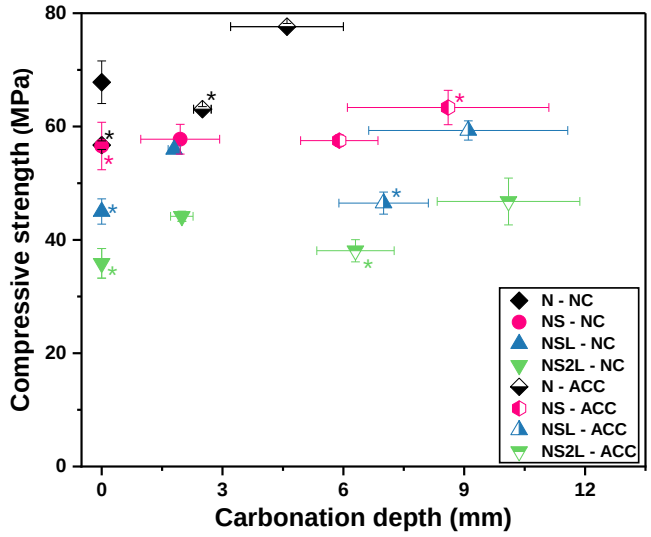

Figure 4.9: Relationship between carbonation depth and compressive strength post 28 and 100 days natural or accelerated carbonation exposure Note: Data points with or without asterisks (*) correspond to 28 or 100 days respectively]

Figure 4.9 shows that there is no direct correlation between the carbonation front and the residual compressive strength. This is particularly noticeable in samples exposed to natural carbonation conditions. Previous studies have identified similar results where it has been

suggested that for materials with compressive strength >40MPa there appears to be some degree of correlation between the compressive strength and carbonation depth (178).

Contrastingly, studies elsewhere reported nearly 50% reduction in compressive strength of slag mortars, but 30% increase in CEM I mortars post 11-15 weeks accelerated exposure (114). This discrepancy can be largely attributed to the use of mortar mixes with high slag replacement (75 wt.%) and 0.75 w/b ratio, relative to ~30 - 50% slag loadings and 0.5 w/b ratio used in the current study. The former case is expected to have a diminishing impact on strength development relative to mortar mixes used in this study.

4.3.4. Transport properties in partially carbonated specimens

4.3.4.1. Unidirectional carbonation performance of mortar cylinders

Figure 4.10 (a – b) shows the carbonation depths of cylinders subjected to unidirectional carbonation for assessing transport properties in carbonated mortar specimens. Similar trend of carbonation performance to the mortar prisms can be noticed, with all composite cement showing higher carbonation depth than CEM I. It is worth noting that, at 28 days natural exposure, carbonation depths < 0.5 mm were recorded unlike in the case of prisms specimens. This is potentially due to surface preparation effects such as using as-cut of cylinders unlike prismatic specimens where moulded or as-cast surface was used for carbonation exposure. Nonetheless, for corresponding carbonation ages of different specimen geometries where carbonation depths were recorded, the values are comparable (within error margins). This suggests that the adopted unidirectional carbonation exposure for cylinders aligns with standardised methods of exposure for prisms. The natural carbonation exposure was carried out for similar duration as accelerated carbonation, and under the same RH [57±3 %] and T [20 ^{o}C] conditions. Therefore, it is expected that the natural carbonation exposure values would serve as reference to elucidate the impact of CO_2 concentration exposure alone. It was expected that natural or accelerated carbonated specimens will reach a comparable degrees of hydration, and consequently comparable initial porosities and degrees of internal saturation, only influenced by the reaction of CO_2 with the hydration products (under accelerated carbonation conditions).

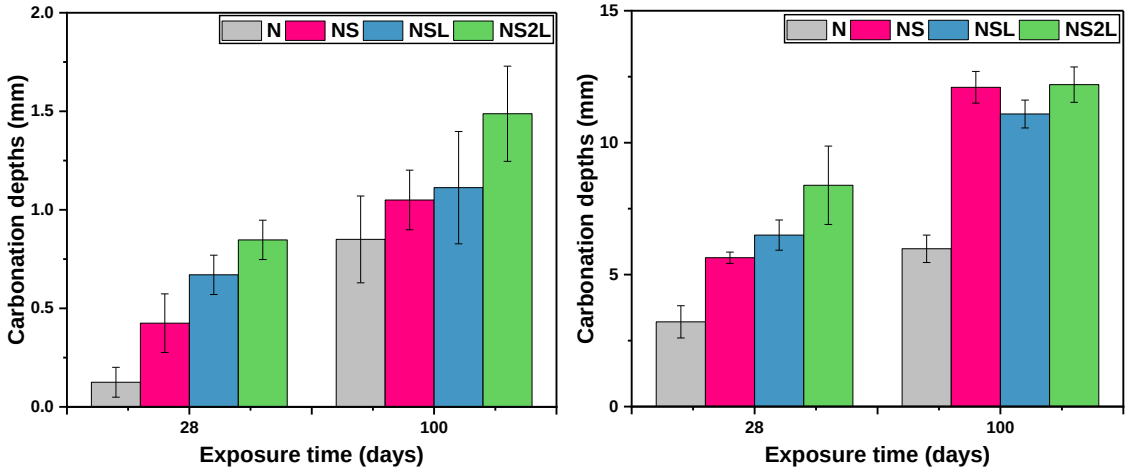

(a) (b)

Figure 4.10: Carbonation depth of mortars (cylinders) exposed to (a) natural or (b) accelerated carbonation. Error bars correspond to one standard deviation of 8 readings (four measurements per each half of axially split cylinder)

4.3.4.2. Water absorption properties of partially carbonated mortars

Figure 4.11(a-d), shows the sorptivity profile of partially carbonated (ambient and accelerated) cylindrical mortars. The sorptivity coefficient (based on the slope of initial linear portion of sorptivity profile) and total water absorption provides a quantitative indication of water absorption properties, as shown in Table 4.6 and Table 4.7 respectively. Analysing the sorptivity coefficients for all mixes, it can be seen that CEM I exhibits an evident reduction in coefficients after 100 days carbonation relative to 28 days, irrespective of the exposure type. For NS, NSL and NS2L, slight increases (within error margins) in sorptivity coefficients are observed at 100 days natural carbonation exposure relative 28 days. Meanwhile reduction in the sorptivity coefficient are observed post 100 days accelerated carbonation relative to 28 days accelerated carbonation, similar to observation of CEM I under post accelerated exposure. Accelerated carbonation generally resulted in an increase in sorptivity coefficients (with error margins) relative to ambient carbonation at 28 and 100 days for NS, NSL and NS2L. Meanwhile, CEM I exhibited a reduction or comparable coefficients under accelerated carbonation relative to ambient exposure. For CEM I based mortars, the reduction in sorptivity coefficient after prolonged accelerated or natural carbonation exposure can be attributed to the densified carbonation layer forming in these materials impeding water admissibility in the capillary pores (179). It is interesting to note that, the accelerated carbonation depth of CEM I at 100 days is comparable to the 28 days carbonation depth (accelerated) of composite

binders, and appears to present comparable sorptivity coefficients, however, as the accelerated carbonation front progressed in the composite mortars, no detrimental changes in the sorptivity coefficients is observed. A similar impact on total water absorption can be seen in Table 4.7, where even though prolonged carbonation resulted in slight increases (within error margins), particularly under accelerated carbonation, the highest increase was < 6.5%. The observed less detrimental influence of increased carbonation front progression on sorptivity coefficient in NS, NSL and NS2L appears to conform to carbonation-blocking effect known to account for reduced water absorption characteristics in CEM I (180). The blocking-effect plausibly influences the characteristics of NS, NSL and NS2L, based on the likelihood of incomplete decalcification in the slag-containing mortars with or without limestone. Although carbonation is expected to modify the pore structure of slag-containing mortars, it is possible that the continuous development of tortuous capillary pore network in the uncarbonated areas, as cement hydration progresses (181), contributes to reduce the overall water penetration in the partially carbonated mortars.

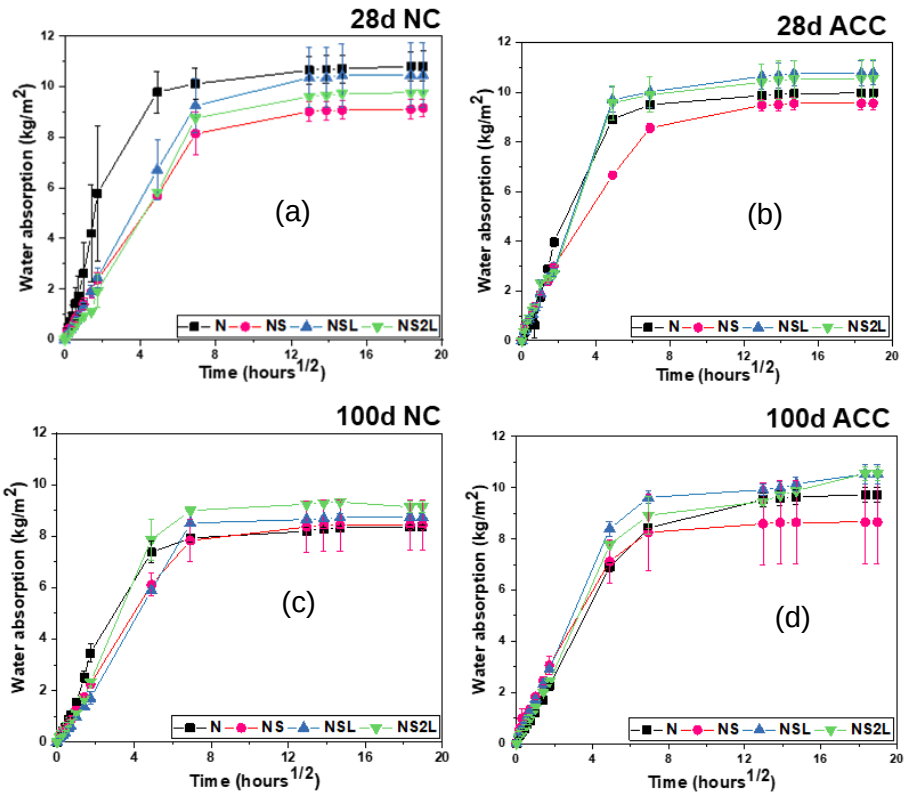

Figure 4.11: Sorptivity profiles of mortar mixes after (a) 28days natural (b) 28days accelerated (c) 100days natural (d) 100days accelerated carbonation. Error bars correspond to one standard deviation of two curves

Table 4.6: Sorptivity coefficients ($kg*m^{-2}*h^{-0.5}$) of partially carbonated cylindrical mortars

	Natural carbonation		Accelerated carbonation	
Mix ID	**28 days**	**100 days**	**28 days**	**100 days**
N	1.57 ± 0.11	1.25 ± 0.06	1.51 ± 0.01	1.26 ± 0.01
NS	1.04 ± 0.11	1.16 ± 0.16	1.22 ± 0.03	1.21 ± 0.28
NSL	1.30 ± 0.29	1.23 ± 0.01	1.58 ± 0.12	1.45 ± 0.06
NS2L	1.02 ± 0.01	1.41 ± 0.08	1.55 ± 0.16	1.37 ± 0.15

Table 4.7: Total water absorption (%mass) of partially carbonated mortars

	Natural carbonation		Accelerated carbonation	
Mix ID	**28 days**	**100 days**	**28 days**	**100 days**
N	7.12 ± 0.20	7.39 ± 0.08	7.38 ± 0.20	7.87 ± 0.79
NS	6.34 ± 0.10	6.57 ± 0.31	6.51 ± 0.56	6.96 ± 0.10
NSL	7.72 ± 1.01	7.22 ± 0.18	8.26 ± 0.28	7.85 ± 0.65
NS2L	7.56 ± 0.48	7.59 ± 0.16	7.88 ± 0.35	8.49 ± 0.38

4.3.4.3. Changes in open porosity of carbonated mortars

Figure 4.12(a-b) shows the vacuum saturated open porosity (%) of oven-dried mortars after 28 days and 100 days of carbonation. There was no significant increase in the open porosity of mortar specimens after 100 days of natural carbonation compared to 28 days of carbonation. Slight increases are observed in samples exposed to accelerated carbonation for a similar exposure duration, particularly in the case of ternary blends where there appears to be a ~7% increase in the post-accelerated carbonation relative to the naturally carbonated mortars at 28 days. However, the porosity changes between 28 days and 100 days accelerated carbonation are comparable for all the ternary cements evaluated. NS exhibited slightly reduced porosity under both exposure conditions and exposure durations relative to the ternary blends, but at higher CO_2 exposure times, the porosities are comparable (within error margins). Overall, there is no indication of detrimental variations on the water accessible porosity induced by accelerated carbonation in the slag-containing mortars with or without limestone compared to CEM I.

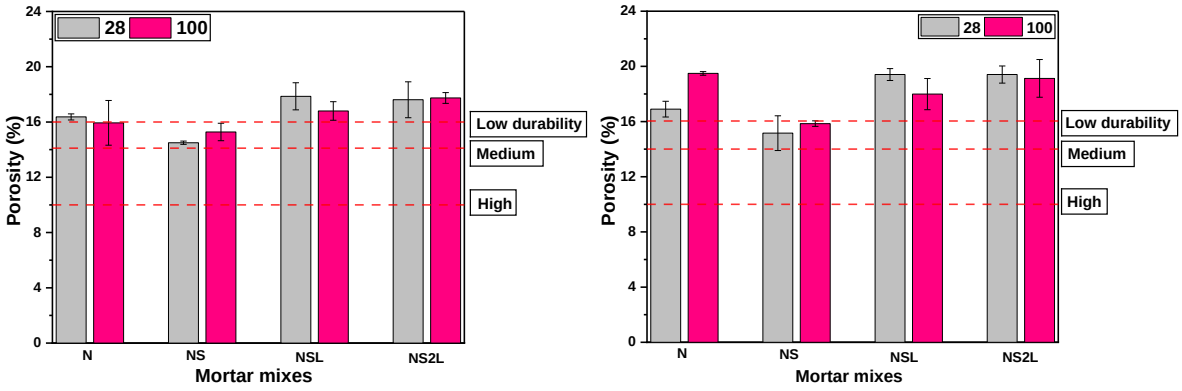

Figure 4.12: Porosity of mortars exposed to (a) natural or (b) accelerated carbonation, as a function of the exposure time. Error bars correspond to one standard deviation of two measurements. Dashed lines correspond to the durability classification proposed by Baroghel-Bouny et al (182).

Based on the Baroghel-Bouny et al (182) performance based durability indicators of cementitious systems, naturally carbonated N and NS mixes can be classified as materials of 'medium durability', while the ternary composite cements based mortars can be categorised as having 'low durability'. All mortar mixes are classified as of low durability after prolonged accelerated carbonation exposure. The increase in porosity due to carbonation is expected in the slag-blended systems (112, 113), the uncarbonated regions can exhibit increased capillary pore volumes, even though their overall pores are expected to be refined, particularly in the ternary blends as observed in (65). Thus the 'net porosity' (difference between carbonated and non-carbonated region) is expected to be relatively greater in the ternary mixes, as the test essentially reports the water-filled capillary porosity. It must be acknowledged that the contribution of increased pore volumes to higher porosities does not necessarily translate into reduced compressive strength as reported in (65). This likely supports the lack of correlation between accelerated carbonation and compressive strength (Figure 4.9).

No direct correlation between the total porosity and the sorptivity coefficient is identified as shown in Figure 4.13. Additional studies analysing pore size distribution are necessary to further understand how the pore structure features of the materials assessed might be influencing the CO_2 diffusivity, and consequently the carbonation progress. Mercury intrusion porosimetry is commonly used for analysing pore size distribution. However, the recommendation of deriving ≤ 6.5 mm^3 test pieces from bulk samples (183), and the potentially damaging impact of applied mercury intrusion pressure on pore structure, particularly for blended systems (184) also cast doubt on the reliability of such techniques.

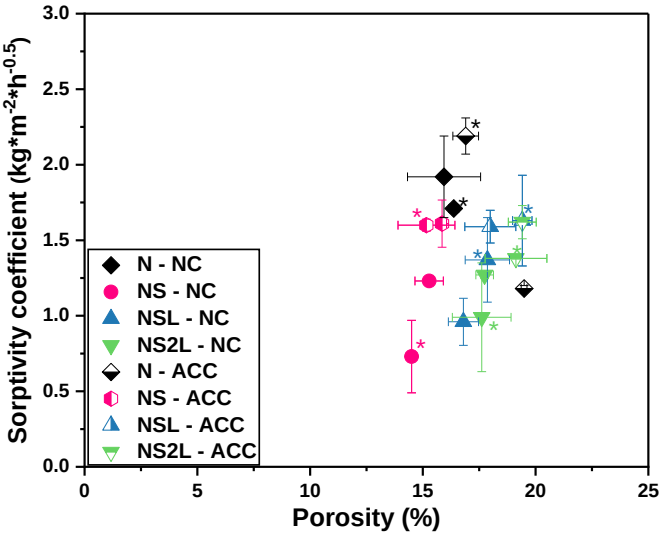

Figure 4.13: Correlation between sorptivity coefficient and porosity of mortar mixes post 28 and 100 days natural or accelerated carbonation exposure Note: Data points with or without asterisks (*) correspond to 28 or 100 days respectively]

4.3.4.4. Bulk conductivity of partially carbonated mortars

Electrical responses change due to microstructural development gives insight into the bulk properties of hardened cementitious material, including total porosity, pore connectivity, pore fluid ionic strength and dielectric properties of the material. It is believed that the pore volume and pore connectivity are the main parameters that influence the bulk conductivity response (185). Thus, electrical response such as conductivity/resistivity can be a very useful indicator of physical structure and resistance to ionic movement within the hydrated cement matrix depending on the binder chemistry and water-binder ratio. Higher resistivity (i.e., lower conductivity) implies discontinuities, or tortuosity of microstructure and vice–versa (186, 187)

In Figure 2.14(a-b), the bulk conductivities of mortar specimens post-natural carbonation are reported. Comparable results for 100 days and 28 days of carbonation exposure are observed, suggesting no significant variations in pore connectivity taking place. This is somehow consistent with the porosity results in Figure 4.12, where negligible changes in total porosity were observed among the specimens (per mix type) upon carbonation. All composite binders based mortars showed three times lower bulk conductivity compared to CEM I, indicating better resistance to ionic ingress. Comparing Figure 2.14 (a) and (b), the bulk conductivity after 28 days accelerated carbonation compares with that of ambient carbonation exposure, even though increased carbonation depths were recorded under accelerated conditions.

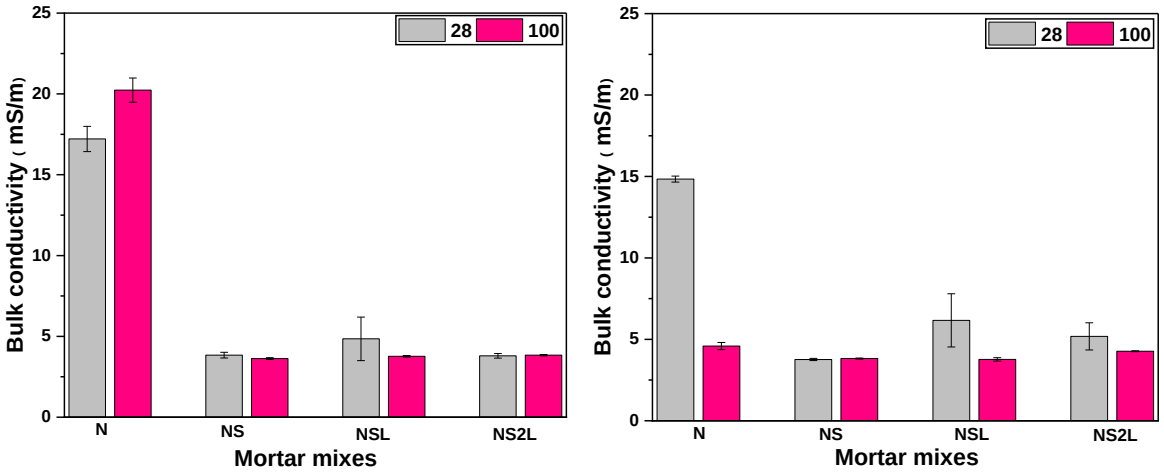

(a) (b)

Figure 4.14: Changes in bulk conductivity post 28 and 100 days of exposure to (a) natural carbonation or (b) accelerated carbonation

It is interesting to note that with the increased carbonation depth after 100 days upon exposure to accelerated carbonation, the bulk conductivities were nearly at parity for all mortar mixes, so that the bulk conductivity of CEM I reduced significantly to comparable levels of the composite cements. While densification of CEM I due to carbonation may be attributable to high resistivity (or reduced conductivity), this reason may not apply to composite binders, as low clinker cement is known to induce coarsening of pore structure during carbonation (188). However, in addition to the findings of less detrimental impact of carbonation on residual strength and the net porosity (difference between carbonated and non-carbonated region) on the composite binders post accelerated carbonation, the lower bulk conductivities suggest that, it is likely the porosity of uncarbonated sections whose microstructure is expected to be more refined than carbonated areas positively contributes to the overall properties of the material, despite experiencing higher carbonation depth.

Figure 4.15 shows that there is no correlation between carbonation depth and bulk conductivity. It is then hypothesised that faster carbonation taking place in composite cements, leading to calcium carbonate polymorphs formation and its precipitation in the pore structure, might mitigate the coarsening of the pore structure. Further studies need to be conducted interrogating the pore size distribution changes upon carbonation of the materials evaluated.

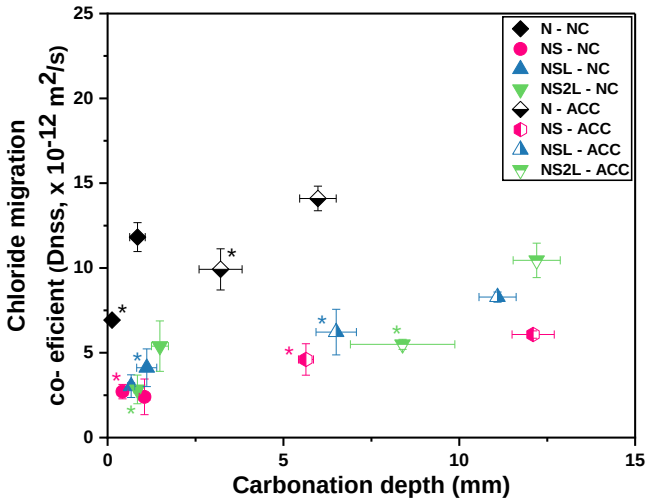

Figure 4.15: Correlation between bulk conductivity vs carbonation depth mortar mixes post 28 and 100days natural carbonation (NC) or accelerated carbonation (ACC). Note: Data points with or without asterisks (*) correspond to 28 or 100 days respectively]

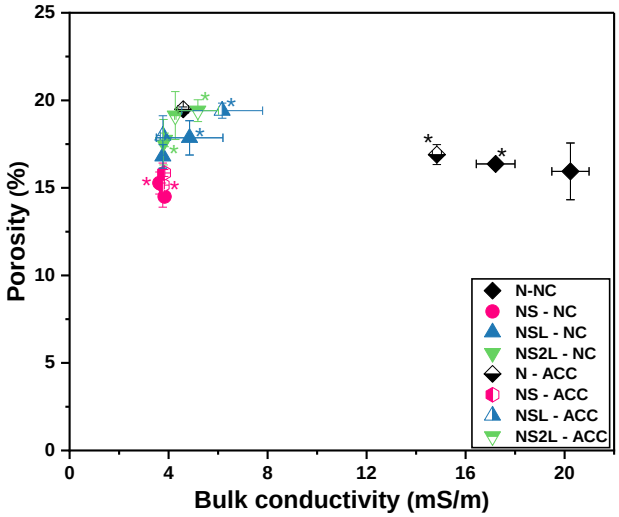

Figure 4.16: Correlation between porosity and bulk conductivity of mortar mixes after 28 and 100 days of natural carbonation (NC) or accelerated carbonation (ACC). Note: Data points with or without asterisks (*) correspond to 28 or 100 days respectively]

Similarly, no correlation between bulk conductivity and porosity was identified (Figure 4.16), and this indicates that the bulk conductivity is not an appropriate measurement for inferring the performance of the carbonated specimens evaluated in this study. That notwithstanding, a lower scatter exist in the natural carbonation data points than accelerated exposure conditions. While both open porosity and bulk conductivity can be related to physical changes

of the pore structure, it has been reported that bulk conductivity measurements are strongly influenced by the chemical composition of the pore solution of the materials evaluated (189). This seems to be the case here, and therefore the results cannot be interpreted as a sole representation of the pore structure of the material.

4.3.4.5. Effect of carbonation on chloride permeability of mortars

The chloride permeability of mortars post 28 days and 100d days of natural or accelerated carbonation exposure are shown in Figure 4.19 (a-b). It is identified that slag-containing mortars with or without limestone show reduced permeability to chlorides than CEM I, irrespective of their high carbonation depths recorded for those mixes. The implications of carbonation on chloride migration coefficient values is more evident after accelerated carbonation (Figure 4.19(b)) when compared to the impact of natural carbonation (Figure 4.19(a)), where an increase in chloride permeability for all mixes post-accelerated carbonation relative was observed. While mortars with 20 wt.% limestone (NS2L) addition exhibited the highest increase in accelerated carbonation depths (~ three fold greater than CEM I) and a net change in chloride migration coefficients at advanced carbonation exposure times (relative to 28 days), its resistance to chloride permeability remains higher than CEM I, and comparable to NSL.

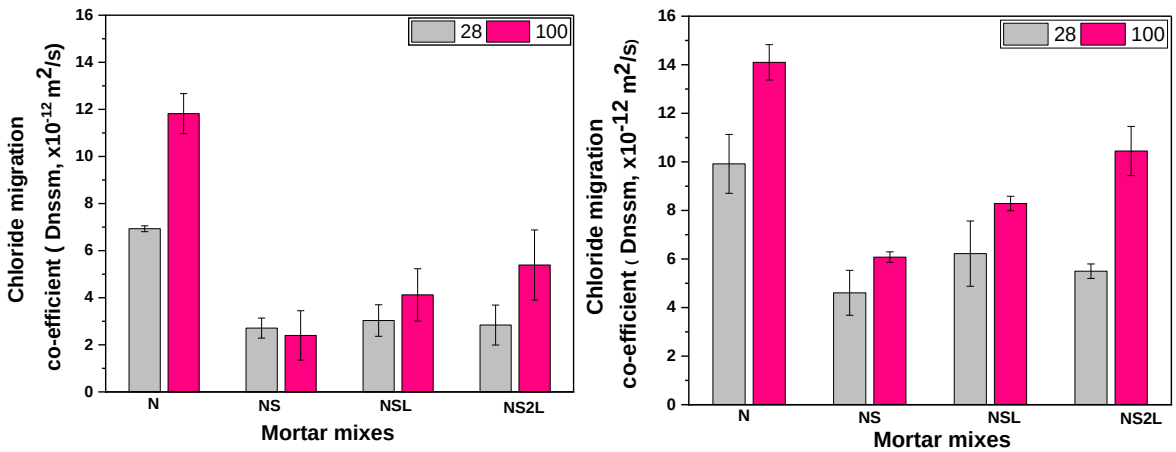

Figure 4.17: Chloride permeability of mortar mixes after 28 and 100 days exposure to (a) natural carbonation or (b) accelerated carbonation

The addition of slag in blended cement is known to improve chloride resistance due to the chloride binding capacity of alumina bearing hydrates including C-(A)-S-H, hydrotalcite like phases, AFm phases and potentially AFm-CO_3^{2-} phases (190-192). It is hypothesised that chemical binding of these phases, particularly in the uncarbonated region is likely contributing to improve the resistance to chloride migration in the slag-containing mixes with or without limestone. In Figure 4.18(a), it is identified that, it there seem not to be a correlation between porosity changes post natural carbonation and chloride permeability particularly in accelerated carbonation exposure samples. Equally no clear correlation between carbonation front progression and chloride permeability is observed (Figure 4.18(b)), independently of the exposure conditions. These suggest that neither porosity nor carbonation progress would be good predictors of chloride permeability performance of slag-containing mixes, due to the chloride binding ability of such mixes.

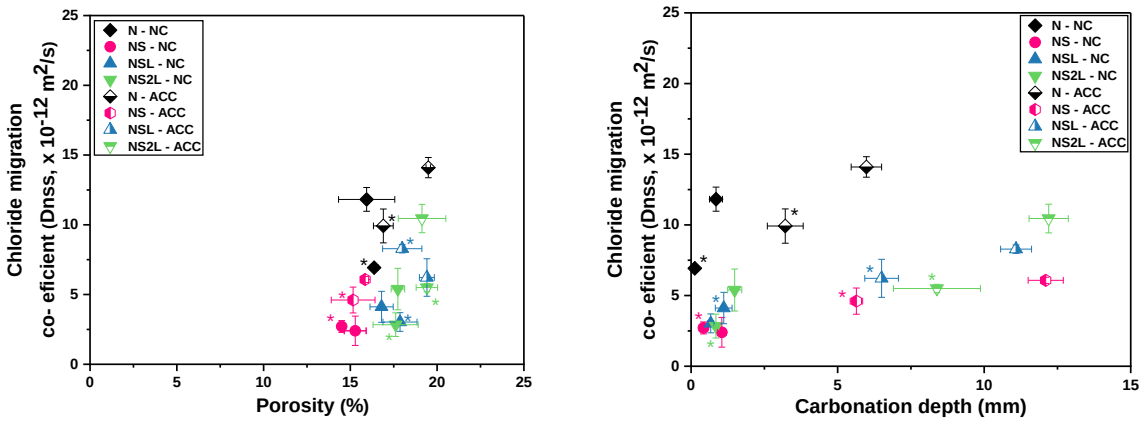

(a) (b)

Figure 4.18: (a) Chloride permeability Vs porosity of mortar mixes after 28 and 100 days of natural/accelerated carbonation, and (b) Chloride permeability Vs Carbonation depth. Note: Data points with or without asterisks (*) correspond to 28 or 100 days respectively]

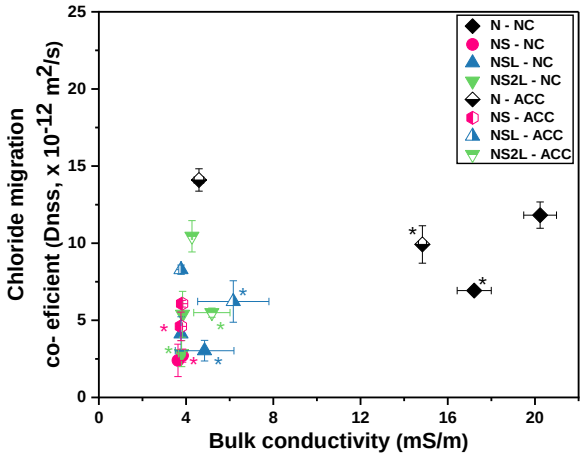

Figure 4.19: Correlation between chloride migration co-efficient and bulk conductivity of mortar mixes post-natural (NC) and accelerated (Acc) carbonation. Note: Data points with or without asterisks (*) correspond to 28 or 100 days respectively]

Furthermore, no correlation between the chloride migration and bulk conductivity is observed (Figure 4.19) either. Although the bulk conductivity of CEM I at 100 days of exposure to accelerated carbonation suggested similar pore connectivity to composite mortars, it did not translate into similar resistance to chloride ingress.

4.4. Conclusions

In this study, the carbonation resistance, and the influence of partial carbonation on transport and durability properties of slag-blended cement based mortars, with and without limestone addition, were investigated. From this study the following conclusions can be drawn.

1. The compressive strength of mortars made of binary slag and ternary slag limestone is comparable to that of CEM I at later curing ages. Mortars with 20 wt.% limestone additions achieve nearly 80% of CEM I strength by 180 days. All composite cements with slag-limestone combination showed continuous development in compressive strength at extended curing times.

2. The carbonation performance of ternary slag limestone blends compares with that of the binary slag cement; while all composite binders show increased carbonation rates relative to CEM I. Despite the high carbonation depths recorded for NS2L, the residual compressive strengths are comparable at 28 days of carbonation exposure for both natural and accelerated carbonation. It is worth noting that slight increases in strength

are observed for the composite binders at 100 days of 3% CO_2 exposure relative to natural carbonation. Such gain in strength cannot be explained considering the porosity of these materials, as the total porosity values are comparable.

3. It is identified that, independently of the relatively higher carbonation depth, slag-containing mortars (with or without limestone) exhibited significantly lower chloride migration coefficients and generally lower bulk conductivities compared to CEM I.

4. Carbonation of mortars influences the initial water absorption properties. The sorptivity coefficient and open porosity of slag-containing mortars with/without limestone do not seem to be significantly impacted by carbonation relative to CEM I. This was an unexpected result given that coarsening of the porosity is expected in blended cements due to carbonation. This might be associated with the tests adopted in this study for indirectly evaluating porosity, and therefore further studies determining pore size distribution of the samples evaluated using techniques that permit the use of representative test pieces relative to the bulk samples from which they are derived.

5. There is no direct correlation between open porosity, strength or bulk conductivity and carbonation depth progress, therefore carbonation performance of slag composite cements cannot be directly inferred from such properties.

6. There is a very good correlation between the natural and accelerated carbonation coefficients calculated based on Fick's law equation and thus gives an indication such correlation can be used for predicting carbonation depths of mortars at different natural exposure times

Overall, it can be concluded that the increased addition of limestone powder to ternary slag-cements leads to comparable performances to that obtained in binary slags mortars, prior and after carbonation exposure. Increased limestone addition resulted in comparable carbonation rates to those of binary slag cement mortars. Even though slag-containing mortars, with or without limestone exhibited inferior carbonation resistance to CEM I, the effects of carbonation-induced pore structural changes are not detrimental to their water absorption and chloride permeability relative to CEM I.

Chapter 5.

5. Engineering and durability properties of Portland cement-slag-limestone composite concretes

5.1. Introduction

There is an increased motivation to reduce the clinker factor in cement and concrete towards curtailing the carbon footprint in the construction industry, and to meet net zero targets (27, 193). One of the strategies adopted to achieve this is by increasing the limestone content in cements, and moving from binary cementitious systems towards multicomponent cements often formulated with reduced clinker contents, SCMs and limestone (3). The improvement in mechanical and durability properties due to limestone addition has been extensively explored in Portland limestone or ternary blends with SCMs. However, the general consensus has been limited to lower levels of limestone addition for assured in-service performance (194, 195). The synergistic benefit of limestone addition in the improvement of hydration kinetics through the provision of additional nucleation sites for clinker and/or slag hydration, as well as its influence on microstructure related properties, has received considerable attention (40, 62, 63, 65). The contribution of limestone in enhancing slag hydration kinetics has been shown to be beneficial in cement with reduced slag content in lieu of increasing limestone powder addition (40, 65). However, these CEM VI cement with high volume replacement of Portland cement with slag and limestone lack an in-service track record. There exist limited studies in the literature on their concrete applications compared to neat and binary slags cement (17, 60, 110). A significant knowledge gap still exists in understanding the evolution of the engineering and durability properties of these concretes. Such knowledge will create the confidence for practitioners to adopt these materials in real practice, and will enable the identification of the potential performance of these materials, considering different exposure

classes imposed by standards. This is essential for their widespread acceptance for their use in structural concrete in critical infrastructure. The reduced amount of available data on some mechanical performance relationships as per existing design codes needs to be validated.

This study reports the mechanical properties, moisture ingress, chloride permeability and electrical resistivity of low carbon concretes made with CEM I and slag-blended composite cements with or without limestone (up to 20 wt.%). The results demonstrate that reducing slag content by adding 10-20 wt.% limestone does not have a significant impact on the mechanical or durability properties of concretes, compared to binary slags and/CEM I concretes.

5.2. Experimental procedures

5.2.1. Concrete mixing and design

The binder content for all the concrete assessed was maintained at 320.3 kg/m^3 which conforms to the limiting values of concrete composition as prescribed by BS EN 206-2021 [in Table F.1 of standard] (73) suitable for carbonation-induced corrosion (XC1-4) and chlorides exposure classes XS (1-2) and XD (1-3). The mix design was developed on volumetric basis, so that cement/binder content as well as the ratio of water-to-binder is kept constant at 0.5. All concrete mixes in this study were moist room cured until testing.

5.2.2. Fresh state properties

The flow properties of all concrete mixes were determined following standardised procedures for slump, flow testing (spread), air content and density as expounded in Chapter 3, Section 3.4.3 and 3.4.4.

5.2.3. Assessment of the mechanical properties of concrete

5.2.3.1. Compressive and flexural strength

Compressive strength evolution of all concrete mixes was determined after 2, 7, 28, 90 and 180 days of curing, on 100 mm cubes in triplicates, as per BS EN 12390-3:2019 (157) standard, applying a load of 6 kN/s. Flexural strength of all concrete mixes was determined

on 100 × 100 × 400 mm prismatic specimens in duplicates, tested at 0.2 kN/s in accordance with BS EN 12390-5:2019.

5.2.3.2. Poisson ratio, static and dynamic modulus of elasticity

Two Ø100 × 200 mm cylindrical specimens were used for the determination of static elastic modulus, and the estimation of Poisson ratios. The preparation of samples for testing and the test procedure are described in Section 3.5.2. Additionally, triplicate 100 mm cubes were monitored for the transit time after 2, 7, 28, 90 and 180 days using a Proceq Pundit PL-200PE test kit equipped with 250 kHz compressional wave transducers. Also, the mass of the three concrete cubes per mix was measured as per BS EN 12390-7: 2019 (162), from which concrete density at testing could be determined as the ratio of measured mass to dimensional volume.

5.2.4. Assessment of the durability properties of concrete

5.2.4.1. Water absorption rate/sorptivity and porosity

Capillary water absorption was conducted in accordance with BS EN 13057:2002 (89) on three cylindrical specimens with a thickness of 50 ± 10 mm and sawn from two (100Ø × 200) mm cylinders at ages 28, 90 and 180 days. The mass changes were determined at predefined times up to 15 days. After the sorptivity test, specimens were vacuum saturatured in water for 24 hours from which the porosity is calculated using the ratio of their weight (%) changes to volume similar to procedure adopted in (173).

5.2.4.2. Resistance to chloride permeability and bulk conductivity

Chloride permeability in concretes was studied on three concrete specimens (100Ø × 50 mm) sawn from central portions of two 100Ø × 200 mm cured cylinders; following the Nordtest NTBUILD 492 chloride migration test (93). For bulk conductivity, the samples to be tested for chloride migration as described above were initially subjected to a potential of 60 V for a period of 60 s, from which values of bulk conductivity (mS/m) was recorded using a PROOVE'it equipment. The automated bulk conductivity test was recorded according to the ASTM 1760 (169) standard.

5.2.4.3. Surface resistivity of concrete

The surface resistivity development was measured on 100Ø × 200 mm cylinders using a handheld Proceq resipod device. A total of 9 readings were taken per cylinder per concrete mix, and the test was conducted on two cylinders immediately after taking out of the moist room.

5.3. Results and discussion

5.3.1. Fresh state properties

The fresh state properties of the concrete mixes are summarised in Table 5.1. It is noted that addition of limestone in the ternary blends slightly improved workability compared to the binary slags, as reflected in the consistency and the flow diameter. The slump and flow classes conform to S4 and F4 respectively as per the BS EN 206:2013+A2:2021 (73). These results are consistent with the fresh properties reported for similar concrete mixes prepared with the finer CEM I 52.5 R cement (60). Overall, the fresh properties including the air content, are comparable to the CEM I concrete, which can be attributable to relatively similar fresh state densities. However, these characteristics would largely be influenced by the relative fineness of the binders and reactivity indices of the slags. Ambient temperature conditions can also influence these properties.

Table 5.1: Fresh state properties of concrete mixes.

Mix ID	Slump (mm)	Slump class	Flow diameter (cm)	Flow class	Air content (%)	Density (Kg/m^3)
N	185		52		1.2	2330
NS	170		48		1.1	2350
NSL	190	S4	54	F4	1.5	2330
NS2L	180		50		1.2	2340

5.3.2. Mechanical performance

5.3.2.1. Compressive and flexural strength

The compressive strength evolution of the concrete mixes after curing ages up to 365 days is shown Figure 5.3(a) for the evaluated concretes. Binary and ternary concrete showed significantly lowered strength (40% reduction) at 2 days of curing compared with CEM I, albeit still meeting typical target strengths criteria of ~10 MPa for formworks removal in construction practice (15, 168). However, continuous strength gain is observed for all concrete mixes at later ages. It is worth noting that, the replacement of slag with limestone had smaller effect on the strength values, particularly after 28d curing. The strength ratios ($f_{cm,2}/f_{cm,28}$) obtained for composite binders (0.3 – 0.4), and CEM I (0.6) show medium and rapid development respectively (73). All composite concretes approached strengths closer to CEM I strength by 28 days and progressively increased towards 365 days; at 28days, NS, NSL and NS2L achieved ~84, 75 and 78 % of CEM I strength, and with further curing time to 180 days, those mixes reached 92, 84 and 80 % strength respectively. There is no marked difference in the strength of ~10 wt.% or ~20 wt.% limestone-added ternary blends, demonstrating the limited dilution effects arising from increased limestone addition. The trend of compressive strength observed here is consistent with what has been reported for the same age of curing of similar mixes and water binder ratio, where ~20 wt.% limestone additions show lower compressive strength to CEM III/A and CEM I (17, 60). Meanwhile, it is also identified that the strength evolution conforms to mortar mixes under curing conditions as discussed in 4.3.1.

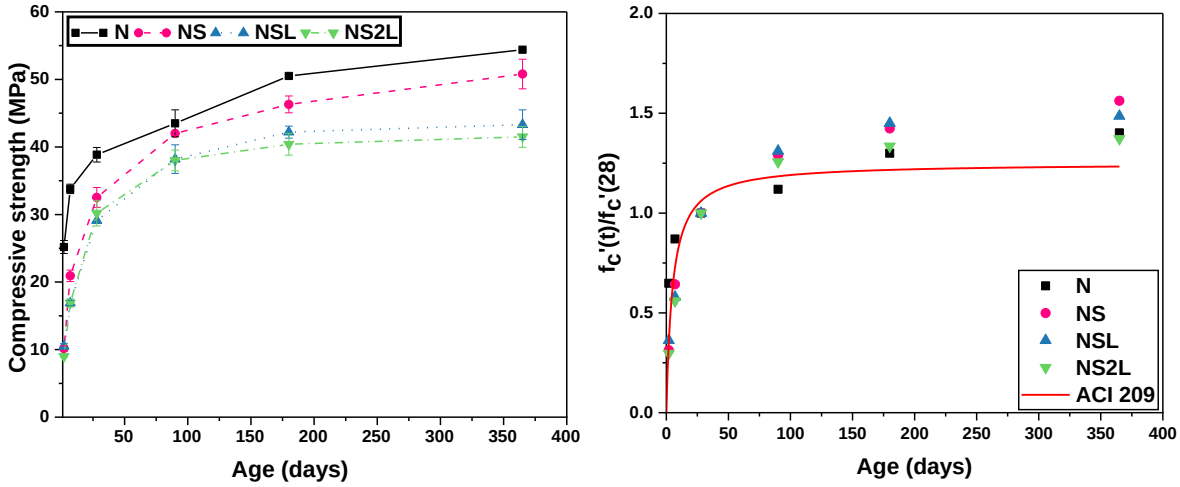

(a) (b)

Figure 5.1: (a) Compressive strength development of cured concrete mixes (error bars corresponds to one standard deviation of three measurements), (b) Comparison of strength

ratios with ACI 209 prediction models (strength is based on cube converted strength; cylinder strength (experimentally determined) = 0.8 * cube strength)

Models exist for time-dependent prediction of compressive strength, such as the ACI 209R-92 (196), which is an empirical model that can be described in Equation 5.1. This relationship considers the strength ratio for any curing time t to the 28 days strength.

$$\frac{f_c'(\mathrm{t})}{f_c'(28)} = \frac{t}{\alpha+\beta t} \qquad \textbf{Eq. 5.1}$$

where; $f_c'(t)$ = compressive strength of concrete at any time t; $f_c'(28)$ = mean 28 days compressive strength (cylinder), and α, β = constants depending and cement and curing type, and appears not to be affected by aggregate (all-light weight, normal weight, and sand lightweight) type.

For a 150Ø x 300 mm cylinder, the model recommends constant values of α = 4, β=0.85 for moist room cured type 1 cement. Assuming the model is valid for the ternary and binary mixes, the strength ratios of experimental compressive strength at all ages, in comparison to ACI 209R-92 strength ratios are shown in Figure 5.3(b). It can be seen that CEM I shows slightly higher strength ratios at the early curing ages, while the slag-containing concretes with or without limestone exhibited lower strength ratio than that predicted by the ACI 209R-92. At 28 days and 90 days of curing, CEM I concrete conforms to the ACI-209 with a significant increase thereafter, demonstrating that this relationship underestimates the strength gain of such concrete beyond 90 days of curing. In the case of NS, NSL and NS2L, progressively higher strength ratios from 28 days than CEM I are observed. The early age characteristics as predicted by ACI-209R-92 agrees with the BS EN 206:2013+A2:2021 (73) classification of strength development based on the strength ratios ($f_{cm,2}/f_{cm,28}$). Thus, while the composite cements show lower early age strength development, after 28 days their rate of strength development progressively exceeds that of CEM I.

The flexural strength of 28 and 180 days cured samples reported in Figure 5.2 shows that the composite concrete exhibit comparable strength to CEM I at early (28 days) and at extended curing ages. The contribution of slag in improving flexural strength of concrete is consistent with the findings of Khatib and Hibbert (53). It does appears that the replacement of slag content with up to 20 wt.% limestone has no adverse impact on the ternary blends, as flexural strength is improved at later ages relative to binary slag levels.

The comparable performance under bending loads of the concrete assessed, despite the different compressive strengths recorded, can be attributable to refined microstructure due to

secondary hydration or better packing density relative to CEM I, particularly around the more porous interfacial transition zone (ITZ) (38, 197). Thus, an improvement in the bond strength of ITZ in NS, NSL and NS2L is likely to contribute to their flexure strength performance, particularly for NSL and NS2L at later curing ages. However, this needs to be evaluated. It must be noted that BS EN 12390-5:2019 (159) currently does not provide precision data for this test method, however, the error (%) for duplicate samples tested in this study lies between 4 to 15%.

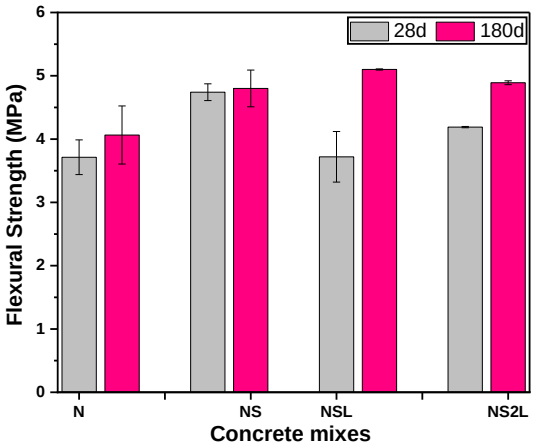

Figure 5.2: Flexural strength evolution of cured concrete prisms (error bars correspond to one standard deviation of two measurements).

5.3.2.2. Empirical and experimental relationship between compressive strength and flexural strength

Design codes, standards and researchers have proposed different approaches to estimate flexural strength from the compressive strength of concrete using analytical relationships. For emerging concretes produced with ternary blended cements, it is important to ascertain the extent of over/under estimation when using these equations to determine their applicability. Figure 5.3 shows experimentally determined flexural strengths in comparison with those estimated values using empirical equations (shown in Table 5.2) using experimentally determined 28 and 180 days compressive cylindrical strengths as input.

Table 5.2: Empirical equation for flexural strength prediction from compressive strength

Design code	Equation (MPa)	Reference
ACI 318 – 19	$Fr = 0.62 * \lambda * (f'_c)^{0.5}$; $\lambda = 1.00$	(67)
CSA A23.3-04	$Fr = 0.6 \lambda (f'_c)^{0.5}$; $\lambda = 1.00$	(198)
NZS 3101:1-2006	$Fr = 0.6 \lambda (f'_c)^{0.5}$; $\lambda = 0.85$	(199)

Where F_r is the flexural strength f'c is the compressive strength and λ is constant based on composition of aggregates or equilibrium density of concrete [normal weight concrete in this case]

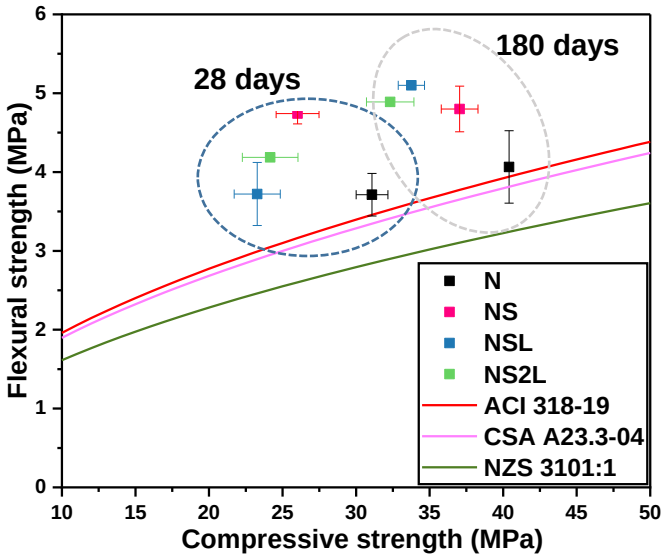

Figure 5.3: Plot comparing experimentally determined flexural strength values, with code predicted equations

The results in Figure 5.3 show that all the concrete mixes assessed conform to the ACI 318-9 and the CSA A23.3-04, while the NZS 3101:1 slightly underestimates, which are safe to use for predicting the values of flexural strength achieved by binary and ternary slag concretes. Overall, this suggests that concrete made from slag composite cement with limestone addition can perform satisfactorily as structural concrete.

5.3.2.3. Poisson ratio estimation

The Poisson ratio determined experimentally was used as input for dynamic elastic modulus calculations for the respective mixes. It was determined from the axial and transverse strains corresponding to 40% of the ultimate load. The computed values for N, NS, NSL and NS2L were 0.13 ± 0.02, 0.14 ± 0.003, 0.15 ± 0.03, and 0.15 ± 0.012, respectively. Concrete with

binary and ternary cements had slightly higher Poisson ratio than CEM I. The obtained results approaches typical values recommended by design codes, such as BS EN 1992-1-1 (Eurocode 2) and *fib* model code, where a general Poisson ratio of 0.2 and 0 is prescribed, for uncracked and cracked concrete respectively (200, 201). However, as experimentally determined Poisson ratios for concretes made with ternary composite binders containing limestone are not often reported in the open literature, the likelihood of overdesign arising from the use of conservative values recommended by design codes is inevitable. Such tendencies are interrogated by comparative analysis of dynamic modulus elasticity computed using experimentally determined Poisson ratio and values specified by BS EN 1992-1-1:2023 (Eurocode 2) in subsequent sections.

5.3.2.4. Static and dynamic modulus of elasticity

The modulus of elasticity of concrete is an important structural design parameter. It is pertinent for serviceability compliance in structural design e.g. for controlling deflection and estimating creep limit states and allowable sway of structures (67). It indicates the stiffness of concrete and it is typically related to the density and compressive strength of concrete using analytical relationships that are commonly used to estimate elastic-modulus for structural design (201-203).

Figure 5.4(a) shows the static modulus of elasticity of concrete mixes. The cylinder compressive strength of N, NS, NSL, and NS2L at the time of testing were 29.81, 29.15, 25.36, and 26.17 MPa, respectively, corresponding to cylinder/cube strength of approximately 0.8 for all mixes. It is identified that slag-containing concretes with/without limestone exhibited comparable elastic behaviour to CEM I under static loads, as reflected in the stress strain relationship as shown in Figure 5.4(b).

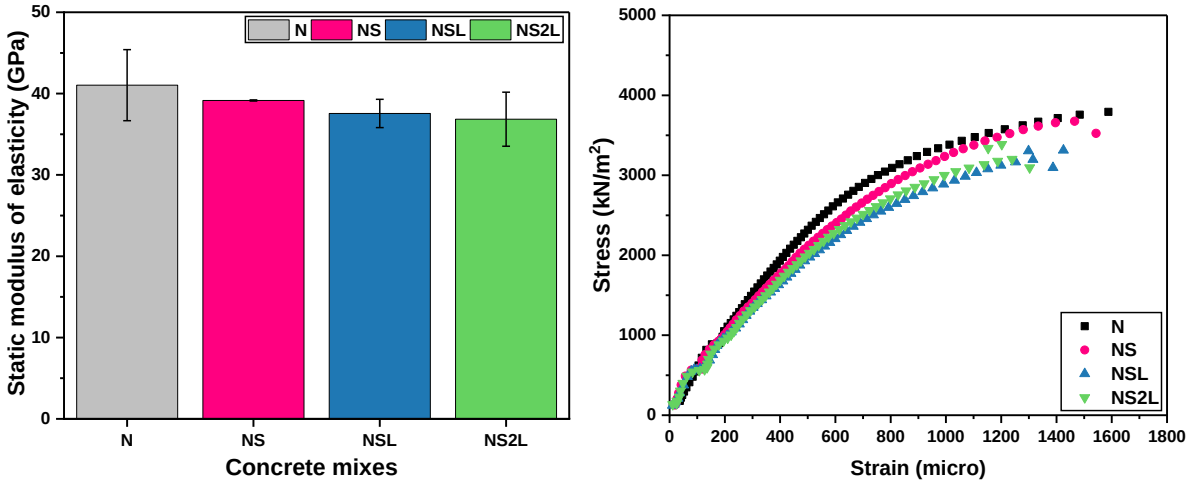

(a) (b)

Figure 5.4: (a) Static elastic modulus of concrete mixes (28 days cured). Error bars corresponds to one standard deviation of two measurements; and (b) stress-strain relationship of concrete mixes (28 days cured)

Additionally, the dynamic elastic modulus of concrete mixes was calculated using Equation 3.5 (see Section 3.5.3). In Figure 5.5(a), the evolution of the dynamic modulus for the concrete mixes is reported. The dynamic elastic modulus of all concrete mixes increased with curing age. Composite cement concrete shows relatively lower modulus from 2 days compared with CEM I concrete, but significant increases are observed from day 7 and compares with CEM I by day 28 up and at advanced curing ages. The results are consistent with other studies, particularly at the early ages (204). The UPV dynamic elastic modulus evolves similarly to the compressive strength as shown in the linear correlation in Figure 5.5(b). Overall, the elastic properties of concrete can be influenced by the aggregate. However, factors such as the aggregate and cement paste interface would play a significant role, as failure would typically proceed in those regions under load for matured concretes. The plausible refinement of the microstructure of concrete, particularly in the ITZ regions, typically reported for slag cement concrete (36) accounts for the improved static and dynamic moduli relative to CEM I for the tested curing ages.

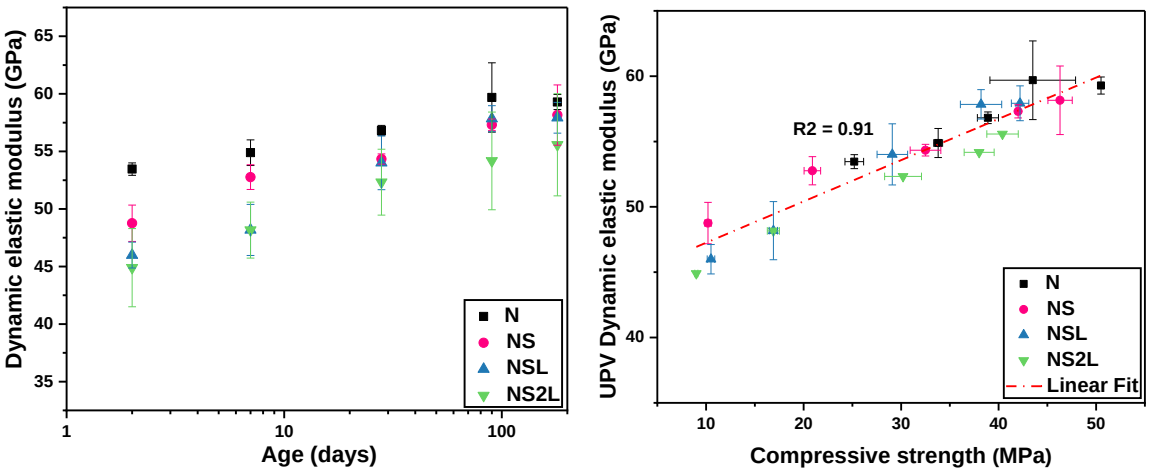

(a) (b)

Figure 5.5: Dynamic modulus of elasticity evolution of cured concrete mixes (error bars correspond to one standard deviation of three measurements) (a) based on experimentally determined Poisson ratios, and (b) linear regression between compressive strength and dynamic elastic modulus of concrete mixes

A comparison was conducted between experimentally determined dynamic elastic modulus and the estimated values calculated according to the BS EN 1992-1-1:2023 (Eurocode 2) or the *fib* model code, which recommend a Poisson ratio of 0.2 for uncracked concrete, and the results are shown in Figure 5.6(a). It is possible to see a direct correlation between the experimental data and estimated results based on Poisson ratios recommended by the design codes. This suggest the proposed values in design codes can be satisfactorily used for structural design of concrete made with the composite cements assessed in this study.

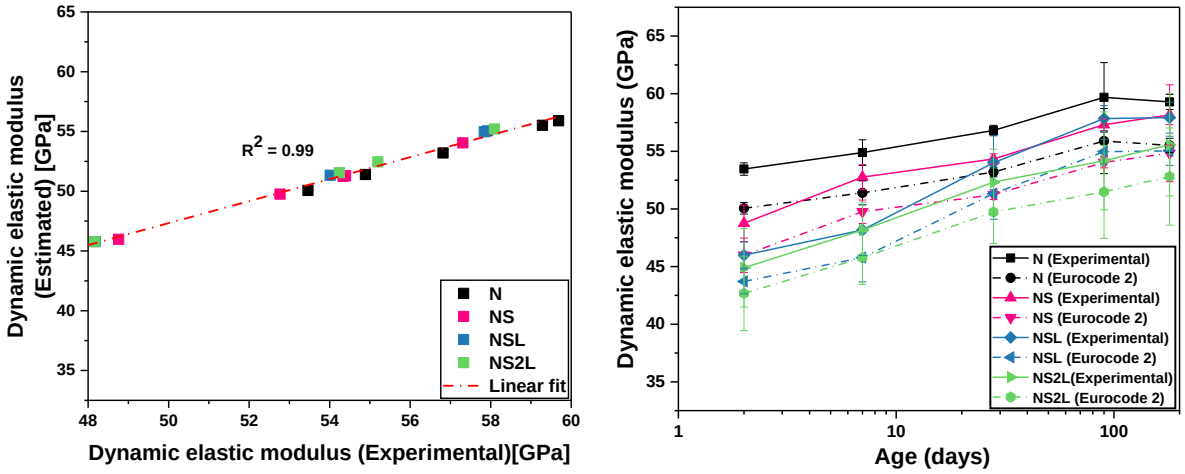

(a) (b)

Figure 5.6: (a) Correlation between dynamic modulus of elasticity based on experimental Poisson ratio and as estimated from design codes(*Fib*/ BS EN 1992-1-1:2023 (Eurocode 2) recommended Poisson ratio (0.2) for uncracked concrete, and (b) Evolution of dynamic modulus of elasticity calculated using the experimentally determined Poisson ratio or the *Fib*/ BS EN 1992-1-1:2023 (Eurocode 2) recommendation (0.2)

However, despite the potential applicability of the Poisson ratio for the structural design of composite cement, a comparison (see Figure 5.6(b)) of dynamic modulus calculated using the experimentally determined Poisson ratios or the prescriptive value of 0.2 in the codes was conducted. It was identified that the computed dynamic modulus based on experimental Poisson values yields nearly +5 GPa more than computation based on recommended values such Poisson ratio prescribed in the BS EN 1992-1-1:2023 (Eurocode 2)/*fib* code. Considering reinforcement bar requirement in structural design is typically dependent on the elastic modulus and Poisson ratios (160), the results here suggest that potential savings in quantities required per concrete cover can be achieved by avoiding overdesign.

5.3.2.5. Correlation of compressive strength and static elastic modulus

Table 5.3 shows a summary of the analytical equations used for estimating static elastic modulus from the mean 28 days compressive strength. Figure 5.7 shows a plot comparing experimentally determined values versus estimates from empirical equations.

Table 5.3: Empirical equation for static modulus prediction from compressive strength

Design code	Equation (GPa)	Reference
ACI 318-19	$4700*(f_c^{0.5})$	(67)
Fib	$(21.5*10^3)*(f_c/10)^{1/3}$	(201)
Eurocode 2	$9500*f_{cm}^{1/3}$	(205)
CSA A23.3-04	$4500\ (f'_c)^{0.5}$	(198)
NZS3101:1-2006	$3220(f'_c)^{0.5}+ 6900$	(199)

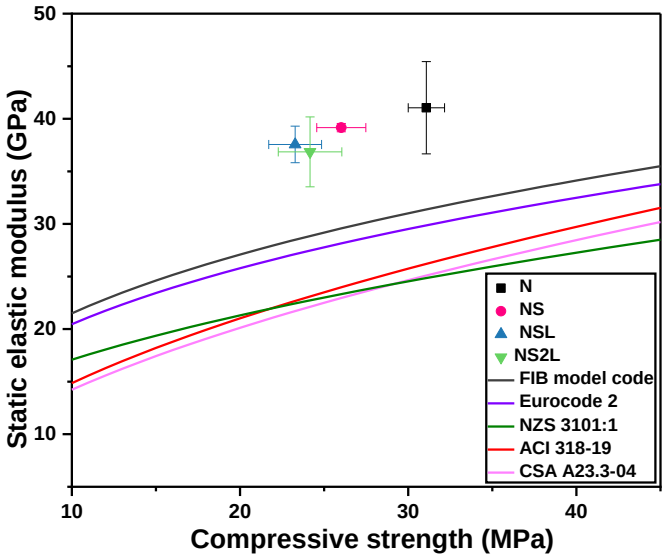

Figure 5.7: 28 day cured concrete static elastic modulus calculated adopting existing empirical models compared with experimentally determined values

The results indicate that slag-blended concretes with up to ~20 wt.% limestone addition evaluated in this study can perform satisfactorily as structural concrete. The *fib* model code and Eurocode 2 exhibit better predictability for concrete mixes assessed here, than the more conservative ACI-318, NZS 3101:1 and CSA A23.3-04.

5.3.3. Durability performance

5.3.3.1. Sorptivity and total porosity

The sorptivity of concrete gives a measure of one-dimensional water admissibility in the capillary pores with respect to time, driven by interfacial pressure gradients, and generally

used as a reasonable durability indicator of pore structure related variations in cementitious materials. Sorptivity profile is obtained from a plot of mass changes versus square root of time.

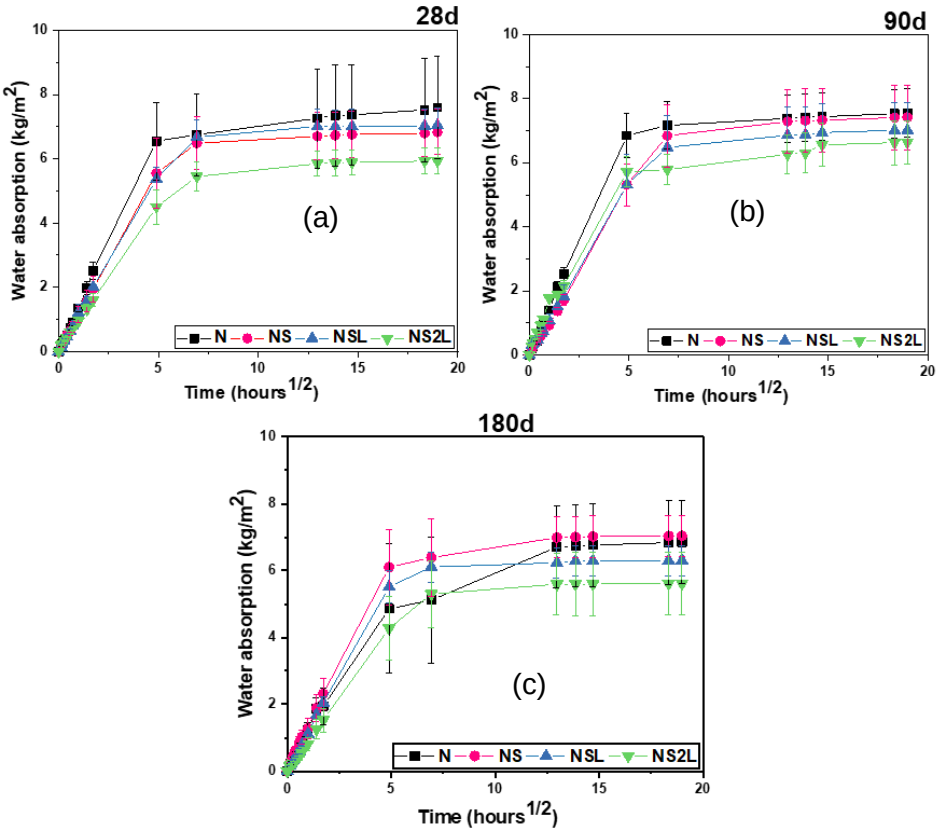

Figure 5.8: Sorptivity profiles of cured concrete samples after (a) 28 days (b) 90 days and (c) 180 days of curing. Average curves of two tested samples are reported, with error bars corresponding to one standard deviation of two curves.

Figure 5.8 shows the sorptivity profile of concrete mixes cured for 28, 90 and 180 days. The kinetics of water ingress can be quantified by the sorptivity coefficient of the concrete mixes are shown in Table 5.4, and it is demonstrated that composite binders show comparable initial water absorption coefficients by 180 days compared to CEM I. The results show that the replacement of slag by ~20% with limestone has no significant impact on the water absorption properties of the concrete mixes evaluated, and it is correspondingly reflected in the similarities in the total water absorbed at all ages for on the concrete mixes. The improved water absorption properties can be attributed to the progressive densification of microstructure with curing age, so that pore refinement in the composite cements contributes to their resistance to moisture ingress. The results corroborates with studies on the impact on limestone on sorptivity (60, 206).

Table 5.4: Sorptivity coefficients ($kg*m^{-2}*h^{-0.5}$) of moist cured concrete mixes

Cured Age	Mix ID			
	N	**NS**	**NSL**	**NS2L**
28	1.08 ± 0.26	0.99 ± 0.18	0.99 ± 0.08	0.81 ± 0.10
90	1.13 ± 0.15	1.01 ± 0.17	0.96 ± 0.18	0.89 ± 0.10
180	0.96 ± 0.19	0.99 ± 0.22	0.94 ± 0.09	0.79 ± 0.19

Table 5.5: Total water absorption (%mass) of moist room cured concretes

Cured Age	Mix ID			
	N	**NS**	**NSL**	**NS2L**
28	6.02 ± 1.53	5.43 ± 1.06	5.93 ± 0.44	5.09 ± 0.63
90	5.7 ± 1.19	6.09 ± 1.21	5.92 ± 0.39	5.11 ± 1.28
180	5.34 ± 1.2	6.28 ± 1.46	5.62 ± 0.52	4.9 ± 0.70

Furthermore, the results of the total porosity of concrete mixes is shown in Figure 5.9. It is observed that the porosity is comparable for all mixes with curing time, with an overall reduction in porosities at prolonged curing ages (when considered within error margins). Considering the classification of concrete durability potential based on the porosities for SCM containing concrete mixes proposed by Baroghel-Bouny et al. (182) it is identified that all the concretes assessed can be classified to present high to medium durability.

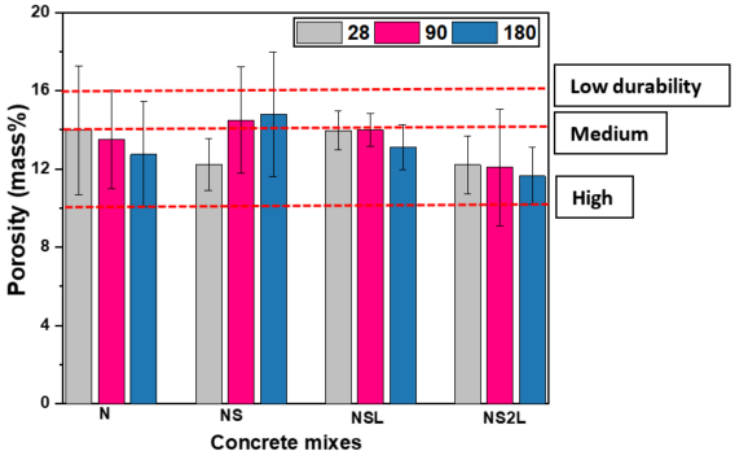

Figure 5.9: Porosity of concrete mixes (error bars corresponds one standard deviation of three measurements); classification based on Baroghel-Bouny et al. (182).

5.3.3.2. Bulk conductivity

Figure 5.10 shows results of bulk conductivities of the concrete studies as a function of their curing age. It can be seen that higher conductivity (lower resistivity) are recorded in CEM I concrete relative to composite binders at all ages. Based on these results it could be thought that the corrosion potential of steel reinforcement on concretes produced with slag or slag + limestone cements is three times higher than that of CEM I concrete due to elevated sulphur species in slags (207), which is conversely to what has been experimentally reported elsewhere for slag-containing concretes (208). Therefore, it can be suggested that there is a need to exercise caution in the use of bulk conductivity as a suitable technique to holistically infer corrosion potential of steel reinforcement in the concretes evaluated in this study.

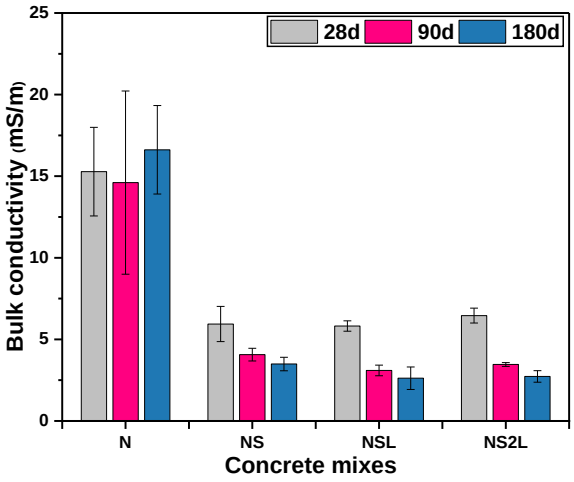

Figure 5.10: Bulk conductivity on concrete mixes (error bars corresponds to one standard deviation of three measurements)

The reduced conductivities potentially arises from discontinuities in the pores structure or increased tortuosity in the composite binders relative to CEM I (39, 181) leading to differences in the internal degree of saturation of the concretes, and also the differences in the ionic composition of the pore water with changes in the binder chemistry.

5.3.3.3. Surface resistivity of concrete

The surface resistivity test is a rapid non-destructive test used for structural health monitoring of concrete structures as an indicator for susceptibility to corrosion, so that higher surface

resistivity would suggest reduced risk of corrosion and vice versa. Based on this, results in Figure 5.11 shows reduced surface resistivity at advanced ages relative to CEM I concrete. This can be attributed to more refined pore structure in slag concretes with or with/without limestone with curing time (65). While this result appears to suggest a potentially reduced risk to corrosion, it must be recognised that the pore solution of the composite systems has reduced alkalis compared to CEM I, so that the response to the resistivity test requires further validation.

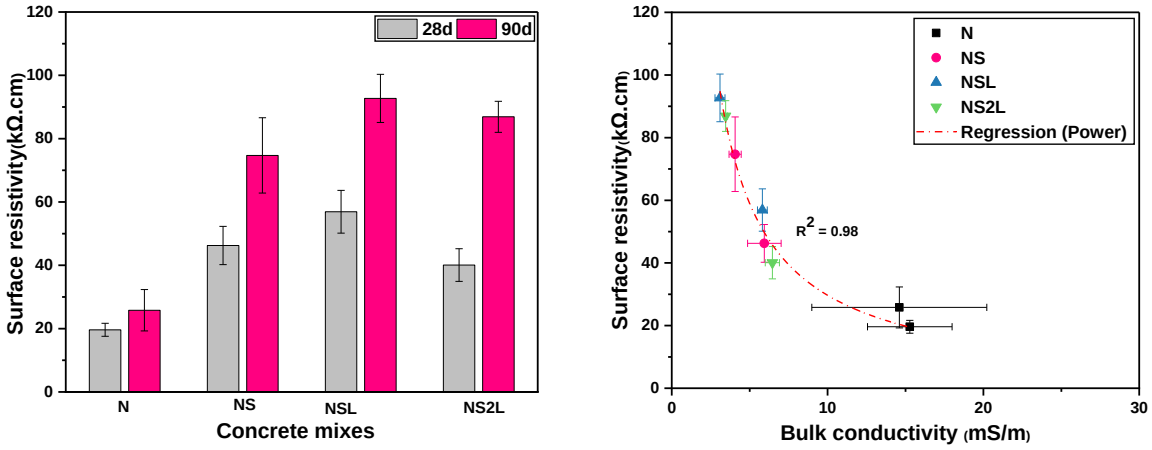

(a) (b)

Figure 5.11: Surface resistivity on concrete mixes (error bars corresponds to 2 cylinders) (b) relationship between surface resistivity and bulk conductivity

Meanwhile, the correlation between bulk conductivity and surface resistivity of the concrete studied (Figure 5.11) is consistent with results reported in other studies (209, 210), however the meaning and relevance of this relationship for concretes with SCMs needs to be further investigated. For example by establishing what boundary conditions or confident intervals under which such relationships can be used to infer pore refinement (tortuosity) and/ or corrosion potential for multicomponent cement systems.

5.3.3.4. Resistance to chloride ions ingress

The NordTest NTBuild 492 has been identified as a relatively precise non steady state method of investigating chloride ingress in SCM containing concretes, when compared to other migration/diffusion test methods (121). The results of chloride migration are shown in Figure 5.12. The calculated non-steady state migration coefficient shows a reduction in chloride permeability of the composite binders containing slag compared to CEM I concrete, which is

consistent with what has been reported by Proske et al. (17). The chloride co-efficient decreases with curing age for all concrete mixes. While NS shows the lowest migration coefficient after 28 days curing, the reduction with curing time is not significant, in comparison to the ternary blends, where up to ~ 50% reduction is observed in their migration coefficients and approaches values of NS at advanced ages.

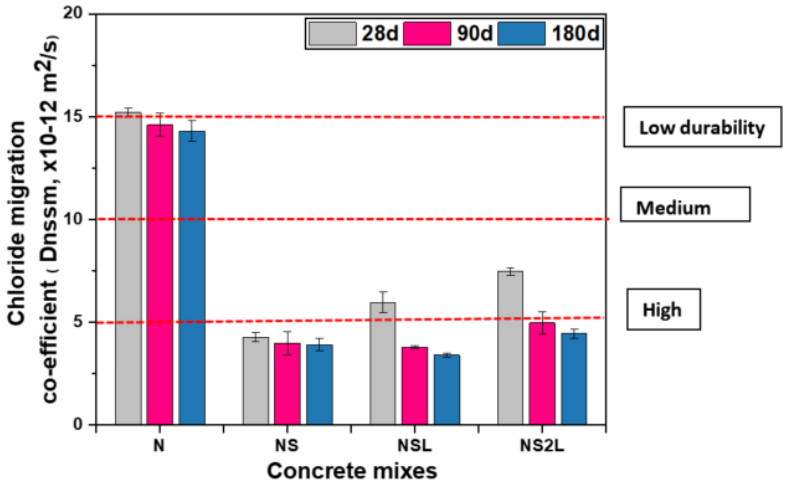

Figure 5.12: Chloride migration coefficients (m^2/s) of concrete mixes after 28, 90 and 180 days (error bars corresponds one standard deviation of three measurements). Durability classification based on Baroghel-Bouny et al. (182).

In slag rich concrete, chloride resistances may be attributed to the formation of Friedel's salt arising from binding between slag hydration products and chloride ions (211), including the likelihood of binding to hydrotalcite like phases (122), however the NTBuild 492 is limited in accounting for such contributions. The assumption of a constant binding capacity and the possibility to reduce with test duration (121) is expected to impact the influence of beneficial binding to chlorides, but does not suggest such chemical process does not play a contributory role. Figure 5.13 shows a linear correlation between the bulk conductivity and the chloride migration coefficient for the concrete mixes assessed, so that higher bulk conductivities are observed in concrete with the higher chloride migration coefficients. The trend is similar to previous studies on other SCMS blended cements (212). Based on durability classifications proposed by Baroghel-Bouny et al. (182, 213), NS, NSL and NSL demonstrate medium to high resistance to chloride permeability with curing age, while N exhibits nearly low chloride permeability. The results suggest that reducing slag content by 20 wt.% with limestone

addition shows satisfactory durability in chloride-laden environments, considering chloride mobility is impeded in a similar manner to binary slags with prolonged curing.

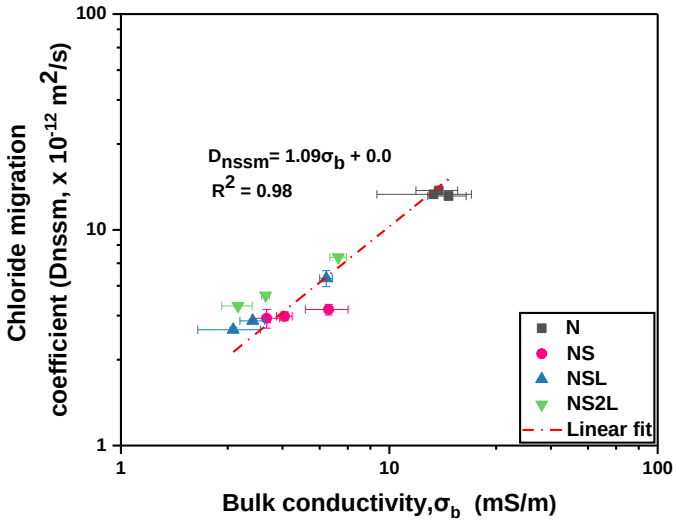

Figure 5.13: Relationship between bulk conductivity and bulk chloride migration co-efficient of 28, 90 and 180 days cured concrete mixes

5.4. Conclusions

Based on the experimental findings on mechanical performance and durability properties of concrete with CEM I, binary cement with 50 wt.% GGBS, ternary cements with GGBS plus 10 wt.% limestone and GGBS plus 20 wt.% limestone, herein labelled as N, NS, NSL and NS2L, the following deductions can be made:

1. Early age compressive strength of concrete with binary and ternary cements is 40% lower than that of concrete made with CEM I. However, all concretes reached ~10MPa or more after 2 days in compliance with requirements for formwork removal in real practice. 28 days compressive strength for concretes with binary and ternary cements was ~30% lower than CEM I but reached designed strength. The compressive strength of NSL and NS2L develops rapidly after 7 days of curing, achieving strength comparable to those identified in blended slag cement concretes (NS).

2. NS exhibit better flexural strength compared with CEM I, however ~10/20% limestone addition has no significant effect on the flexural strength of NSL/NS2L. NSL and NS2L exhibit comparable flexural strength at advanced curing age. Existing equations

considering flexural strength in structural design codes can be utilised for slag-limestone composite cements concretes.

3. The dynamic elastic modulus of NS, NSL and NS2L are lower at day 2 relative to CEM I but increase significantly after 7 days of curing, and are comparable to CEM I by 28 days and 180 days.

4. Replacing Portland cement with slag leads to a significant reduction of the chlorides migration coefficient, and the addition of up to ~20% limestone slightly increased the chloride permeability of NS2L relative binary slags, albeit about 3 folds less than the migration coefficient of CEM I by 180 days curing age. The correlation between bulk conductivity and surface resistivity demonstrates the influence of pore refinement or tortuosity, even when the influence of chloride binding capacity due to slags is not considered.

5. The sorptivity coefficient, total water absorption and water accessible porosity demonstrate that slag-containing concretes with or without limestone does not exhibit detrimental water absorption properties relative to CEM I, and it is more evident at prolonged curing ages.

6. The relatively higher surface resistivity of ternary blends suggests increased tortuosity and the potential to reduce migration of free chlorides.

Overall, it can be concluded that replacing slag with up to 20% limestone powder does not adversely affect the mechanical and durability performance of concretes made from them. These concrete exhibit satisfactory performance comparable to not only binary slags but CEM I in certain cases. Assessment of their conformance to design codes suggest they can be satisfactorily used as structural concrete.

Chapter 6.

6. Carbonation performance of composite Portland cement-slag-limestone concrete and its impact on chloride permeability

6.1. Introduction

Corrosion of steel reinforcement in structural concrete is believed to be associated with the carbonation of the binding phase (causing reductions in pH) and/or the penetration of chlorides through the concrete cover layer. Recent evidence has demonstrated that carbonation alone does not led to corrosion of steel (99) in all cases, as other factors such as pore structure and moisture content at the steel-concrete-interface play a key role in destabilizing the passivation layer formed in the steel surface. In the case of concretes produced with SCMs, it is known that carbonation can lead to an increased porosity and reduction of strength properties. Therefore it is critical to assess how carbonation might impact other durability phenomenon, particularly chlorides permeability, to ensure the suitability of using multicomponent cement systems with up to 50% GGBS (with limestone addition) as structural concrete.

This appears to have been addressed in some standards by increasing the cover depth (214, 215), potentially aiming at delaying the progression of carbonation/pH loss towards steel reinforcement. However, it remains largely unknown how carbonation progress will modify the overall permeability properties of novel concrete. The main concern, which needs to be addressed, is how variations in pore structure induced by increased carbonation rates in concretes made with modern cements could trigger the ingress of other deleterious species such as chlorides. This reinforces the urgent need to understand the underlying degradation mechanisms of SCM concrete systems under multiple environmental exposure, which reflects realistic service conditions.

It is also worth noting that reports on the carbonation performance of concretes made with CEM VI(S-LL) are limited, and their carbonation service life has largely not been considered. Several carbonation service life prediction models have been developed based on the square root of time where the carbonation front progression is considered to evolve proportionally with square root of time (216), according to Fick's law. This has been expanded to improved physicochemical models taking into account the combined influence of moisture exchange between hydrates and exposure environment, the coupled impact of carbonation-induced changes in the amount of carbonatable materials and carbonation products (217), porosity evolution and water saturation (218). Even though these new models account for different limiting factors, and independently show comparable results to experimental data, they require solving complex analytical equations and input parameters likely to vary by cement combinations or mix design. Thus, a one-size-fits-all carbonation model appears near impossible.

Meanwhile, it also been shown that accelerated carbonation rates can be used for carbonation service life prediction and have been validated using independent experimental natural carbonation data in literature (177). This approach can potentially minimise the need to account for complex physico-chemical/reactive transport mechanisms, and thus can be conveniently used for cement systems with limited inputs in reactive transport models. For example, according to Sisomphon and Franke (177), for a given accelerated carbonation coefficient, carbonation depths under ambient conditions can be estimated from Equation 4.1 (Chapter 4; Section 4.3.2) derived from Fick's law of diffusion, and then integrated into the square root of time equation.

In response to the current knowledge gap and the highlighted practical needs, this study pursues an understanding of the impact of carbonation on the transport of chlorides and moisture in partially carbonated concretes produced with CEM I, binary slag (~50 wt.%), and ternary slag composite cement with ~10 and ~20 wt.% limestone addition. The carbonation performance under ambient and accelerated exposure (3% CO_2 and 60% RH) was assessed using a phenolphthalein pH indicator. Residual compressive strengths post-carbonation were tested at 100 days for both exposure types, and further tested after ambient exposure for 365 days. Shrinkage evolution was monitored under carbonation exposure up to 28 days. Concrete cylinders unidirectionally exposed to natural or accelerated carbonation were used for investigating the implications of carbonation on bulk conductivity, chloride permeability and water ingress. It is identified that although carbonation rates increased in slag-containing concretes with or without limestone, they exhibited comparable or better shrinkage performance, chloride resistance and water absorption properties compared to CEM I.

Carbonation service life prediction also gave an indication the concretes made from composite cements can potentially satisfy cover depths in some design code for at least 50 service life.

In addition to this chapter, further studies on the combined action of compressive load and carbonation on transport properties are discussed.

6.2. Experimental procedures

The experimental methods in this chapter follows the same protocol implemented on the mortar scale study for investigating carbonation performance, residual strength and impact of carbonation on transport properties as described in Section 4.2.2 and 4.2.3. This includes sample preparations and preconditioning procedures. Meanwhile the concrete mixes evaluated are the same as studied in Chapter 5.

In the current study based on concrete scale, carbonation evolution was monitored on 75 × 75 × 200 mm prisms each at 7, 28, 70, and 100 days of exposure to 3% CO_2 accelerated carbonation and corresponding natural carbonation. Natural carbonation depth was further measured up to 365 days using an extra prism. The residual strength of 75 mm cubes dry cut from carbonated 75 × 75 × 200 mm prisms were tested after 100- and 365-days carbonation exposure.

The impact of carbonation on transport properties was determined in cylindrical samples with comparable dimension and counts as in the case of mortars (Chapter 4). Thus, the chloride permeability, sorptivity and porosity of ten (100Ø × 50 ± 5 mm) concretes unidirectionally exposed to carbonation were tested post 28 and 100 days per exposure type. One cylinder per age was used for carbonation depth monitoring.

Additionally, the shrinkage evolution of 75 × 75 × 200 mm prisms under both natural and accelerated carbonation. The methodology is described below.

6.2.1. Carbonation shrinkage

Shrinkage evolution was monitored using wireless data loggers. Each side of a 75 x 75 x 200 mm prism, adjacent to the as-cast surface was appended with a 120 Ω, 60mm strain gauge. A detailed description of sample preparation is provided in Section 3.5.7.1. Here, 28 days cured prism appended with two strain gauges on opposite sides (75 × 200mm surface) was used per exposure type. The surface prepared, and strain gauged prisms connected to data

loggers were subsequently stored in a climatic chamber. Shrinkage data collection progressed for an initial 14 day preconditioning (57±3 %RH, and 20 ^{o}C), as per accelerated carbonation standard recommendation (219). Then prisms were transferred to a 3% [CO_2] accelerated carbonation chamber for a further 28 days. The shrinkage evolution under natural carbonation was logged for 42 days (14 days preconditioning + 28 days carbonation). It is acknowledged that shrinkage data from two or more prisms would reduce errors in data. However, due to constraints such as the carrying capacity of the environmental chamber (at the time of the experiment), shrinkage data from one specimen (average of measurements from two sides) is reported for a qualitative assessment of the impact of carbonation on shrinkage.

6.3. Results and discussion

6.3.1. Carbonation performance of concrete mixes

The carbonation depths of the concrete mixes was measured on freshly split surfaces by spraying the samples with a phenolphthalein indicator (1 g phenolphthalein in 100 ml IPA) on concrete mixes carbonated under both exposure conditions, as illustrated for concretes subjected to 100 days accelerated carbonation in Figure 6.1.

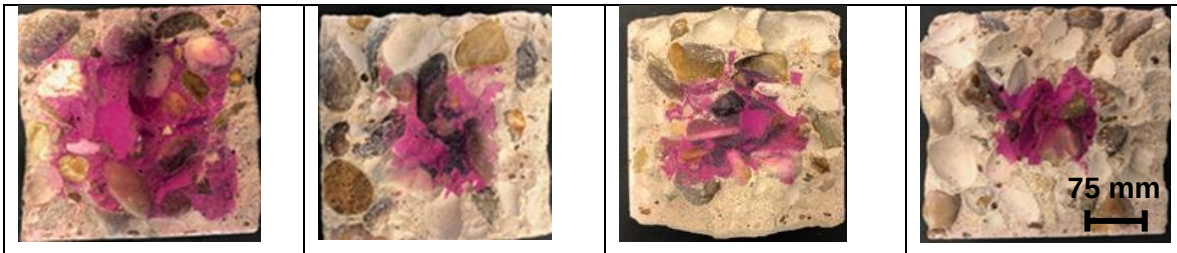

(a)	(b)	(c)	(d)

Figure 6.1: Photographs of carbonated concretes showing the carbonated (colourless) and non-carbonated (fuchsia) regions of the tested samples. These images correspond to samples exposed for 100 days to accelerated carbonation. (a) N (b) NS (c) NSL (d) NS2L

Figure 6.2(a) shows the carbonation depth evolution under accelerated carbonation, and the corresponding carbonation coefficients calculated using the Fick's equation are shown in Figure 6.2(b). The results reveal an increased rate of carbonation in the slag-containing concretes (with or without limestone) relative to CEM I, as shown in the overall accelerated carbonation coefficients summarised in Table 6.1. Comparing the slag-containing mixes, NS,

NSL and NS2L exhibit similar carbonation depth evolution by 100 days of accelerated carbonation. Overall, it is further identified in Table 6.2 that the percentage change in carbonation rates between two successive ages reduces as the accelerated carbonation exposure time approaches 100 days. For example, in NS2L the change (%) between 7 and 28 days is 18.5% while the change in carbonation rates (%) between 70 -100 days is 16.7%. This suggests a potential retarding effect with exposure time for all mixes.

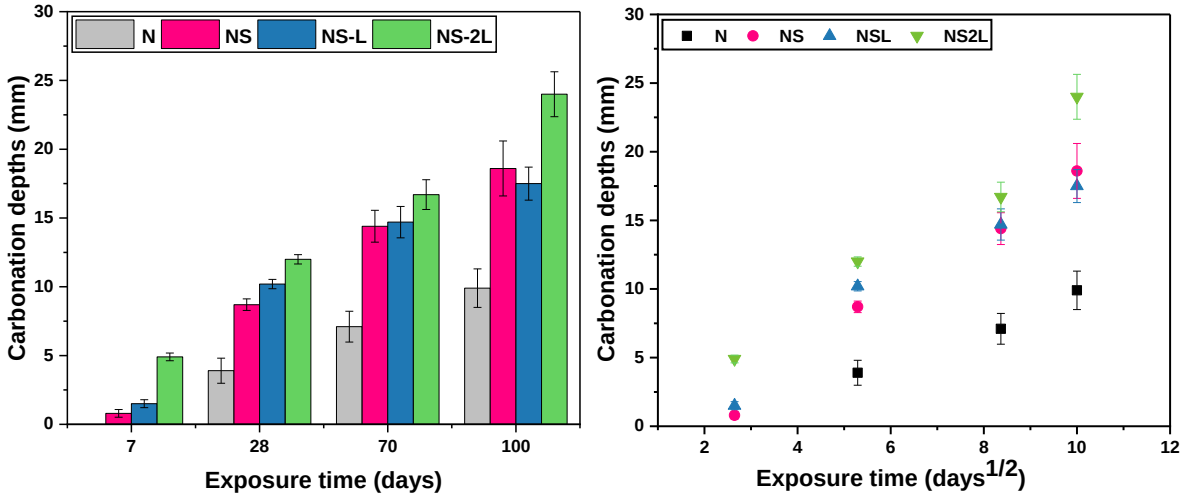

(a) (b)

Figure 6.2: (a) Carbonation depth of concretes exposed to accelerated carbonation up to 100 days. (b) The correlation between accelerated carbonation depth and the square root of time. The values reported correspond to the average of 16 readings (four per side), and error bars correspond to one standard deviation of such measurements

Table 6.1: Accelerated carbonation coefficient (mm*days$^{-0.5}$) of concrete prisms based on slope of linear regression in figure 6.2(b)

Mix ID	N	NS	NSL	NS2L
Carbonation coefficient (mm*days$^{-0.5}$)	1.21 ± 0.16	2.65 ± 0.24	2.60 ± 0.45	2.45 ± 0.23
R^2	0.97	0.98	0.92	0.97

Table 6.2: Accelerated carbonation coefficient (mm*days$^{-0.5}$) of concrete prisms as a function of exposure time

Mix ID	Exposure time (days)			
	7	**28**	**70**	**100**
N	-	0.73	0.85	0.99
NS	0.32	1.64	1.72	1.86
NSL	0.56	1.92	1.75	1.75
NS2L	1.84	2.26	2.00	2.40

The carbonation depth evolution of concrete mixes under natural exposure for a period of 365 days is shown in Figure 6.3(a). The overall carbonation coefficients tabulated in Table 6.3 showed increased depths in NS, NSL and NS2L relative to the CEM I at all exposure times. Both exposure methods show a similar trend in the carbonation rates of the concrete mixes. It is identified that the carbonation rates of slag-containing concrete with/without limestone demonstrate a twofold increase irrespective of exposure type. The carbonation rates identified for binary and ternary slag concrete relative to CEM I are consistent with the findings reported by Proske et al (17). Similar to observation under accelerated carbonation, Table 4.2 suggests a reduction in the percentage change (considered between two successive ages) in natural carbonation coefficient with exposure time by 365 days.

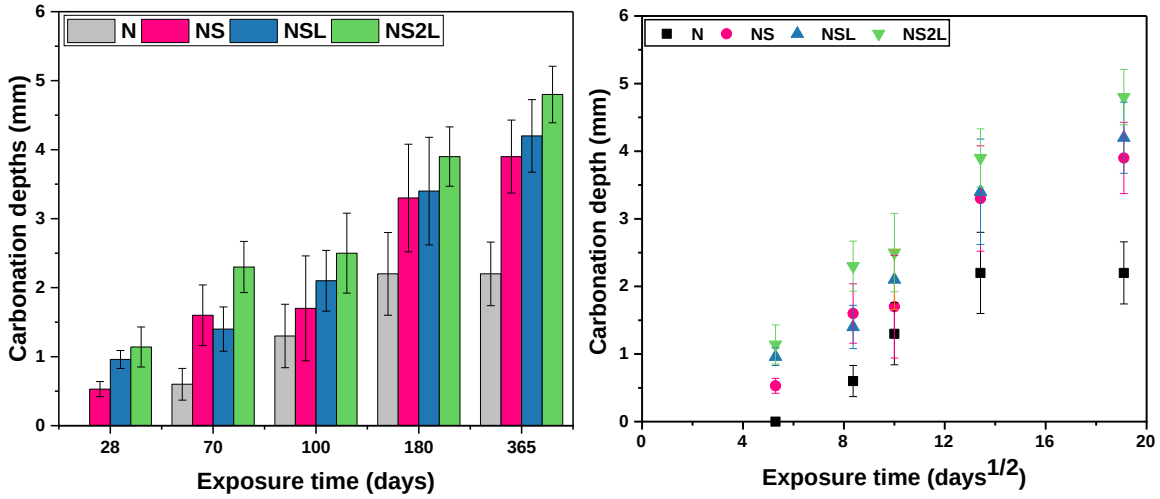

(a) (b)

Figure 6.3: (a) Carbonation depth of concretes exposed to natural carbonation up to 1 year. (b) The correlation between natural carbonation depth and the square root of time. Values

reported correspond to the average of 16 readings (four per side), and error bars correspond to one standard deviation of such measurements

Table 6.3: Natural carbonation coefficient (mm*days$^{-0.5}$) of concrete prisms based on slope of linear regression in figure 6.3(b)

Mix ID	N	NS	NSL	NS2L
Carbonation coefficient (mm*days$^{-0.5}$)	0.12 ± 0.02	0.21 ± 0.02	0.22 ± 0.01	0.26 ± 0.01
R^2	0.90	0.97	0.99	0.99

Table 6.4: Natural carbonation coefficient (mm*days-0.5) of concrete prisms as a function of exposure time

Mix ID	Exposure time (days)				
	28	**70**	**100**	**180**	**365**
N	-	0.07	0.13	0.17	0.11
NS	0.10	0.19	0.17	0.25	0.21
NSL	0.18	0.17	0.21	0.25	0.22
NS2L	0.22	0.27	0.25	0.29	0.25

The reduced carbonation performance of the composite cements concrete is attributable to their reduced CO_2 buffer capacity compared to CEM I systems (19) due to their lower clinker content. Discrepancies in the carbonation rates between mortars (Chapter 4) and concretes are identified; the natural and accelerated carbonation rates increased by an average factor of 1.69±0.10 and 2.54±0.19 respectively in the concrete specimens. Although similar hydrates will be forming in both systems, differences in the carbonation rates are due to variations in paste volumes in mortars and concrete. In addition, the characteristics of interfacial transition zones on mortar and concrete scale are largely different and would influence CO_2 diffusivities differently. That notwithstanding, size effect of the different surface areas/ exposed CO_2 ratio in the different scales (mortar = 1600 mm^2; concrete = 5625 mm^2) can also be a contributing factor, but this would require validation using different specimen dimension at the same scale of mortar or concrete. Such discrepancies can be obviated by normalisation of carbonation rates by carbonated area, but as can been seen in the scatter in measured carbonation depths on both mortar and concrete scales, this can result in biased comparisons. Thus while studies on mortar should be considered as a standalone chapter, comparisons to concrete scale would focus on similarities in trends where possible.

Table 6.5: Estimated natural carbonation coefficient from accelerated carbonation coefficient based on Equation 4.1

Mix ID	Measured (Experimental): *K_{NC}	Measured (Experimental): *K_{ACC}	Estimated K_{NC} from K_{ACC} at 3%
	Slope	Slope	[CO_2]
N	0.12 ± 0.02	1.21 ± 0.16	0.14 ± 0.01
NS	0.21 ± 0.02	2.65 ± 0.24	0.31 ± 0.02
NSL	0.22 ± 0.01	2.60 ± 0.45	0.30 ± 0.04
NS2L	0.26 ± 0.01	2.45 ± 0.23	0.28 ± 0.02

*K_{ACC} = Accelerated carbonation coefficient (mm*day$^{-0.5}$); K_{NC} = Natural carbonation coefficient (mm*day$^{-0.5}$)

Overall it is worth noting that carbonation rates in the mortar scale also followed the 2-fold increase in NS, NSL and NS2L relative to CEM I, similar to observation on the concrete scale. Towards estimating the natural carbonation coefficient from accelerated coefficients, when Equation 4.1 is applied, the results tabulated in Table 6.5 show the estimated carbonation coefficients (within error margins) are comparable to experimental values, consistent with findings on the mortar scale.

6.3.1.1. Carbonation Service life prediction, and comparison with BS 8500-1:2023

Figure 6.4 shows a 100-year carbonation service life prediction of carbonation front progression based on Equation 4.1. The basis for proposing service life models as against model based on Equation 4.1 proposed by Sisomphon and Franke (177) has been attributed to non-existence of correlation between ambient and natural carbonation coefficients in some studies. Contrary to such reports, the comparable experimental and estimated natural carbonation coefficients as derived from accelerated carbonation coefficients at both mortar and concrete scales suggest Equation 4.1 can be used for predicting the long-term carbonation depth evolution. Thus, rearranging Equation 4.1 (see Section 4.3.2), the Sisomphon and Franke equation can be expressed as follows:

$$K_{Nc} = K_{Acc} * \frac{\sqrt{C_{NC}}}{\sqrt{C_{Acc}}} = K_{Acc} * \frac{\sqrt{0.04}}{\sqrt{3}} = 0.115 = 0.1K_{Acc} \quad \textbf{Eq. 6.1}$$

*Where; K_{ACC} = Accelerated carbonation coefficient (mm*day$^{-0.5}$); K_{NC} = Natural carbonation coefficient (mm*day$^{-0.5}$); C_{ACC} = CO_2 concentration under natural carbonation(3%) ; and C_{NC}(mm) = CO_2 concentration under natural carbonation (0.04 % as adopted in (103))*

It is worth noting, that a primary assumption using Sisomphon and Franke equation is that CO_2 diffusivity reduces at prolonged carbonation ages. This assertion holds for this study as identified in mortar specimens (Section 4.3.2) and concretes, where age-specific carbonation rates followed a reducing trend by 2 years (mortars) or 365 years (concretes) of natural carbonation exposure, and by 100 days of accelerated carbonation exposure.

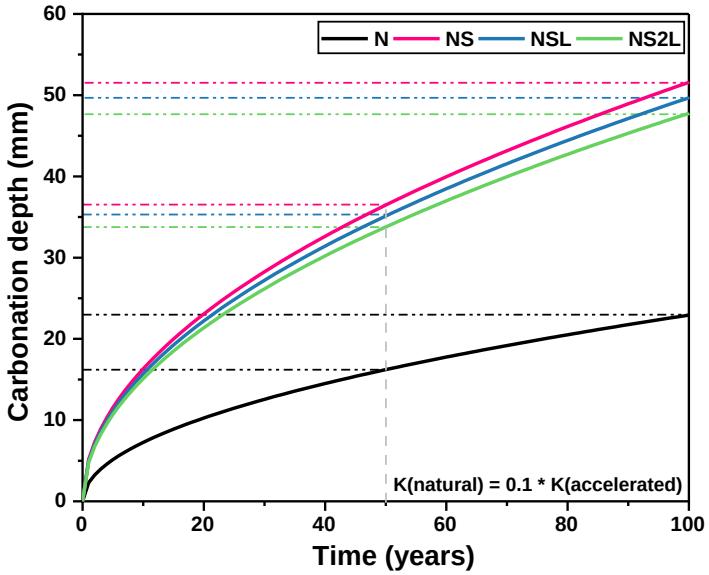

Figure 6.4: 100-year carbonation depth prediction of concrete mixes [Marked lines on Y-axis show predicted carbonation depths corresponding to 50/100 years service life for respective concrete mixes]. The BS 8500-1:2023 recommended cover depths are shown in Table 6.6

The CEM I concretes consistently exhibit a reduced carbonation depth up to 100 years of exposure relative to NS, NSL and NS2L, while all the slag-containing concretes with or without limestone exhibit similar depths. The practical relevance can be determined when the predicted carbonation depth are correlated with prescribed cover depths in accordance with standards, for example with BS-8500:1. The depths corresponding to design life of structural concretes at 50 and 100 years are tabulated in Table 6.6. While high carbonation depths are evident in concretes made with composite cements, the predicted values appear to be within limits of cover depths recommended by the BS 8500-1:2023 for concretes incorporating multicomponent cement systems (based on 28 days design strength, C25/30 in this study). In

addition, considering carbonation tests under sheltered (ambient exposure without direct contact with rainfall) conditions have often reported higher depths than unsheltered (ambient exposure with direct contact with rainfall) conditions (220), it is likely that concretes made with composite cements will perform satisfactorily under field condition. However, caution needs to be exercised in these predictions by validation with long-term carbonation depth monitoring, and the need to account for effect of loading for carbonation service life predictions. It is however interesting to note that the BS 8500:1 also suggests, for a C25/30 concrete, the binary and ternary slags are unsuitable for structural applications with exposure class XC3 (moderate humidity) at risk of corrosion-induced carbonation intended for 100 years service. The projected carbonation depth by 100 years as shown in Table 6.6 gives an indication such exclusions in the standard need careful reconsideration. Meanwhile, the predicted depths, for example at 50 years is nearly 2-times less than the cover depth prescribed by the BS 8500-1:2023, suggesting potential use of excess materials that have a bearing on cost and overall carbon footprints. This negates the cost-cutting potential of multicomponent systems (by reducing slag use in lieu of limestone), and net carbon reduction tendencies.

Table 6.6: Predicted natural carbonation depths (see Figure 6.4) at 50 and 100 years compared to BS 8500-1:2023 recommended cover depth for concrete containing carbon reinforcing steel or prestressed elements with an intended working life >= 50 years (Table a.4a in BS 8500:1:2023) or 100 (Table a.5a in 8500:1:2023) years for corrosion induced carbonation (XC 3 : moderate humidity)

Concrete Mix ID	**50 years Predicted Carbonation depth (mm)**	**50 years Cover depth (mm)**	**100 years Predicted Carbonation depth**	**100 Cover depth (mm)**
N	16.2	45 + Δc	22.9	60 + Δc
NS	36.5		51.6	No classification
NSL	35.1	≥ 65 + Δc	49.7	for C25/30
NS2L	33.8		47.8	

Δc = allowance for workmanship

6.3.2. Compressive strength of carbonated concretes

Figure 6.5 (a) shows the compressive strength evolution of carbonated 75 mm concrete cubes after 100 days of natural or accelerated carbonation, in addition to the tested compressive strength after 365 days of natural carbonation exposure. It is identified that the compressive

strength of concrete made from composite cements are comparable to CEM I post 100 days of natural carbonation, and with increasing strength gain by 365 days exposure. N and NS exhibited higher strength gain than NSL and NS2L from 100 days exposure to 365 days. Comparing the strength evolution between 100 to 365 days naturally carbonated samples, herein referred to as air curing (60% RH), there is weak evidence that the compressive strength of carbonated samples are reduced compared to 90 days to 365 days moist cured concretes (see Figure 5.1(a) in Section 5.3.2.1) at similar ages. Contrary to findings elsewhere (221) for slag-based concretes, the compressive strength is comparably independent of the curing type. An explanation for this discrepancy can be attributed to significant variations in the fineness of slag used in both studies, where slags with 3-folds less blaine were used in the current study. High fineness slag would increase water demand, thus less evaporable water is expected in hardened concrete for the same water-to-binder ratio, which when rapidly lost under air curing would negatively affect the progress of secondary hydration. Additionally, high autogenous shrinkage in slag concretes (204, 222), can potentially induce microcracking due to greater use up of an expected limited amount of evaporable water via self-desiccation when using high blaine slags. These combined effects will have a negative impact on strength.

Meanwhile, after 100 days of accelerated carbonation, it is identified that N, NS and NSL exhibit significant increases in strength with values slightly lower to those recorded at 365 days of natural carbonation. Conversely, NS2L reported a reduction in strength after 100 days of accelerated carbonation.

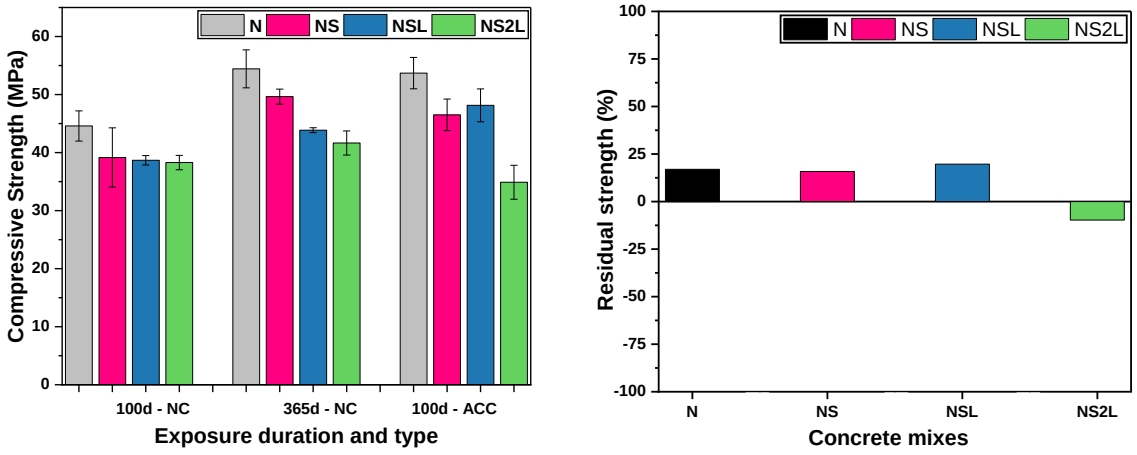

(a) (b)

Figure 6.5: (a) Compressive strength of concretes post 100 days of natural carbonation (NC), 365 days natural and 100 days of accelerated (ACC) carbonation (b) Residual compressive strength (carbonated (ACC) strength/ carbonated (NC) strength) after 100 days

of carbonation exposure. Error bars correspond to the standard deviation of two measurements

The residual strength (%), as determined from the ratio of 100 days accelerated carbonated strength to 100 days natural carbonated strength (reference) expressed as a percentage change is shown in Figure 6.5(b). N, NS, and NSL exhibited relatively increased (~20%) compressive strength in accelerated carbonated samples than the corresponding natural carbonated samples, NS2L shows nearly 10% reduction post accelerated carbonation strength, suggesting a retarding impact of carbonation on strength development of NS2L relative to other mixes. However, while there exists such a reduction in the 100-day accelerated compressive strength of NS2L relative to the reference sample (natural carbonation); it is observed that the 100-day accelerated compressive strength value is indeed 15% greater than the design strength of NS2L. This suggests that the long-term influence of carbonation on pore structure is not necessarily detrimental to strength development, as concrete can maintain strength above design strength. It also becomes apparent that consideration of 28-day design strength as limiting values for conformance to cover depth for XC3/XC4 exposure classes unfavourably excludes the suitability of NS, NSL and NS2L concretes intended for 100 years service life.

Strength gain in CEM I can be attributed to densification effects due to greater buffer capacity (100, 176), while decalcification is expected to be dominated in highly carbonated areas of NS, NSL and NS2L (112, 113). Based on the results, it can be argued that the impact of decalcification is limited or partial on strength development, particularly for NS and NSL, and even if it is to a higher degree in NS2L, this is insufficient to reduce post-carbonated strength below design strength.

6.3.3. Shrinkage evolution of carbonated concretes

In real practice, concrete would often undergo drying in combination with carbonation at moderate to low humidity conditions, and the dimensional instability of concrete structures that occurs when concrete is not under load is shrinkage (131). Figure 6.6(a-b) shows the shrinkage evolution of 28 days cured concrete mixes under natural carbonation or accelerated conditions. Under natural carbonation, the ternary blends show reduced shrinkage strain relative to binary slag and CEM I; binary slag (~50 wt.%) exhibits comparable shrinkage to CEM I under ambient conditions. Meanwhile, under accelerated conditions, slag-containing concretes with or without limestone shows reduced shrinkage relative to CEM I. However, the

ternary blends similarly show reduced shrinkage to binary slag under accelerated conditions. Under similar preconditioning, the impact of carbonation on shrinkage is not evident, but its influence can be seen under accelerated carbonation conditions where increased shrinkage is observed relative to natural carbonation exposure beyond the preconditioning period, for a similar exposure duration. Nonetheless, the increase in shrinkage due to carbonation is marginal in the ternary blends. These observations are consistent with other studies (17, 223) that have shown improvement in drying shrinkage of slag-limestone concrete relative to CEM I when assessed via experimental and analytical methods.

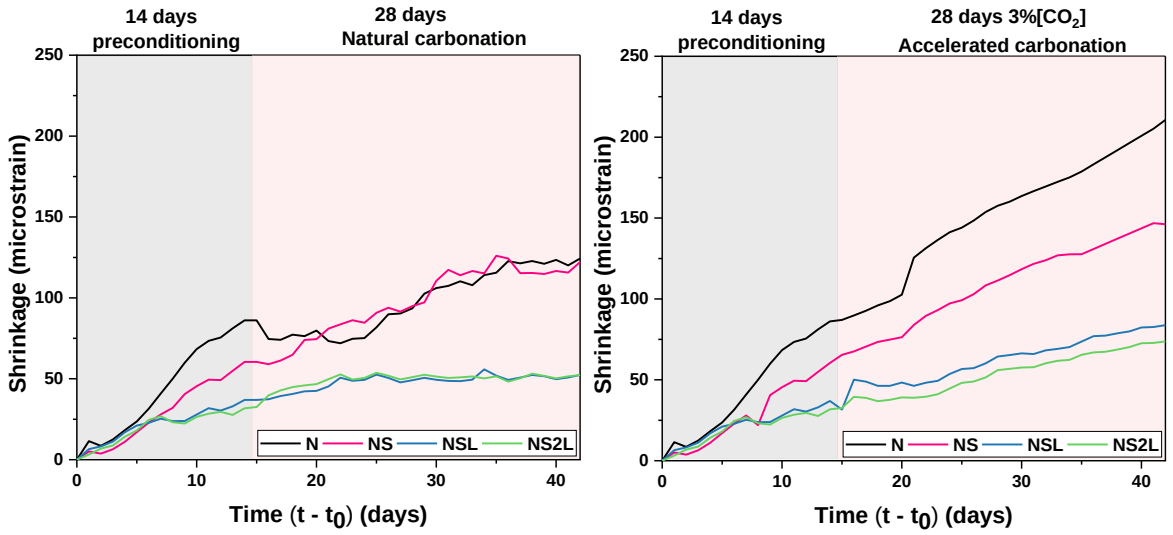

(a) (b)

Figure 6.6: Shrinkage evolution of 28 days cured concrete mixes exposed to (a) natural (ambient) carbonation for 42 days or (b) (3% CO_2) accelerated carbonation for 28 days (+14 days preconditioning)

A plausible explanation of the performance identified under natural carbonation can be linked to the microstructure differences of the cements evaluated. In blended slag systems, a reduced amount of C-(A)-S-H might be forming compared to CEM I particularly at early curing durations, which potentially translates into a reduced bound water removal during drying, in addition to restraining effects imposed by unreacted limestone filler acting as additional aggregate (224). This is consistent with the fact that concretes with higher limestone addition (and consequently less slag) exhibited a reduced shrinkage, this being more noticeable as limestone addition increased. The marginal increases in shrinkage under accelerated conditions relative to ambient conditions suggest that increased carbonation rates in ternary

mixes in particular has limited impact on their dimensional stability in the long term. The less pronounced impact of porosity under accelerated carbonation as observed in Figure 6.9 underpins such an assertion, considering high carbonation did not translate into increased open porosities, which have a bearing on pore volumes, and hence dimensional stabilities. The results are consistent with the observed residual strengths in this study (Figure 6.5) where increased carbonation shrinkage could have resulted in significant strength loss due to microcracking or coalescence of any pre-existing microcracks, which was not the case. The reduced cracking tendency or propagation can be attributed to the lessening action of the carbonation layer on moisture movement, hence the reduced strain (142). It is worth noting that CEM I systems have been reported to exhibit reduced strains (102) at 15% [CO_2] and 65% relative humidity (RH). It thus becomes important to also assess if the marginal strains recorded for the ternary mixes under accelerated carbonation are retained under combined load and accelerated carbonation.

6.3.4. Studies on partially carbonated concrete cylinders

6.3.4.1. Carbonation depth evolution of carbonated cylinders

The carbonation depths of cylinders subjected to unidirectional carbonation are shown in Figure 6.7(a) and Figure 6.7(b) after natural and accelerated carbonation respectively. In all exposure types, NS, NSL and NS2L recorded higher carbonation depth relative to CEM I, similar to the trends exhibited by the carbonated prisms previously discussed. As can be seen in Figure 6.7(c), it is also identified that the carbonation coefficients of prismatic specimens also compared to cylinders exposed to 1-dimensional CO_2 ingress, where a strong correlation exist in experimental data.

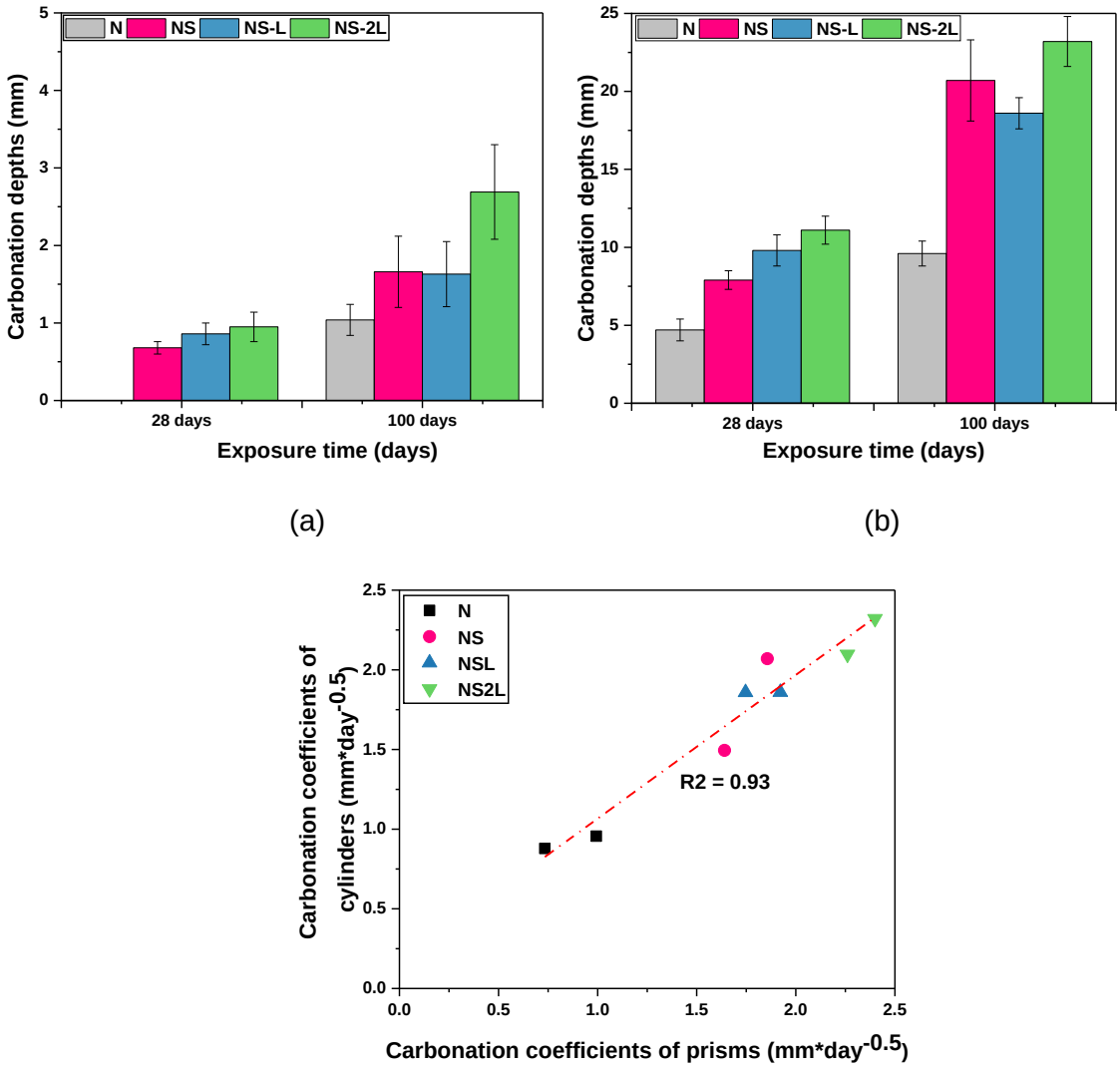

Figure 6.7: Carbonation depth of concrete cylinders after 28 days and 100 days (a) natural, (b) accelerated carbonation exposure and (c) correlation between accelerated carbonation coefficients (28 and 100 days) of prisms and cylindrical specimens

The results in Figure 6.7(c) demonstrate that similar carbonation depths are recorded for specimens of different geometries under the same carbonation exposure conditions such as those specified in the BS EN 12390-12:2022 (166). Meanwhile, the cylindrical concrete subjected to unidirectional carbonation shows different carbonation depths relative to mortar cylinders (Section 4.3.4.1) under similar exposure conditions. This follows the explanation attributable to the discrepancies in carbonation depth reported for prismatic specimens at different scales (mortar or concretes) as discussed in Section 6.3.1.

6.3.4.2. Variation in water absorption properties in carbonated concretes

The water absorption characteristics of concretes give insight into the porosity and their pore structure connectivity. Thus, the admissibility of water into capillary pores serves as useful durability indicator (87, 88), and it is typically quantified by measurements such as sorptivity coefficient; essentially the ratio of mass changes at different times to the square root of time. Sorptivity profiles of partially carbonated cylinders post 28 and 100 days of natural or accelerated carbonation exposure are shown in Figure 6.8(a-d). The sorptivity profiles show comparable trends, however the nuances in suction properties can be seen in the concrete mixes quantified in Table 6.7 and Table 6.8 as sorptivity coefficient and total water absorption respectively.

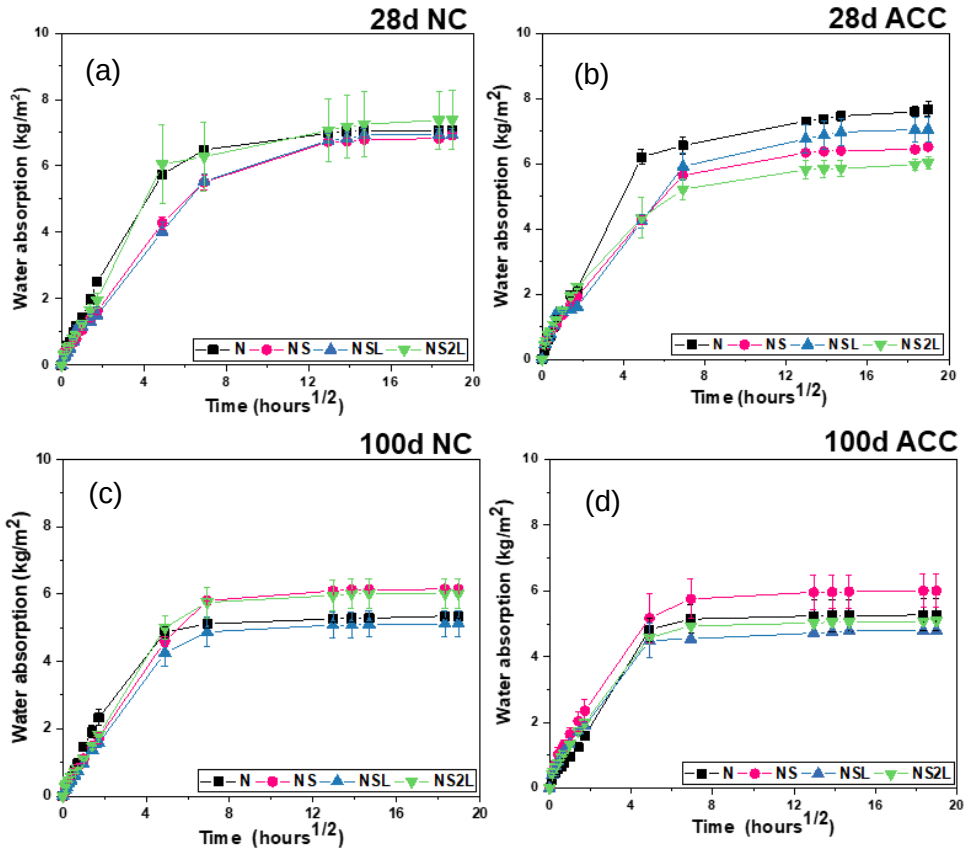

Figure 6.8: Sorptivity profiles of concrete mixes after (a) 28days of natural, (b) 28days of accelerated, (c) 100days natural and (d) 100days accelerated carbonation exposure

CEM I shows a decreased sorptivity coefficient post prolonged carbonation relative to 28 days carbonation, and independent of the carbonation exposure type. Meanwhile, the composite binders generally demonstrated increased sorptivity coefficient (all mixes, including NSL when

considered with error margins) post 100 days carbonation irrespective of exposure type. That notwithstanding, comparing the mixes by specific exposure types and age, it is not conclusive that CEM I demonstrated reduced sorptivity coefficients relative to composite cements. For example, even though post 100 days natural carbonation, NS, NSL and NS2L generally show an increase relative to CEM I, the 100 days post accelerated carbonation (considered as the extreme scenario) show comparable values for all mixes (including NSL when considered within error margins).

Table 6.7: Sorptivity coefficients ($kg*m^{-2}*h^{-0.5}$) of 28 days carbonated concrete mixes after natural or accelerated carbonation exposure. Error values correspond standard deviation of two curves

	Natural carbonation		Accelerated carbonation	
Mix ID	**28 days**	**100 days**	**28 days**	**100 days**
N	0.96 ± 0.12	0.79 ± 0.03	1.11 ± 0.06	0.94 ± 0.12
NS	0.79 ± 0.04	0.84 ± 0.001	0.77 ± 0.02	0.99 ± 0.21
NSL	0.78 ± 0.04	0.85 ± 0.12	0.79 ± 0.08	0.73 ± 0.3
NS2L	0.97 ± 0.25	0.99 ± 0.09	0.72 ± 0.11	0.90 ± 0.003

Findings in partially carbonated concretes exposed to natural conditions can be explained by the influence exerted by continuous hydration in the uncarbonated region (internal curing) relative to the smaller carbonated section identified in the samples evaluated. In the natural carbonated area, it is expected that the pore refinement characteristics of blended slag concrete counteract changes in porosity associated with decalcification of hydrated phases at slow carbonation rates, which potentially contributed to a the overall lower sorptivity coefficients relative to CEM I (180), post 28 days. While CEM I coefficients reduce after 100 days natural carbonation, and composite cements increase, the changes are less detrimental (< 8%). The evident reduction in sorptivity coefficients of CEM I post 100 days of accelerated carbonation relative to 28 days, unlike when compared to NS, NSL and NS2L is attributable to densification of microstructure due to carbonated phases in the pore system (179), and continued clinker hydration for the duration of the test. However, the comparable sorptivity coefficients under the severest conditions (post 100 days accelerated exposure) suggest that factors, other than or in addition to carbonation-induced decalcification, influence the sorptivity under accelerated carbonation. It is also worth noting that the potential impact of carbonation shrinkage-induced microcracking is not prevalent, as discussed in Section 6.3.3.

Table 6.8 shows the total water absorption of concrete mixes. Under natural carbonation, NS2L shows slightly higher water absorption at 28 days but exhibits comparable values by

100 days ambient exposure similar to the water absorption of CEM I at 100 days. This gives an indication of less detrimental impact under prolonged carbonation exposure. Similarly, for accelerated exposure, increased carbonation front did not translate into increased water absorption by 100 days accelerated exposure. Similar reasons attributable to sorptivity properties also explains the water absorption post-carbonation exposure.

Table 6.8: Total water absorption (%mass) of 28 and 100 days carbonated concrete mixes under natural or accelerated exposure. Error values correspond to standard deviation of two measurements

	Natural carbonation		Accelerated carbonation	
Mix ID	**28 days**	**100 days**	**28 days**	**100 days**
N	5.38 ± 0.44	5.0 ± 0.32	5.8 ± 0.52	5.43 ± 0.14
NS	5.15 ± 0.1	5.66 ± 0.25	4.82 ± 0.24	5.44 ± 0.95
NSL	4.77 ± 0.14	4.91 ± 0.23	5.29 ± 0.24	4.48 ± 0.10
NS2L	5.51 ± 0.55	5.15 ± 0.20	5.27 ± 0.10	4.84 ± 0.10

When the combined influence of carbonated (pore structure changes) and uncarbonated regions (continued hydration and consequent pore refinement) on sorptivity are considered, it can be concluded that the addition of limestone does not have a significant detrimental impact on the water absorption properties of the ternary mixes. This is consistent with findings reported by Chen et al. (206), who demonstrated that limestone fines reduced water permeability and sorptivity in cured concrete. Thus, the uncarbonated region most likely undergoing hydration (albeit slow) could exert resistance to moisture ingress due to pore structure refinement, which has a bearing on the overall moisture penetrability.

Comparing the water absorption properties on the concrete and mortar scale, while the sorptivity coefficients present similar range of values, it appears the water absorption values on the mortar scale are slightly elevated. The explanation for this can be attributable to potential sensitivity of the mortar sample to preconditioning during oven drying due to relatively high paste volume (88) compared to concretes.

6.3.4.3. Changes in volume of permeable voids

The results for vacuum saturated porosity of the partially carbonated concrete mixes are shown in Figure 6.9. As can be seen there is no marked changes in porosity at the early and advanced exposure times, irrespective of the exposure method.

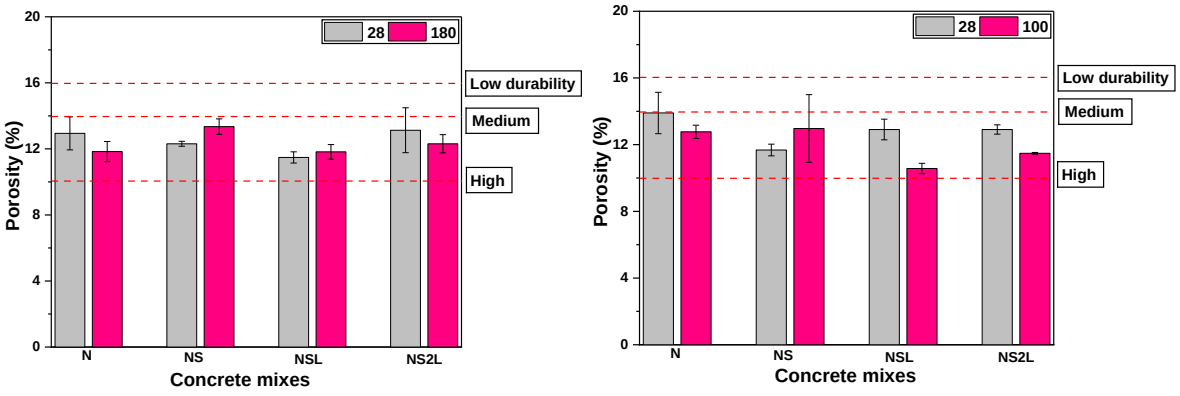

Figure 6.9: Total porosity changes in carbonated concrete mixes after (a) 28 and 100 days of natural carbonation and (b) 28 and 100 days of accelerated carbonation exposure

No significant changes in the total porosity are observed, consistent with the post-carbonation compressive strength recorded, where residual strength (Figure 6.5) exhibited no reduction in strength below design strength even for fastest carbonating concrete with high limestone content (NS2L) (Figure 6.7(a-b)). Similarly, the potential influence of carbonation-induced pore structural changes appears to be less evident when the net total porosity is considered based on the influence of both carbonated and uncarbonated regions. Porosity classification following Véronique Baroghel-Bouny's (182) performance-based durability indicators of cementitious systems shows all concretes exhibited medium to high durability irrespective of the exposure type and age of exposure.

Discrepancies are observed between mortar (Section 4.3.4.3) and concrete. Despite about 1.5-fold increase in carbonation depth at prolonged natural or accelerated carbonation exposure when evaluating concrete relative to the mortar specimens, the porosities of the concrete mixes generally show reduced porosity compared to mortars.

6.3.4.4. Effect of carbonation on bulk conductivity

Figure 6.10(a-d) shows the bulk conductivities of concrete mixes after 28 days and 100 days of natural or accelerated carbonation exposure, and superimposed with corresponding carbonation depths. The bulk conductivities of slag-containing concretes with or without limestone are lower relative to CEM I, irrespective of the carbonation exposure type at 28 and 100 days. Under natural carbonation, the bulk conductivities of all concrete mixes are comparable for 28 and 100 days exposure. Meanwhile under accelerated carbonation

exposure, the bulk conductivity of CEM I reduces relative to corresponding natural carbonation exposure ages, while no changes are observed for NS, NSL and NS2L independent of exposure type and age. The result suggest that the higher carbonation depth in NS, NSL and NS2L relative to CEM I does not translate into noticeable changes in bulk conductivity in all cases. This conforms to the lack of direct dependency between carbonation depth and bulk conductivity as observed on studies on mortar scale (see Section 4.3.4.4).

The result show that the observed reductions in the bulk conductivity of CEM I post accelerated exposure was significant when increased carbonation depth was recorded. As can be seen in Figure 6.10(d), the bulk conductivity at 100 days of accelerated carbonation reduces to bulk conductivity levels comparable to NS, NSL and NS2L. The reduction in bulk conductivity in CEM I with increasing carbonation depth is plausibly due to well-known densification effects related to carbonation by-products in the carbonated area (179), potentially imposing discontinuities in the pore system.

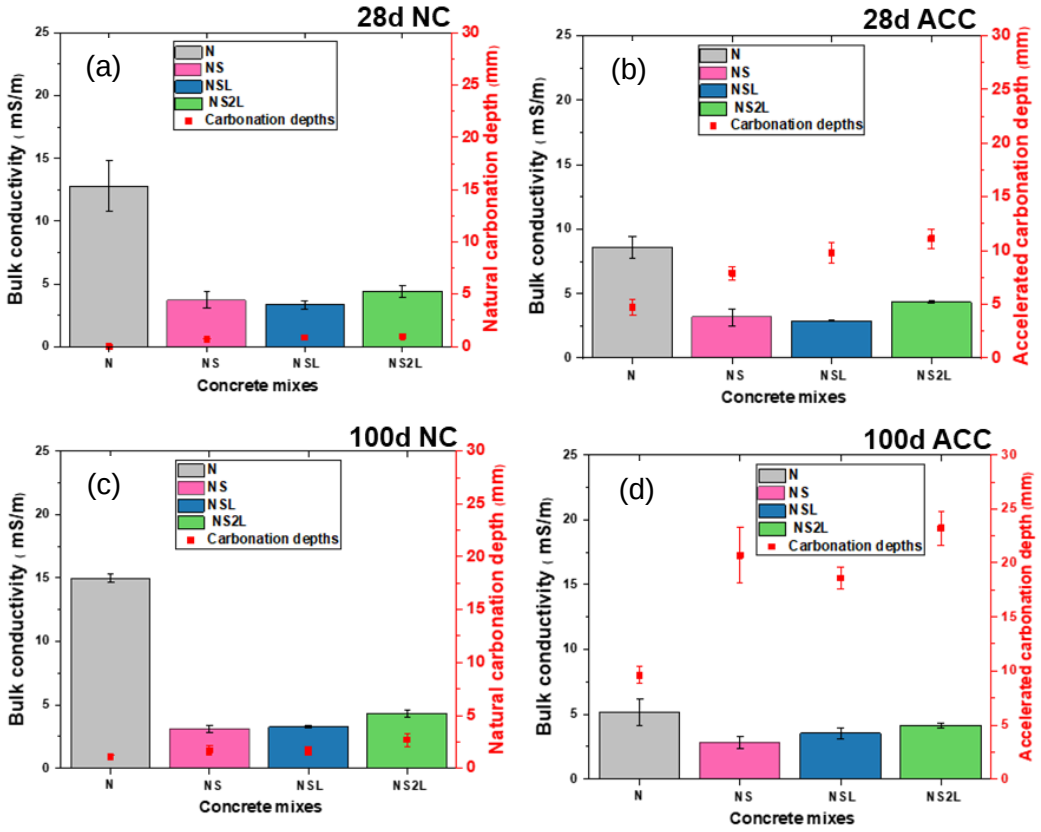

Figure 6.10: Bulk conductivity (mS/m) of concrete mixes after (a) 28 days of natural carbonation (b) 28 days of accelerated carbonation, (c) 100 days of natural carbonation, and (d) 100 days of accelerated carbonation

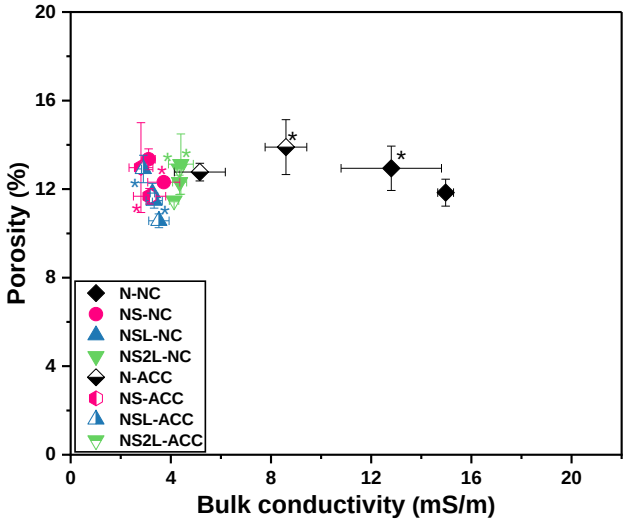

Figure 6.11: Porosity Vs Bulk conductivity of concrete mixes after 28 and 100 days natural/accelerated carbonation. Note: Data points with or without asterisks (*) correspond to 28 or 100 days respectively]

This assertion may not apply to NS, NSL and NS2L as the bulk conductivities were comparably independent on the exposure type and duration. The unnoticeable variation in bulk conductivity with increased carbonation depth in NS, NSL and NS2L suggests that other factors in addition to pore structural changes, including chemical factors such as ionic pore solution (189), are unaccounted for by the bulk conductivity measurements. The bulk conductivity results are somehow consistent with total porosity (Figure 6.9) and water absorption properties (Table 6.7, Table 6.8) observed in the concretes after accelerated 100 days carbonation exposures, where negligible differences were observed, even when higher carbonation depths were recorded. It is also worth mentioning that similar changes in bulk conductivities were also observed for studies on the mortar scale (see Section 4.3.4.4). That notwithstanding, no correlation exist between the bulk conductivity and porosities as shown in Figure 6.11. Considering relatively higher carbonation rates but lower porosities were observed on the concrete scale compared to the mortar, similarities in their bulk conductivities suggest factors other than solely physical effects control the bulk conductivity.

6.3.4.5. Impact of carbonation on chloride ingress

Figure 6.12 (a-d) shows the chloride permeability of the carbonated concretes, where it can be seen that CEM I exhibits inferior chloride permeability to NS, NSL and NS2L for all ages and carbonation exposure conditions assessed. While the chloride migration coefficient of all

concrete mixes after 28 days and 100 days of natural carbonation are comparable, they increased upon accelerated carbonation. The increase in migration coefficients post-accelerated carbonation is more evident after 100 days of exposure, where higher values were observed in the concretes made with ternary cements. It is worth noting however that, while the carbonation depth of NS2L concrete was ~3 folds greater than in CEM I, the increase in its chloride permeability is nearly less than 50% that of CEM I.

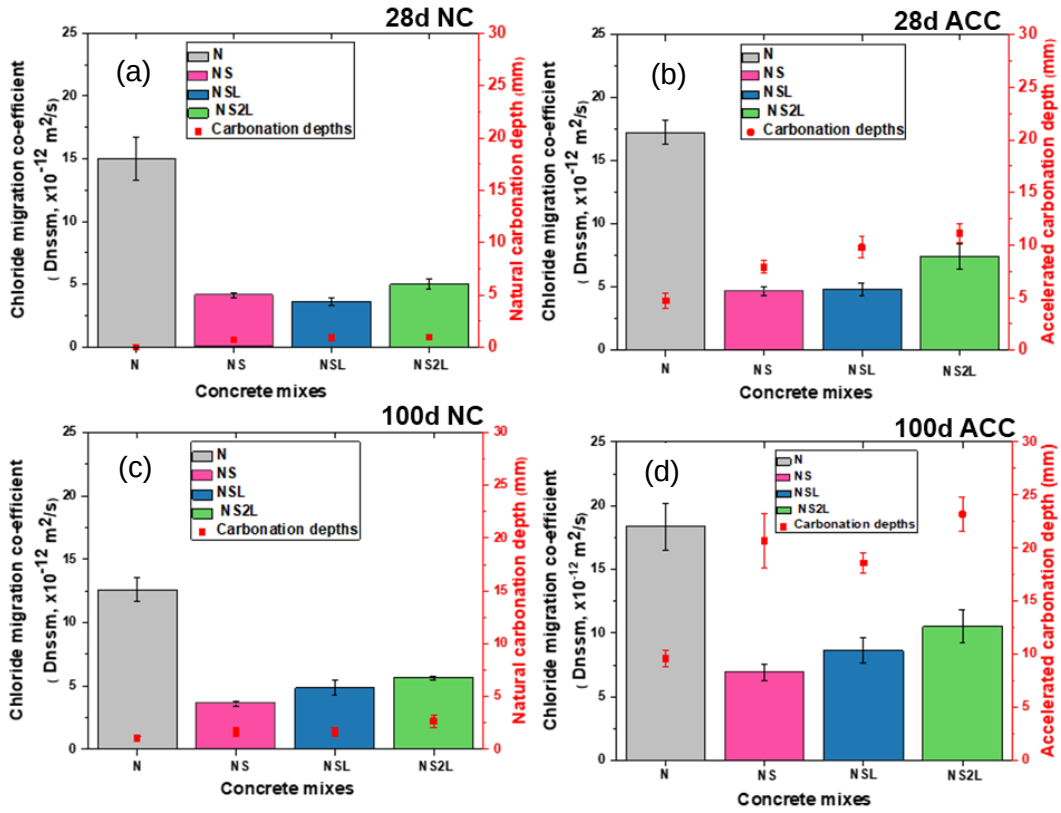

Figure 6.12: Chloride migration co-efficient (m^2/s) of concrete mixes after (a) 28 days of natural carbonation, (b) 28 days of accelerated carbonation, (c) 100 days of natural carbonation, and (d) 100 days of accelerated carbonation

The results can be explained by a combination of physical and chemical factors. Slag addition to NS, NSL and NS2L results in hydrates that can chemically bind/adsorb chlorides including C-A-S-H, hydrotalcite like phases, AFm phases and potentially AFm-CO_3^{2-} phases (190-192). This induces a lower chloride migration in the slag-blended system, with or without limestone, when compared to CEM I in all cases. The physical influence can be considered in terms of refined pore structure (due to continued hydration in the uncarbonated zone, albeit a reduced rate) and pore volume changes in the carbonated zones. Such changes are expected to be

more detrimental in NS, NSL and NS2L relative to CEM I due to their overall inferior carbonation depths. However, at advanced accelerated carbonation ages, the chloride permeability of concretes made from blended cements are still significantly less than CEM I. No correlation between the porosity and chloride permeability (Figure 6.13), nor porosity and bulk conductivity (Figure 6.11) was identified in the concretes evaluated, which confirms that chemical factors are likely dominating the performance of the materials when exposed to chlorides.

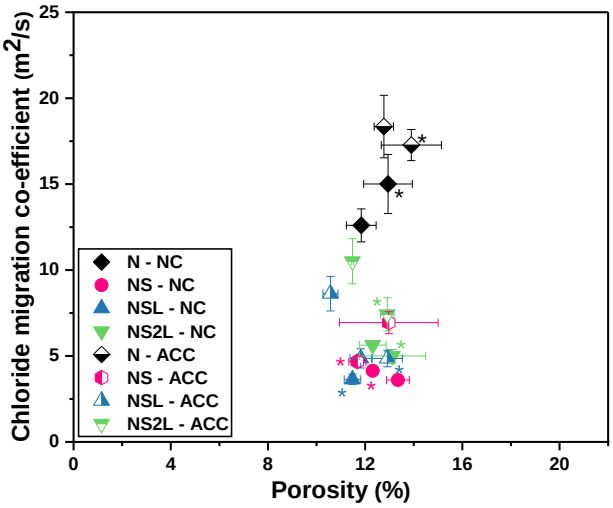

Figure 6.13: Chloride permeability Vs porosity of concrete mixes after 28 and 100 days natural/accelerated carbonation. Note: Data points with or without asterisks (*) correspond to 28 or 100 days respectively]

The findings on the influence of carbonation on chloride permeability are consistent with other studies on binary slag (114), and ternary slag-fly ash (94) hardened mortars and concretes, which are largely based on prolonged exposure to chlorides based on diffusion.

6.3.4.6. Impact of carbonation on chloride ingress relative to cured concrete

Towards assessing the extent of variations in chloride permeability due to carbonation, the post-carbonated chloride permeability was compared to corresponding cured 28 days concretes as shown in Figure 6.14. Based on the observations in concretes studied in Chapter 5; Section 5.3.3.4, all concrete mixes exhibited reducing permeability to chlorides with curing age from 28 days to 180 days, independent of mix design. This suggests that the 28 days cured chloride migration coefficient can be considered as the worst-case scenario of chloride

permeability in this study. Thus, it can be argued that the worst performance of concretes post-carbonation can be assessed when benchmarked or referenced with the 28 days cured chloride migration coefficient. It must be also acknowledged that all specimens prior to carbonation were 28 days cured, which further justifies their use as reference values.

In Figure 6.14(a), it can be seen that all concrete mixes exposed to natural carbonation do not show any reduction in performance by 100 days when compared to with 28 days cured concretes. Meanwhile in Figure 6.14(b), while CEM I exhibited increased chloride permeability post 28 days and 100 days accelerated carbonation relative to the 28 days cured uncarbonated concretes, the slag-containing concretes with or without limestone showed reduced post 28 days carbonation chloride permeability but increased post 100 days. However, the increase in chloride permeability post 100 days accelerated carbonation is marginal in NS, NSL and NS2L. These marginal increases are also significantly lower when compared to the chloride permeability of 28 days cured CEM I.

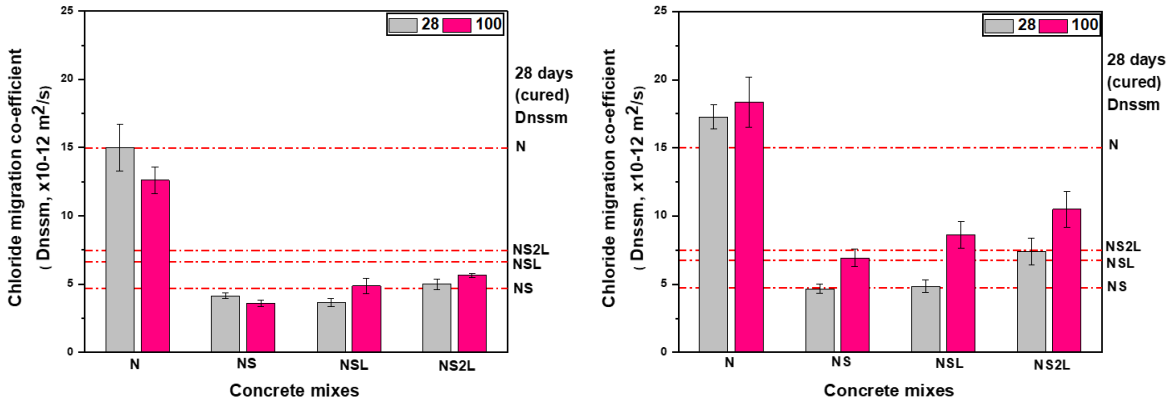

Figure 6.14: Chloride permeability of concrete mixes after 28 and 100 days exposure to (a) natural carbonation or (b) accelerated carbonation, benchmarked against 28 days coefficients determined in cured concrete pre-carbonation

The less detrimental impact of natural carbonation is plausibly due to ongoing hydration (albeit slow) in the non-carbonated region contributing to mitigate the effect of carbonation. A combination of pore refinement on chloride permeability observed for cured concretes (explained in detail in Section 5.3.3.4) in addition to chemical interaction with chlorides likely account for this. However, for the accelerated carbonated concretes, the influence of ongoing hydration is likely diminished particularly with significant carbonation depths as the chloride

permeability varies from the chloride permeability of cured concretes. Nevertheless, the reduced net influence of carbonation on NSL and NS2L relative to CEM I also suggest that effects of their carbonation-induced pore structure related variations on chloride permeability might also be limited.

6.4. Conclusions on carbonation performance of composite Portland cement-slag-limestone concrete and its impact on chloride permeability

Based on the experimental findings on the influence of carbonation on the transport properties of concrete made from CEM I, binary cement with ~50% GGBS, ternary cement with GGBS plus ~10% limestone and GGBS with ~20% limestone corresponding to N, NS, NSL and NS2L, respectively, the following deductions can be made:

1. CEM I concrete exhibited high resistance to carbonation relative to the slag-containing concrete, with or without limestone, at all durations of natural or accelerated carbonation exposure. Meanwhile, binary slags and ternary slags concrete exhibited comparable carbonation resistance.

2. While NS, NSL and NS2L showed inferior carbonation performance relative to CEM I, carbonation service prediction gives an indication of potential serviceability up to 50 years for binary and ternary concrete, when benchmarked with cover depth recommendations in the BS 8500-1:2023.

3. The residual compressive strength of all concrete mixes after carbonation based on ratios of natural to accelerated carbonation for the same age (100 days) shows an increase in strength for N, NS and NSL, while NS2L exhibited a decrease in strength. However, concrete with the least post-carbonation strength (NS2L) remain higher than its design strength. This indicates that the continued hydration (slow) of the binder is positively contributing to the strength gain of the material, even at moderate RH (57%), such as the one adopted for inducing natural or accelerated carbonation. The result also suggest carbonation-induced strength can potentially influence the long-term performance of concretes studied, particularly NS2L.

4. Drying shrinkage under ambient conditions is reduced in concretes made with composite cements relative to CEM I. While a similar trend was observed under accelerated carbonation, marginal shrinkage strains were observed in the ternary mixes. Nonetheless, higher carbonation rates did not translate into significant strains

in NS, NSL and NS2L relative to CEM I. Maximum of ~75 microstrain increase (compared to ambient conditions) was found for CEM I concrete and increase of about ~25-30 microstrains was found for NS, NSL and NS2L due to accelerated carbonation.

5. Studies of water absorption properties showed that CEM I exhibited decreased sorptivity coefficient after 100 days carbonation relative to 28 days carbonation, irrespective of the carbonation exposure conditions. NS, NSL (NSL when considered with error margins), NS2L generally demonstrated increased sorptivity coefficient post 100 days carbonation irrespective of exposure type. In addition, there is no marked change in the total porosity of the samples neither at early nor at later exposure times, independently of the exposure condition adopted (natural vs accelerated). This might be indicating that carbonation is most likely inducing changes in the pore size distribution of the materials evaluated, but no changes in the total porosity are taking place. This is somehow consistent with the compressive strength recorded for carbonated samples, where residual strength exhibited no reduction below design strength, even for NS2L concrete with the worst carbonation performance.
6. It can further be concluded that reducing slag content in blended cements for ~10 or ~20% limestone addition to produce ternary cements does not significantly compromise their chloride resistance when both binary and ternary forms are subjected to similar carbonation exposure conditions.
7. It is identified that no clear correlation exist between compressive strength, porosity, bulk conductivity, sorptivity coefficient and carbonation rate similar to finding on the mortar scale. Therefore, none of those parameters can be directly used to solely infer potential longevity of slag-based concretes.

Overall, it can be concluded that reducing slag content in blended cements for ~10 or ~20% limestone addition has no detrimental impact on the carbonation performance of their ternary blended mixes with high limestone content. Meanwhile it also is identified that, while the carbonation rates of slag-containing concretes with or without limestone exhibit relatively higher carbonation rates to CEM I, this does not translate into detrimental impairment of their known resistance to chlorides under curing conditions. For a similar exposure duration to a carbonation environment, it is hypothesised that concretes made from composite cement with up to 20 % limestone addition can demonstrate better resistance to chloride-induced corrosion than CEM I despite their poor carbonation resistance.

Based on the understanding developed on the carbonation performance of ternary systems relative to binary and CEM I, an additional study to interrogate the performance of these systems under carbonation exposure while being subjected to mechanical loads are further

discussed. Furthermore, how the coupled actions influence transport properties is also reported.

6.5. Combined action of compressive load and carbonation on transport properties of composite concrete

The dimensional stability in stressed states for concrete made with ternary cements and higher SCMs replacement contents is not well understood, particularly when the concrete undergoes carbonation. In this study, the dimensional changes of blended slag cement concretes, with or without limestone, subjected to simultaneous compressive stress and accelerated carbonation are reported. Six concrete specimens per mix made with CEM I, CEM I + slag or ternary slag–limestone cements were cured for 7 days before subjecting them to a ~30% stress/strength ratio uniaxial compressive loading under natural and accelerated (3% CO_2) carbonation for up to 28 days. The results show that the total strain evolution of ternary CEM I-slag concretes with ~10-20 wt.% limestone addition was comparable to that of binary CEM I-slag concretes, both of which showed lower deformation compared to CEM I under natural or accelerated carbonation. However, greater strains were recorded under accelerated carbonation exposure, and the increase was more pronounced in the ternary binder concretes. The loaded concretes exhibited less (micro) cracking tendencies, which might be potentially reducing the carbonation rates compared to non-loaded concretes. The results indicate that partial substitution of CEM I with slag + ~20% limestone did not significantly reduce carbonation resistance nor dimensional stability of the concrete. It is also identified that the combined action of loading and carbonation has no detrimental impact on strength or transport properties of concretes made with composite slag-rich cements.

6.5.1. Experimental procedure

The concrete mixes used in this study were based on the mix design used in Chapter 5. Six 75 × 75 × 200 mm concrete prisms per mix were cast and cured in the moist room for 7 days. A conservative approach was adopted for loading concrete specimens at 7 days to accommodate any uncertainties during loading of the ternary mixes (particularly NS2L) which have limited body of knowledge on their engineering properties. After curing, the concrete prisms were surface air-dried and then surface prepared for strain gauge appendage and subsequent loading as discussed below.

6.5.2. Sample preparation and loading setup

The surface-dried 75 × 75 × 200 mm concrete specimens were instrumented with 60 mm, 120-Ohm strain gauges using lightly applied and sanded adhesive to ensure continuous contact to flattened surface prior to attaching the strain gauges. This was to enhance bonding to concrete. The bonded strain gauges were then lead-soldered to wires, which were subsequently connected to separate channels on a data logger. Concrete specimens were centrally positioned in the loading rig equipped with a 15-tonne load cell. Centred specimens allowed for efficient and sustained load transfer to concrete specimens. Each loading rig consisted of one load cell and four strain gauges (2 per either side of upper and lower prism) per set connected to channels via quarter bridge completions to the data logger. Strain data logging frequency was on hourly basis. A detailed description of the setup configuration has been provided in Section 3.5.4 and 3.5.5.

6.5.3. Combined action of loading and carbonation

Following the sample surface preparation and the loading rig set up, two 75 × 75 × 200 mm prisms per loading rig per concrete mix were exposed to natural or accelerated carbonation while being subjected to compressive load. The applied stress (kN) was ~30% of their compressive strength determined prior to loading, in accordance with EN 12390-17:2019 (165), and calculated as 63.4, 38.6. 37.1 and 37.1 kN for N, NS, NSL and NS2L, respectively. The applied stress corresponds to the same stress strength ratio of 1.88 for all mixes. The elastic strain was captured immediately load was applied. Furthermore, the strain evolution was automatically recorded for loaded concretes subjected to accelerated [3% (CO_2), 60% RH, and 20^{o}C] and natural carbonation [60 %RH, and 20 ^{o}C] for 28 days. Accelerated carbonation was induced according to EN 12390-12:2020 (166); without the sample preconditioning step. The strain data acquisition in the closed environmental chamber during accelerated carbonation with load employed the wireless data logging system with remote transmission capability of strain data to a computer. After the duration of the loading cycle, the loaded prisms were dismounted for further testing without monitoring the recovery strain. The dismounted prisms are addressed as pre-loaded concretes in this chapter.

For all loaded concretes, complementary specimens were kept under the same environmental conditions as the loaded concretes, but without load, and were monitored for carbonation depth after 28 days. The non-loaded specimens were surface prepared similar to loaded concretes to ensure similar surface areas for CO_2 ingress. The strain (shrinkage) evolution was however, not monitored for the non-loaded concretes. It is worth highlighting that the

measurement from non-loaded concretes could be used to calculate creep (strain) by subtracting the shrinkage values from the total strain of loaded samples. However, this is not pursued considering the focus of this study was to compare the progression of carbonation front in both cases. The deformational characteristics of loaded samples are addressed by reporting the total strain. The unstressed concretes are interchangeably addressed as non-loaded, no load, not loaded or without load in this chapter.

It is worth mentioning that the exposed surfaces of concretes were adjacent to the as-cast surface due to experimental constraints as described in Section 3.5.7.2. The adopted methods nonetheless agree with recommended surfaces suitable for CO_2 ingress reported in a RILEM TC 281-CCC document (117) when prismatic specimens are used for studying combined action of load and carbonation. However, different reasons such as the influence of as-cast surface and bottom-cast surfaces on CO_2 diffusivity were cited in the RILEM TC 281-CCC for such recommendation. This indirectly affirms the robustness of the adopted experimental methodology.

6.5.3.1. Carbonation performance and residual strength

One 75 × 75 × 200 mm per mix of the loaded concretes was used for carbonation depth monitoring and subsequently tested for compressive strength. The carbonation depths of loaded concretes were determined by spraying phenolphthalein in isopropanol (IPA) solution on freshly sliced concretes. After measuring the carbonation depths, the same samples were used for compressive strength testing towards assessing their residual strengths. Compressive strength was determined on 75 mm cubes in duplicates at a 6 kN/s loading rate based on BS EN 12390-3:2019 (157), with 75 × 75 mm^2 plates placed at top and bottom of the tested concrete. Similarly, the non-loaded concretes were correspondingly tested for compressive strength post-carbonation depth measurement. The pre-loaded and non-loaded concretes were tested post 28 days of natural or accelerated carbonation exposure, including concretes loaded for 200 days.

6.5.3.2. Coupled effect of compressive loading and carbonation on water absorption properties of concrete

For assessing the impact of the combined action of loading and carbonation on transport properties, 50 × 50 × 75 mm slices per mix were obtained from one of the pre-loaded 75 × 75

× 200 mm concrete specimens for water absorption testing. A similar number of slices were obtained from the non-loaded concrete. The water absorption testing including sample preparation, preconditioning, sorptivity and vacuum saturated porosity (%) testing are described in detail in Chapter 3, Section 3.5.8.4. Sorptivity profiles were plotted as mass change at predefined times against the square root of time up to 15 days from which the initial and final sorptivity coefficients could be calculated. The total porosity or volume of permeable voids was calculated as the ratio of their weight (%) changes (after vacuum water saturation) to sample volume. Testing was conducted on pre-loaded and non-loaded concretes post 28 days of natural or accelerated carbonation, as well as on the concrete loaded for 200 days.

6.6. Results and discussion

6.6.1. Impact of sustained compressive load on carbonation depths

The carbonation depths of concretes subjected to compressive load (~30% of the 7 days compressive strength) and the corresponding non-loaded concretes are shown in Figure 6.15. Independent of the loading and carbonation exposure condition, the binary and ternary mixes exhibited increased carbonation depth in comparison to CEM I. Meanwhile, it is also identified that the binary mixes show comparable carbonation resistance to ternary mixes. For concretes exposed to 28 days of natural carbonation without load, it can been seen that carbonation depth was only recorded in the concretes made with binary and ternary cements. Conversely, no identified carbonation depths can be recorded for the loaded concretes under natural carbonation exposure conditions, independently of the concrete mix design. However, when the duration of combined natural carbonation with loading was extended to up to 200 days, the progression of carbonation becomes evident. The unnoticeable carbonation front in loaded specimens after 28 days of exposure, may potentially be associated with partial closure of early-age microcracks, which impeded the ingress of CO_2 as suggested in (13). However, with prolonged ambient carbonation exposure under load, the tendencies of microcracking coalescence (81) potentially influenced CO_2 diffusivity resulting in the observed carbonation depth after 200 days natural carbonation. The result suggests concretes made with composite cements can be used in stressed state in early phases of construction with limited carbonation progress, however further investigation is required for validating these potential phenomena.

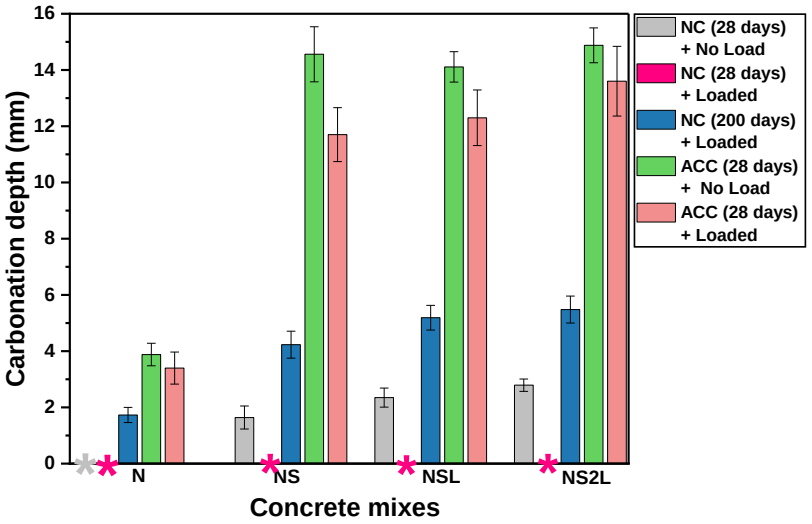

Figure 6.15. Carbonation depths after 28 and 200 days of exposure to ambient/natural (NC) or 28 days accelerated (ACC) carbonation for stressed (loaded) and non-stressed (non-loaded) concretes. * *denote no depth recorded for the concrete mix corresponding to the colour code of exposure type*

For the concretes subjected to accelerated carbonation with or without loading, CEM I exhibited relatively lower carbonation depth relative to the slag-containing concretes with or without limestone. However all concretes appear to show lowered carbonation depth in their stressed state relative to the unstressed states. The results are consistent with findings of the interlaboratory studies of the RILEM TC 281-CCC (117), where concretes stressed at 30% load level exhibited reductions in carbonation depths. It appears the stress influences the carbonation shrinkage microcracking tendencies, likely restraining volumetric changes of the specimens and therefore preventing significant changes in pore connectivity, consequently mitigating diffusivity of CO_2 into the samples. This likely led to the reductions in carbonation depth identified in the loaded specimens compared to the non-loaded concretes.

Meanwhile, it is also worth mentioning that the RILEM TC 281-CCC recommended the use of 90 days cured concretes made with SCMs (such as slags) for studying the combined effect of loading and carbonation (117). However, it is interesting to note that the carbonation depths for CEM I and slags concretes under loading conditions in this study demonstrated comparable carbonation depths to the RILEM TC 281-CCC, even when 90days cured concretes were exposed 20% CO_2 concentration at 30% stress levels for similar exposure duration (28 days) to this study. The findings from this study suggest that shortened curing time in both exposure methods is not expected to have detrimental impact on carbonation depth in their stressed state. It must be acknowledged that the age of loading will also influence

the strain evolution of concretes irrespective of stress type (225, 226). Thus, the recommendation for the use of 90 days cured concretes made from SCMs for studies on the combined action of load and carbonation, may not give a true picture of the performance composite concretes in early age use as structural concrete.

Meanwhile, it must be highlighted that conditions of temperature and relative humidity under accelerated carbonation were under highly stable (57±3 RH% and 20±3 ^{o}C) conditions, while natural carbonation exposure presented fluctuations in relative humidity and temperature. However, the conditions under natural exposure was maintained at 60±10 RH% and 20±3 ^{o}C as can be seen in Figure 6.16. Thus, this provides a basis for comparison of specimens kept in both environments, considering the range of values are comparable.

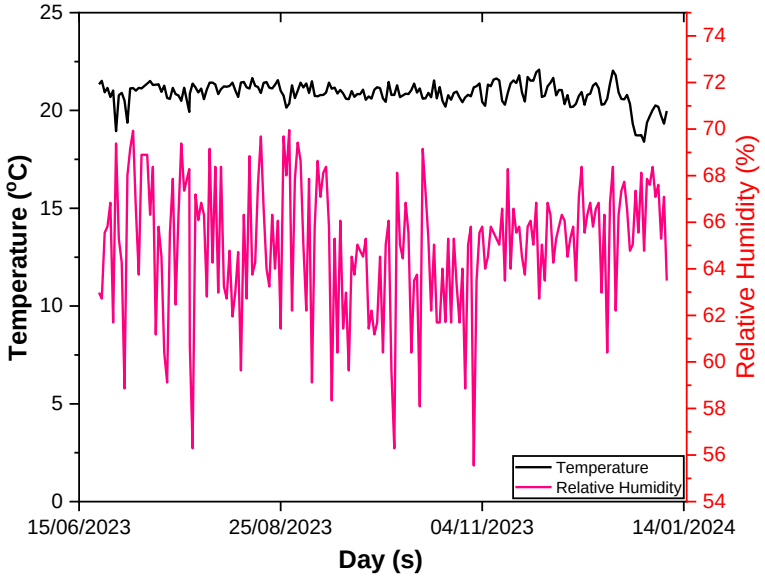

Figure 6.16: Temperature (^{o}C) and relative humidity (%) evolution in natural environment

6.6.2. Residual compressive strength

Figure 6.17(a) and Figure 6.17(b) show the compressive strength results of stressed and unstressed concretes after natural and accelerated carbonation respectively. In Figure 6.17(a), for all the concrete mixes, there is no marked change in the 28 days post-natural carbonation strength of loaded or non-loaded concretes. The binary and ternary mixes exhibit slightly reduced strength post 28 days loading relative to CEM I. However, it is also observed that, at an extended loading period of up to 200 days, the binary and ternary achieve strength closer to CEM I, this being more noticeable in the ternary mixes. Similar increases in compressive strength have been reported for binary slag concretes exposed to carbonation

for up to 20 years, with or without load (227, 228). The comparable strengths suggest the phase assemblage evolution, and hence pore structure development appears not to be influenced by the progress of natural carbonation, even under stressed state. This is evidenced when the post-natural carbonation compressive strength with or without load is compared to the 28 days cured strength (reported in Section 5.3.2.1), where all concretes achieve comparable or better compressive strength, irrespective of the loading type or mix design. This indicates that early age loading does not necessarily lead to strength loss of the concretes below their design strength. This appears to be the case even when the load is sustained for prolonged periods, particularly in the case of NSL and NS2L. This is consistent with findings elsewhere on the performance of concretes loaded within their serviceability limit (118, 229). It is also noticeable that the strength evolution of loaded concretes between 28 days and 200 days when compared to that of the water-cured concretes for similar time frames, it appears the strength gain for the same concrete mixes is dissimilar. Considering the effect of different relative humidity, it is worth noting that, for a comparable age interval, moist room cured (95%RH) concretes (see Figure 5.1(a) in Section 5.3.2.1) appeared to exhibit higher strength gain (% change) than those exposed to carbonation conditions (60%RH); natural carbonation in this case. This appears to indicate that the concrete curing at 60 %RH under loading could have a negative impact on strength development, but nonetheless well above its design strength. An obvious explanation can be attributed to the different degrees of hydration, which is expected to be higher under moist curing, while in the case of drying, an outward movement of moisture could mean a reduced rate of ongoing hydration.

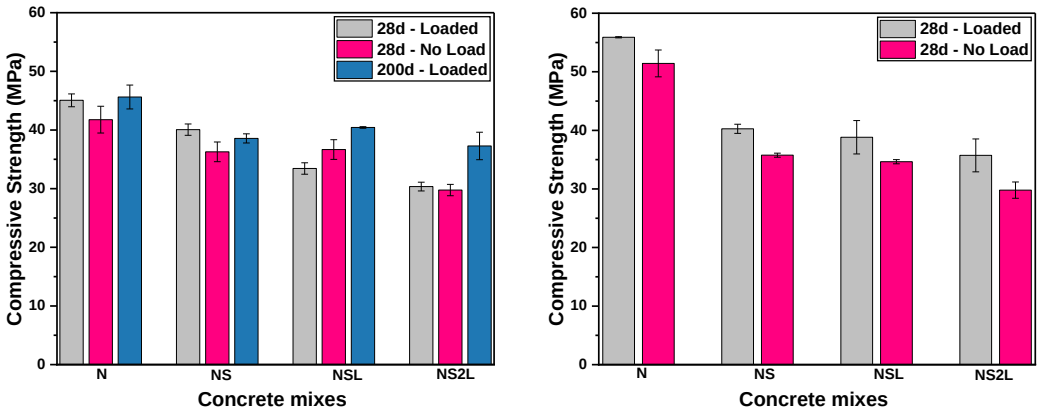

Figure 6.17: Compressive strength of stressed and unstressed concretes under carbonation exposure to (a) natural (b) accelerated conditions. Error bars correspond to standard

deviation of two measurements

Furthermore, the compressive strength of 28 days accelerated carbonated concrete with or without load is shown in Figure 6.17(b). It can be seen that the stressed concretes exhibited slightly increased strength compared to their unstressed states. This phenomenon can be attributed to reduced diffusion pathways for CO_2 ingress due to stress-induced partial closure of potential carbonation shrinkage-induced microcracks. This means that the influence of slow internal curing on strength gain is more likely than unstressed concretes. The results are consistent with the reduced carbonation depth recorded (Figure 6.15) for stressed concretes relative to unstressed concretes. This suggests that the effect of microcracking due to carbonation-induced shrinkage on strength loss is potentially minimised. It is also likely that pore densification is occurring under loading conditions resulting in a reduced CO_2 ingress rate (103), thus contributing to much higher strength increases. The influence of pore structure is not conclusive in the results, considering for a given porosity, a wide range of compressive strength is identified in both exposure types with or without load as shown in Figure 6.18(a) and (b). It is however noteworthy that the less detrimental impact of accelerated carbonation in stressed state (considering strength does not fall below design strength) suggest that, strength loss due to long-term natural carbonation (at least up to the time it would take to attain measured accelerated carbonation depths under load in this study) is less likely when composite cements are used for producing structural concrete. However, prolonged studies are required to further elucidate the observed mechanical performance.

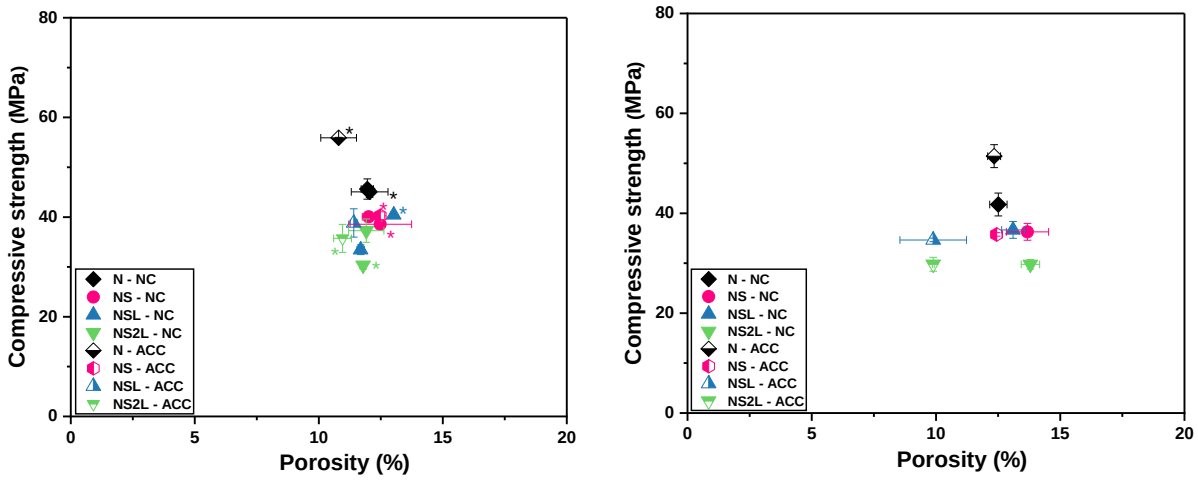

Figure 6.18: compressive strength vs porosity for concretes exposed to natural/accelerated carbonation (a) with load [Note: Data points with or without asterisks (*) correspond to 28 or 200 days respectively] OR (b) without load

The results obtained for accelerated carbonation also suggest that the performance of slag-containing containing concretes with or without limestone shows their suitability for carbonation curing application considering the less detrimental impact on mechanical properties upon accelerated CO_2 exposure (230). Overall, all concrete mixes are expected to show satisfactory in-situ compressive strength when used as structural concretes.

6.6.3. Total strain evolution

The total strain is the summation of shrinkage and load-induced strain (231). In addition to humidity conditions, several factors including cement paste content, cement type, age of loading, aggregate concentration, aggregate type and testing method can influence the dimensional stability of concrete (138, 225, 232). Under carbonating conditions, the influence of carbonation shrinkage is expected to contribute to the overall measured strain. Thus, the overall measured strain under carbonation exposure and load can be used for the assessment of the time-dependent dimensional stability of concrete specimens. This can give an indication of the potential serviceability of concrete structures particularly those produced with composite cements, which have a limited track record. Figure 6.19(a) and (b) show total strain under natural or accelerated carbonation exposure, respectively. Under both exposure conditions, it is identified that slag-containing concretes, with or without limestone, exhibit reduced strain

relative to CEM I-based concrete. However, the magnitude of strain is greater in accelerated carbonation when compared to natural exposure conditions.

For CEM I concrete, after extended exposure times (150 days in stressed state) as shown in Figure 6.19(c), the maximum strain values recorded are comparable to those of concretes exposed to accelerated carbonation for ~15 days. Meanwhile, NS, NSL and NS2L attain the maximum strain at ~10 days. The results give an indication that slag-containing concretes with/without limestone subjected to loading while exposed to accelerated carbonation can be expected to undergo deformations ~3 times higher than what can be expected under service natural carbonation conditions. This can be related to a relatively greater degree of phase changes at 3% CO_2 and associated volume changes. Nonetheless, the measured strains are still lower relative to OPC. Similar results of reduced deformations of slag-containing concrete, with or without limestone, relative to OPC have been reported in the literature (17, 232).

The improved performance of binary and ternary mixes can be associated with a combination of factors including modulus of elasticity (225) and applied stress strength ratios. It can also be related to the properties of hydrates as nano/micro-chemo-mechanical studies have demonstrated close agreement with macroscopic loading experiments (233, 234). Generally, the hydrates in slag-containing concrete are dominated by aluminium-substituted calcium silicate hydrate (C-(A)-S-H), which directly affects not only the mechanical properties but also volumetric deformations. The Al-substituted C-S-H affects dimensional stability via alterations in the volume of gel pores (large), mean chain length and the basal unit which, overall reduces deformation with reducing Ca/Si ratio (137, 235). However, in the case of C-S-H (dominant phase in OPC), micromechanical properties are somewhat retarded due to stiffer silica chains and reduced defects at higher Ca/Si; increased isotropy degree (136). The implication of dominant hydrates in slag-based concretes can explain the relatively reduced strain evolution in NS, NSL and NS2L relative to CEM I irrespective of the exposure type. Meanwhile, the increased magnitude of strain under accelerated carbonation is plausibly due to increased carbonation-induced shrinkage in the composite cement systems, associated with additional pore volume changes from phase assemblages other than carbonation of relatively large amount of portlandite in the case of CEM I, which is known to exhibit infinitesimal (small) carbonation shrinkage (179). It thus appears there is limited compensation to stresses due to shrinkage (carbonation) by applied load under accelerated carbonation than under natural exposure. This probably also accounts for the increased magnitude of the total strains in NS, NS, NS2L under accelerated carbonation.

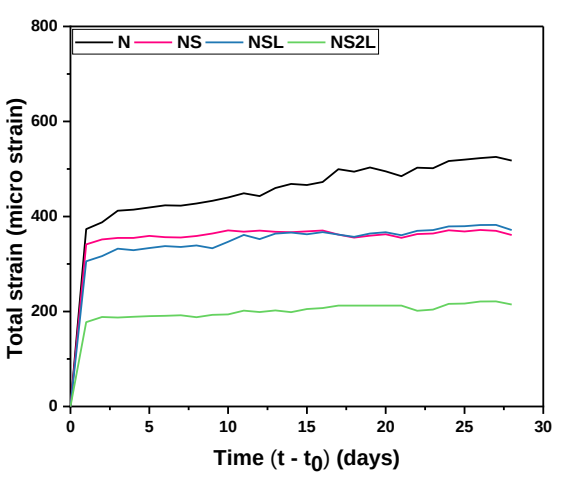

(a)

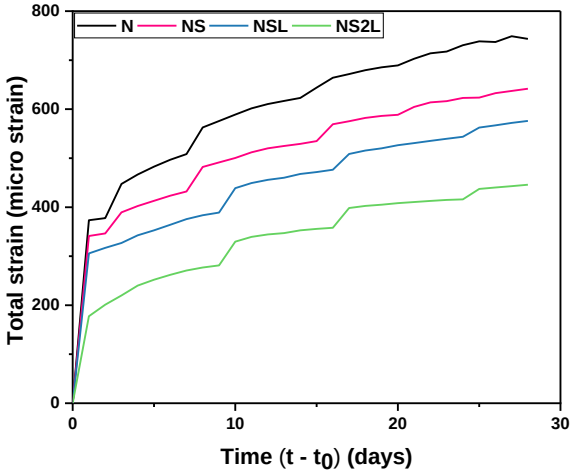

(b)

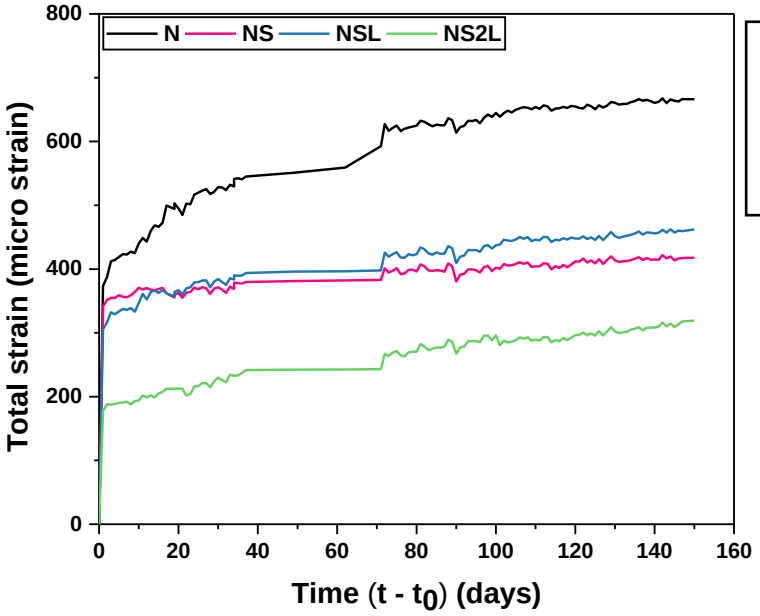

Total strain data collected for 150 days, but loading continued up to 200 days

(c)

Figure 6.19. Strain evolution of stressed concrete exposed to (a) natural, (b) accelerated carbonation for 28 days and (c) concretes exposed to natural carbonation for 200 days. (t = time; t_o = day corresponding to first day of loading concrete)

In addition, all concrete mixes were applied with same strength/stress ratio of 1.88. Under similar stress/strength ratio, it is expected that the stiffest concrete (highest elastic modulus) would record highest strain (236). As can be seen from Section 5.3.2.4 (Figure 5.4), CEM I demonstrates higher stiffness relative to the binary and ternary mixes and thus plausibly explains the increased initial and total strain evolution of CEM I relative to NS, NSL and NS2L. However, considering the initially applied load is based on the strength at the age of loading,

it may be practical to account for the time-dependent compressive strength evolution. This is however out of the scope of the current study.

It must also be highlighted that even though the loading cycle progressed up to 200 days under natural carbonation with the applied load recorded by the data logger, the strain gauges malfunctioned at 150 days. Hence, the reported total strain evolution up to 150 days in Figure 6.19(c). This also explains why studies of water transport after carbonation with load as discussed below follow testing on 200 days of loaded concretes.

6.6.4. Water absorption properties of stressed and carbonated concretes

Figure 6.20(a-e) shows the sorptivity profiles of 75 x 75 x 50 mm loaded and non-loaded concretes under natural and accelerated carbonation exposure conditions. The respective water absorption properties as quantified in terms of sorptivity coefficient and total water absorption (%mass) are shown in Table 6.9 and Table 6.10 respectively. The sorptivity coefficient after 28 days natural carbonation reduces in concretes subjected to the combined action of carbonation and load relative to the unstressed concretes. This is particularly the case for NS, NSL and NS2L, with the reduction for all mixes being more evident with prolonged loading and natural carbonation exposure. It can be seen that the extension of the loading duration to 200 days did not increase the sorptivity coefficients beyond the values obtained for the 28 days of non-loaded concretes. Meanwhile, comparing the impact of stress under accelerated and natural carbonation exposure on sorptivity, the overall effect of accelerated carbonation is not conclusive. However, there is an indication of slight increases in N, NSL and NS2L. The impact of load and carbonation on water ingress becomes more apparent when variations in total water absorption are considered, where a reduction in loaded samples relative to non-loaded samples under natural carbonation can be seen. Overall, a similar trend is observed in accelerated carbonation when loaded concretes are compared to non-loaded concretes. The reduction in water absorption at the early carbonation exposure times of stressed concretes compared to the unstressed concretes can be attributed to the partial closure of microcracks. Meanwhile, the densification effects of concretes in stressed states can also account for the observed phenomenon (13). Similar findings have been reported for slag systems damaged up to 90% of their failure loads, yet exhibited improved sorptivity properties, attributable to the self-healing potential of SCMs (77). While results of total strain evolution showed higher magnitudes under accelerated carbonation (as discussed in Section 6.3.3), and suggest an increased tendency of coalescence of microcracks, which can be

consequential to water ingress properties, this is not evident, based on the measured properties.

Under non-loading conditions, the sorptivity coefficients post-accelerated carbonation follow a similar trend as observed in Section 6.3.4.2 (Table 6.7). This suggest that even though CEM I appears to show increased sorptivity at 28 days, densification effects may become evident with prolonged accelerated carbonation, where all mixes tend to exhibit comparable coefficients. Similarly, the total water absorbed appear to be comparable for each exposure type with no indication detrimental increases.

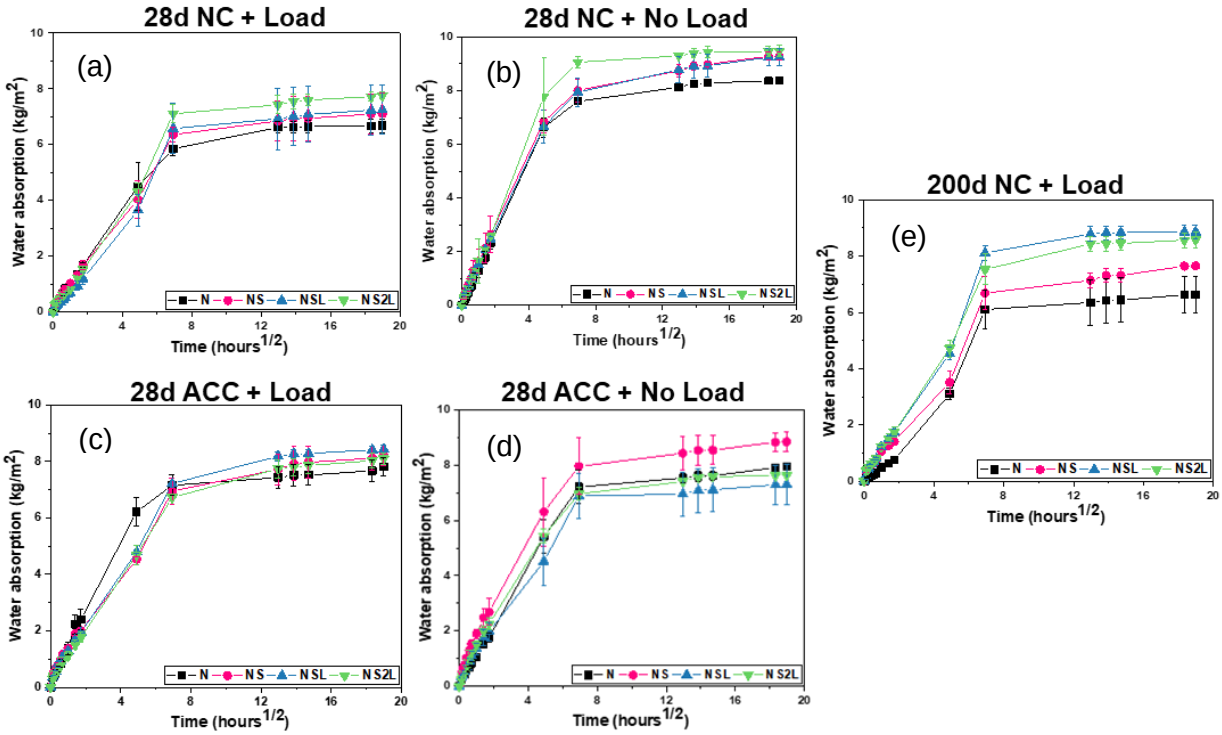

Figure 6.20: Sorptivity profiles of concrete mixes (a) 28 days loaded concrete under natural carbonation (NC) conditions, (b) 28 days non-loaded concrete +NC; (c) 28 days loaded concrete under accelerated carbonation (ACC) conditions, (d) 28 days non-loaded concrete + ACC (e) 200 days loaded concrete + NC

Table 6.9: Sorptivity coefficients of concrete exposed to natural or accelerated carbonation with or without load at various exposure durations

Mix ID	Natural carbonation			Accelerated carbonation	
	28d - Load	28d- No Load	200d-Load	28d - Load	28d – No Load
N	1.01 ± 0.03	0.78 ± 0.15	0.62 ± 0.10	1.07 ± 0.08	1.04 ± 0.14
NS	0.90 ± 0.05	1.37 ± 0.42	0.67 ± 0.13	0.82 ± 0.05	1.09 ± 0.30
NSL	0.70 ± 0.16	1.33 ± 0.18	0.88 ± 0.06	0.88 ± 0.0004	0.82 ± 0.22
NS2L	0.82 ± 0.08	0.98 ± 0.18	0.92 ± 0.08	0.87 ± 0.08	1.00 ± 0.04

Table 6.10: Total water absorption (%mass) of concretes exposed to natural or accelerated carbonation with or without load at various exposure durations

Mix ID	Natural carbonation			Accelerated carbonation	
	28d - Load	28d - No Load	200d-Load	28d - Load	28d – No Load
N	5.03 ± 0.37	5.22 ± 0.09	5.07 ± 0.02	4.38 ± 0.29	5.13 ± 0.08
NS	4.97± 0.02	5.79 ± 1.16	5.4 ± 0.31	5.1 ± 0.19	5.14 ± 0.12
NSL	4.94 ± 0.03	5.65 ± 0.09	5.56 ± 0.02	4.95 ± 0.14	4.95 ± 0.09
NS2L	5.02 ± 0.13	5.81 ± 0.14	4.98 ± 0.18	4.67 ± 0.19	5.40 ± 0.46

6.6.5. Changes in total porosity of stressed and carbonated concretes

The results of total porosity after 28 days natural or accelerated carbonated concretes, with or without load, are reported in Figure 6.21(a-b). Under natural carbonation exposure, the results give an indication that the impact of loading on pore structural development leads to reduced porosity relative to non-loaded concretes. For accelerated carbonation, CEM I exhibits reduced porosity under load relative to non-loaded concretes. In the slag-containing concretes with or without limestone, similar porosities are observed for both loading states for NS, NSL and NS2L but relatively lower porosities in the ternary blends. When the porosity variations in the accelerated carbonated concretes are compared to the natural carbonated concretes for the same age (28 days) with load, it shows slightly reduced porosity in CEM I which can be explained by carbonation-induced densification. Meanwhile the slag-containing concretes with or without limestone remain comparable. The reduced porosity can be attributable to densification effect arising from pore volume reduction under loading conditions relative to non-loaded states, and reported to be more evident in CEM I systems than in slag-systems (13). However, it appears the densification effect is more relevant under accelerated conditions with load, and further explains the increased strengths relative to natural

carbonation. Meanwhile, contrary to the similar pore size distributions and crack patterns reported for natural and 3% accelerated exposure (237), when considered in the context of partially carbonated concretes, they may exhibit different load-induced variations. It is however observed that, while the loading and exposure type exert different influences on porosity, classification considering the durability indicator proposed by Baroghel-Bouny (182) suggests all concretes show satisfactory performance.

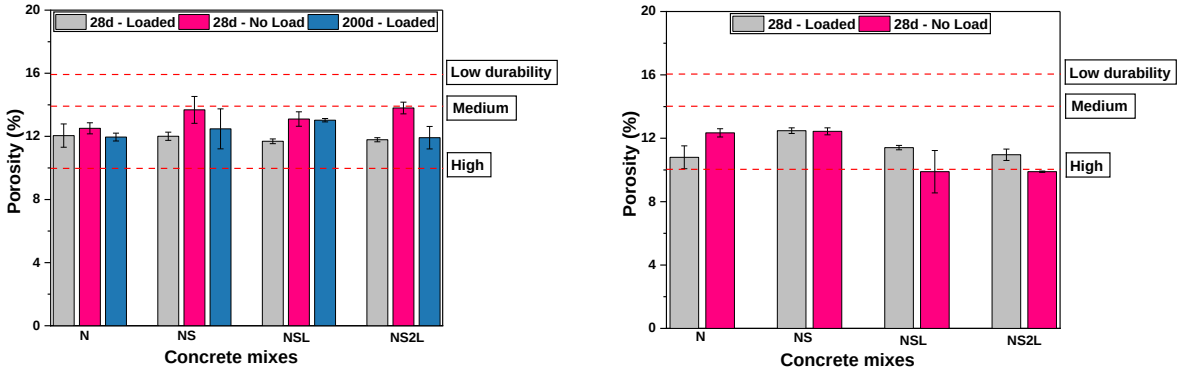

Figure 6.21: Total Porosity changes with or without load of concretes exposed to (a) natural or (b) accelerated carbonation

6.7. Conclusions on studies on the combined action of compressive load and carbonation on transport properties of composite concrete

This study's experimental findings and analysis demonstrate the need to deepen the understanding of engineering and durability aspects of low carbon concretes when subjected to mechanical loads toward replicating near realistic conditions. These findings indicate the need for critically considering the effect of loading in service life predictions of structural concrete to minimise over or under estimation. Based on the results discussed above, the following inferences are drawn:

1. A reduced progression of carbonation front was observed in loaded concrete during early times of exposure, independently of the cement composition, under natural exposure conditions. Conversely, carbonation depths increased significantly under accelerated exposure, with comparable values being recorded for stressed and unstressed CEM I concrete, but slight reductions were observed for NS, NSL and NS2L concrete, when exposed

to carbonation under a stressed state. In all cases when carbonation depths were recorded, CEM I exhibited greater carbonation resistance.

2. Early age loading (such as 7 days cured) of concretes made with composite cements has no detrimental impact on carbonation, when compared to non-loaded concretes. However further investigation is required to understand the causes of this phenomenon.

3. Significant increase in total deformation were recorded under accelerated carbonation exposure conditions, compared to natural exposure for all mixes. While there was about 2.5-fold increase in total strain for CEM I, there was about 5-folds increase in the magnitude of total strain in the slag-containing concretes, with or without limestone. The addition of ~10-20 wt.% limestone in lieu of slag content induces similar dimensional stability to binary slag-containing concretes.

4. The concrete mixes investigated under compressive stress exhibited a reduction in water admissibility particularly at early ages for natural carbonation, which seems to be significantly dependent on the type of carbonation exposure and stress state. Overall, the total water absorption gives an indication of reduction in absorbed water in loaded samples relative to non-loaded samples for both exposures.

5. The changes in total porosity in concretes subjected to accelerated carbonation compared to the natural carbonation, for the same age and when subjected to load, are slightly reduced in CEM I concrete. However, the porosity of the slag-containing concretes, with or without limestone, shows an overall comparable porosity to CEM I. All concretes exhibit medium to high durability when assessed based on post-carbonation porosities irrespective of loading or exposure condition following the Baroghel-Bouny classification of concrete durability performance.

6. It is identified that accelerated carbonation, with or without loading, of slag-containing concretes, with or without limestone, has no detrimental impact on their compressive strength. This suggests that the concrete mixes evaluated in this study can perform satisfactorily when used as structural concrete despite their increased carbonation susceptibility.

Chapter 7

7. Conclusions and recommendations

7.1. Conclusions

This research investigated the mechanical and durability performance of mortars and concretes made from multicomponent cements with varying slag loadings and limestone powder addition, in comparison with binary and CEM I cements. The implications of the systematic exposure of mortars and concretes to carbonation and chloride ingress were investigated, in addition to the influence of the combined action of compressive load and carbonation on water absorption properties. Based on the research findings discussed in the thesis, general conclusions for the experimental chapters are hereby highlighted.

7.1.1. Carbonation performance of mortars made from Portland-slag-limestone

Mortar samples were exposed to natural (ambient CO_2, 57±3 %RH, and 20 ^oC) and accelerated (3% CO_2, 57±3 %RH, and 20 ^oC) unidirectional carbonation, followed by rapid chloride permeability testing (NTBuild 492). It was identified that mortars made from binary and ternary slags-limestone exhibited inferior carbonation performances relative to CEM I under both ambient and accelerated exposure. Even though the slag-based mortars with or without limestone exhibited higher carbonation rates, studies on the potential impact of carbonation-induced variations in pore structure related properties indicated that their water absorption properties and permeability to chlorides are not significantly impacted. Mortars made from ternary cements with increased limestone addition (PC + slag + ~20wt.% limestone) even though exhibit significantly high carbonation depths, they demonstrate significantly lower permeability to chlorides than CEM I. Ternary cements with lower (~10 wt.%) or higher (~20 wt.%) limestone addition shows comparable performance to permeability to chlorides post-carbonation exposure.

7.1.2. Implication on mechanical and durability performance of concretes made from ternary slag blends with high limestone powder addition

Concrete samples were moist room cured for different durations and the evolution of mechanical and durability properties were tested. Studies on compressive strength evolution up to 365 days demonstrated that the early age strength of slag-containing concretes with or without limestone generally exhibited reduced early age compressive strength (day 2). However the strength progressively approaches the compressive strength of CEM I concrete from 90 days onwards, so that concretes made from cements with ~20% limestone addition were able to achieve 80% of CEM I compressive strength. This study also showed that there was no significant impact of reducing slag content in ternary mixes using ~10-20 wt.% powdered limestone on flexural strength (at 28 days and 180 days) and elastic moduli (at 28 days) compared to CEM I mixes. The compressive strength, flexural strength and static elastic moduli of concretes made from multicomponent systems when benchmarked with various international design codes exhibited conformance, similar to CEM I. The investigation of transport properties including sorptivity and chloride permeability tests show composite cements containing powdered limestone as high as ~20 wt.% had no detrimental implications on their resistance to chlorides or moisture. The beneficial effect of pore refinement resulted in improved surface resistivity and transport properties of concretes containing multi-component cements. These results demonstrate that powdered limestone additions can be effectively used for reducing both CEM I and slag contents to produce low carbon concrete for structural applications.

7.1.3. Influence of high carbonation rates of Portland-cement slag limestone concretes on chloride and moisture resistance

Concrete samples were assessed for their carbonation rates, how it affects the chloride permeability and water absorption characteristics. The shrinkage evolution due to accelerated carbonation was monitored. The studies on carbonation and its effect on the chloride permeability of concrete made from high carbonating binary and ternary cements, revealed similar performances to the studies on the mortar scale. The 50-100 years carbonation service life prediction gives an indication that concretes made from ternary slag cements with ~10-20% are within the cover depth limit for exposure classes XC3/XC4. It was also established that even though concrete made from ternary slag-cement was adversely impacted by 100 days accelerated carbonation exposure, the impact on chloride permeability is significantly lower relative to CEM I which exhibited higher carbonation resistance. Furthermore, despite the higher carbonation rates in the binary and ternary mixes, a relatively reduced carbonation-

induced shrinkage was observed relative to CEM I, indicating their dimensional stability is not compromised due to high carbonation rates.

7.1.3.1. Impact of coupled action of carbonation and sustained compressive loads on transport properties of concrete

Finally, on the findings for combined action of carbonation and uniaxial compressive load, it was observed that loading of concretes within the elastic region (~30%) generally resulted in hindered progression of carbonation front relative to non-loaded concretes and appeared to be independent of concrete mix design or carbonation exposure type. The strain evolution of loaded concretes under accelerated carbonation was of increased magnitude in the binary and ternary cements relative to CEM I when their respective strain evolution is compared to their corresponding strain evolution under ambient exposure. Overall, binary and ternary cements show reduced total strain than CEM I for both ambient and accelerated exposure. The early age loading of slag-containing concretes has no detrimental impact on their long-term total strain evolution relative to CEM I. Following the simultaneous exposure of concretes to compressive load and carbonation, the combined influence on sorptivity coefficient after 28 days of natural carbonation shows a reduction in stressed concretes relative to the unstressed concretes, with no detrimental impact of load on sorptivity coefficients post 200 days of loading. Similarly, accelerated carbonation with load was not significantly impacted compared to non-loaded states. Furthermore, the studies on the coupled action of load and carbonation show reduced water accessible porosity under load relative to non-loaded concretes for natural carbonation conditions. Meanwhile, for accelerated carbonation, CEM I concretes exhibited reduced porosity under load relative to non-loaded conditions. In the binary slag and ternary slag-limestone concretes, comparable open porosities were observed for both loading states for NS, NSL and NS2L but with relatively lower porosities in the ternary blends.

7.2. Recommendations

The findings presented in this work have focused on investigating the long-term performance of slag-containing mortars and concretes with or without limestone (~10-20 wt.%) relative to CEM I. Variations in durability performance under single or multiple exposure conditions, and with or without load, were determined to define the engineering and durability properties of such materials. Some further work towards expanding the body of knowledge in the experimental methodology and research findings are hereby discussed.

- The experimental methodology adopted in this study for studying the impact of carbonation on moisture and chloride ingress followed the use of samples unidirectionally carbonated, and then subsequently exposed to chlorides or moisture. While the adopted approach provides a practical approach for accounting for multiple durability exposures, the methodology can further be defined considering exposure classes based on cyclic environmental exposures, using combinations of wet-dry cycles of unidirectional carbonation exposure followed by chloride permeability testing. This can be pursued using controlled environmental chambers equipped with wet-dry cycles or direct exposure of samples to external weather conditions subject to rain and/or dry conditions. Additionally, even though it is envisaged that carbonation would proceed relatively earlier (from formworks removal) than other exposures, the case of unidirectional chloride exposure followed by carbonation can further be explored, as this is also likely. This can give insights into whether chloride ions in the near-surface cover depth can present a retarding impact on carbonation progress.

- In this study, carbonation-induced pore structural variations were evaluated by sorptivity coefficient, total water absorption and open porosity. Even though they are quantitative, they only give a qualitative meaning to the variations in pore size distribution post-carbonation. Limitations exist for commonly used mercury intrusion porosimetry for pore size distribution, pertaining to aspect ratio of test pieces derived from bulk materials. Complementary studies to determine pore structural changes post-carbonation can be conducted by employing high spacial resolution techniques such as X-ray computed tomography to holistically characterise the porosity and pore size distribution. This would contribute to identifying the key physical factors influencing post-carbonation properties such as chloride resistance and strength, while also giving insight into pore structure related carbonation shrinkage.

- The assessment of the combined action of loading and accelerated carbonation can be extended from sustained compressive loading to specimens subjected to tensile loading using similar strength/stress ratios. The boundaries of research can be extended into the adoption of biaxial stresses. Meanwhile, recovery strain after unloading concretes can be monitored for further assessment on closure of microcracks.

- Towards assessing transport properties for concretes simultaneously subjected to load and carbonation, the use of large specimens can be beneficial as it can allow for the coring of samples thus removing bottlenecks related to specimen geometry required for other complementary durability testing such as chloride permeability testing which require cylindrical samples. This however requires purpose-built loading rigs that allow for the application of high stress levels, as loading rigs that were used in the current study required extremely high torque to reach the highest applied load of 63.4 kN. Additionally, the use of walk-in carbonation chambers is necessary to adequately upscale these studies.

- Carbonation service life prediction was addressed in this study. The chloride permeability post-carbonation was also explored. An additional study dependent on the chloride exposure method is to conduct chloride content profiling on concretes systematically subjected to carbonation exposure (with or without load) and then chlorides. This can then be used to give insight into realistic service life prediction for corrosion initiation for a given concrete cover depth.

- Although this study gave some insights into the dimensional stabilities of the concrete mixes. An additional study can pursue the measurement of shrinkage evolution of unloaded specimens corresponding to the age of loaded concretes, which when subtracted from the total strain can be used to estimate the creep performance of the concrete mixes. That notwithstanding, using modern modelling approaches, the experimental results obtained in the loading studies can be used for extrapolating long-term dimensional stabilities, while validating with experimental studies beyond standard durations of PhD studies in the UK.

In summary, this work contributes to the development of an experimental methodology to realistically study the implications of combined action of load and carbonation on the performance of low carbon cements such as those made from Portland cement-slag-

limestone. However there still exist opportunities to expand and revisit this methodology to further understand such complex phenomena. The results from this research provide novel insight about composite slag concretes performance evaluated under close to realistic exposure conditions, accounting for the effect of load and multiple environmental exposure. This highlights the need for adopting performance based durability assessment of concretes, given that conventional and prescriptive evaluation of materials to infer their longevity (e.g. considering strength and porosity values) do not seem to provide a good indication of how these novel concretes will perform when exposed to CO_2.

References

1. Koch, G. Cost of corrosion. In: *Trends in oil gas corrosion research technologies*. 2017, pp.3-30.

2. Stewart, M.G., Wang, X. and Nguyen, M.N. Climate change adaptation for corrosion control of concrete infrastructure. *Structural Safety.* 2012, **35**, pp.29-39.

3. *BS EN 197-5. Portland-composite cement CEM II/C-M and Composite cement CEM VI.* BSI London, 2021.

4. *BS 8500-2. Concrete. Complementary British Standard to BS EN 206. Specification for constituent materials and concrete.* BSI London, 2023.

5. Yao, Y., Wang, L. and Wittmann, F.H. *Publications on durability of reinforced concrete structures under combined mechanical loads and environmental actions: an annotated bibliography.* Aedificatio Publishers, 2013.

6. Song, Z., Zhang, Y., Liu, L., Pu, Q., Jiang, L., Chu, H., Luo, Y., Liu, Q. and Cai, H. Use of XPS for quantitative evaluation of tensile-stress-induced degradation of passive film on carbon steel in simulated concrete pore solution. *Construction and Building Materials.* 2021, **274**, p.121779.

7. Zhang, Y. and Poursaee, A. Passivation and corrosion behavior of carbon steel in simulated concrete pore solution under tensile and compressive stresses. *Journal of Materials in Civil Engineering.* 2015, **27**(8), p.04014234.

8. Samaha, H.R. and Hover, K.C. Influence of microcracking on the mass transport properties of concrete. *Materials Journal.* 1992, **89**(4), pp.416-424.

9. Hearn, N. Effect of shrinkage and load-induced cracking on water permeability of concrete. *Materials Journal.* 1999, **96**(2), pp.234-241.

10. Picandet, V., Khelidj, A. and Bastian, G. Effect of axial compressive damage on gas permeability of ordinary and high-performance concrete. *Cement and concrete research.* 2001, **31**(11), pp.1525-1532.

11. Sugiyama, T., Bremner, T.W. and Holm, T.A. Effect of stress on gas permeability in concrete. *Materials Journal.* 1996, **93**(5), pp.443-450.

12. Francois, R. and Maso, J. Effect of damage in reinforced concrete on carbonation or chloride penetration. *Cement and concrete research.* 1988, **18**(6), pp.961-970.

13. Liu, Z., Van den Heede, P., Zhang, C., Shi, X., Wang, L., Li, J., Yao, Y. and De Belie, N. Influence of sustained compressive load on the carbonation of concrete containing blast furnace slag. *Construction and Building Materials.* 2022, **335**, p.127457.

14. El-Chabib, H. and Syed, A. Properties of self-consolidating concrete made with high volumes of supplementary cementitious materials. *Journal of Materials in Civil Engineering.* 2013, **25**(11), pp.1579-1586.

15. Darquennes, A., Roziere, E., Khokhar, M.I.A., Turcry, P., Loukili, A. and Grondin, F. Long-term deformations and cracking risk of concrete with high content of mineral additions. *Materials and structures.* 2012, **45**(11), pp.1705-1716.

16. Shariq, M., Prasad, J. and Abbas, H. Creep and drying shrinkage of concrete containing GGBFS. *Cement and Concrete Composites.* 2016, **68**, pp.35-45.

17. Proske, T., Rezvani, M., Palm, S., Müller, C. and Graubner, C.-A. Concretes made of efficient multi-composite cements with slag and limestone. *Cement and Concrete Composites.* 2018, **89**, pp.107-119.

18. Shah, V. and Bishnoi, S. Carbonation resistance of cements containing supplementary cementitious materials and its relation to various parameters of concrete. *Construction and Building Materials.* 2018, **178**, pp.219-232.

19. Leemann, A. and Moro, F. Carbonation of concrete: the role of CO2 concentration, relative humidity and CO2 buffer capacity. *Materials and structures.* 2017, **50**(1), p.30.

20. Sulapha, P., Wong, S., Wee, T. and Swaddiwudhipong, S. Carbonation of concrete containing mineral admixtures. *Journal of Materials in Civil Engineering.* 2003, **15**(2), pp.134-143.

21. Worrell, E., Price, L., Martin, N., Hendriks, C. and Meida, L.O. Carbon dioxide emissions from the global cement industry. *Annual review of energy the environment.* 2001, **26**(1), pp.303-329.

22. Mehta, P.K. and Meryman, H. Tools for reducing carbon emissions due to cement consumption. *Structure Magazine.* 2009, **1**(1), pp.11-15.

23. Damtoft, J.S., Lukasik, J., Herfort, D., Sorrentino, D. and Gartner, E.M. Sustainable development and climate change initiatives. *Cement and concrete research.* 2008, **38**(2), pp.115-127.

24. Gartner, E. and Sui, T. Alternative cement clinkers. *Cement and concrete research.* 2018, **114**, pp.27-39.

25. Sharp, J., Gartner, E. and Macphee, D. Novel cement systems (sustainability). Session 2 of the Fred Glasser Cement Science Symposium. *Advances in cement research.* 2010, **22**(4), pp.195-202.

26. IEA, W., CSI. *Cement Technology Roadmap 2009–Carbon emissions reductions up to 2050.* Paris, France, 2009.

27. Environment, U., Scrivener, K.L., John, V.M. and Gartner, E.M. Eco-efficient cements: Potential economically viable solutions for a low-CO2 cement-based materials industry. *Cement and concrete research.* 2018, **114**, pp.2-26.

28. Scrivener, K., Martirena, F., Bishnoi, S. and Maity, S. Calcined clay limestone cements (LC3). *Cement and concrete research.* 2018, **114**, pp.49-56.

29. Douglas, E. and Brandstetr, J. A preliminary study on the alkali activation of ground granulated blast-furnace slag. *Cement and concrete research.* 1990, **20**(5), pp.746-756.

30. De Belie, N., Soutsos, M. and Gruyaert, E. *Properties of fresh and hardened concrete containing supplementary cementitious materials.* Springer, 2018.

31. Lothenbach, B., Scrivener, K. and Hooton, R. Supplementary cementitious materials. *Cement and concrete research.* 2011, **41**(12), pp.1244-1256.

32. *ASTM C618 - 23E1. Standard Specification for Coal Ash and Raw or Calcined Natural Pozzolan for Use in Concrete.* West Conshohocken, PA, USA: American Society for Testing Materials, 2023.

33. Skibsted, J. and Snellings, R. Reactivity of supplementary cementitious materials (SCMs) in cement blends. *Cement and concrete research.* 2019, **124**, p.105799.

34. Scrivener, K.L., Lothenbach, B., De Belie, N., Gruyaert, E., Skibsted, J., Snellings, R. and Vollpracht, A. TC 238-SCM: hydration and microstructure of concrete with SCMs. *Materials and structures.* 2015, **48**(4), pp.835-862.

35. Berodier, E. and Scrivener, K. Understanding the Filler Effect on the Nucleation and Growth of C- S- H. *Journal of the American Ceramic Society.* 2014, **97**(12), pp.3764-3773.

36. Wu, K., Shi, H., Xu, L., Ye, G. and De Schutter, G. Microstructural characterization of ITZ in blended cement concretes and its relation to transport properties. *Cement and concrete research.* 2016, **79**, pp.243-256.

37. Durdziński, P.T., Ben Haha, M., Zajac, M. and Scrivener, K.L. Phase assemblage of composite cements. *Cement and concrete research.* 2017, **99**, pp.172-182.

38. Scrivener, K.L., Crumbie, A.K. and Laugesen, P. The interfacial transition zone (ITZ) between cement paste and aggregate in concrete. *Interface science.* 2004, **12**(4), pp.411-421.

39. Berodier, E. and Scrivener, K. Evolution of pore structure in blended systems. *Cement and concrete research.* 2015, **73**, pp.25-35.

40. Adu-Amankwah, S., Zajac, M., Stabler, C., Lothenbach, B. and Black, L. Influence of limestone on the hydration of ternary slag cements. *Cement and concrete research.* 2017, **100**, pp.96-109.

41. Lothenbach, B., Le Saout, G., Gallucci, E. and Scrivener, K. Influence of limestone on the hydration of Portland cements. *Cement and concrete research.* 2008, **38**(6), pp.848-860.

42. Pu, Q., Jiang, L., Xu, J., Chu, H., Xu, Y. and Zhang, Y. Evolution of pH and chemical composition of pore solution in carbonated concrete. *Construction Building Materials.* 2012, **28**(1), pp.519-524.

43. De Weerdt, K., Plusquellec, G., Revert, A.B., Geiker, M.R. and Lothenbach, B. Effect of carbonation on the pore solution of mortar. *Cement and concrete research.* 2019, **118**, pp.38-56.

44. Pal, S., Mukherjee, A., Pathak, S.J.C. and Research, C. Investigation of hydraulic activity of ground granulated blast furnace slag in concrete. 2003, **33**(9), pp.1481-1486.

45. Bougara, A., Lynsdale, C. and Milestone, N.B. Reactivity and performance of blastfurnace slags of differing origin. *Cement and Concrete Composites.* 2010, **32**(4), pp.319-324.

46. Kocaba, V., Gallucci, E. and Scrivener, K.L. Methods for determination of degree of reaction of slag in blended cement pastes. *Cement and concrete research.* 2012, **42**(3), pp.511-525.

47. Hinrichs, W. and Odler, I. Investigation of the hydration of Portland blastfurnace slag cement: hydration kinetics. *Advances in Cement Research.* 1989, **2**(5), pp.9-13.

48. Babu, K.G. and Kumar, V.S.R. Efficiency of GGBS in concrete. *Cement and concrete research.* 2000, **30**(7), pp.1031-1036.

49. Taylor, R., Richardson, I.G. and Brydson, R.M.D. Composition and microstructure of 20-year-old ordinary Portland cement–ground granulated blast-furnace slag blends containing 0 to 100% slag. *Cement and concrete research.* 2010, **40**(7), pp.971-983.

50. Beushausen, H., Alexander, M. and Ballim, Y. Early-age properties, strength development and heat of hydration of concrete containing various South African slags at different replacement ratios. *Construction and Building Materials.* 2012, **29**, pp.533-540.

51. Lang, E. Blast furnace cements. *Structure and performance of cements.* 2002, pp.310-325.

52. Ukpata, J.O., Basheer, P.A.M. and Black, L. Performance of plain and slag-blended cements and mortars exposed to combined chloride–sulfate solution. *Advances in cement research.* 2018, **30**(8), pp.371-386.

53. Khatib, J.M. and Hibbert, J.J. Selected engineering properties of concrete incorporating slag and metakaolin. *Construction and Building Materials.* 2005, **19**(6), pp.460-472.

54. De Schutter, G. Hydration and temperature development of concrete made with blast-furnace slag cement. *Cement and concrete research.* 1999, **29**(1), pp.143-149.

55. Bamforth, P. In situ measurement of the effect of partial portland cement replacement using either fly ash or ground granulated blast-furnace slag on the performance of mass concrete. *Proceedings of the Institution of Civil Engineers.* 1980, **69**(3), pp.777-800.

56. Güneyisi, E., Özturan, T., Gesoğlu, M.J.C. and Composites, C. A study on reinforcement corrosion and related properties of plain and blended cement concretes under different curing conditions. 2005, **27**(4), pp.449-461.

57. Giergiczny, Z., Glinicki, M.A., Sokołowski, M. and Zielinski, M. Air void system and frost-salt scaling of concrete containing slag-blended cement. *Construction and Building Materials.* 2009, **23**(6), pp.2451-2456.

58. Tsivilis, S., Batis, G., Chaniotakis, E., Grigoriadis, G., Theodossis, D.J.C. and research, c. Properties and behavior of limestone cement concrete and mortar. 2000, **30**(10), pp.1679-1683.

59. Palm, S., Proske, T., Rezvani, M., Hainer, S., Müller, C. and Graubner, C.-A. Cements with a high limestone content – Mechanical properties, durability and ecological characteristics of the concrete. *Construction and Building Materials.* 2016, **119**, pp.308-318.

60. Adu-Amankwah, S., Zajac, M., Skocek, J., Ben Haha, M. and Black, L. Relationship between cement composition and the freeze–thaw resistance of concretes. *Advances in cement research.* 2018, **30**(8), pp.387-397.

61. Palm, S., Müller, C., Proske, T., Rezvani, M. and Graubner, C.-A. Concrete application of clinker-efficient cements. *Advances in cement research.* 2019, **31**(5), pp.225-234.

62. Heikal, M., El-Didamony, H. and Morsy, M.S. Limestone-filled pozzolanic cement. *Cement and concrete research.* 2000, **30**(11), pp.1827-1834.

63. Ye, G., Liu, X., De Schutter, G., Poppe, A.M. and Taerwe, L. Influence of limestone powder used as filler in SCC on hydration and microstructure of cement pastes. *Cement and Concrete Composites.* 2007, **29**(2), pp.94-102.

64. Dedeloudis, C., Zervaki, M., Sideris, K., Juenger, M., Alderete, N., Kamali-Bernard, S., Villagrán, Y. and Snellings, R. Natural Pozzolans. In: De Belie, N. et al. eds. *Properties of Fresh and Hardened Concrete Containing Supplementary Cementitious Materials: State-of-the-Art Report of the RILEM Technical Committee 238-SCM, Working Group 4*. Cham: Springer International Publishing, 2018, pp.181-231.

65. Zajac, M., Skocek, J., Adu-Amankwah, S., Black, L. and Ben Haha, M. Impact of microstructure on the performance of composite cements: Why higher total porosity can result in higher strength. *Cement and Concrete Composites.* 2018, **90**, pp.178-192.

66. Menéndez, G., Bonavetti, V. and Irassar, E.F. Strength development of ternary blended cement with limestone filler and blast-furnace slag. *Cement and Concrete Composites.* 2003, **25**(1), pp.61-67.

67. *Building Code Requirements for Structural Concrete (ACI 318-19).* Farmington Hills, MI 48331: American Concrete Institute, 2019.

68. Neville, A.M. *Properties of concrete*. Longman London. 1995, 4, pp.482-529.

69. Mehta, P.K. and Monteiro, P.J.M. Concrete Microstructure, Properties, and Materials. In: 3rd ed. ed. New York: McGraw-Hill, 2006, p.122.

70. Hooton, R.D. Current developments and future needs in standards for cementitious materials. *Cement and concrete research.* 2015, **78**, pp.165-177.

71. Hooton, R.D. Future directions for design, specification, testing, and construction of durable concrete structures. *Cement and concrete research.* 2019, **124**, p.105827.

72. Beushausen, H., Torrent, R. and Alexander, M.G. Performance-based approaches for concrete durability: State of the art and future research needs. 2019, **119**, pp.11-20.

73. *BS EN 206:2013+A2. Concrete — Specification, performance, production and conformity.* London: British Standards Institute, 2021.

74. Nganga, G., Alexander, M. and Beushausen, H. Practical implementation of the durability index performance-based design approach. *Construction and Building Materials.* 2013, **45**, pp.251-261.

75. Güneyisi, E. and Gesoğlu, M. A study on durability properties of high-performance concretes incorporating high replacement levels of slag. *Materials and structures.* 2008, **41**, pp.479-493.

76. Balonis, M., Glasser, F.P.J.C. and Research, C. The density of cement phases. 2009, **39**(9), pp.733-739.

77. Maddalena, R., Taha, H. and Gardner, D. Self-healing potential of supplementary cementitious materials in cement mortars: Sorptivity and pore structure. *Developments in the Built Environment.* 2021, **6**, p.100044.

78. Chen, J., Song, X., Zhao, T. and Tian, L. Service life prediction of lining concrete of subsea tunnel under combined compressive load and carbonation. *Journal of Wuhan University of Technology-Mater. Sci. Ed.* 2010, **25**(6), pp.1061-1064.

79. Acker, P. and Ulm, F.-J. Creep and shrinkage of concrete: physical origins and practical measurements. *Nuclear engineering design.* 2001, **203**(2-3), pp.143-158.

80. Tamtsia, B.T. and Beaudoin, J.J. Basic creep of hardened cement paste A re-examination of the role of water. *Cement and concrete research.* 2000, **30**(9), pp.1465-1475.

81. Loo, Y.H. A new method for microcrack evaluation in concrete under compression. *Materials and structures.* 1992, **25**, pp.573-578.

82. Von Greve-Dierfeld, S., Lothenbach, B., Vollpracht, A., Wu, B., Huet, B., Andrade, C., Medina, C., Thiel, C., Gruyaert, E. and Vanoutrive, H. Understanding the carbonation of concrete with supplementary cementitious materials: a critical review by RILEM TC 281-CCC. *Materials and structures.* 2020, **53**(6), pp.1-34.

83. Yaman, I., Hearn, N. and Aktan, H. Active and non-active porosity in concrete part I: experimental evidence. *Materials and structures.* 2002, **35**(2), pp.102-109.

84. Sidney Mindess, J.F.Y., David Darwin. *Concrete*. Prentice Hal. 2002, pp.477-448.

85. Picandet, V. and Khelidj, A. Gas and water permeability of cracked concrete. In, 2003.

86. Gerard, B., Reinhardt, H. and Breysse, B. Measured transport in cracked concrete. *Rilem report.* 1997, (16), pp.265-324.

87. Hall, C. Water sorptivity of mortars and concretes: a review. *Magazine of concrete research.* 1989, **41**(147), pp.51-61.

88. Castro, J., Bentz, D. and Weiss, J. Effect of sample conditioning on the water absorption of concrete. *Cement Concrete Composites.* 2011, **33**(8), pp.805-813.

89. BS EN 13057. Products and systems for the protection and repair of concrete structures. Test methods. Determination of resistance of capillary absorption. 2002.

90. Ollivier, J.-P., Torrenti, J.-M. and Carcassés, M. *Physical properties of concrete and concrete constituents.* Wiley Online Library, 2012.

91. M. Moini, K.S.I.F.-V.S.M.L.T.P.S.C. and Beyene, M. Durability of Concrete Mixtures Containing Supplementary Cementitious Materials in Rapid Chloride Permeability Test. *ACI Materials Journal.* **116**(5).

92. Shafikhani, M. and Chidiac, S. Quantification of concrete chloride diffusion coefficient–A critical review. *Cement and Concrete Composites.* 2019, **99**, pp.225-250.

93. *Nordtest NTBuild 492. Concrete, Mortar, Cement Based Repair Materials: Chloride Migration Coefficient from Non-steady State Migration Experiments.* 1999.

94. Li, K., Zhang, Y., Wang, S. and Zeng, J. Impact of carbonation on the chloride diffusivity in concrete: experiment, analysis and application. *Materials and structures.* 2018, **51**(6), p.164.

95. Banthia, N., Biparva, A. and Mindess, S. Permeability of concrete under stress. *Cement and concrete research.* 2005, **35**(9), pp.1651-1655.

96. Bao, J. and Wang, L. Combined effect of water and sustained compressive loading on chloride penetration into concrete. *Construction and Building Materials.* 2017, **156**, pp.708-718.

97. Djerbi Tegguer, A., Bonnet, S., Khelidj, A. and Baroghel-Bouny, V. Effect of uniaxial compressive loading on gas permeability and chloride diffusion coefficient of concrete and their relationship. *Cement and concrete research.* 2013, **52**, pp.131-139.

98. Kermani, A. Permeability of stressed concrete: Steady- state method of measuring permeability of hardened concrete studies in relation to the change in structure of concrete under various short- term stress levels. *Building research and information.* 1991, **19**(6), pp.360-366.

99. Angst, U., Moro, F., Geiker, M., Kessler, S., Beushausen, H., Andrade, C., Lahdensivu, J., Köliö, A., Imamoto, K.-i. and von Greve- Dierfeld, S. Corrosion of steel in carbonated concrete: mechanisms, practical experience, and research priorities–a critical review by RILEM TC 281-CCC. *RILEM Technical Letters.* 2020, **5**, pp.85-100.

100. Castellote, M., Fernandez, L., Andrade, C. and Alonso, C. Chemical changes and phase analysis of OPC pastes carbonated at different CO 2 concentrations. *Materials and structures.* 2009, **42**(4), pp.515-525.

101. McPolin, D., Basheer, P., Long, A., Grattan, K. and Sun, T. New test method to obtain pH profiles due to carbonation of concretes containing supplementary cementitious materials. *Journal of Materials in Civil Engineering.* 2007, **19**(11), pp.936-946.

102. Jerga, J.J.C. Physico-mechanical properties of carbonated concrete. *Construction Building Materials.* 2004, **18**(9), pp.645-652.

103. Liu, Z., Van den Heede, P., Zhang, C., Shi, X., Wang, L., Li, J., Yao, Y., Lothenbach, B. and De Belie, N. Carbonation of blast furnace slag concrete at different CO2 concentrations: Carbonation rate, phase assemblage, microstructure and thermodynamic modelling. *Cement and concrete research.* 2023, **169**, p.107161.

104. Leemann, A., Nygaard, P., Kaufmann, J. and Loser, R. Relation between carbonation resistance, mix design and exposure of mortar and concrete. *Cement and Concrete Composites.* 2015, **62**, pp.33-43.

105. Lollini, F. and Redaelli, E. Carbonation of blended cement concretes after 12 years of natural exposure. *Construction and Building Materials.* 2021, **276**, p.122122.

106. Shi, Z., Lothenbach, B., Geiker, M.R., Kaufmann, J., Leemann, A., Ferreiro, S. and Skibsted, J. Experimental studies and thermodynamic modeling of the carbonation of Portland cement, metakaolin and limestone mortars. *Cement and concrete research.* 2016, **88**, pp.60-72.

107. Dhandapani, Y., Santhanam, M., Kaladharan, G. and Ramanathan, S. Towards ternary binders involving limestone additions — A review. *Cement and concrete research.* 2021, **143**, p.106396.

108. Auroy, M., Poyet, S., Le Bescop, P., Torrenti, J.-M., Charpentier, T., Moskura, M. and Bourbon, X. Impact of carbonation on unsaturated water transport properties of cement-based materials. *Cement and concrete research.* 2015, **74**, pp.44-58.

109. Wowra, O. Effects of carbonation to microstructure and pore solution. In: *International RILEM Workshop on Frost Resistance of Concrete*: RILEM Publications SARL, 2002, pp.61-68.

110. Lauch, K.-S. and Dieryck, V. Durability of concrete made with ternary cements containing slag or fly ash and limestone filler. *Int RILEM Conf Mater Syst Struct Civ Eng Conf Segm Concr with SCM's.* 2016.

111. Femenias, Y.S., Angst, U., Moro, F. and Elsener, B. Development of a novel methodology to assess the corrosion threshold in concrete based on simultaneous monitoring of pH and free chloride concentration. *Sensors.* 2018, **18**(9), p.3101.

112. Borges, P.H., Costa, J.O., Milestone, N.B., Lynsdale, C.J. and Streatfield, R.E. Carbonation of CH and C–S–H in composite cement pastes containing high amounts of BFS. *Cement and concrete research.* 2010, **40**(2), pp.284-292.

113. Wu, B. and Ye, G. Development of porosity of cement paste blended with supplementary cementitious materials after carbonation. *Construction and Building Materials.* 2017, **145**, pp.52-61.

114. Hren, M., Bokan Bosiljkov, V. and Legat, A. Effects of blended cements and carbonation on chloride-induced corrosion propagation. *Cement and concrete research.* 2021, **145**, p.106458.

115. Wan, X.M., Cao, W.Q., Zhao, T.J. and Fan, H. Service Life Prediction Based on Carbonation Reliability Theory for Reinforced Concrete under Mechanical Load. *Advanced Materials Research.* 2011, **243-249**, pp.1156-1162.

116. Wan, X., Wittmann, F. and Zhao, T.-j. Influence of mechanical load on service life of reinforced concrete structures under dominant influence of carbonation. *Restoration of Buildings Monuments.* 2011, **17**(2), pp.103-110.

117. Yao, Y., Wang, L., Li, J., De Belie, N., Shi, X., Van den Heede, P., Zhang, C., Liu, Z., Talakokula, V., Jin, Z., Xiong, C., Lu, J., Kamali-Bernard, S., Bansal, T., Li, B., Wang, Z. and Huang, Y. Report of RILEM TC 281-CCC: effect of loading on the carbonation

performance of concrete with supplementary cementitious materials — an interlaboratory comparison of different test methods and related observations. *Materials and structures.* 2023, **56**(6), p.110.

118. Claisse, P. and Dean, C. Compressive strength of concrete after early loading. *Proceedings of the Institution of Civil Engineers-Construction Materials.* 2013, **166**(3), pp.152-157.

119. Galan, I. and Glasser, F.P. Chloride in cement. *Advances in cement research.* 2015, **27**(2), pp.63-97.

120. Ben-Yair, M. The effect of chlorides on concrete in hot and arid regions. *Cement and concrete research.* 1974, **4**(3), pp.405-416.

121. Tang, L., Nilsson, L.-O. and Basheer, P.M. *Resistance of concrete to chloride ingress: Testing and modelling.* CRC Press, 2011.

122. Machner, A., Zajac, M., Ben Haha, M., Kjellsen, K.O., Geiker, M.R. and De Weerdt, K. Chloride-binding capacity of hydrotalcite in cement pastes containing dolomite and metakaolin. *Cement and concrete research.* 2018, **107**, pp.163-181.

123. Lizarazo Marriaga, J. and Claisse, P. The influence of the blast furnace slag replacement on chloride penetration in concrete. *Ingeniería e Investigación.* 2011, **31**(2), pp.38-47.

124. Otieno, M., Beushausen, H. and Alexander, M. Effect of chemical composition of slag on chloride penetration resistance of concrete. *Cement and Concrete Composites.* 2014, **46**, pp.56-64.

125. Lim, C.C., Gowripalan, N. and Sirivivatnanon, V. Microcracking and chloride permeability of concrete under uniaxial compression. *Cement and Concrete Composites.* 2000, **22**(5), pp.353-360.

126. Yoo, S.-W. and Kwon, S.-J. Effects of cold joint and loading conditions on chloride diffusion in concrete containing GGBFS. *Construction and Building Materials.* 2016, **115**, pp.247-255.

127. Neubauer, C., Bergstrom, T., Sujata, K., Xi, Y., Garboczi, E. and Jennings, H. Drying shrinkage of cement paste as measured in an environmental scanning electron microscope and comparison with microstructural models. *Journal of Materials Science.* 1997, **32**(24), pp.6415-6427.

128. Hamed, E. and Lai, C. Geometrically and materially nonlinear creep behaviour of reinforced concrete columns. 2016, **5**, pp.1-12.

129. Bažant, Z.P. and Jirásek, M. Basic Properties of Concrete Creep, Shrinkage, and Drying. In: Bažant, Z.P. and Jirásek, M. eds. *Creep and Hygrothermal Effects in Concrete Structures*. Dordrecht: Springer Netherlands, 2018, pp.29-62.

130. Hubler, M.H., Wendner, R. and Bažant, Z.P. Comprehensive Database for Concrete Creep and Shrinkage: Analysis and Recommendations for Testing and Recording. *ACI Materials Journal.* 2015, **112**(4).

131. Neville, A.M. *Properties of concrete*. Longman London. 1995, 4, pp.426-445.

132. Bažant, Z., Donmez, A., Masoero, E. and Aghdam, S.R. Interaction of concrete creep, shrinkage and swelling with water, hydration, and damage: Nano-macro-chemo. In: *CONCREEP 10*. 2015, pp.1-12.

133. Jennings, H.M. Colloid model of C− S− H and implications to the problem of creep and shrinkage. *Materials and structures.* 2004, **37**(1), pp.59-70.

134. Vandamme, M., Ulm, F.-J. and Fonollosa, P. Nanogranular packing of C–S–H at substochiometric conditions. *Cement and concrete research.* 2010, **40**(1), pp.14-26.

135. Bažant, Z.P. and Jirásek, M. *Creep and hygrothermal effects in concrete structures.* Springer, 2018.

136. Abdolhosseini Qomi, M.J., Krakowiak, K.J., Bauchy, M., Stewart, K.L., Shahsavari, R., Jagannathan, D., Brommer, D.B., Baronnet, A., Buehler, M.J. and Yip, S. Combinatorial molecular optimization of cement hydrates. *Nature Communications.* 2014, **5**(1), p.4960.

137. Wang, J., Hu, Z., Chen, Y., Huang, J., Ma, Y., Zhu, W. and Liu, J. Effect of Ca/Si and Al/Si on micromechanical properties of C(-A)-S-H. *Cement and concrete research.* 2022, **157**, p.106811.

138. Pickett, G. The effect of change in moisture-content on the crepe of concrete under a sustained load. In: *Journal Proceedings*, *1942*, 1942, pp.333-356.

139. Chern, J.-C. and Chan, Y.-W. Deformations of concretes made with blast-furnace slag cement and ordinary portland cement. *Materials Journal.* 1989, **86**(4), pp.372-382.

140. Brooks, J.J., Wainwright, P.J. and Boukendakji, M. Influence of slag type and replacement level on strength elasticity, shrinkage and creep of concrete. *Special Publication.* 1992, **132**, pp.1325-1342.

141. Khatri, R.P., Sirivivatnanon, V. and Gross, W. Effect of different supplementary cementitious materials on mechanical properties of high performance concrete. *Cement and concrete research.* 1995, **25**(1), pp.209-220.

142. Neville, A.M. *Properties of concrete*. Longman London. 1995, 4, p.441.

143. Alahmad, S., Toumi, A., Verdier, J. and François, R. Effect of crack opening on carbon dioxide penetration in cracked mortar samples. *Materials and structures.* 2009, **42**(5), pp.559-566.

144. *BS 7979. Specification for limestone fines for use with Portland cement.* London: BSI Standards Limited, 2016.

145. *BS EN 196-1. Methods of testing cement. Determination of strength.* London: British Standards Institution, 2016.

146. Hupp, B.N. and Donovan, J.J. Quantitative mineralogy for facies definition in the Marcellus Shale (Appalachian Basin, USA) using XRD-XRF integration. *Sedimentary Geology.* 2018, **371**, pp.16-31.

147. Chatterjee, A.K. Handbook of analytical techniques in concrete science and technology: principles, techniques and applications. In: Ramachandran, V.S. and Beaudoin, J.J. eds. Elsevier, 2000.

148. Fawcett, T.G., Blanton, J.R., Kabekkodu, S.N., Blanton, T.N., Lyza, J. and Broton, D. Best references for the QPA of Portland cement. *Powder Diffraction.* 2022, **37**(2), pp.68-75.

149. Taylor, H.F. *Cement chemistry.* Thomas Telford London, 1997.

150. Diab, A.M., Mohamed, I.A. and Aliabdo, A.A. Impact of organic carbon on hardened properties and durability of limestone cement concrete. *Construction and Building Materials.* 2016, **102**, pp.688-698.

151. *BS EN 933-1: 2012. Tests for geometrical properties of aggregates-Part 1: Determination of particle size distribution-Sieving method.* London, UK: British Standards Institution 2012.

152. *BS EN 1097-6 . Tests for mechanical and physical properties of aggregates.* London: British Standard Institution, 2022.

153. *BS EN 12390-2. Testing hardened concrete. Making and curing specimens for strength tests.* London: British Standards Institution, 2019.

154. *BS EN 12350-2. Testing fresh concrete. Slump-test.* London: British Standards Institution, 2019.

155. *BS EN 12350-5. Testing Fresh Concrete. Flow Table Test.* London: British Standard Institute, 2019.

156. *BS EN 12350-6. Testing Fresh Concrete. Density.* London, UK: British Standard Institute

2019.

157. *BS EN 12390-3. Testing Hardened Concrete: Compressive Strength of Test Specimens.* London, UK: British Standard Institute, 2019

158. *BS EN 1015-11: Methods of test for mortar for masonry–Part 11: Determination of flexural and compressive strength of hardened mortar.* London: BSI, 2019.

159. *BS EN 12390-5. Testing Hardened Concrete. Flexural Strength of Test Specimens.* London: British Standard Institution, 2019.

160. *ASTM C469/C469M. Standard Test Method for Static Modulus of Elasticity and Poisson's Ratio of Concrete in Compression.* West Conshohocken, PA: ASTM International, 2022.

161. *BS EN 12504-4. Testing concrete. Determination of ultrasonic pulse velocity.* London: British Standards Institution, 2021.

162. *BS EN 12390-7. Testing Hardened Concrete: Density of Hardened Concrete.* British Standards Institution, 2019.

163. *ASTM C-597: Standard test method for pulse velocity through concrete.* West Conshohocken, PA, USA: American Society for Testing and Materials 2002.

164. Anson, M. and Newman, K. The effect of mix proportions and method of testing on Poisson's ratio for mortars and concretes. *Magazine of concrete research.* 1966, **18**(56), pp.115-130.

165. *BS EN 12390-17. Testing Hardened Concrete - Determination of creep of concrete in compression.* London: BSI, 2019.

166. *BS EN 12390-12: Determination of the carbonation resistance of concrete — Accelerated carbonation method.* London, UK: British Standards Institution, 2020.

167. Guri, M., Zadov, B. and Elovici, Y. Odini: Escaping sensitive data from faraday-caged, air-gapped computers via magnetic fields. *IEEE Transactions on Information Forensics and Security.* 2019, **15**, pp.1190-1203.

168. Khokhar, M.I.A., Rozière, E., Turcry, P., Grondin, F. and Loukili, A. Mix design of concrete with high content of mineral additions: Optimisation to improve early age strength. *Cement and Concrete Composites.* 2010, **32**(5), pp.377-385.

169. ASTM C 1760. Standard test method for bulk electrical conductivity of hardened concrete. 2012.

170. *BS 1881-208. Recommendations for the determination of the initial surface absorption of concrete.* London: British Standards Institution, 1996.

171. Ismail, I., Bernal, S.A., Provis, J.L., San Nicolas, R., Brice, D.G., Kilcullen, A.R., Hamdan, S. and van Deventer, J.S.J. Influence of fly ash on the water and chloride permeability of alkali-activated slag mortars and concretes. *Construction and Building Materials.* 2013, **48**, pp.1187-1201.

172. Gallé, C. Effect of drying on cement-based materials pore structure as identified by mercury intrusion porosimetry: A comparative study between oven-, vacuum-, and freeze-drying. *Cement and concrete research.* 2001, **31**(10), pp.1467-1477.

173. Dhandapani, Y., Sakthivel, T., Santhanam, M., Gettu, R. and Pillai, R.G. Mechanical properties and durability performance of concretes with Limestone Calcined Clay Cement (LC3). *Cement and concrete research.* 2018, **107**, pp.136-151.

174. Mounanga, P., Khokhar, M.I.A., El Hachem, R. and Loukili, A. Improvement of the early-age reactivity of fly ash and blast furnace slag cementitious systems using limestone filler. *Materials and structures.* 2011, **44**(2), pp.437-453.

175. Pane, I. and Hansen, W. Investigation of blended cement hydration by isothermal calorimetry and thermal analysis. *Cement and concrete research.* 2005, **35**(6), pp.1155-1164.

176. Cui, H., Tang, W., Liu, W., Dong, Z. and Xing, F. Experimental study on effects of CO2 concentrations on concrete carbonation and diffusion mechanisms. *Construction and Building Materials.* 2015, **93**, pp.522-527.

177. Sisomphon, K. and Franke, L. Carbonation rates of concretes containing high volume of pozzolanic materials. *Cement and concrete research.* 2007, **37**(12), pp.1647-1653.

178. Leemann, A. and Moro, F. Carbonation of concrete: the role of CO2 concentration, relative humidity and CO2 buffer capacity. *Materials and structures.* 2016, **50**(1), p.30.

179. Dias, W.P.S. Reduction of concrete sorptivity with age through carbonation. *Cement and concrete research.* 2000, **30**(8), pp.1255-1261.

180. da, S., Pedrosa, R., Lameiras, F.S. and Vasconcelos, W. Carbonation-Related Microstructural Changesin Long-Term Durability Concrete. *Materials Research.* 2002, **5**.

181. Vigor, J.E., Prentice, D.P., Xiao, X., Bernal, S.A. and Provis, J.L. The pore structure and water absorption in Portland/slag blended hardened cement paste determined by synchrotron X-ray microtomography and neutron radiography. *RSC advances.* 2024, **14**(7), pp.4389-4405.

182. Baroghel-Bouny, V. Which toolkit for durability evaluation as regards chloride ingress into concrete? Part II: Development of a performance approach based on durability indicators and monitoring parameters. In: *2004*, pp.137-163.

183. Hearn, N. and Hooton, R.D. Sample mass and dimension effects on mercury intrusion porosimetry results. *Cement and concrete research.* 1992, **22**(5), pp.970-980.

184. Day, R.L. and Marsh, B.K. Measurement of porosity in blended cement pastes. *Cement and concrete research.* 1988, **18**(1), pp.63-73.

185. Dhandapani, Y. and Santhanam, M. Assessment of pore structure evolution in the limestone calcined clay cementitious system and its implications for performance. *Cement and Concrete Composites.* 2017, **84**, pp.36-47.

186. Andrade, C., Blanco, V.M., Collazo, A., Keddam, M., Nóvoa, X.R. and Takenouti, H. Cement paste hardening process studied by impedance spectroscopy. *Electrochimica Acta.* 1999, **44**(24), pp.4313-4318.

187. Dhandapani, Y. and Santhanam, M. Investigation on the microstructure-related characteristics to elucidate performance of composite cement with limestone-calcined clay combination. *Cement and concrete research.* 2020, **129**, p.105959.

188. Shah, V., Scrivener, K., Bhattacharjee, B. and Bishnoi, S. Changes in microstructure characteristics of cement paste on carbonation. *Cement and concrete research.* 2018, **109**, pp.184-197.

189. Lübeck, A., Gastaldini, A.L.G., Barin, D.S. and Siqueira, H.C. Compressive strength and electrical properties of concrete with white Portland cement and blast-furnace slag. *Cement and Concrete Composites.* 2012, **34**(3), pp.392-399.

190. Ke, X., Bernal, S.A. and Provis, J.L. Uptake of chloride and carbonate by Mg-Al and Ca-Al layered double hydroxides in simulated pore solutions of alkali-activated slag cement. *Cement and concrete research.* 2017, **100**, pp.1-13.

191. Nielsen, E.P., Herfort, D. and Geiker, M.R. Binding of chloride and alkalis in Portland cement systems. *Cement and concrete research.* 2005, **35**(1), pp.117-123.

192. Mapa, D.G., Zhu, H., Nosouhian, F., Shanahan, N., Riding, K.A. and Zayed, A. Chloride binding and diffusion of slag blended concrete mixtures. *Construction and Building Materials.* 2023, **388**, p.131584.

193. Shah, I.H., Miller, S.A., Jiang, D. and Myers, R.J. Cement substitution with secondary materials can reduce annual global CO2 emissions by up to 1.3 gigatons. *Nature Communications.* 2022, **13**(1), p.5758.

194. Hawkins, P., Tennis, P.D. and Detwiler, R.J. *The use of limestone in Portland cement: a state-of-the-art review.* Portland Cement Association Skokie, IL, USA, 1996.

195. Tennis, P.D., Thomas, M.D.A. and Weiss, W.J. *State-of-the-Art Report on Use of Limestone in Cements at Levels of up to 15%.* 2011.

196. *ACI 209R-92. Prediction of creep, shrinkage, and temperature effects in concrete structures, In: ACI Manual of Concrete. Practice Part 1: materials and general properties of concrete; 1994.* 2004.

197. Duan, P., Shui, Z., Chen, W. and Shen, C. Enhancing microstructure and durability of concrete from ground granulated blast furnace slag and metakaolin as cement replacement materials. *Journal of Materials Research and Technology.* 2013, **2**(1), pp.52-59.

198. *CSA A23. 3-04 - Design of Concrete Structures.* . Mississauga, ON, Canada: Canadian Standard Association. 2004.

199. *NZS-3101: Concrete structures standard—The design of concrete structures*. NZS Wellington, New Zealand: Standards New Zealand. 2006.

200. *BS EN 1992-1-1:2004 +A1 (2014). Eurocode 2: Design of concrete structures.* London: British Standard Institute,

201. Taerwe, L. and Matthys, S. *Fib model code for concrete structures 2010*. Ernst & Sohn, Wiley. 2013.

202. Shariq, M., Prasad, J. and Masood, A. Studies in ultrasonic pulse velocity of concrete containing GGBFS. *Construction and Building Materials.* 2013, **40**, pp.944-950.

203. Zhou, Y., Gao, J., Sun, Z. and Qu, W. A fundamental study on compressive strength, static and dynamic elastic moduli of young concrete. *Construction and Building Materials.* 2015, **98**, pp.137-145.

204. Bouasker, M., Khalifa, N.E.H., Mounanga, P. and Ben Kahla, N. Early-age deformation and autogenous cracking risk of slag–limestone filler-cement blended binders. *Construction and Building Materials.* 2014, **55**, pp.158-167.

205. *BS EN 1992-1-1. Eurocode 2: Design of concrete structures.* London: British Standard Institute, 2023.

206. Chen, J.J., Kwan, A.K.H. and Jiang, Y. Adding limestone fines as cement paste replacement to reduce water permeability and sorptivity of concrete. *Construction and Building Materials.* 2014, **56**, pp.87-93.

207. Yeau, K.Y. and Kim, E.K. An experimental study on corrosion resistance of concrete with ground granulate blast-furnace slag. *Cement and concrete research.* 2005, **35**(7), pp.1391-1399.

208. Rodulfo, P., Wang, B., Gupta, R., Sharma, L. and Mukhopadhyaya, P. Relationship between electrical Conductivity, Half cell Potential, Linear polarization resistance and Macrocell current of cementitious repair materials. *Construction and Building Materials.* 2023, **401**, p.132733.

209. Ghosh, P. and Tran, Q. Correlation Between Bulk and Surface Resistivity of Concrete. *International Journal of Concrete Structures and Materials.* 2015, **9**(1), pp.119-132.

210. Jagan, G. and Gary, C. Resistivity Tests for Concrete—Recent Field Experience. *ACI Materials Journal.* **113**(4).

211. Saillio, M., Baroghel-Bouny, V., Barberon, F.J.C. and Materials, B. Chloride binding in sound and carbonated cementitious materials with various types of binder. 2014, **68**, pp.82-91.

212. Wilson, W., Georget, F. and Scrivener, K. Unravelling chloride transport/microstructure relationships for blended-cement pastes with the mini-migration method. *Cement and concrete research.* 2021, **140**, p.106264.

213. Baroghel-Bouny, V., Kinomura, K., Thiery, M. and Moscardelli, S. Easy assessment of durability indicators for service life prediction or quality control of concretes with high volumes of supplementary cementitious materials. *Cement and Concrete Composites.* 2011, **33**(8), pp.832-847.

214. BSI. *BS 8500-1: 2015+ A2: 2019. Concrete. Complementary British Standard to BS EN 206. Method of specifying and guidance for the specifier.* London: British Standard Institution, 2019.

215. *BS 8500-1. Concrete. Complementary British Standard to BS EN 206. Method of specifying and guidance for the specifier.* London: British Standard Institution, 2023.

216. Tuutti, K. Service Life of Structures with Regard to Corrosion of Embedded Steel. *ACI Symposium Publication.* **65**.

217. Papadakis, V.G., Vayenas, C.G. and Fardis, M. A reaction engineering approach to the problem of concrete carbonation. *AIChE Journal.* 1989, **35**(10), pp.1639-1650.

218. Metalssi, O.O., Aït-Mokhtar, A. and Turcry, P. A proposed modelling of coupling carbonation-porosity-moisture transfer in concrete based on mass balance equilibrium. *Construction and Building Materials.* 2020, **230**, p.116997.

219. BS EN 12390-12: Determination of the carbonation resistance of concrete — Accelerated carbonation method. 2020.

220. Huy Vu, Q., Pham, G., Chonier, A., Brouard, E., Rathnarajan, S., Pillai, R., Gettu, R., Santhanam, M., Aguayo, F., Folliard, K.J., Thomas, M.D., Moffat, T., Shi, C. and Sarnot, A. Impact of different climates on the resistance of concrete to natural carbonation. *Construction and Building Materials.* 2019, **216**, pp.450-467.

221. Atiş, C.D. and Bilim, C. Wet and dry cured compressive strength of concrete containing ground granulated blast-furnace slag. *Building and Environment.* 2007, **42**(8), pp.3060-3065.

222. Lim, S.N. and Wee, T.H. Autogenous shrinkage of ground-granulated blast-furnace slag concrete. *Materials Journal.* 2000, **97**(5), pp.587-593.

223. Rezvani, M., Proske, T. and Graubner, C.-A. Modelling the drying shrinkage of concrete made with limestone-rich cements. *Cement and concrete research.* 2019, **115**, pp.160-175.

224. Kwan, A.K.H., McKinley, M. and Chen, J.-J. Adding limestone fines as cement paste replacement to reduce shrinkage of concrete. *Magazine of concrete research.* 2013, **65**(15), pp.942-950.

225. Neville, A.M. Creep of concrete as a function of its cement paste content. *Magazine of concrete research.* 1964, **16**(46), pp.21-30.

226. Forth, J. Predicting the tensile creep of concrete. *Cement and Concrete Composites.* 2015, **55**, pp.70-80.

227. Litvan, G.G. and Meyer, A. Carbonation of granulated blast furnace slag cement concrete during twenty years of field exposure. *ACI Symposium Publication.* 1986, **91**, pp.1445-1462.

228. Osborne, G.J. Durability of Portland blast-furnace slag cement concrete. *Cement and Concrete Composites.* 1999, **21**(1), pp.11-21.

229. Vivek, K.S., Vinod Kumar, K. and Subba Reddy, Y.V. Influence of early age loading on compressive strength of M25 fly ash concrete. *Materials Today: Proceedings.* 2023.

230. Monkman, S. and Shao, Y. Carbonation curing of slag-cement concrete for binding CO 2 and improving performance. *Journal of Materials in Civil Engineering.* 2010, **22**(4), pp.296-304.

231. McDonald, D.B., Brooks, J.J., Burg, R.G., Daye, M.A., Gardner, N.J. and Novak, L.C. Report on factors affecting shrinkage and creep of hardened concrete reported by ACI committee 209. *American Concrete Institute (ACI): Farmington Hills, MI, USA.* 2014, pp.1-12.

232. Li, J. and Yao, Y. A study on creep and drying shrinkage of high performance concrete. *Cement and concrete research.* 2001, **31**(8), pp.1203-1206.

233. Vandamme, M. and Ulm, F.J. Nanoindentation investigation of creep properties of calcium silicate hydrates. *Cement and concrete research.* 2013, **52**, pp.38-52.

234. Zhang, Q., Le Roy, R., Vandamme, M. and Zuber, B. Long-term creep properties of cementitious materials: Comparing microindentation testing with macroscopic uniaxial compressive testing. *Cement and concrete research.* 2014, **58**, pp.89-98.

235. Wilson, W., Sorelli, L. and Tagnit-Hamou, A. Unveiling micro-chemo-mechanical properties of C–(A)–S–H and other phases in blended-cement pastes. *Cement and concrete research.* 2018, **107**, pp.317-336.

236. Neville, A.M. *Properties of concrete*. Longman London. 1995, 4. 416.

237. Auroy, M., Poyet, S., Le Bescop, P., Torrenti, J.-M., Charpentier, T., Moskura, M. and Bourbon, X. Comparison between natural and accelerated carbonation (3% CO2): Impact on mineralogy, microstructure, water retention and cracking. *Cement and concrete research.* 2018, **109**, pp.64-80.